THE OPTIMIZATION OF HALOGEN-BONDING ARYL-ETHYNYL RECEPTORS

by

THAÍS PETERSON DE FARIA

A DISSERTATION

Presented to the Department of Chemistry and Biochemistry
and the Division of Graduate Studies of the University of Oregon
in partial fulfillment of the requirements
for the degree of
Doctor of Philosophy

September 2022

DISSERTATION APPROVAL PAGE

Student: Thaís Peterson de Faria

Title: The Optimization of Halogen-Bonding Aryl-Ethynyl Receptors

This dissertation has been accepted and approved in partial fulfillment of the requirements for the Doctor of Philosophy degree in the Department of Chemistry and Biochemistry by:

Dr. Amanda Cook	Chairperson
Dr. Darren Johnson	Advisor
Dr. Michael Haley	Advisor
Dr. Ramesh Jasti	Core Member
Dr. Anne Zemper	Institutional Representative

and

Krista Chronister	Vice Provost for Graduate Studies

Original approval signatures are on file with the University of Oregon Division of Graduate Studies.

Degree awarded September 2022.

DISSERTATION ABSTRACT

Thaís Peterson de Faria

Doctor of Philosophy

Department of Chemistry and Biochemistry

September 2022

Title: The Optimization of Halogen-Bonding Aryl-Ethynyl Receptors

Supramolecular chemistry is an ever-growing area in science that studies noncovalent interactions between small molecules and/or ionic species through molecular recognition or self-assembly. Host-guest chemistry is a branch of this field that pulls a lot of inspiration from nature in hopes to harness synthetic control for a broad range of applications, including encapsulation for pollution remediation, cellular ion transport channels in therapeutics, and anion sensing for *in vivo* cell imaging.

Hydrogen bonds are the most popularly studied noncovalent interaction because of their rich presence in naturally occurring processes, their strength, and directionality. In the past 20 years, halogen bonds have emerged as another prominent form of intermolecular interaction that have similar directionality as hydrogen bonds but have shown to bind guests more competitively in water–a medium that makes up most of the applications of these systems.

In this dissertation, we aim to modify mono- and bi-dentate arylethynyl halogen bond (XB) scaffolds with the purpose of optimizing their selectivity of binding target analytes in polar solvents. In Chapter II, we attempt to synthesize a zwitterionic bi-dentate XB host receptor that features propyl sulfonate, a water-solubilizing functional group, in hopes to measure its binding affinity with phosphate in aqueous media.

In Chapter III, we assess the influence of substituent effects, by modifying tunable groups with various EWGs and EDGs, in neutral versus charged receptors in a family of novel *meta* "one-armed" receptors. In Chapter IV, we continue the investigation of mono-dentate arylethynyl receptors by studying the binding geometry of the *ortho* isomer. Through the comparison of the two isomers (*ortho* and *meta*), we can elucidate chloride's affinity to each binding pocket size. In Chapter IV, we also serendipitously discover a novel vinylic XB donor that is shown to participate in halogen bonding with chloride in a crystal structure. The following results of the binding geometries, experimental binding trends, and theoretical calculations can heavily influence future designs of small-molecule, halogen bonding receptors from this scaffold family to bind to smaller anions more successfully.

This dissertation contains previously published, soon to be published, and unpublished co-authored materials.

CURRICULUM VITAE

NAME OF AUTHOR: Thaís Peterson de Faria

GRADUATE AND UNDERGRADUATE SCHOOLS ATTENDED:

University of Oregon, Eugene
Florida State University, Tallahassee

DEGREES AWARDED:

Doctor of Philosophy, Chemistry, 2022, University of Oregon
Master of Science, Chemistry, 2017, Florida State University
Bachelor of Science, Chemistry, 2015, Florida State University

AREAS OF SPECIAL INTEREST:

Physical Organic Chemistry
Supramolecular Chemistry
Anion Binding

PROFESSIONAL EXPERIENCE:

Research and Development Intern, Thermo Fisher Scientific, June-December, 2022

Graduate Research Fellow, University of Oregon, 2019-2022
Graduate Teaching Fellow, University of Oregon, 2017-2019
Graduate Teaching Fellow, Florida State University, 2015-2017

GRANTS, AWARDS, AND HONORS:

Knight Campus Undergraduate Scholars Program, University of Oregon, 2021

Graduate Student Award for Excellence in the Teaching of Chemistry, University of Oregon, 2017

Promising Scholar, University of Oregon, 2017

Women in Defense–Central Florida Woman in STEM, Florida State University, 2015

Graduate Student Award for Excellence in the Teaching of Chemistry, Florida State University, 2014-2015

Florida Bright Futures Scholarship, Florida State University, 2011-2015

Sarasota Selby Foundation Academic Scholar, Florida State University, 2011-2014

PUBLICATIONS:

Mohamed, R.K.; Mondal, S.; Jorner, K.; Faria Delgado, T.; Ottosson, H.; Alabugin, I.V. The Missing C1-C5 Cycloaromatization Reaction: Triplet State Antiaromaticity Relief and Self-terminating Photorelease of Formaldehyde for Synthesis of Fulvenes from Enynes. *J. Am. Chem. Soc.*, **2015**, *137* (49), 15441–15450.

Fargher, H. A.; Nickels, R. A.; de Faria, T. P; Haley, M. M.; Pluth, M. D.; Johnson, D. W. Deuterium Equilibrium Isotope Effects in a Supramolecular Receptor for the Hydrochalcogenide and Halide Anions. *RSC Adv.*, **2021**, *11*, 26581.

de Faria, T. P.; Bates, H. J.; Trom, A. S.; Longnight, F. I. D.; Miller, M. P.; Zakharov, L. N.; Haley, M. M.; Johnson, D. W. Substituent Effects In a Series of Compact Arylethnyl "Monodentate" Halogen Bonding Hosts for Anions. *Manuscript in prep*.

Bard, J. P.; Bolton, S. G.; Howard, H. J.; McNeill, J. N.; de Faria, T. P.; Zakharov, L. N.; Pluth, M. D.; Johnson, D. W.; Haley, M. M. Utilization of the 2-λ^5-Phosphaquinolin-2-one Scaffold as a non-cytotoxic, pH-stable, and Lysosome Targeting Cell Imaging Reagent. *Manuscript in prep.*

ACKNOWLEDGMENTS

I would like to preface this section with the understanding that no one can accomplish great things alone. There are many people, both from my professional and personal communities, that I would like to articulate my appreciation for helping me attain this goal:

I will begin with expressing my gratitude to all those who helped advise, mentor, and mold me as a young scientist at my alma mater, Florida State University, with special thanks to Dr. Igor Alabugin, Dr. Rana Mohamed, Dr. Gabriel Gomes, Dr. David Delgado, Dr. Paula Delgado, and Dr. Henry Martinez.

To my student mentors at the University of Oregon, Dr. Lisa Eytel, Dr. Jeremy Bard, and Dr. Hazel Fargher, I recognize the time and effort you voluntarily put into helping me better myself as a writer, scientist, and mentor, and, for that, I will be forever indebted to you.

To my current (and recently graduated) lab mates, Dr. Jess Lohrman, Dr. Hazel Fargher, Faith, Scout, Hannah, Luca, Willow, Alex, and Doug, going into work never felt like a burden. In addition to the constant conversations that revolved around projects, group jobs, and scientific advice, we always found a way to have fun. We annoyed one another by dancing and scream-singing in lab while running columns, we argued over how to rank random foods, objects, or activities, and we bonded over playing word games like Wordle and the NYT Crosswords. I recognize that this PhD experience is uncommon, and I couldn't be happier to have shared that with you all. Faith, Scout, and Hannah, this whole dissertation would not have unfolded the way it did without you three.

To my close friends, Dr. Claire Otteson, Dr. Kiana Kawamura, Dr. Hannah Bates, Dr. Terri Lovell, and our respective fur children, Juno, Beans, Cora, Max, Ezra, Kali, Chloe and Lilah. Thank you for being there to laugh, cry, rejoice, and suffer with me through it all. I am so proud of us and all that we went through. To the friends I call family, Katelynn and Thomas Adams, Natalie Fontanes, Julia Howe, Dr. Alanna Condren, and Andres Crucet-Choi. Even with what feels like an insurmountable distance some days, thank you for being some of my greatest cheerleaders throughout this process.

To my partner, Daniel Dougherty, thank you for being my rock. Thank you for easing my panic through your unconditional love, support, and encouragement. Thank you for welcoming me into your life and allowing me to become a part of your beautiful family– it has been one of my greatest blessings in Eugene.

To my mom and dad, I could never even dream of being where I am today without your unlimited support, wisdom, love, and sacrifice. Thank you for always encouraging me to be push myself to be the best student I could be, thank you for actively listening to me when I tell you all about my projects, roadblocks, and drama, thank you for teaching me to be light-hearted and outgoing, and, of course, thank you for always, always, *always* being there, even thousands of miles away. The appreciation I have for you both is hard to put into words. To the rest of my family, both in the US and Brasil, thank you for being pillars in my life and being the first to teach me about the importance of community.

I would like to thank my committee members, Dr. Amanda Cook, Dr. Ramesh Jasti, and Dr. Anne Zemper for your guidance, advice, and mentoring throughout graduate school. To my advisors, Mike and Darren, working under and with you has been

such a gift. I have learned to be a leader, a scholar, and a well-rounded professional scientist under your wings. I'm looking forward to making you proud throughout my career in industry. I would also like to thank the NIH (R01-GM087398) and the University of Oregon for funding.

Finally, I want to especially acknowledge the community that the DWJ lab has worked so hard to build and cultivate over many years–it is a rare gem in the field of science. Thank you, Darren and all my lab mates, past and present, for making our lab and office setting a truly welcoming, healthy, and positive workplace.

Para minha mãe e meu pai –

por todos os sacrifícios que vocês fizeram para que eu pudesse chegar até aqui; eu não seria quem eu sou hoje sem vocês na minha vida

TABLE OF CONTENTS

LIST OF FIGURES

LIST OF TABLES

Table Page

LIST OF SCHEMES

Scheme Page

CHAPTER I

INTRODUCTION

This chapter contains excerpts from a review that is *in preparation* to published and was written by Thaís P. de Faria and Hannah J. Bates with editorial assistance Douglas H. Banning, Dr. Trevor A. Shear, and Professors Michael M. Haley and Darren W. Johnson.

This article accounts the science and history behind anion binding, host-guest chemistry, and some of the first papers on the Johnson/Haley anion recognition works that foreshadow future work that will be highlighted herein. However, this is by no means a comprehensive review of the field; rather, a few pertinent examples have been selected for discussion to give a general overview of the state of the field.

Anions are prevalent in the human body and vital to life. They play a variety of different roles from producing electrical signals to maintaining cell volume.[1] While there are many anions present in living systems, chloride (Cl^-) and the protic forms of phosphate (i.e. HPO_4^{2-}, $H_2PO_4^-$) play a critical role in maintaining basic metabolic pathways within the human body.

Two types of phosphorous species (organic and inorganic) are prevalent in our body's biological processes. An example of organic phosphates are the nucleotide phosphates found in adenosine monophosphate, diphosphate, and triphosphate (AMP, ADP, and ATP, respectively), molecules known for supplying energy for most biological

reactions, participating in metabolism, and transferring genetic information.[2] Inorganic phosphates, on the other hand, play a part in bone formation and help maintain bone density.[3] They are normally seen in adult human serum at concentration levels of 0.8-1.45 mM;[4] however, when present in excess, inorganic phosphates can ultimately lead to cardiovascular disease due to vascular calcification and renal failure.[5] Deficient concentration of inorganic phosphate can lead to negative physical effects, like osteomalacia, central nervous system dysfunction, and muscle weakness, amongst many other disorders.[6]

Chloride anions are found within human cells in concentration levels between 5 and 15 mM[1] and are vital to cellular processes, including balancing the charges of transfer proteins and building membrane potential. The natural role and regulation of Cl^- is so critical that there are even chloride transport channels in intracellular organelles and the plasma membrane.[7,8] Mutations of these channels lead to disruption of chloride movement in and out of the cell and have been linked to many genetic diseases, such as cystic fibrosis and the degeneration of muscles.[9]

Because these anions play such important roles within the human body, there is significant interest for their detection and monitoring in physiologically-relevant media. Previous approaches to quantify the concentration of these anions has largely involved dialysis and sample dilution,[10,11] microelectrodes (for measurement within individual cells),[12,13] and imaging using yellow fluorescent proteins.[14,15] These detection methods all have major drawbacks, including difficulty in performing the measurements, pH sensitivity, and low selectivity. Because of these challenges, the use of supramolecular chemistry in this area of research has been of growing interest, as supramolecular host-

guest chemistry is well studied and often allows for the ability to fine-tune the electronic and steric properties of the hosts used.[16–19] Recently, attention has shifted to the use of these small molecule sensors that can reversibly bind and display either a colorimetric or fluorescent response upon anion binding and, finally, can be performed *in vivo*.[2,20–25]

Many research groups have been attempting to conquer the feat of designing and Developing a small molecule receptor that displays a selective preference for reversibly binding one targeted anion over others, that is sensitive enough to detect minute concentrations, and that exhibits some form of optoelectronic response to binding.[19,26,27] One example of a small molecule receptor that has shown reversible binding to dihydrogenphosphate ($H_2PO_4^-$) in dimethyl sulfoxide (DMSO) involves a scaffold with a hydrogen-bond donating (bis)thiourea motif (**Figure 1.1a**); however, the receptor has a modest limit of detection, requiring at least ~1 mM concentration of analyte for detection.[28] Another example of promising binding to $H_2PO_4^-$ in acetonitrile includes a redox-based sensor that contains a ferrocene unit in addition to hydrogen-bond (HB) donors (**Figure 1.1b**).[29] The HB units provide initial binding, but after oxidation of ferrocene, the host-guest interactions get further stabilized with the electrostatic interactions of the ferrocenium moieties.[30] In addition to binding strongly with the phosphate anion, it also binds well with fluoride, and, therefore, lacks selectivity. A more recent example of phosphate anion detection comes from Sessler et al., who synthesized

an indole-based receptor that showed promising colorimetric response upon binding (**Figure 1.1c**); however, this receptor lacks water solubility.[31]

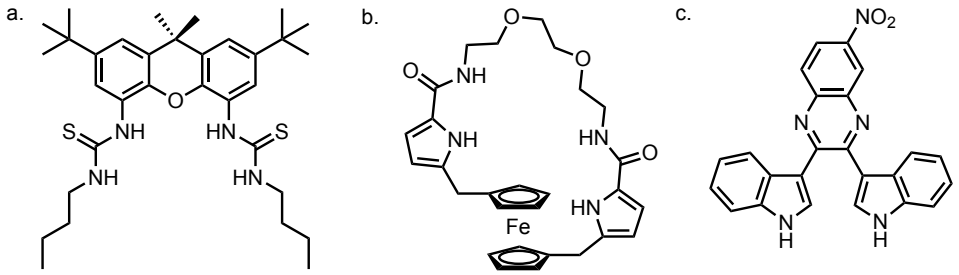

Figure 1.1. Examples from the literature of phosphate receptors containing a) bis-urea motifs, b) hydrogen-bond donors and ferrocene motifs, and c) indoles.

Some examples of successful receptors and sensors that are able to detect chloride through non-covalent interactions include: 1) nucleic acid-based hosts that can detect anions over a wide pH range, but they either lack anion specificity because of their ion-pairing recognition mechanism or lack functionality for targeting some cellular compartments;[32–35] 2) chloride-templated rotaxanes that use redox-active interlocked systems to act as electrochemical sensors for anions, although binding only occurred in minimally polar solvents and did not show fully reversible oxidation;[36] 3) foldamers that have the ability to selectively coil around chloride and bind it tightly (albeit, the energy of organization of the helix was only optimal in certain solvents);[37–42] and numerous others.[43–46]

The original, or Gen 1, host-guest receptors to emerge from the Johnson and Haley labs have shown to bind a range of anions through non-covalent, reversible interactions.[47–52] The tunable scaffold includes urea (HB) motifs (**Figure 1.2a**) as well as three functional groups (R, R', and R") that can be synthetically modified to optimize the optoelectronics, selectivity, and binding properties of the receptors. In addition, the

conjugated backbone of the arylethynyl scaffold has allowed for some receptors to show

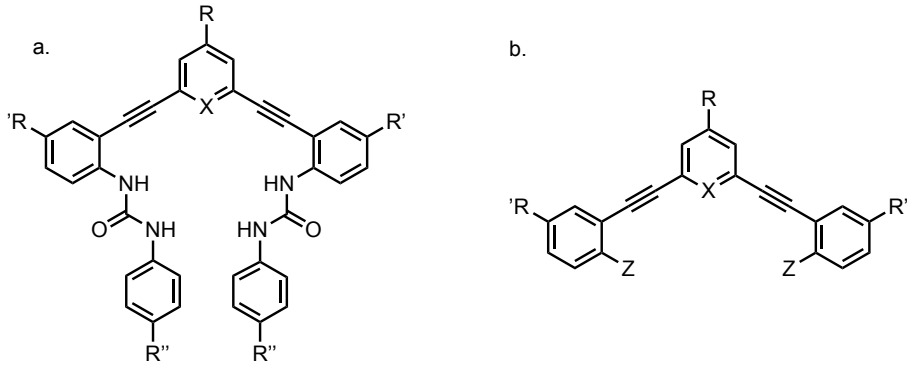

Figure 1.2. Receptor scaffolds for a) Gen 1, hydrogen-bonding where X=N, N^+–R, CH; R= H, Me, F, OMe; R'= H, ^{t}Bu, CF_3, SO_2Me, SO_2CF_3 ; R''= H, NO_2, CF_3, OMe and b) Gen 2, halogen bonding where X=N, CH; R= H, Me, sulfopropyl, R'= H, ^{t}Bu, CF_3, SO_2Me, SO_2CF_3; Z= H, I, Br. The central aromatic ring containing X is referred to as the core of the receptor, and the ligands attached to the core referred to as arm(s).

a fluorometric response upon binding.[47–49] Finally, all but one of the recent Johnson/Haley receptors have only demonstrated anion binding in organic media or wet organic solvents, which does not necessarily reflect a physiologically-relevant environment.

The most promising arylethynyl bis-urea scaffold to show chloride binding *in water* was synthesized and studied by Michelle Watt et al. in 2015.[21] The way that solubility was achieved in this case was by protonating the core pyridine nitrogen using 1% TFA in water. The most notable result in this paper was that a "turn-on" fluorescence was reported in water/DMSO mixtures and increased with a higher percentage of water added, peaking at about 80% water.[21] The observed fluorescence was attributed to a mechanism called "aggregation-induced emission" (AIE), that occurs through J-aggregation and is widely used in fluorophores to sense analytes.[53] Although titration studies demonstrated a strong selectivity for chloride, the receptor exhibited weak

binding ($K_a \leq 100\ M^{-1}$) in DMSO/H_2O mixtures and the fluorescence was not strong enough for *in vivo* cell studies. Alas, the search for a water-soluble arylethynyl receptor that can selectivly bind to chloride in aqueous media and displays strong fluorescent properties has continued in the Johnson/Haley lab.

Firstly, to accomplish the goal of using our supramolecular receptors in physiological environments we have to optimize the reversible interactions in polar, protic solvents, like water. Sensing anions in water is a difficult mission for chemists due to the inherently low charge density which is a consequence of the large anion size. This makes the non-covalent electrostatic interactions between anions and receptors less efficient. In addition to this, anions have high free energies of solvation in water;[54] consequently, the receptors must energetically compete with the medium.[55] According to Hunter et al., a promising strategy to achieve aqueous anion detection employs halogen bonding (XB) interactions, which exhibit stronger anion binding in polar, protic solvents than do HB interactions.[56]

Halogen bonding is a type of reversible non-covalent binding interaction that has been gaining interest in the scientific community since it was first reported.[57] The nature of this interaction was defined by IUPAC in 2013[58] as: R—X···Y, where X is a polarizable halogen covalently bound to an R group and Y is an electronically-dense halogen bond acceptor (**Figure 1.3**). This attractive interaction is facilitated by the halogen atom's ability to shift electron density with the help of the covalently bonded R group and, thus, reveal an area of positive electrostatic potential, named the σ-hole for its electron deficiency, directly opposite to the R–X σ-bond.[59] Since the σ-hole is located on the opposite side of halogen X to the R—X bond, the covalently attached "R" substituent

influences the size of the partially positive hole with its electron-withdrawing character. The more withdrawing the substituent, R, the larger the σ-hole and, therefore, the stronger the binding to the XB acceptor. Surrounding the σ-hole are areas of high electronegativity and this feature gives the σ-hole its strong directionality, demonstrating a strong preference for non-covalent bonding at a 180˚ angle from the XB acceptor.[60,61]

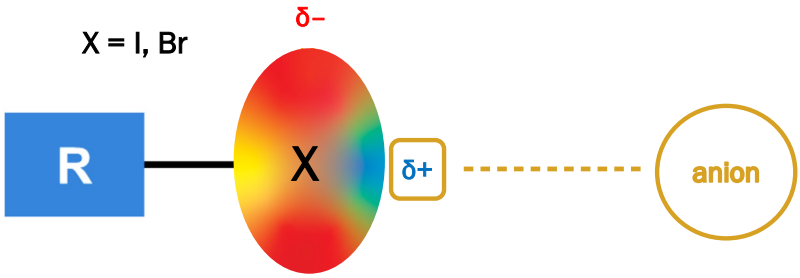

Figure 1.3. A pictogram that represents halogen bonding.

New anion receptors, or Gen 2 receptors (**Figure 1.2b**), were developed in the Johnson/Haley lab to utilize halogen bonding. In place of the bis-urea hydrogen binding motif found in Gen 1 receptors, iodine was installed as a halogen bond donor in the binding pocket. To enhance the XB interactions, strong electron-withdrawing functional groups at the R' positions can be used to increase the polarization of XB donors, and consequently, the strength of binding.

Dr. Jessica Lohrman synthesized and characterized the first XB Johnson/Haley receptor (**Figure 1.4a**).[62] It was shown to bind to the halide anion family, as well as produce a "turn-on" fluorescence response; however, the receptor was not sufficiently soluble in water for biological studies. Since the desired applications of this receptor require water solubility, modifications to achieve solvation in aqueous media must be made. On the basis of preliminary unpublished results with the original XB receptor exhibiting a high affinity to binding phosphate in organic solvents, we propose that by

making further changes to the XB scaffold, it would be possible to achieve the desired goal of maximizing water solubility (**Figure 1.4b**) with selective binding to phosphate. The results of these studies are discussed in Chapter II.

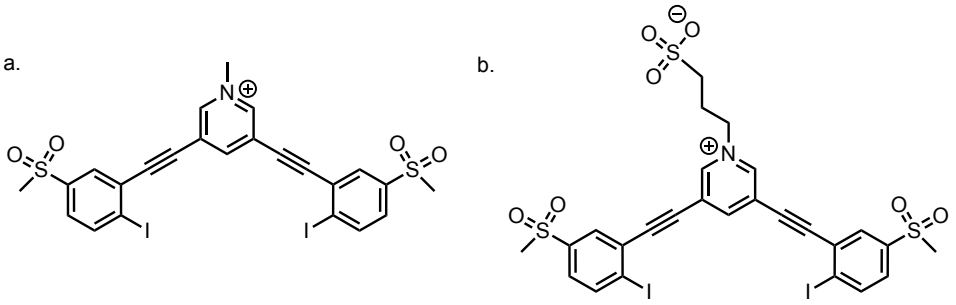

Figure 1.4. a) The first XB receptor which is not soluble in 100% water informing modifications for b) a water-soluble receptor.

We then set out to explore what is herein described as Gen 3 receptors (**Figure 1.5**) in Chapters III and IV. These receptors were, again, highly influenced by Dr. Lohrman's XB receptor.[62] With the target analyte chloride proving to be too small for the binding pocket available in the "two-arm" receptor, more simplified "one-armed" analogues were designed with: the purpose of simplifying/creating a smaller pocket for the receptors, converting their preference of binding chloride over iodide and studying their geometry of binding.

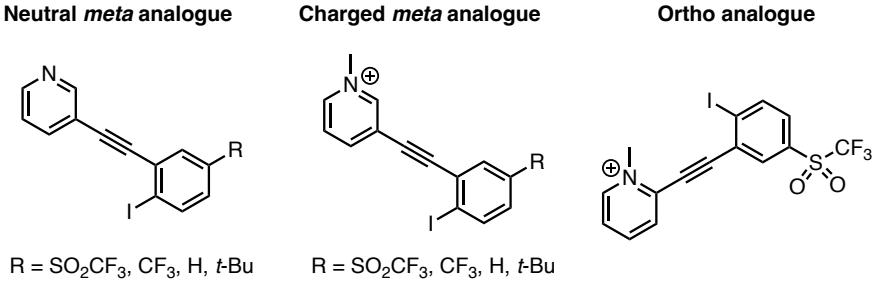

Figure 1.5. Receptors studied in Chapters III (*meta*) and IV (*ortho*).

In Chapter III, we investigate the *meta* isomer of the "one-armed" receptor (**Figure 1.5**) and discover that, in addition to halogen bonding, this receptor also utilizes hydrogen-bonding to non-covalently bind to the anionic guests. The smaller hybrid–part XB, part HB–pocket was able to reverse the preference of binding seen in Gen. 2 receptors, now binding the smaller halides better than the larger (i.e. the target analyte, chloride, exhibited strongest binding). This study also revealed that the strongest contributor to the XB donor's σ-hole is the methyl pyridinium ion located on the core aryl ring and that the tunable functional groups on the XB donor's aryl ring play little part in increasing strength of binding through thorough theoretical, solution- and solid-state experimental structure/property relationship studies.

Chapter IV continues the study of "one-armed" receptors by investigating the *ortho* isomer (**Figure 1.5**) where we reveal that the geometry and binding motifs are similar to that of the *meta* receptors studied in Chapter III; however, the hybrid pocket is even smaller, showing an even stronger preference of binding chloride over iodide. The results illustrated in this chapter also delve deeper into an unexpected synthetic side product that is the first ever reported vinylic XB donor, whose crystallographic data shows participation in non-covalent halogen bonding.

Considering the significance of anions and the roles they play in biological and environmental systems, the need for monitoring their concentrations in aqueous media is continuously growing. To this end, this thesis focuses on the use and optimization of tunable halogen bonding, water-soluble receptors that can selectively bind to analytes of interest.

CHAPTER II

BUILDING HALOGEN-BONDING RECEPTORS FOR PHOSPHATE ANION RECOGNITION IN AQUEOUS MEDIA

The contents of this chapter contain unpublished materials that was written by Thaís de Faria with editing assistance by Darren W. Johnson and Michael M. Haley and Dr. Jeremy P. Bard. All synthesis and characterization were performed by Thaís de Faria with advice and guidance by Darren W. Johnson, Michael M. Haley, and Dr. Jessica A. Lohrman.

2.1 Introduction

Anions are ubiquitous in nature, playing important roles in the body like sending neural signals and maintaining cell processes, in the agricultural field where they are key players in fertilizer, and a variety of disparate areas of interest.[1,2] Specifically, the phosphate anion is one of the three key components of fertilizer and plays a significant part in bone formation.[2] One crucial factor in an anion's ability to function properly is that it must be within a specific concentration threshold. For example, an excess of inorganic phosphate (above 1.45 mM)[3] in the blood serum could be an indication of kidney failure and could be caught early with monitoring.[4,5] Overfertilization is also a prevalent issue in the agricultural industry. Phosphorus in runoff from rural lands has

been identified as an influential factor in pollution as it aids in the process of eutrophication of water bodies like lakes and streams.[6] These are only a few of the many reasons why it is imperative to have the capability of detecting, monitoring, and measuring the presence of anions in aqueous media.

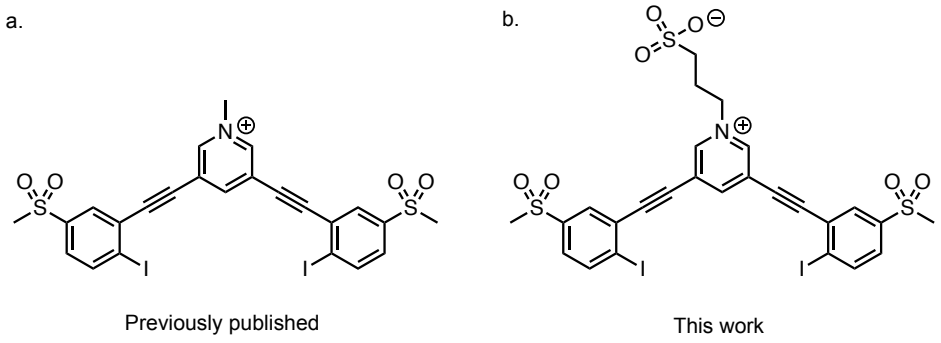

Figure 2.1. a) The first generation XB receptor which is not soluble in 100% water informing modifications for b) a water-soluble XB receptor.

The first halogen-bonding receptor to come out of the DWJ/Haley labs[7] (**Figure 2.1a**) shows strong preliminary binding to inorganic phosphate and borderline water solubility. In order to maximize aqueous solubility, the original XB pyridine receptor will be modified through the addition of a charged sulfopropyl group upon the central pyridine nitrogen (**Figure 2.1b**), a moiety that has been shown to increase the aqueous solubility of organic molecules such as polymers and proteins.[8] The modifications proposed for the promising phosphate receptor will keep the same motifs as the original (a pyridinium ion and the methylsulfone electron-withdrawing substituent), but will install an added charged functional group, creating a novel zwitterionic aryl-ethynyl scaffold. This character will promote solubility of the receptor in water. The fluorometric response upon binding of phosphate ions (with the novel receptor) will be tested in aqueous media.

2.2 Results and Discussion

Starting with commercially available 4-(methylthio)aniline, **1**, oxidation with $ZnCl_2$ and H_2O_2 in the presence of DBU was used to afford sulfone **2** (**Scheme 2.1**). Iodination followed by subsequent triazene formation gave iodotriazene **4**. Sonogashira cross-coupling with trimethylsilylacetylene (TMSA) was performed to generate TMS-protected acetylene **5**. Deprotection of the ethynyl group in **5** with base followed

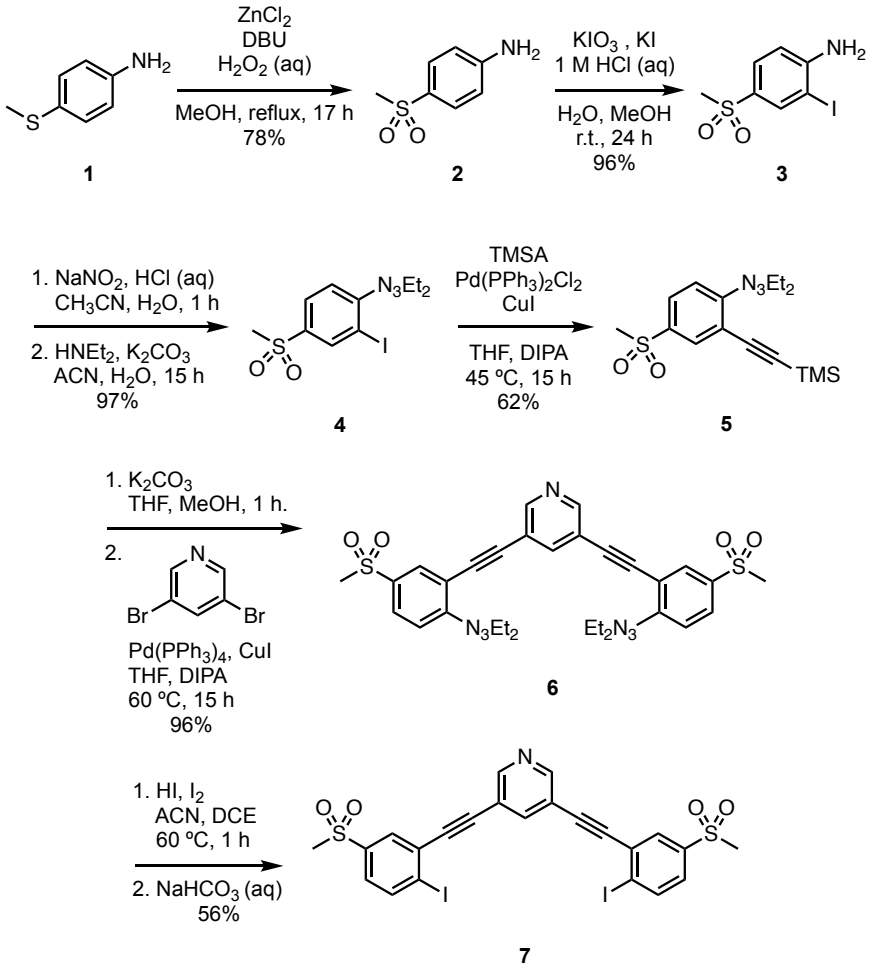

Scheme 2.1. Synthetic route to advanced halogen-bonding receptor intermediate and sulfonate coupling partner.

immediately with a Sonogashira cross-coupling with 3,5-dibromopyridine formed bis-triazene **6**. The final step to reach the key precursor is an iodine substitution reaction that replaces the triazene substituent with halogen bond donating iodine atoms in host **7**.

The last step in the synthetic route, sulfopropylation of the pyridine core, has never before been attempted on this scaffold; however, it has been shown to occur with a variety of aromatic nitrogen organic compounds, especially in the synthesis of water-soluble, zwitterionic polymers.[9] One reported method of attaching the sulfonate chain to pyridine-based molecules includes the addition of 1,3-propanesultone in toluene at 50 ºC.[10] A proof of concept reaction with this method was first performed on 3,5-dibromopyridine, proving to be successful through NMR spectroscopy which can be found in Appendix A (**Figure A.7**) as well as displaying promising solubility in water (**Scheme 2.2**).

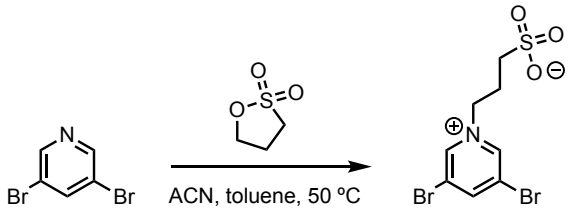

Scheme 2.2. Proof-of-concept reaction for the sulfopropylation of the pyridine core using the simpler di-bromopyridine derivative.

When this reaction was applied to the more complex coupling partner, **7**, it showed no signs of reactivity, instead affording only starting materials (**Scheme 2.3**). This is likely a result of the decrease in nucleophilicity of the lone pair of electrons on the pyridine core of the scaffold due to the highly electron-withdrawing SO_2CH_3 appendages. An expansive screening of conditions was attempted based off of the proof-of-concept reaction to attach the charged propyl sulfonate moiety onto the scaffold precursor, including: changing the solvent so we could run the reaction at higher reflux temperatures, and so we could explore the solubility of starting materials; running the reactions under inert conditions to see if water or air was impeding the reaction from proceeding forward; and notably, attempting a microwave reaction that showed promise in reacting electron-deficient aromatic nitrogens with 1,3-propanesultone.[8]

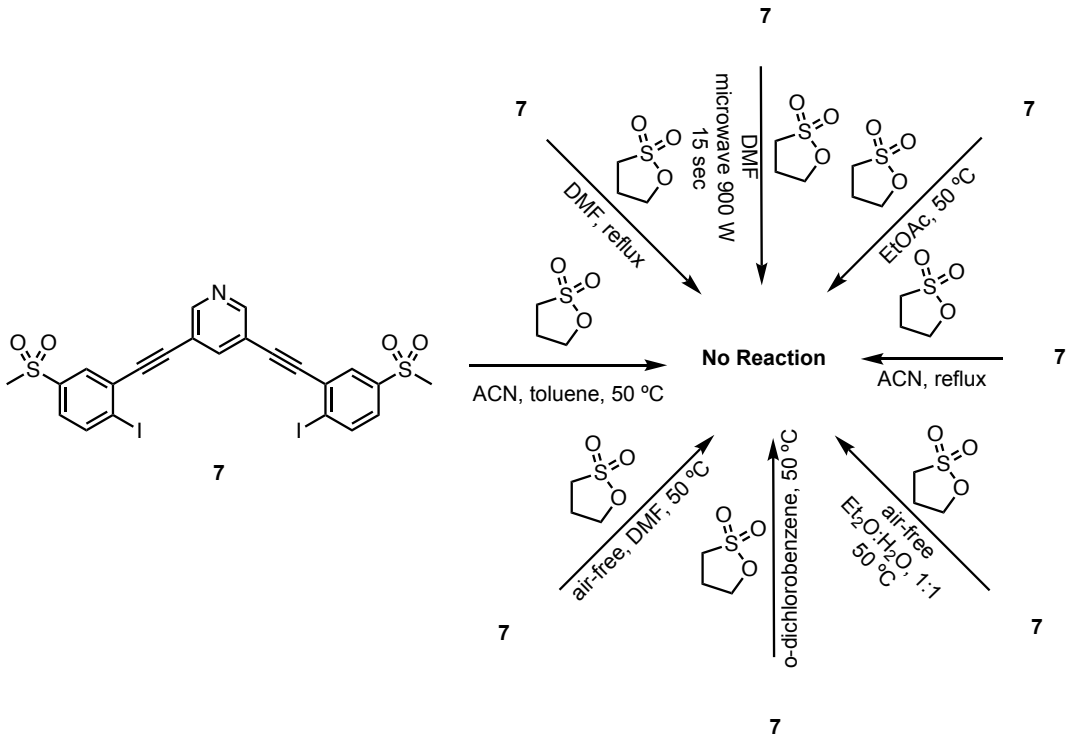

Scheme 2.3. Unsuccessful attempts at sulfopropylation of precursor, **7**. Unless otherwise noted, all reactions were run overnight.

Of these, the reaction conditions that showed the greatest potential of success (**Scheme 2.4**) occurred when DMF was heated with starting material, **7**, to 65 ºC *before* adding propanesultone. The reaction mixture was then allowed to reflux overnight. This set of conditions resulted in a precipitate crashing out of solution upon cooling the reaction flask.

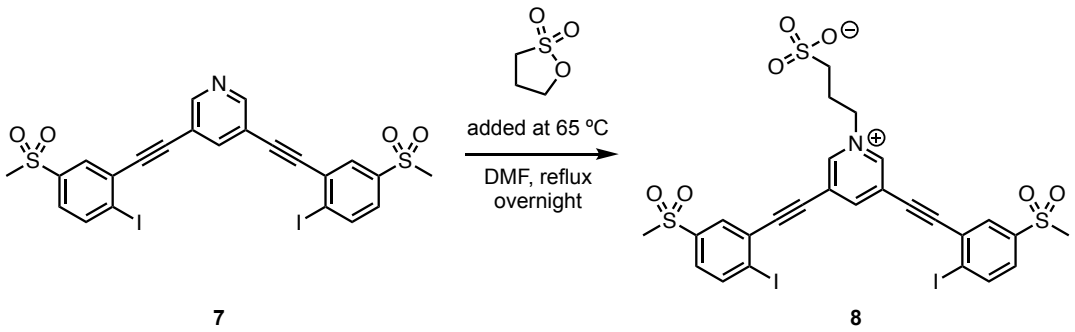

7 8

Scheme 2.4. Reaction scheme of the most promising conditions.

The resulting precipitate proved to be difficult to characterize. The "go-to" organic chemistry characterization technique, NMR spectroscopy, could not be used due to the insoluble nature of the precipitate. Solubility studies were performed in a variety of organic solvents (including, but not limited to, DMSO, dichloroethane, dioxane, hexanes, dichloromethane, ethyl acetate, acetone) and water (at low pH, high pH, brine).

The stubborness of the precipitate to go into solution was an undesired, albeit, anticipated property of the desired receptor.[11] Because the final product is a zwitterion, or a single molecule that contains both a discrete positive and a discrete negative charge within its structure, aggregation is expected. However, zwitterionic aggregates are typically solvated with the aid of salts that play a role in breaking up charges,[12] so we also attempted to dissolve the precipitate with aqueous (like NaCl) and organic (like TBACl) salts. Neither lead to success.

The lack of solubility led to the need to characterize the powder through the use of ATR-FTIR (**Figure 2.2a**). The IR data showed the growth of promising peaks between 1200-1100 cm^{-1} in the spectrum of the precipitate (green trace) when compared to that of the starting material (red trace). The peaks in this range have been associated with similar (poly)zwitterions in literature[11] (**Figure 2.2b)**. With this preliminary support of the formation of product, further studies will need to be performed to confirm the structure as well as explore possible binding capabilities.

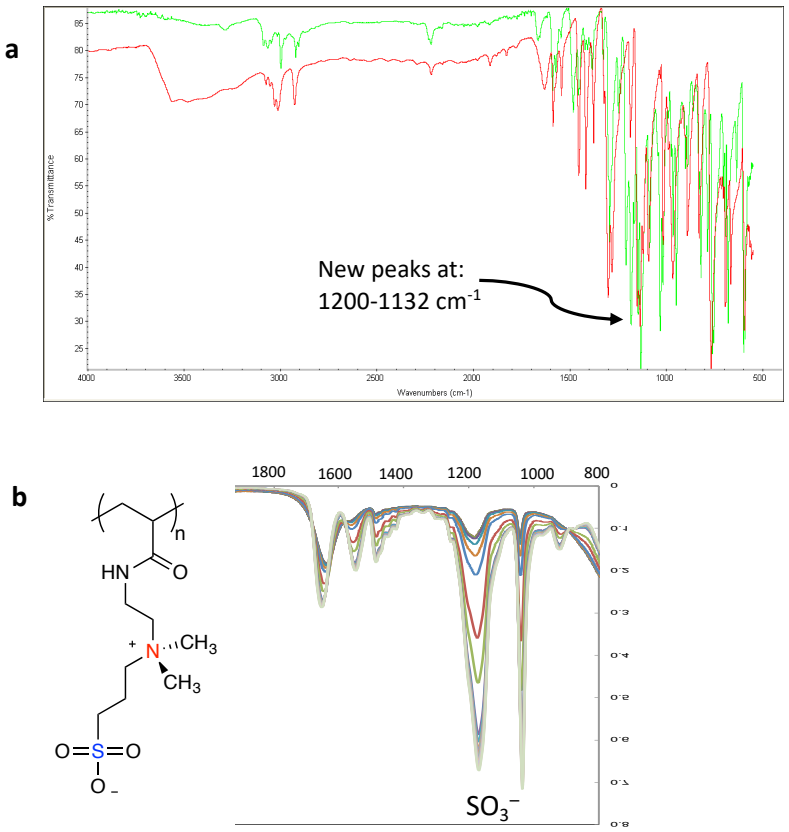

Figure 2.2. a) ATR-FTIR of the starting material shown in red and the potential product shown in green; b) Literature ATR-FTIR of a polyzwitterion with a propanesulfonate functional group. The sulfonate group was labelled to be in the 1200 cm^{-1} range. Data obtained from ref 11.

2.3 Future Directions

Specific ion effects (SIE)–the intrinsic effect of an ion's identity to properties on a system–have been studied for many years, but first started with Lewith and Hofmeister.[12,13] Hofmeister divvied up the anions into two categories: kosmotropes that precipitate (or "salt-out") proteins and chaotropes that help to dissolve (or "salt-in") proteins.[13]

Anions: $C_4H_4O_6^{2-} > SO_4^{2-} > HPO_4^{2-} > C_3H_5O(CO_2)_3^{3-} > CH_3CO_2^- > HCO_3^- > CrO_4^{2-} > Cl^- > NO_3^- > ClO_3^-$

Cations: $Li^+ > K^+ \approx Na^+ > NH_4^+ > Mg^{2+}$

" >" implies that the ion has a greater ability to "salt-out" proteins.

In order to continue this project, the first consideration is to perform a more complete and extensive solubility study with the complete Hofmeister series of salts since it has been used to probe changes in the physical properties of zwitterionic polymers, from lubrication of their surfaces[14] to their behaviors in solution.[11] If this successfully dissolves the zwitterionic receptor, characterization of the complete, novel XB receptor with appended sulfopropyl solubilizing group would be necessary to further confirm the success of the final reaction. Then, a suite of anion binding studies – via UV/VIS titrations – should be performed on the receptor to look for specific anion sensitivity and to calculate binding constants, as well as look for and measure any fluorescent or colorimetric responses upon binding.

The ultimate goal for the sensor is to achieve the aqueous solubility needed for it to be applicable for measuring anion concentrations within biological media, including

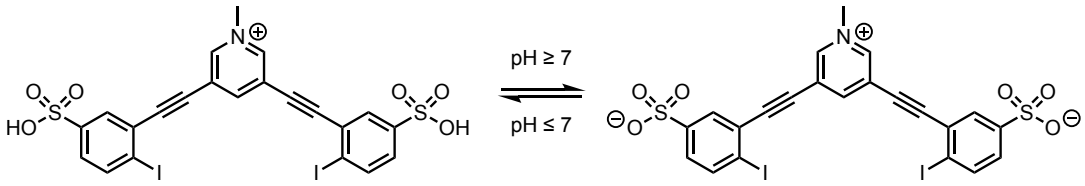

Figure 2.3. Scaffold with sulfonic acids as an alternative plan to solubilize XB receptor.

human serum and living cells.[15] If the receptor is either not water soluble enough for analysis in aqueous solutions or is unable to be synthesized, different steps towards achieving water solubility must be taken. This includes a new scaffold that maintains the methyl pyridinium core but modifies the methylsulfone R' position to sulfonic acid functional groups, which are commonly used to promote water solubility in fluorescent probes (**Figure 2.3**).[16]

If water solubility is achieved as is, preliminary studies on the receptor will need to be taken to see if it is able to be applied in cell studies – this includes its ability to be uptaken by cells. If it is not seen with the current desired scaffold, novel designs must be taken to incorporate functional groups that permit permeation into cell membranes.[17]

CHAPTER III

SUBSTITUENT EFFECTS IN A SERIES OF COMPACT ARYLETHNYL "MONODENTATE" HALOGEN BONDING HOSTS FOR ANIONS

This chapter includes material from a co-authored manuscript in preparation by Thaís P. de Faria, Hannah J. Bates, A. Scout Trom, Faith I. D. Longnight, Michael P. Miller, Lev N. Zakharov, Michael M. Haley, and Darren W. Johnson. The experimental work was done by me or A. S. Trom, F. I. D. Longnight under my direction; computational analysis by M. P. Miller under my direction; mass spectrometry characterization by H. J. Bates; crystal characterization by L. N. Zakharov; writing by me and H. J. Bates with editorial assistance by all co-authors.

3.1 Introduction

Anions are ubiquitous in nature—they play especially critical roles within our cells as well as in our external environment. Some of the most fundamental anions, the halides (I^-, Br^-, Cl^-, F^-), are crucial to human health and well-being. Examples include the misregulation of chloride in cells associated with disease states like cystic fibrosis[1] and iodine deficiency causing thyroid disease and goiter formation.[2] Despite their significance, non-covalent binding of these anions still proves to be difficult for several reasons, but most notably because the entire halide family shares the same spherical shape, similar basicities for the three heaviest halides, and only slightly increasing sizes,

leaving little margin for error when designing a suitable selective binding pocket. Additionally, anions are well-solvated, particularly by the polar, protic media that make up many of the more interesting applications of these systems, *in vivo* sensing, for example.[3–5] In fact, the Hofmeister series illustrates how, especially as halides get smaller, the energy required to free a halide anion from water becomes increasingly costly in energetic terms.[6,7] In spite of these challenges, there have been many supramolecular systems that successfully bind anions, like chloride, in competitive polar protic solvents.[8–12] Many of these hydrogen bonding hosts feature multi-dentate coordination that seems necessary for these hosts to compete in aqueous media. Further preorganization through macrocyclization often further enhances binding, although can be synthetically challenging and may make cellular uptake and compatibility less likely, per Lipinski's Rules, for *in vivo* cell studies.[13,14]

Recent work in the field of host-guest chemistry has expanded the supramolecular toolset beyond that of traditional hydrogen-bonding (HB) to now also include σ-hole interactions, like those seen in halogen-,[15] chalcogen-,[16] and pnictogen-bonding.[17,18] Previous studies by other groups have shown that halogen-bonding (XB), while often comparable in strength to hydrogen-bonding, tends to be favored in polar protic solvents.[9,19,20] For this reason, our group, among many others, has recently begun investigating halogen bonding as a tool for binding halides and other anions.[21–24] The work we present here was largely influenced by our previously studied bis-aryl-ethynyl or "two-armed" receptors (**Figure 3.1a**), whose pocket size seemed to be too large to accommodate our target anion, chloride.[22]

A crystallographic study showed the "two-arm" receptor changing configurations and binding chloride out of the intended pocket, unlike larger anions like iodide which fit well. The new studies reported herein focus in on a compact "one-armed" structure (**Figure 3.1b and 3.1c**) that (1) eliminates the pre-determined pocket in hopes to shift binding preference to chloride over iodide and (2) enables the study of small, discreet changes on binding geometry.[25,26]

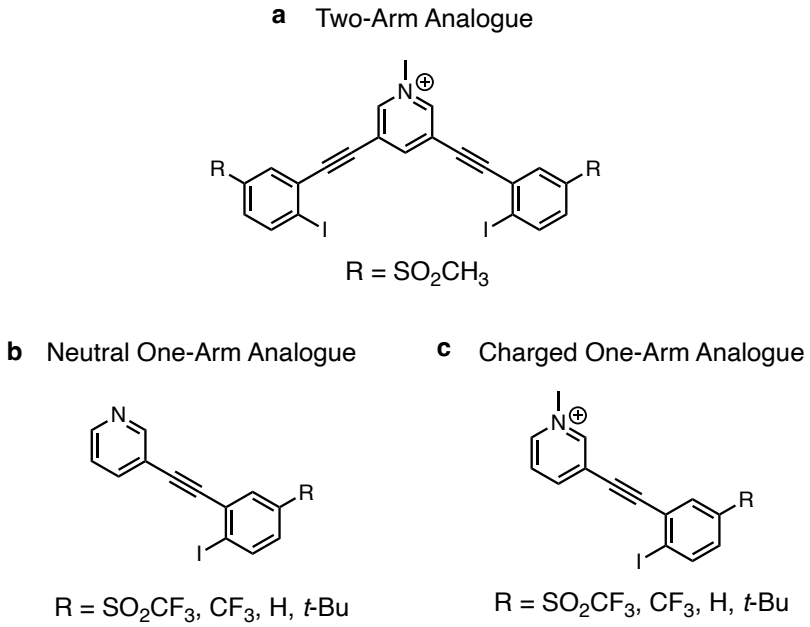

Figure 3.1. Previously studied bis-arylethynyl XB receptor, **a**. Novel "one-armed" neutral, **b**, and charged, **c**, arylethynyl receptors.

This paper will also describe the modification of the R substituents and how various electron-withdrawing and -donating groups affect the binding affinity in neutral *vs* charged receptors in this family. These results will allow for a number of observations to be made about the fundamental nature of the halogen bond—something often reductively characterized as an attractive R–X -- :A interaction (where R is a sufficiently electron withdrawing atom, X is a halide and A is an anion or other Lewis base)—through a structure-property relationship study.[27]

3.2 Results and Discussion

Electrostatic potential surface (ESP) maps were generated for all potential neutral, **4a-d**, and charged, **5a-d**, host receptors (**Figure 3.2**) to see which synthetic alteration would have the greatest effect on the XB donor's ability to noncovalently bind guests: the positively charged *N*-methylpyridinium core, or the tunable R groups attached to the "arm" of the receptors. The results of the maps corroborate trends our group has seen in previous computational studies.[22] When looking at the area of partial positivity—quantified and described as $V_{s,max}$—created from the σ-hole of the XB donor, it shows a decrease in magnitude of about 11 kcal/mol as the R-groups *para* to the iodo XB donor

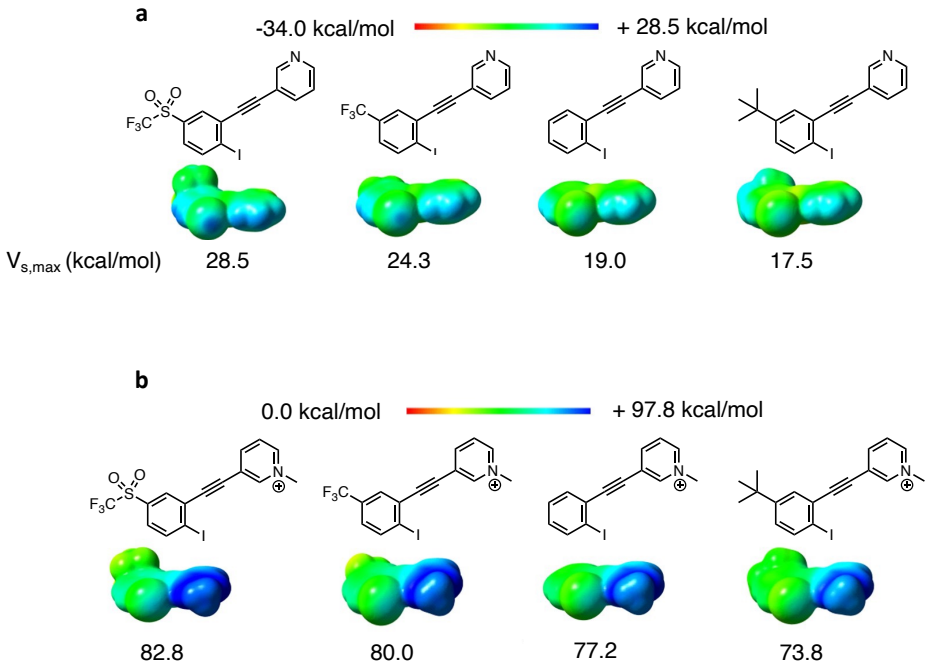

Figure 3.2. ESP maps of the entire family of receptors with the σ-hole values underneath each structure. Neutral structures are in panel **a**, and methylated structures in panel **b**. This figure clearly illustrates the outsized effect the methylated pyridinium unit plays in polarizing our halogen bond donor (compared to the changing ID of the FG para to it).

become more electron-donating in the neutral pyridyl receptors **4a-d**. In the pyridine-N-Me cationic receptors **5a-d**, the change is similar with a 9 kcal/mol decrease across the series of electron withdrawing/donating R-groups. However, when comparing the neutral receptors with similar σ_p values as their charged analogues, the $V_{s,max}$ values significantly increase with a ~54-58 kcal/mol difference providing evidence that what contributes more in the XB σ-hole enhancement of these arylethynyl scaffolds is the presence of the cationic *N*-methylpyridinium core, despite its distance from the XB donor.

To further verify this theoretical trend, all the scaffolds were synthesized for later solution-state binding studies, according to the modular synthetic path shown in **Scheme 3.1**. The starting aniline with the desired R-group was iodinated using KI and KIO_3 to furnish **1a-d**. Diazotization of the aniline group followed by trapping with Et_2NH

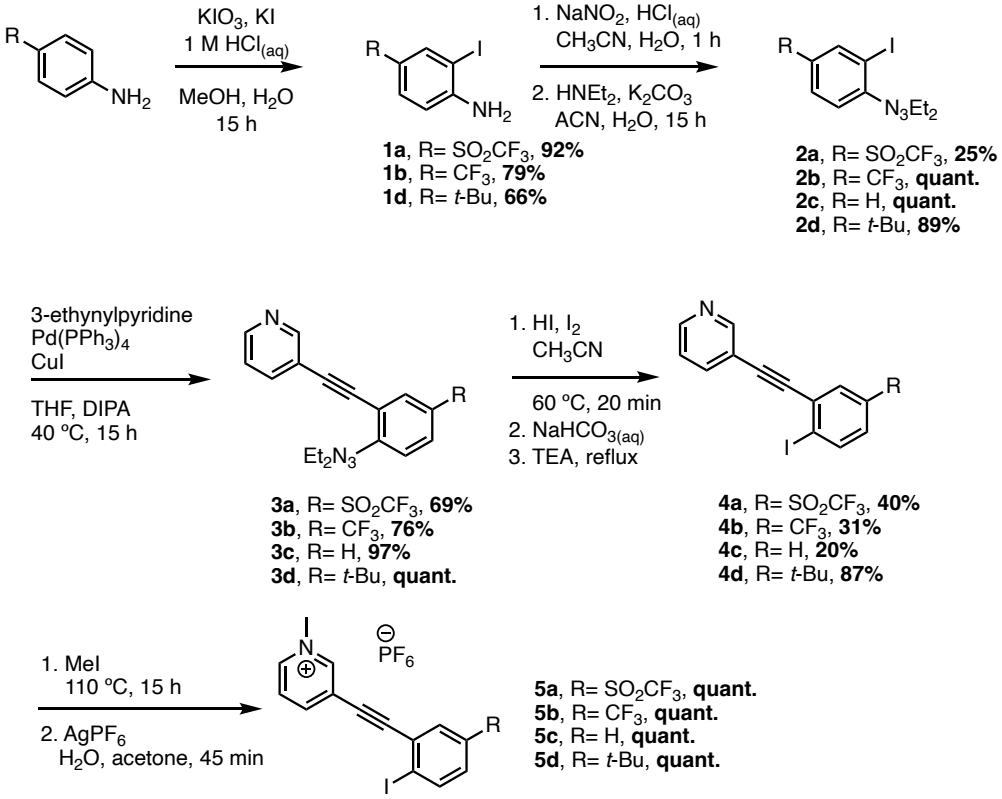

Scheme 3.1. Synthetic pathway and yields for the formation of the neutral, **4a-d**, and charged, **5a-d**, receptors.

afforded triazenes **2a-d**. Next, Sonogashira cross-coupling with 3-ethynylpyridine gave compounds **3a-d**. The triazene group was then transformed into an iodine, the XB donor chosen for each of our scaffolds, by heating with HI/I_2 to produce neutral hosts **4a-d**. The neutral receptors were transformed into the charged receptors through alkylation using MeI with I^- as the counter ion, **5a-d • I**$^-$. To enhance the apparent association constants for these charged receptors, the iodide counterion was then exchanged for the less competitive PF_6^- (**5a-d • PF$_6^-$**).

The solution-state binding trend seen between our group's previously studied two-arm analogue and the series of halides showed that the preferred binding pocket fit best with the largest anion, iodide;[22] bromide demonstrated the second-strongest affinity and chloride last. To test the hypothesis that the two-arm pocket was too large to preferentially bind chloride over larger anions, ^{1}H NMR titrations were performed with 1 mM solutions of single arm host receptor, **5a • PF$_6^-$**, and 20-30 mM guest solutions of the tetrabutylammonium salts of chloride, bromide, and iodide in CD_3CN. Association constants (K_a) were determined by tracking proton peaks and fitting the change in chemical shift to a 1:1 binding model using the Bindfit software.[28,29] Receptor **5a • PF$_6^-$** bound to Cl^-, Br^-, and I^- with K_a values of 137, 104, and 103 M^{-1}, respectively, demonstrating a modest yet inverse trend seen from our previous two-arm host analogue. This provides evidence that by changing the size of the pocket and reducing the entropic penalty associated with the previous host's pre-organization, it is possible to shift the preference of anionic guest to slightly favor chloride despite the fact that iodide typically features stronger halogen bonding interactions in polar solvents, presumably due to lower solvation energies.[30] The proton peaks that exhibited the largest change in chemical

environment helped to elucidate the solution-state binding geometry of the receptors, which matched that of the calculated lowest energy state of the charged receptor (**Figure 3.2**) with the iodine XB donor facing the methylated pyridinium core.

In all cases, the two hydrogens active in binding the halide guests are the pyridyl C–H in between the alkyne and the N atom, and one of the C–Hs of the pyridinium methyl group (**Figure B.1**). A similar geometry was observed in the solid-state crystal data of our analogous bidentate XB host receptor that showed binding with the XB donor twisted out of the too-large pocket and HB participation by the polarized C–Hs on the core and the methyl of the pyridinium. Neutral receptors **4a-d** did not show measurable binding to chloride in acetonitrile, demonstrating that XB donors with σ-holes with $V_{s,max}$ of ~17-29 kcal/mol may not be significantly electron-withdrawn to participate in halogen binding. Charged receptors **5a-d•PF_6^-**, and most notably those with lower σ_p values, were still able to bind to chloride in a trend that follows well with their calculated $V_{s,max}$ values (**Table 3.1**).

Table 3.1. Binding constants, in M–1, of charged receptors 5a-d with guest chloride and their calculated *σ*-hole values in kJ/mol.

	5a • PF_6^-	**5b • PF_6^-**	**5c • PF_6^-**	**5d • PF_6^-**
K_a with Cl^- (M^{-1})	137 ± 5	120 ± 6	98 ± 4	85 ± 2
$V_{s,max}$ (kJ/mol)	82.8	80.0	77.2	73.8

With the binding constants determined, we sought out to better comprehend the receptors' binding sensitivity to chloride through the use of the Hammett relationship ($\log(K_a^R/K_a^H)$ vs σ_p) by fitting the K_as to **Equation 3.1**.

$$\log \frac{K_a^R}{K_a^H} = \rho\sigma_p + \varepsilon \qquad (3.1)$$

Plotting these values against the σ_p of the R substituents revealed that there is a weak linear response between the K_a and the electron-donating/-withdrawing nature of the substituent (**Figure 3.3**). The equation inset in **Figure 3.3** describes the parameters of the linear fit, resolved through linear regression. The slope of the line's positive magnitude tells us that chloride binding is favored with more electron-withdrawing *para* R substituents. The value of ρ, 0.173, reveals that the halogen bond in this system is less sensitive to substituent effects compared to the standard, benzoic acid; therefore, the σ_p of the tunable R group is a statistically insignificant predictor of binding sensitivity in the one-armed arylethynyl receptor, further corroborating the hypothesis that the methylpyridinium dominates this family of receptors' binding affinity compared to the *para* R–X's σ_p values. This result is contrary to what we found for CH H-bond donors in related neutral bis-arylethynyl urea scaffolds. The CH hydrogen-bonding motifs in those systems were more susceptible to *para* substituent effects than that of our novel XB

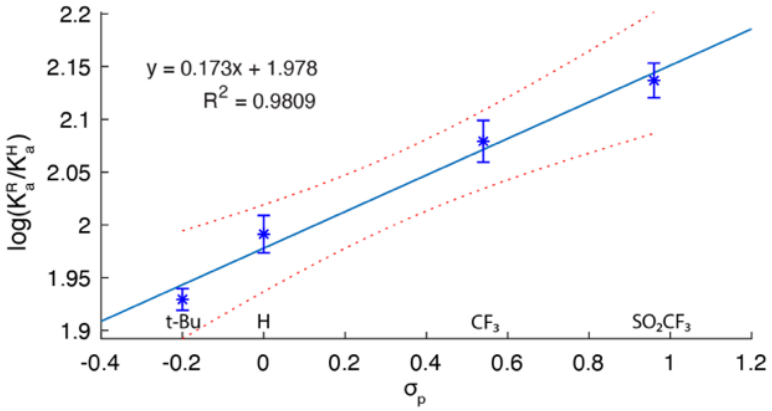

Figure 3.3. Hammett plot between **5a-d** and I^-. The slope of the line indicated that substituents in this receptor has little role in affecting the sensitivity of the halogen-bond donor. The dotted lines represent the 95% confidence interval.

receptor with a ρ value of 0.71.[31] It remains to be determined if substituent effects in charged CH receptors would be mitigated by the overall charge of the host, a topic we will address in the future.

After getting a handle on the one-armed XB receptors' binding geometries and properties in solution-state, we set out to study solid-state binding geometries. Crystals suitable for x-ray diffraction were grown of **5a,d•I⁻** (**Figures 3.4b and 3.4d**) from a 2:1 mixture of CH_2Cl_2:acetone via slow evaporation. These structures

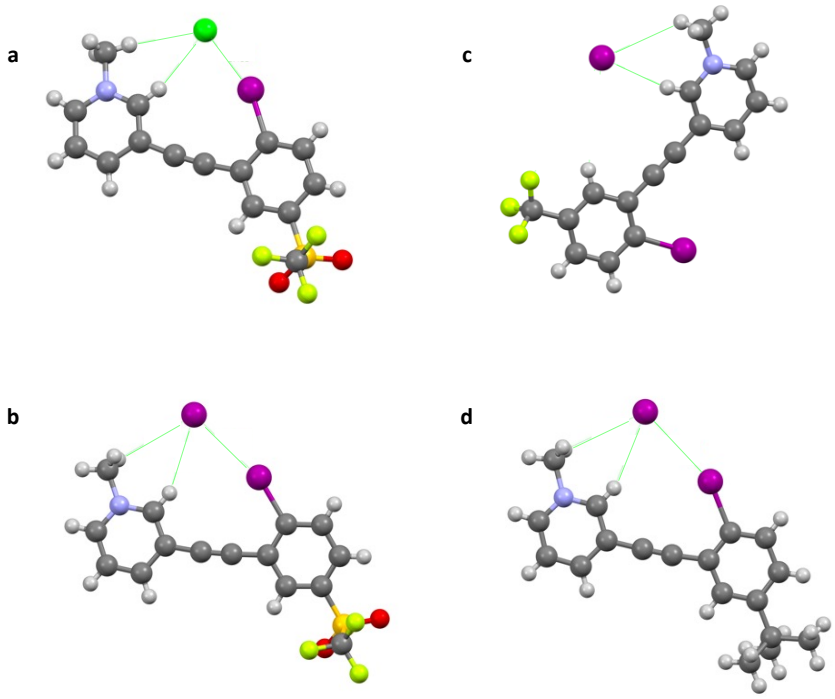

Figure 3.4. Crystals structures of: (**a**) **5a** binding to chloride; (**b**) **5a** binding to iodide; (**c**) **5b** binding to iodide; and (**d**) **5d** binding to iodide.

revealed that the solid-state geometry of binding is similar to what we see in solution-state. Atomic distances calculated in the crystal structures were less than the sum of the van der Waals radii of the guest and the iodine XB donor, the aryl H, and the methyl H. These results indicate supramolecular binding occurs with

not only our intentional XB donor, but also with the polarized CHs as H-bond donors.

Table 3.2. XB or HB distances, in Å, of receptors **5a**, **5b**, and **5d** binding to chloride or iodide as calculated from their crystal structures in **Figure 3.4**.

	5a • Cl^-	**5a • I^-**	**5b • I^-**	**5d • I^-**
$C–H_{aryl}$ -- X^- distance (Å)	2.904	3.173	2.928	3.187
$C–H_{me}$ -- X^- distance (Å)	2.833	3.522	3.626	3.558
C–I -- X^- distance (Å)	3.403	3.705	N/A	3.824

When comparing the binding distances in **5a** and **5d**, both binding I^-, in the solid-state (**Table 3.2**), there is little difference in either of the C–H--I^- distances of the HB donors – about 0.01-0.03 Å. The distance between the XB donor and iodide, C–I--X^-, however, shows an order of magnitude greater difference with 0.12 Å. Receptor **5a**, with the most electron-withdrawing substituent, showed a closer distance of guest to XB donor than **5d**, the receptor with the most electron-donating substituent, suggesting that even in solid-state binding, there is a slight preference for substituents with electron-withdrawing characteristics.

Crystals of **5a•Cl^-** were grown from a 1:2 acetone:CH_3CN mixture via evaporation. When comparing the SO_2CF_3 receptor, **5a**, binding to the largest guest, I^-, and smallest guest, Cl^-, an even larger shift is observed. The aryl C–H--I^- distance changes by 0.27 Å, the methyl C–H--I^- by 0.69 Å, and the C–H--X^- by 0.30 Å with the guest halide becoming more tightly bound to the receptor with decreasing size of the anion. This trend is also shown subtly in the solution-state binding studies with a stronger K_a observed for chloride over iodide by 27 M^{-1}.

Finally, crystals of **5b•I^-** (**Figure 3.4c**) were grown from a mixture of 1:1:1 CH_2Cl_2:acetone:CH_3CN. The crystals in this sample showed solid state binding of

iodide with only the HB donors, C–H(aryl and methyl)--I^-, which appeared to hold no trend with the previous bonding distances. The aryl C–H to iodide distance is 2.93 Å, the second shortest aryl C–H to iodide distance of the four crystal structures; however, the methyl C–H to iodide distance is 3.63 Å, the largest methyl C–H to iodide distance. Notably, this structure is showing a binding geometry with the XB donor facing away from the iodide guest and not participating in binding at all. This result begs further investigation to help understand the significance of solvent effects in supramolecular binding through crystal packing of host-guest molecules.

3.3 Conclusion

In conclusion, the data reported for this compact series of receptors suggest that when designing XB receptors with an arylethynyl foundation, a charged pyridinium core will provide a greater enhancement to the size and strength of the σ-hole than any adjacent functional groups. This knowledge allows for the purpose of the R group to shift away from that of only a XB enhancer to, instead, a number of other purposes including being a modular handle for other desired applications, such as polymerization, increased water-solubility, various cell compartment targeting functional groups, fluorophores, etc. without disrupting the most important portion of the anion recognition (the charge-polarized XB donor). Additionally, recognizing that the R-group does not contribute significantly to the polarization of the XB donor in these charged hosts allows for future host-guest chemists to dodge the synthetic pitfalls that come with appending extremely electron withdrawing functional groups, like SO_2CF_3. These design principles, in addition

to the binding demonstrated by the halogen/hydrogen bonding receptor in a polar solvent, will inform future host receptors for the halide anions.

CHAPTER IV

ORTHO 1-ARM HALOGEN-BONDING ARYLETHYNYL SCAFFOLDS

This chapter contains unpublished work that was done by Thaís P. de Faria and Mark Butters-Blakely under Thaís's direction and written by Thaís P. de Faria, with editorial assistance by Jacob T. Mayhugh, and Professors Michael M. Haley and Darren W. Johnson. This chapter also contains an excerpt from a review *in preparation* to be published with Thaís P. de Faria, Hannah J. Bates, Michael M. Haley, and Darren W. Johnson as co-authors. (Same review as Chapter I.)

4.1 Introduction

Chloride is a small anion of the spherical halide family, and it plays several critical roles in cellular processes.[1] Its concentration levels within human cells (between 5-15 mM)[1] are mitigated through chloride transport channels.[1–3] Diseases, like cystic fibrosis (CF), are caused by genetic mutations that prevent smooth movement through these transport channels and, thus, trap chloride inside of cells leading to mucous-lined lungs.[4,5] The most exhaustive form of clinically testing chloride concentrations and diagnosing cystic fibrosis is through sweat testing (ST).[6] In a "gold standard" sweat test performed using the Gibson and Cooke technique, a patient has electrodes placed on their arms or legs and is administered electrical stimulation to collect their sweat over 30

minutes.[7] Although this method of examination has been useful, there are many limitations including: 1) insufficient sweat collection in infants; 2) late onset CF shows slow progression of lung disease and is, therefore, harder to identify through ST; and 3) the accuracy of the ST depends highly on the technicians and laboratories that perform them, so countries that have low socioeconomic status also suffer from concomitantly poor diagnoses.[6,8,9]

Scientists in the field of supramolecular chemistry have started to tackle this problem by synthesizing host-guest molecules designed to selectively target and bind chloride using reversible interactions.[10–12] A recent receptor by Lohrman et al., using halogen-bonding (XB) as the binding motif (**Figure 4.1**), demonstrated strong non-covalent interactions with the anions in the halide family.[13] The results from that paper showed a preference for the bulkier iodide guest over chloride, influencing our study towards shrinking the arylethynyl scaffold's binding pocket with a "one-arm" analogue.

The monodentate *meta* (XB) receptor (**Figure 4.1**), analyzed in Chapter III, was able to reduce the size of the binding pocket and, therefore, invert the preference of binding from iodide to chloride, but not by a large threshold (103 and 137 M^{-1}, respectively). This study will continue this investigation by considering the XB receptor's *ortho* isomer, which will possess an even smaller binding pocket (**Figure 4.1**). Chapter III also elucidated that the main contributor to σ-hole generation, and therefore binding strength, of the iodo XB donor was the methyl pyridinium cation. This work allows us to explore whether the effect of the pyridinium cation has a larger influence *via* resonance in the novel *ortho* receptor or *via* induction in the *meta* receptor; moreover, this study will allow us to elucidate chloride's affinity to each binding pocket, guiding future chloride

receptor design principles. Amidst these studies, an unforeseen reaction side product led to a serendipitous discovery of the, to our knowledge, first reported vinylic XB donor participating in halogen bonding with chloride.

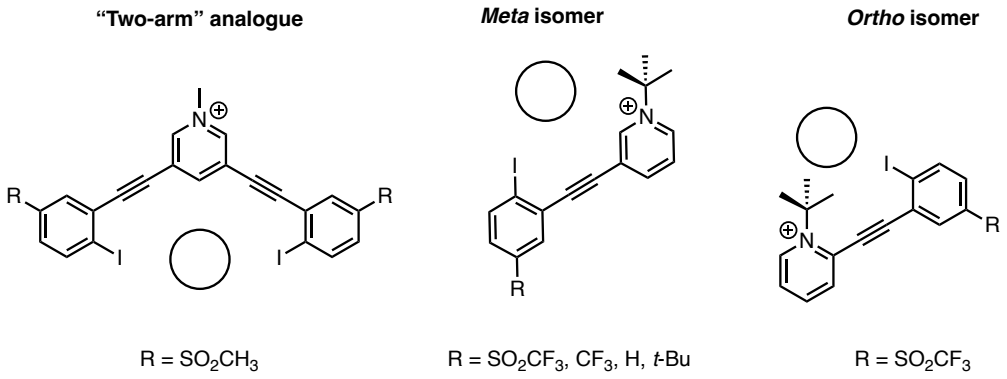

Figure 4.1. Previously published "two-arm" analogue and its preferred bidentate binding pocket; Chapter III's monodentate *meta* isomer and its smaller binding pocket; this work's monodentate *ortho* isomer featuring the smallest binding pocket.

4.2 Results and Discussion

To synthesize the *ortho* isomer of the XB receptor, the aniline starting material, **1**, was first protected with acetic anhydride so that the trifluoromethylthio functional group could undergo harsh oxidation conditions with mCPBA to afford the desired sulfone, **3** (**Scheme 4.1**). Here, the aryl amide was deprotected to afford **4** under basic conditions. Iodination followed by triazene formation resulted in Sonogashira cross-coupling partner, **6**, that was reacted with 2-ethynylpyridine to give advanced intermediate, **7**. The halogen bond donor, **9**, was then installed by transforming the triazene to an iodine. Finally, the neutral receptor was methylated with MeI and the counterion exchanged from iodide, I^-,

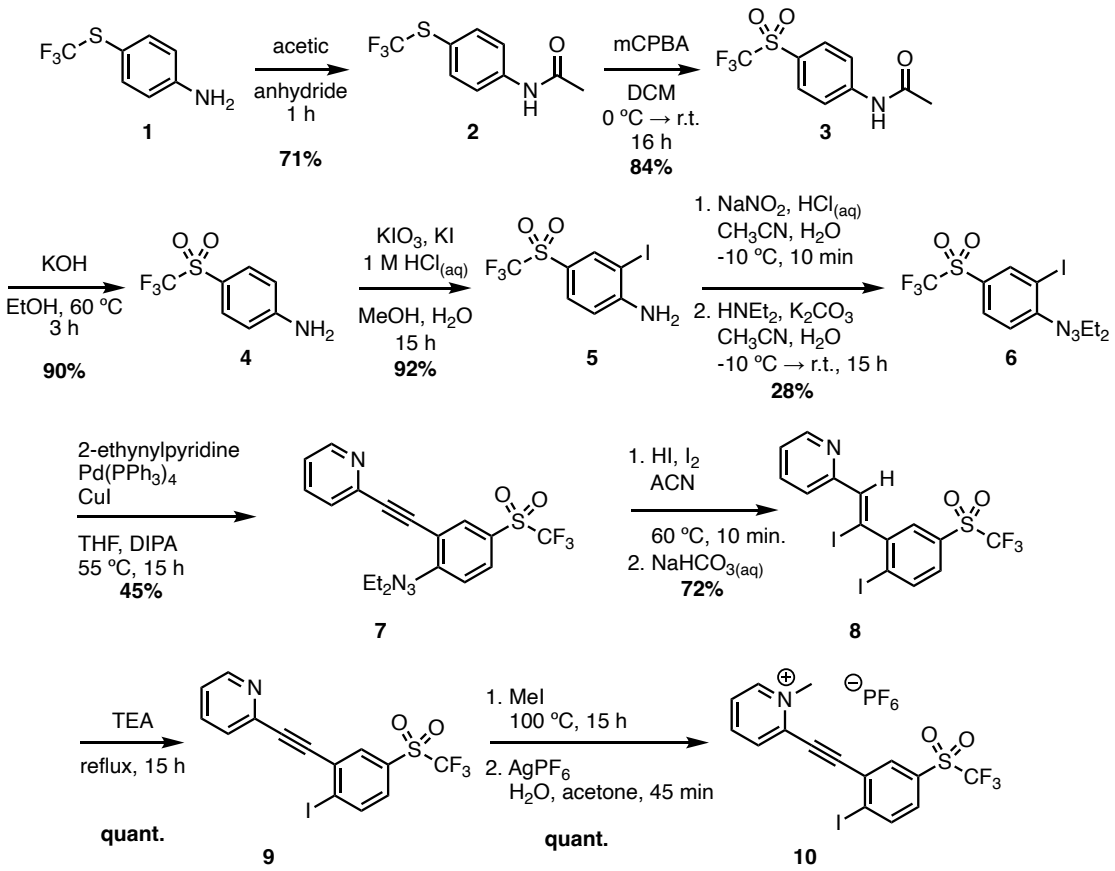

Scheme 4.1. Synthetic pathway to get to the final *ortho* isomer receptor, **10**.

to the non-coordinating PF_6^- to yield the final *ortho* receptor, **10** as its hexafluorophosphate salt.

The multi-step synthesis proved to be challenging, changing the reactivity of many well-known, literature-precedented reactions, due to the withdrawing nature of the trifluoromethylsulfone functional group. Notably, the reaction that transforms the triazene, **7**, into the XB donor iodine, **9**,[14] resulted in an unexpected major product that displayed one extra hydrogen in its ^{1}H NMR spectrum. After further characterization with ^{13}C NMR and ES-ToF Mass Spectrometry, it was revealed that HI added along the backbone of the electron-deficient alkyne; however, the regioselectivity of the addition

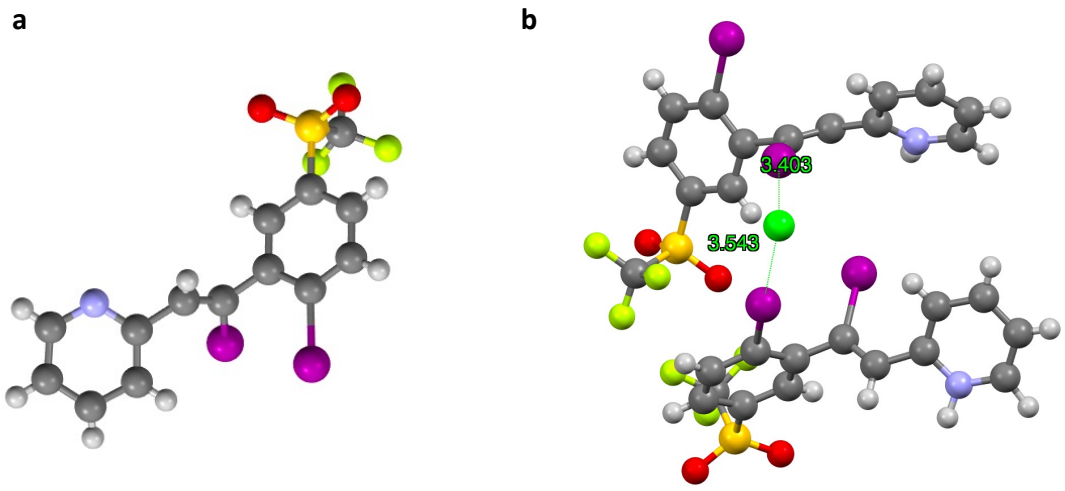

Figure 4.2. a) the crystal structure of molecule **8** that displays both the vinylic and aryl XB donors, and b) a subsection of the crystal packing to highlight the aryl and vinylic XB donors of the protonated form, **H8**$^{+}$, binding to chloride.

remained unknown until the crystals of molecule **8** were grown and analyzed (**Figure 4.2a**). Nevertheless, the most remarkable finding here was a crystal structure of **H8**$^{+}$**–** presumably protonated from trace HCl in $CHCl_3$ during recrystallization–demonstrating a quite surprising vinylic XB donor participating in halogen-bonding with chloride (**Figure 4.2b**).

The subsection of the crystal packing highlights 2 host receptors binding to one chloride guest. The calculated distance from C–I_{vinyl} --- Cl^- is 3.403 Å, about 0.14 Å shorter than C–I_{aryl} --- Cl^-. When looking at a more complete (albeit crowded) picture of host:guest binding of receptor **H8**$^{+}$ in the solid state, (**Figure 4.3**), it is clear that there are two additional hydrogen-bonding (HB) interactions to note and a total of a 4:1 host:guest binding ratio. The shortest bond length in the crystal structure comes from the protonated pyridinium N–H --- Cl^- at 2.10 Å, and the second of the two HB donors is found off the

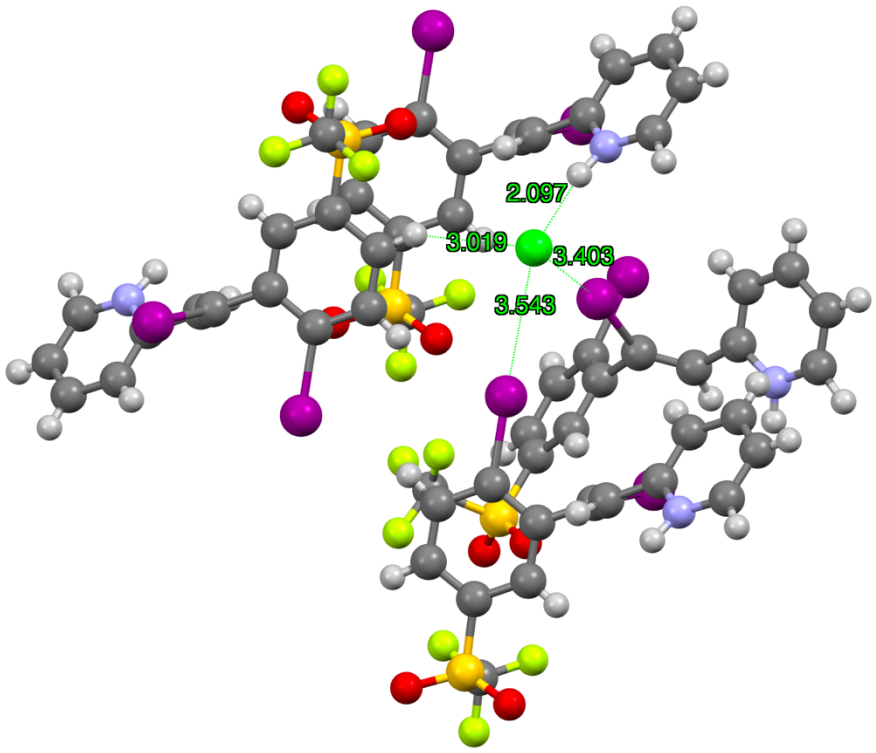

Figure 4.3. A snapshot of the crystal packing that demonstrates two hydrogen-bonding and two halogen-bonding interactions of 4 **H8**$^+$ molecules to one chloride guest.

carbon that is *ortho* to the trifluoromethyl sulfone, *meta* to the aryl XB donor, and *para* to the alkyne with a C–H_{aryl} distance of 3.05 Å.

The crystal structures implored us to obtain solution-state binding constants of **H8**$^+$ with chloride, but, to our dismay, the receptor did not show appreciable binding of iodide (in competition with the PF_6^- counterion) in acetonitrile with any of the anionic halide family which led us to continue with the synthesis of the *ortho* receptor. Yields from the iodination of the triazene host intermediate, **7**, were still grim–as **8** was, repeatedly, the major product. To increase the overall yield on the synthetic pathway, the alkene was reacted with TEA at reflux overnight to eliminate HI and reform the desired alkyne.

Once the final receptor, **10**, was synthesized, ^{1}H NMR titrations were conducted in $CDCl_3$ with 1 mM host concentration and ~20-30 mM guest concentration. Solution-state binding constants (K_a) for **10 • Cl**, **10 • Br**, and **10 • I** were determined to be 131 ± 12, 118 ± 5, and 78 ± 5 M^{-1}, respectively; the *meta* receptor bound to chloride, bromide, and iodide at constants of 137 ± 5, 104 ± 12, 103 ± 13 M^{-1}, respectively. The difference in binding constants from chloride to iodide in the *meta* receptor is only ~34 M^{-1}, whereas in the *ortho* receptor, it was found to be ~53 M^{-1}. These results provide evidence towards the hypothesis that the binding pocket of the "one-armed" receptor's *ortho* isomer would be smaller than that of the *meta* isomer, and would, therefore, allow for more selectivity of the host to bind chloride over iodide. When comparing *meta* • Cl^- to *ortho* • Cl^-, however, the binding constants are the same (within experimental error). This preliminary evidence shows that there may be no measurable difference in the withdrawing nature of the methyl pyridinium cation; whether it be resonance or inductive effect, either connectivity has the same influence on the overall anion binding strength.

4.3 Conclusions and Future Studies

In this study, it was confirmed through comparison of the *meta* monodentate receptor to its *ortho* isomer, the binding pocket is tailored more towards chloride than iodide with heightened preorganization. This project also led to a fortuitous discovery of a novel vinylic halogen-bond donor binding to chloride in a 4:1 ratio in a crystal structure.

Lastly, the question on whether there would be different binding strengths due to distinct resonance or inductive electron-withdrawing effects from the methyl pyridinium cation being *ortho* or *meta* to the alkyne (and therefore the XB donor), was answered. When comparing the K_as of the *ortho* and *meta* receptors binding to one of the smallest anions of the halide series, chloride, there was insignificant difference in affinity. This result, however, can still be expanded on with more thorough future investigations.

When reviewing the results from Chapter III, solution- and solid-state evidence supported theoretical calculations that the largest contributor to the σ-hole size, and therefore binding strength, is the cationic methyl pyridinium functional group at the core of the receptor. The LFER study also showed that, although the tunable functional groups (Rs in **Figure 4.1**) played little part in the overall electron deficiency of the XB donor, chloride binding was still favored with electron-withdrawing groups (EWGs) *para* to the XB donor. Another, similar, LFER study could be conducted for this series to to see if there is stronger preference for EWGs in the *ortho* receptor's binding affinities with chloride.

A preliminary study was done to see if this project would be worth pursuing. The CF_3 derivative of the *ortho* receptor was synthesized by Mark Butters-Blakely and a single ^{1}H NMR titration was done (**Figure 4.4**). Receptor $\mathbf{10^{CF_3} \bullet PF_6}$ was found to bind Cl^- with a K_a of 59 M^{-1} ± 1.4% in $CDCl_3$. Although this value has not yet been

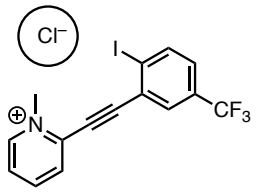

Figure 4.4 Receptor $\mathbf{10^{CF_3} \bullet Cl^-}$

corroborated, it has a notably weaker binding interaction than we have seen in any of our other titrations with the *meta* receptors–including with the slightly electron-donating *t*-Bu group that bound at 83 M^{-1}. If upheld, this data point shows promise that a new LFER study with a series of *ortho* receptors could further shine a light on how the electronics of the methyl pyridinium cation influences the XB donor's σ-hole.

CHAPTER V

CONCLUDING REMARKS

In this dissertation, I have introduced and demonstrated the versatility in the arylethynyl receptor scaffold's ability to be modified in order to tune the selectivity of binding to anionic guests. Chapter I highlights the prevalence of the anions chloride and inorganic phosphate both in our external and internal environments and, therefore, the importance of monitoring their concentrations *in situ* or *in vivo*. This chapter also goes into a brief review of the advancements in technologies of anion sensing and where supramolecular chemistry fits in that narrative. Chapter II discusses a body of work related to a bi-dentate arylethynyl halogen bonding (XB) receptor that aims to bring our scaffolds into water by appending a propyl sulfonate functional group onto the molecule. Chapter III begins the development of a novel generation of our scaffold: a simplified mono-dentate halogen bonding receptor for the purpose of binding to smaller guests, like chloride. In this chapter, we performed thorough structure/property relationship studies which showed that the largest contributor to the XB donor's σ-hole generation is the methyl pyridinium cation and not the suspected functional groups *para* to the XB donor. The new, smaller binding pocket also shifted the receptor's preference to chloride over the bulkier iodide and displayed both XB and HB motifs. Chapter IV continues the investigation of this study by looking at an isomer (*ortho*) of the original (*meta*) mono-dentate receptor. We found that the shrunken hybrid binding pocket on this scaffold demonstrated a greater preference for binding chloride compared to the *meta* isomer.

Finally, the synthesis in Chapter IV also led us to a serendipitous discovery of a receptor that exhibits a novel vinylic XB donor participating in halogen bonding with chloride in a crystal structure.

In conclusion, the findings within this dissertation provide nuanced information about halogen bonding arylethynyl receptors. The detailed understanding will help influence future designs of these scaffolds to better and more selectively bind anions of interest.

APPENDIX A

SUPPLEMENTARY CONTENT FOR CHAPTER II

Experimental Details

Materials and Methods.

Unless otherwise noted all reactions were run open to the atmosphere and consequently were exposed to air and water. All reagents were used as purchased from commercial sources. The ^{1}H NMR, ^{13}C NMR, and ^{19}F spectra were obtained using a Bruker 500 MHz spectrometer (^{1}H 500 MHz and ^{13}C 126 MHz). All ^{1}H NMR and ^{13}C NMR chemical shifts (δ) are reported in parts per million and referenced to residual solvent peaks ($CHCl_3$: ^{1}H 7.26 ppm, ^{13}C 77.16 ppm; $(CH_3)_2CO$: ^{1}H 2.05ppm, ^{13}C 29.84 and 206.26 ppm; CH_3CN ^{1}H 1.94 ppm, ^{13}C 118.26 and 1.32 ppm).

Full Receptor Synthesis.

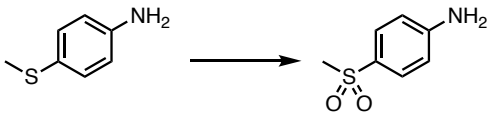

4-(methanesulfonyl)aniline, 2.

4-(methylthio)aniline (6.00 mL, 48.27 mmol) was added to a round bottom flask and dissolved in 50 mL MeOH. Then, $ZnCl_2$ (0.66 g, 4.83 mmol) 1,8-diazabicyclo[5.4.0]undec-7-ene, or DBU (1.8 mL, 12.07 mmol), and H_2O_2 (30% in H_2O, 50 mL) was added to the flask in that order. When the H_2O_2 was added, the solution

changed from a clear brown to an opaque white color. The reaction mixture was left stirring and heated at reflux overnight, then at room temperature for two days. The now yellow crude reaction mixture was diluted with H_2O and extracted with ethyl acetate. The organic layer was washed with water, brine, dried (Na_2SO_4) and concentrated to afford a yellow precipitate. The crude product was purified by flash chromatography (1:9 ethyl acetate:dichloromethane) to afford pure yellow solid (6.1 g, 74% yield). ^{1}H NMR (500 MHz, Chloroform-*d*) δ 7.69 (d, *J* = 8.6 Hz, 2H), 6.71 (d, *J* = 8.7 Hz, 2H), 4.19 (s, 1H), 3.00 (s, 3H).

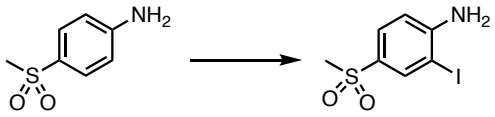

2-iodo-4-(methanesulfonyl)aniline, 3.

The aniline starting material, **2** (6.00 g, 35.04 mmol) was dissolved in 40 mL methanol. In another flask, KIO_3 (2.62 g, 12.27 mmol) and KI (3.83 g, 23.48 mmol) were dissolved in 100 mL water. The aqueous solution was added to the solution containing the aniline derivative then 1 M HCl (39 mL) was added dropwise. After the reaction stirred at room temperature overnight, the mixture was extracted with ethyl acetate. The combined organic layers were then washed with $Na_2S_2O_3$, $NaHCO_3$, water, and brine, then dried (Na_2SO_4) and concentrated to afford yellow solid product with no need for further purification (10 g, 96% yield). ^{1}H NMR (500 MHz, Chloroform-*d*) δ 8.18 (d, *J* = 2.0 Hz, 1H), 7.67 (dd, *J* = 8.4, 2.1 Hz, 1H), 6.77 (d, *J* = 8.4 Hz, 1H), 4.67 (s, 2H), 3.02 (s, 3H).

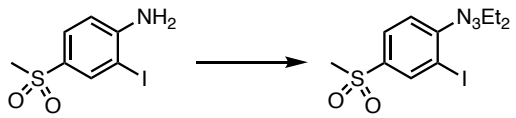

2-iodo-4-(methanesulfonyl)triazene, 4.

The iodoaniline derivative, **3** (6.00 g, 20.19 mmol) was dissolved in 30 mL acetonitrile and set to cool at -10 ºC. Concentrated HCl (13.5 mL) was added to the flask. In another flask, a solution of $NaNO_2$ (3.34 g, 48.47 mmol) in 30 mL water was prepared. The aqueous $NaNO_2$ solution was added dropwise to the solution of the iodoaniline derivative and left to stir at -10 ºC. This reaction mixture was monitored by TLC for consumption of starting material. Once consumed, the reaction mixture was added to a quench solution of: $HNEt_2$ (20.9 mL, 0.201 mol) and K_2CO_3 (16.19 g, 0.117 mol) in 50 mL of acetonitrile and 100 mL of water at -10 ºC. This quenched reaction mixture was allowed to warm up to room temperature while continuously stirring overnight. The reaction was extracted with ether and the combined organic layers were washed with $Na_2S_2O_3$, $NaHCO_3$, water, and brine. The organic layer was collected and dried (Na_2SO_4) and concentrated to afford the crude iodotriazene that was purified by column chromatography (gradient from pure hexanes to 1:9, dichloromethane:hexanes) to afford pure iodotriazene (7.5 g, 98% yield). ^{1}H NMR (500 MHz, Chloroform-*d*) δ 8.37 (d, *J* = 2.1 Hz, 1H), 7.80 (dd, *J* = 8.5, 2.1 Hz, 1H), 7.48 (d, *J* = 8.5 Hz, 1H), 3.86 (qd, *J* = 7.2, 2.0 Hz, 4H), 3.05 (s, 3H), 1.35 (dt, *J* = 28.1, 7.2 Hz, 6H).

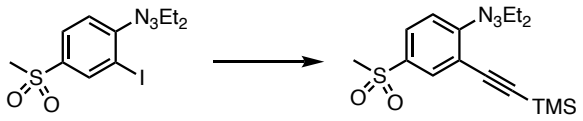

4-(methanesulfonyl)-2-((trimethylsilyl)ethynyl)triazene, 5.

After a mixture of 10 mL tetrahydrofuran and 10 mL acetonitrile, iodotriazene, **4** (10.10 g, 26.5 mmol), $Pd(PPh_3)_2Cl_2$ (1.86 g, 2.65 mmol) and CuI (0.51 g, 2.65 mmol) was outgassed with $N_{2\,(g)}$ for 20 minutes. The alkyne, TMSA (7.5 mL, 52.99 mmol) was then added dropwise. The reaction was allowed to stir at room temperature under a steady flow of $N_{2\,(g)}$ overnight. The reaction mixture was run through a silica/celite plug and washed with DCM to afford the crude product that was then purified by column chromatography (gradient from pure hexanes to 2:8, ethylacetate:hexanes) to afford a pure brown oil. (5.2 g, 56% yield). ^{1}H NMR (500 MHz, Chloroform-*d*) δ 8.03 (d, *J* = 2.2 Hz, 1H), 7.74 (dd, *J* = 8.7, 2.2 Hz, 1H), 7.55 (d, *J* = 8.6 Hz, 1H), 3.85 (q, *J* = 7.2 Hz, 4H), 3.03 (s, 3H), 1.34 (dt, *J* = 32.4, 7.1 Hz, 6H), 0.24 (s, 9H).

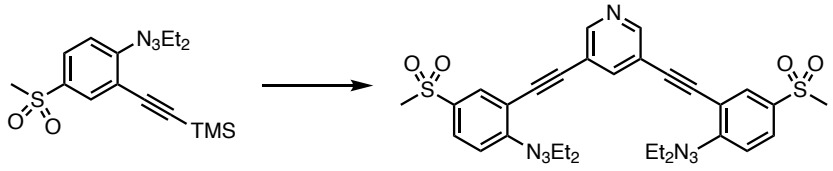

Bis-triazene, 6.

Ethynyltriazene, **5** (5.18 g, 14.7 mmol) was dissolved in 20 mL of a 1:1 THF:MeOH mixture and set stirring in a RBF. K_2CO_3 (16.3 g, 117.78 mmol) was then added to the solution and left stirring until the SM had disappeared by TLC (~1 h). The reaction mixture was diluted with H_2O, extracted with ethyl acetate, and washed with water and brine. The solution was then dried, and solvent was removed *in vacuo* to furnish the deprotected alkyne in quantitative yields. While this was going on, a RBF of 20 mL THF

and 20 mL DIPA was outgassed with N_2 for at least forty minutes. Once isolated, the alkyne (4.41 g, 15.79 mmol) was dissolved in a minimal amount of THF and outgassed for at least 1 min./mL of solvent. After outgassing, 3, 5-dibromopyridine (1.25 g, 5.26 mmol), $Pd(PPh_3)_4$ (0.61 g, 0.526 mmol), and CuI (0.10 g, 0.526 mmol) were added to the RBF with the THF/DIPA mixture and set to stir. The separate solution of deprotected alkyne in THF was then cannulated dropwise to the dibromopyridine/catalyst mixture and the reaction was left stirring at 55 °C overnight. The next day, the reaction was passed through a silica/celite plug, washed with DCM, and concentrated to afford the crude product that was purified by column chromatography (gradient from 1:9, DCM:hexanes to 100% DCM) to afford an off-white solid product (3.0 g, 90% yield). ^{1}H NMR (500 MHz, Chloroform-*d*) δ 8.66 (d, *J* = 2.0 Hz, 2H), 8.11 (d, *J* = 2.2 Hz, 2H), 7.87 (t, *J* = 2.0 Hz, 1H), 7.82 (dd, *J* = 8.7, 2.2 Hz, 2H), 7.64 (d, *J* = 8.7 Hz, 2H), 3.90 (dq, *J* = 11.5, 7.2 Hz, 8H), 3.08 (s, 6H), 1.37 (dt, *J* = 24.5, 7.1 Hz, 12H).

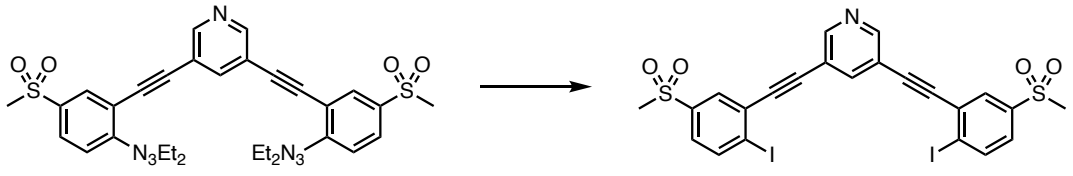

Diiodide, 7.

HI (1.56 mL, 11.83 mmol) and I_2 (3.00 g, 11.83 mmol) were dissolved in ACN (50 mL) then set stirring at 60 °C. While the first solution was coming up to temperature the bistriazene, **6** (1.56 g, 2.37 mmol) was dissolved in ACN (50 mL). The triazene solution was then added dropwise into the first flask and stirred at 60 °C while monitoring via TLC. After the SM was consumed, the mixture was extracted with ethyl acetate and washed with $NaHCO_3$, $Na_2S_2O_3$, water x2 each, then brine. The organic layer was then

dried with Na_2SO_4 and concentrated to form an oil which was purified on silica via column chromatography (gradient from 100% hexanes to 3:7 ethylacetate:hexanes) to afford a yellow oil (1.6 g, 98% yield). ^{1}H NMR (500 MHz, Chloroform-*d*) δ 8.83 (d, *J* = 1.9 Hz, 2H), 8.14 (d, *J* = 8.3 Hz, 2H), 8.09 (d, *J* = 2.3 Hz, 2H), 8.06 (t, *J* = 2.0 Hz, 1H), 7.59 (dd, *J* = 8.3, 2.2 Hz, 2H), 3.09 (s, 6H).

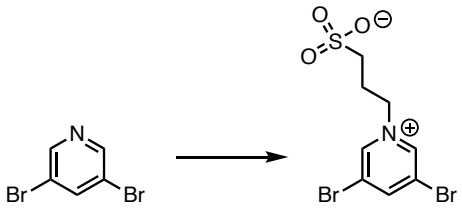

Pyridinesultone.

3, 5-dibromopyridine (0.5 g, 2.11 mmol) was dissolved into 10 mL CAN and set to stir in an ice bath. Propanesultone (0.185 mL, 2.11 mmol) in 5 mL toluene was slowly added to the cooled dibromopyridine solution. After addition, the mixture was *slowly* heated to 50 ºC and left to stir overnight. The resulting precipitate was filtered *via* vacuum filtration and washed with ether 3 times. No yield was noted as this was a proof-of-concept reaction. ^{1}H NMR (500 MHz, Deuterium Oxide) δ 9.28 (d, *J* = 1.7 Hz, 2H), 9.07 (d, *J* = 1.7 Hz, 1H), 4.81 (d, *J* = 9.8 Hz, 2H), 3.05 (t, *J* = 7.2 Hz, 2H), 2.50 (p, *J* = 7.3 Hz, 2H).

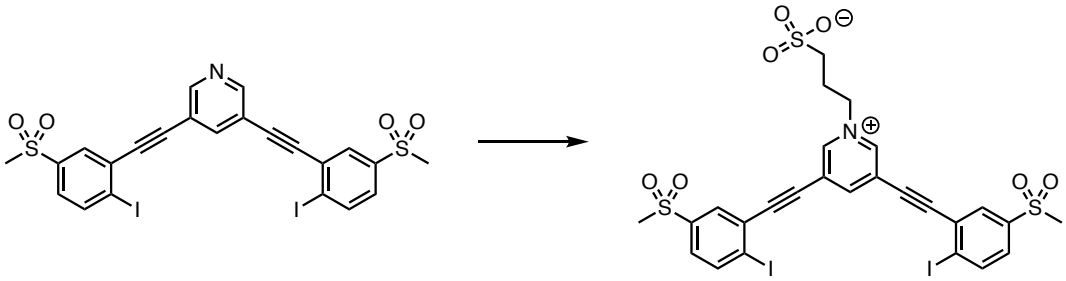

Sulfopropyl zwitterionic receptor, 8.

Diiodide, **7** (0.30 g, 0.436 mmol), was dissolved in 10 mL DMF and started to heat. When the reaction temperature got to be 60-70 ºC, propanesultone (0.10 mL, 1.14 mmol) was added to the flask and became a clear red/orange color. The reaction mixture was then allowed to stir at reflux overnight. The next day, the reaction was opaque brown. Hot filtration was performed to collect the precipitate.

NMR Spectra

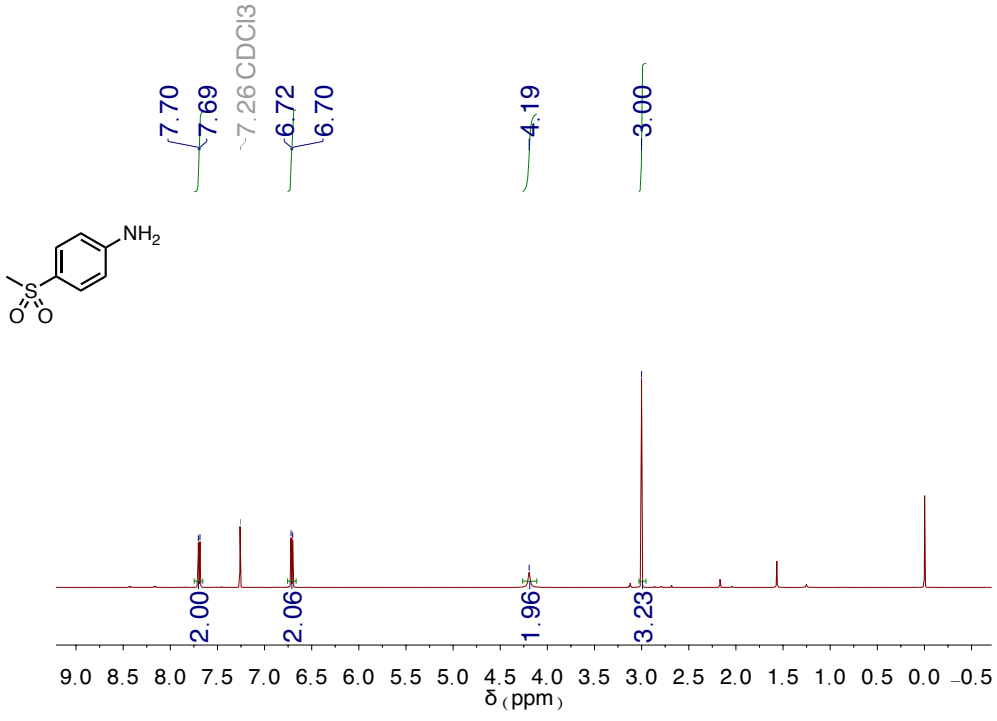

Figure A.1. ^{1}H NMR spectrum of **2**.

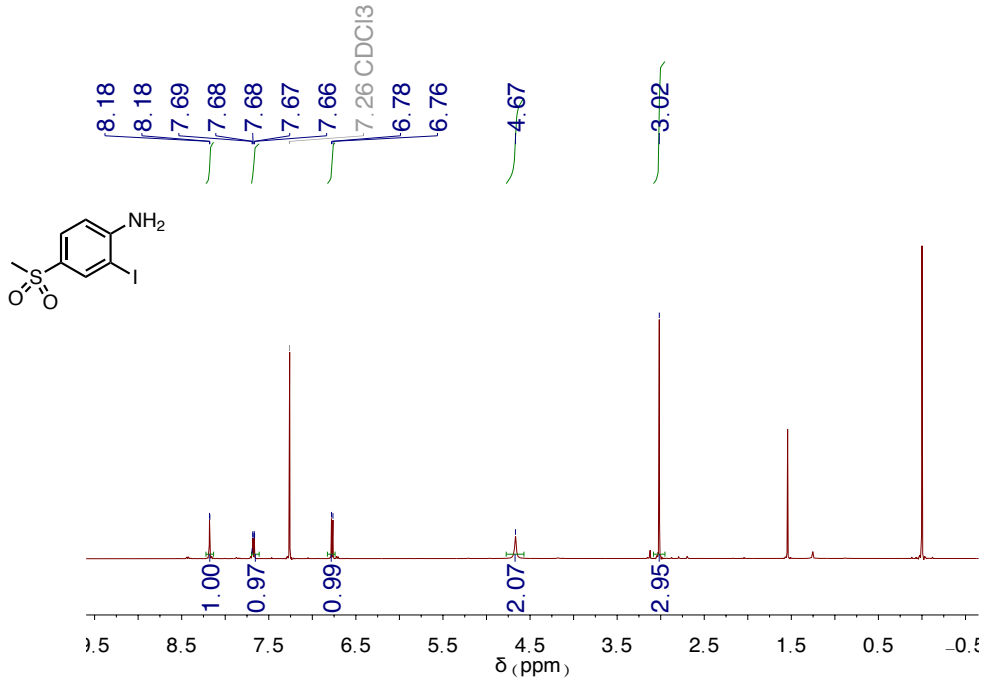

Figure A.2. ^{1}H NMR spectrum of **3**.

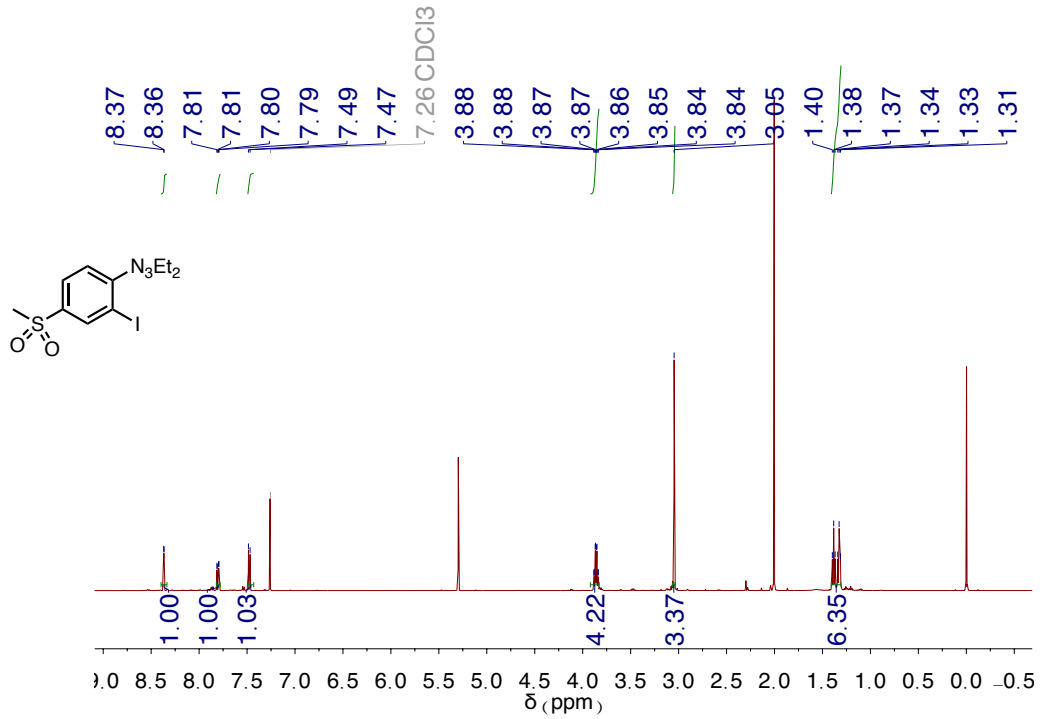

Figure A.3. ^{1}H NMR spectrum of **4**.

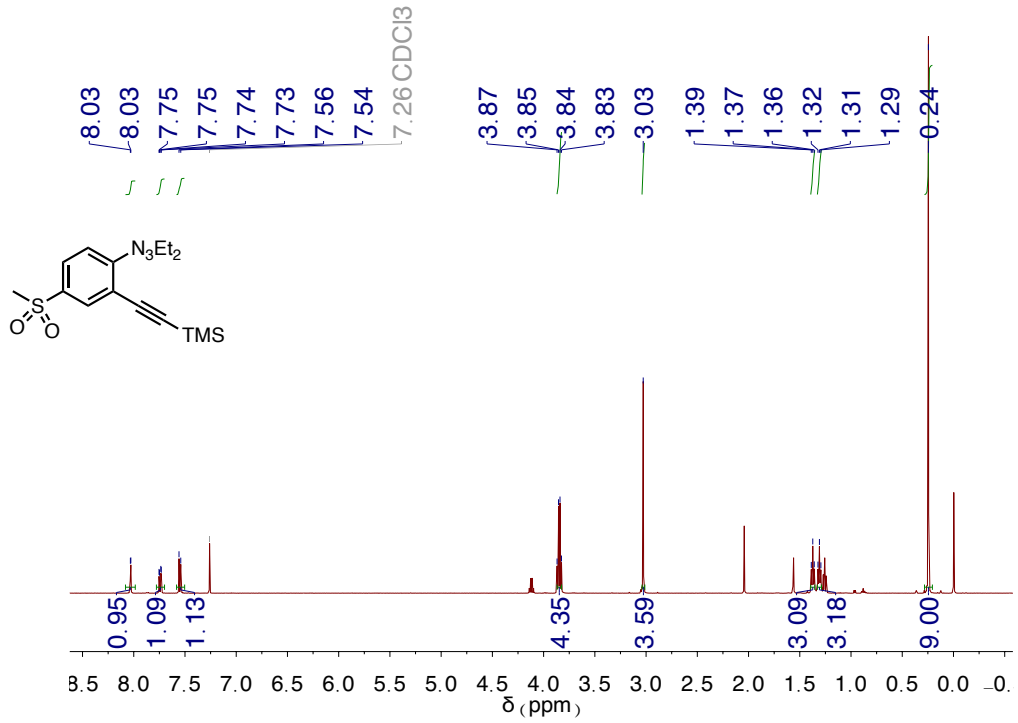

Figure A.4. ^{1}H NMR spectrum of **5**.

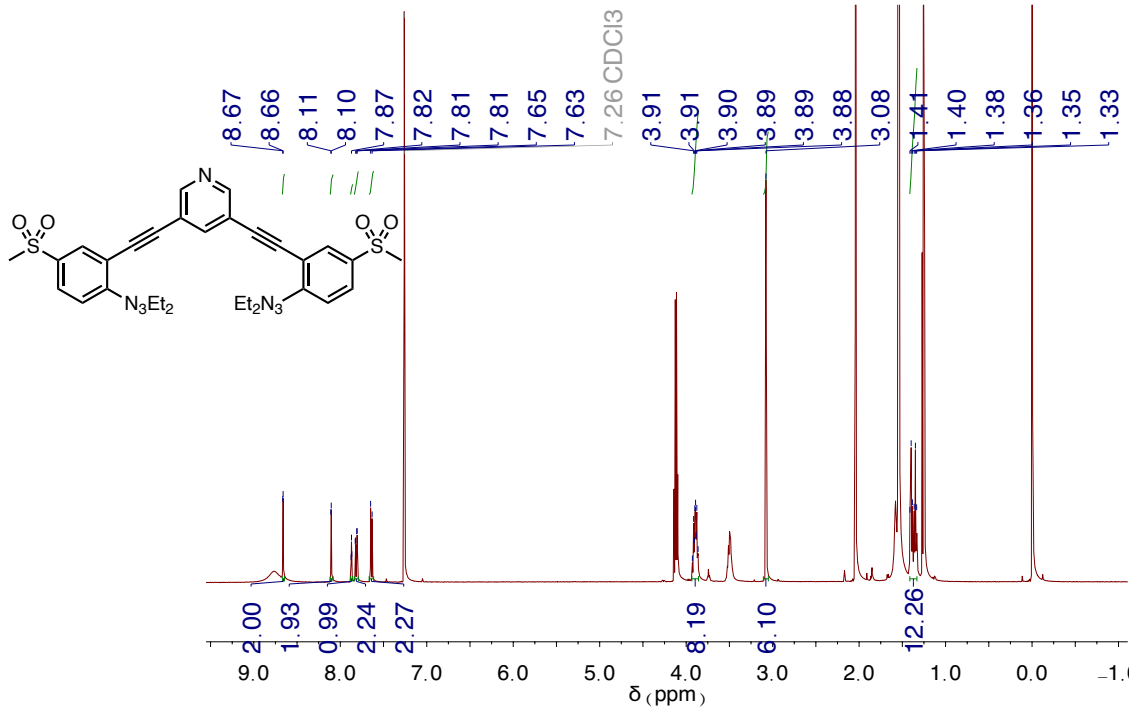

Figure A.5. ^{1}H NMR spectrum of **6**. Wet with ethyl acetate.

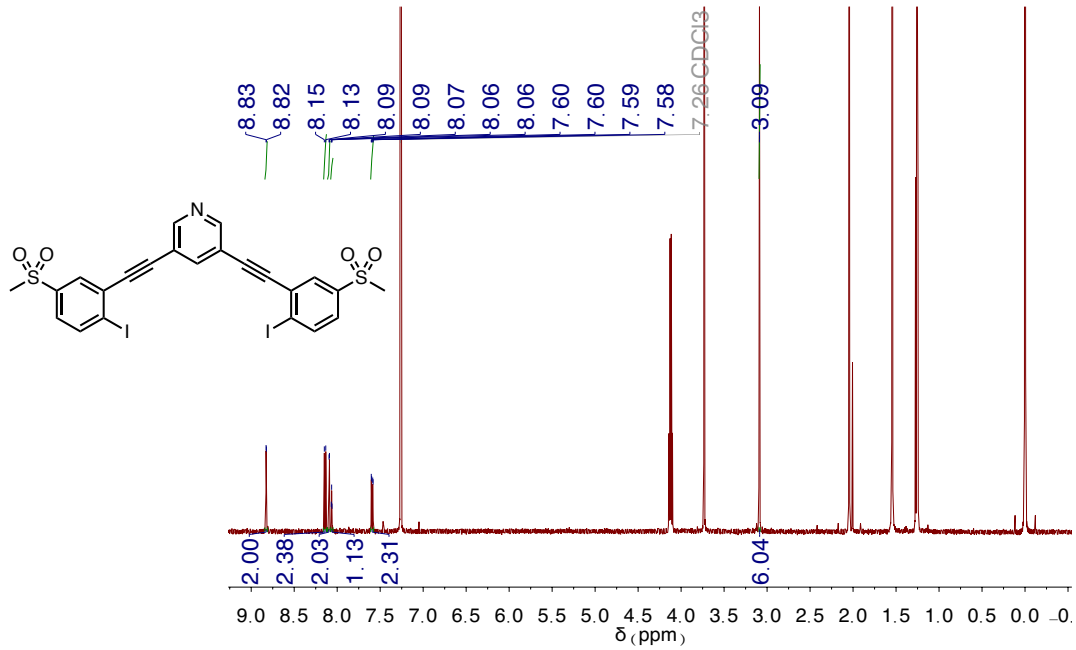

Figure A.6. [1]H NMR spectrum of **7**. Wet with ethyl acetate.

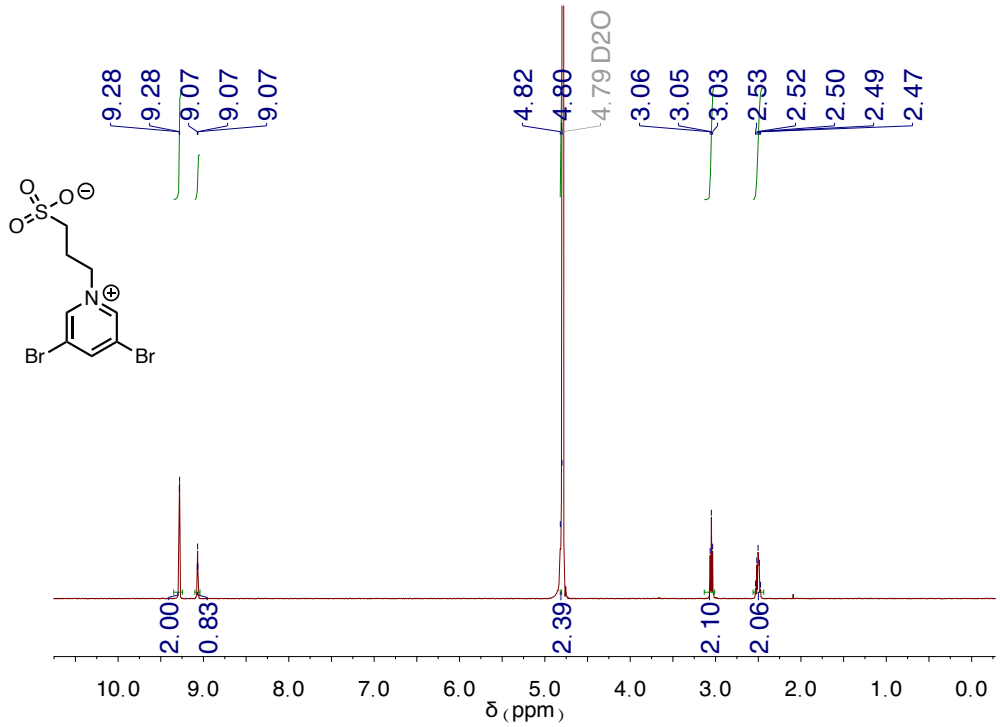

Figure A.7. [1]H NMR spectrum of pyridinesultone.

Infrared Radiation (IR) Spectroscopy.

Nicolet 6700 IR Spectrometer analysis of powders and films used to analyze **7** and the potential product precipitate. No sample preparation required.

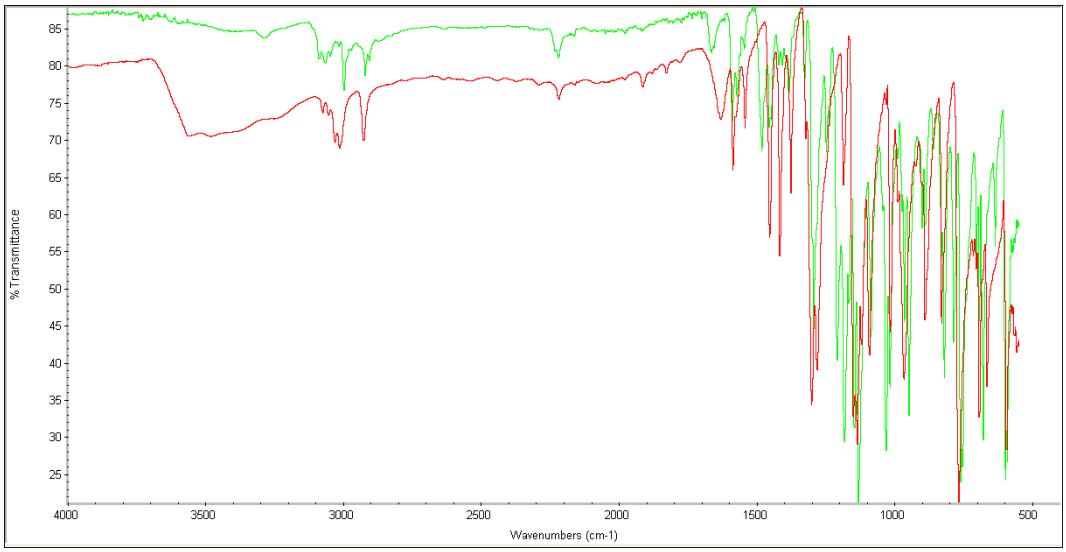

Figure A.8. IR spectra of **7**, red trace, and of the potential zwitterionic product, green trace.

APPENDIX B

SUPPLEMENTARY CONTENT FOR CHAPTER III

Experimental Details

Materials and Methods.

Unless otherwise noted all reactions were run open to the atmosphere and consequently were exposed to air and water. All reagents were used as purchased from commercial sources. The ^{1}H NMR, ^{13}C NMR, and ^{19}F spectra were obtained using a Bruker 500 MHz spectrometer (^{1}H 500 MHz, ^{13}C 126 MHz, ^{19}F 471 MHz), and the ^{1}H NMR titrations were performed on a Varian 500 MHz spectrometer (^{1}H 500.10 MHz) using *d3*-ACN. All ^{1}H NMR and ^{13}C NMR chemical shifts (δ) are reported in parts per million and referenced to residual solvent peaks ($CHCl_3$: ^{1}H 7.26 ppm, ^{13}C 77.16 ppm; $(CH_3)_2CO$: ^{1}H 2.05ppm, ^{13}C 29.84 and 206.26 ppm; CH_3CN ^{1}H 1.94 ppm, ^{13}C 118.26 and 1.32 ppm). Masses for novel compounds were determined with a Waters Xevo G2-XS ToF spectrometer.

Full Receptor Synthesis.

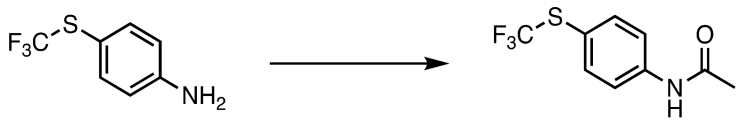

4-(trifluoromethylthio)acetamide.

4-(trifluoromethylthio)aniline (7.4 mL, 71.8 mmol) was added under N_2 to an oven-dried, vacuum-cooled round bottom flask. Acetic anhydride (10.2 mL, 108 mmol) was added to the flask dropwise and a white precipitate crashed out upon addition. The mixture was stirred at room temperature for one hour. Afterwards, the solid was dissolved using ethyl acetate and washed with water and brine. The organic layer was dried (Na_2SO_4), filtered, and concentrated to give the crude protected aniline. The white powdered product was purified by running the crude product through a plug with dichloromethane. (12 g, 71% yield). ^{1}H NMR (500 MHz, Acetone-d_6) δ 9.44 (s, 1H), 7.80 (d, J = 8.7 Hz, 2H), 7.63 (d, J = 8.7 Hz, 2H), 2.11 (s, 3H).

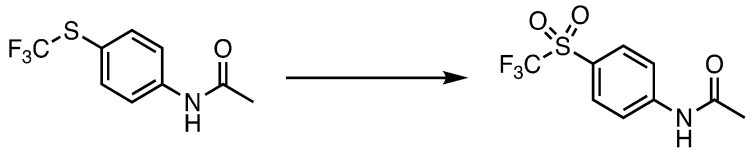

N-[4-[(trifluoromethyl)sulfonyl]phenyl]acetamide.

In an oven-dried, vacuum-cooled round bottom flask, the 4-(trifluoromethyl)thio phenyl acetamide (12 g, 51.0 mmol) was dissolved in 200 mL of dry dichloromethane and cooled to 0 ºC. mCPBA (26 g, 153 mmol) was added in 4 portions under a heavy $N_{2\,(g)}$ flow. The

reaction was allowed to warm up to room temperature while stirring overnight. The reaction mixture was diluted with more dichloromethane and $Na_2S_2O_3$ was used to quench any excess mCPBA. The mixture was extracted with dichloromethane and the combined organic layers were washed with $Na_2S_2O_3$, $NaHCO_3$, water and brine, then dried (Na_2SO_4) and concentrated to afford a white precipitate (11.4 g, 84% yield). ^{1}H NMR (500 MHz, Acetone-d_6) δ 9.84 (s, 1H), 8.08 – 8.00 (m, 4H), 2.18 (s, 3H).

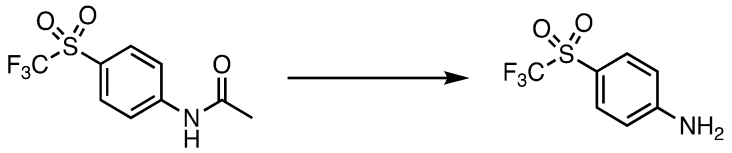

N-[4-[(trifluoromethyl)sulfonyl]phenyl]aniline.

N-[4-[(trifluoromethyl)sulfonyl]phenyl]acetamide (6.2 g, 23.15 mmol) was dissolved in 200 mL of EtOH; KOH (1.43 g, 25.46 mmol) was added, and the reaction mixture was set to 60 ºC and allowed to stir. After 3 hours, the mixture was concentrated to afford a crude solid which was then dissolved in water. White precipitate formed and collected via vacuum filtration to afford pure product (4.7 g, 90% yield). ^{1}H NMR (500 MHz, Chloroform-*d*) δ 7.75 (d, *J* = 8.8 Hz, 2H), 6.75 (d, *J* = 8.8 Hz, 2H), 4.54 (s, 2H).

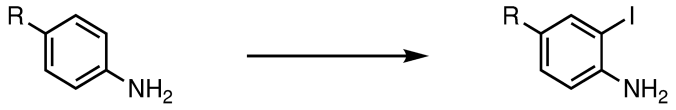

Iodoaniline derivatives, 1a-d.

The aniline derivative (20.76 mmol, 1.0 equiv.) was dissolved in 40 mL methanol. In another flask, KIO_3 (7.27 mmol, 0.35 equiv.) and KI (13.7 mmol, 0.66 equiv.) were dissolved in 100 mL water. The aqueous solution was added to the solution containing

the aniline derivative then 1 M HCl (23 mL, 1.1 equiv.) was added dropwise. After the reaction stirred at room temperature overnight, the mixture was extracted with ethyl acetate. The combined organic layers were then washed with $Na_2S_2O_3$, $NaHCO_3$, water, and brine, then dried (Na_2SO_4) and concentrated to afford crude product.

R= SO_2CF_3 (red/brown solid, 92% yield). ^{1}H NMR (500 MHz, Chloroform-*d*) δ 8.22 (d, *J* = 2.1 Hz, 1H), 7.74 (dd, *J* = 8.6, 2.1 Hz, 1H), 6.81 (d, *J* = 8.6 Hz, 1H), 4.99 (s, 2H). ^{13}C NMR (126 MHz, $CDCl_3$) δ 153.83, 142.11, 132.45, 123.86, 121.27, 118.88, 118.68, 116.09, 113.44, 81.85, 77.16. ^{19}F NMR (471 MHz, $CDCl_3$) δ -78.79. MASS SPEC NEEDED.

R= CF_3 (brown solid, 79% yield). ^{1}H NMR (500 MHz, Chloroform-*d*) δ 7.87 (s, 1H), 7.38 (dd, *J* = 8.5, 2.2 Hz, 1H), 6.74 (d, *J* = 8.4 Hz, 1H), 4.41 (s, 2H).

R= H commercially available

R= *t*Bu (brown solid, 66% yield). ^{1}H NMR (500 MHz, Chloroform-*d*) δ 7.65 (d, *J* = 1.7 Hz, 1H), 7.19 (d, *J* = 2.0 Hz, 1H), 6.70 (d, *J* = 8.4 Hz, 1H), 3.99 (s, 2H), 1.28 (d, *J* = 1.7 Hz, 9H).

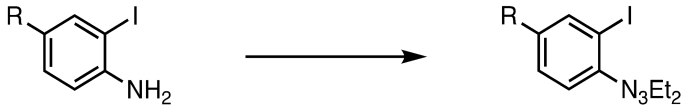

Iodotriazene derivatives, 2a-d.

The iodoaniline derivative (8.55 mmol, 1.0 equiv.) was dissolved in 30 mL acetonitrile and set to cool at -10 ºC. Concentrated HCl (5.7 mL, 8.0 equiv.) was added to the flask. In another flask, a solution of $NaNO_2$ (20.51 mmol, 2.4 equiv.) in 30 mL water was prepared. The aqueous $NaNO_2$ solution was added dropwise to the solution of the iodoaniline derivative and left to stir at -10 ºC. This reaction mixture was monitored by

TLC for consumption of starting material. Once consumed, the reaction mixture was added to a quench solution of: $HNEt_2$ (85.45 mmol, 10 equiv.) and K_2CO_3 (49.56 mmol, 5.8 equiv.) in 50 mL of acetonitrile and 100 mL of water at -10 ºC. This quenched reaction mixture was allowed to warm up to room temperature while continuously stirring overnight. The reaction was extracted with ether and the combined organic layers were washed with $Na_2S_2O_3$, $NaHCO_3$, water, and brine. The organic layer was collected and dried (Na_2SO_4) and concentrated to afford the crude iodotriazene that was purified by column chromatography (gradient from pure hexanes to 1:9, dichloromethane:hexanes) to afford pure iodotriazene.

R= SO_2CF_3 (orange solid, 25% yield). ^{1}H NMR (500 MHz, Chloroform-*d*) δ 8.11 (d, *J* = 2.2 Hz, 1H), 7.56 (dd, *J* = 8.6, 1.9 Hz, 1H), 7.27 (d, *J* = 8.7 Hz, 1H), 3.60 (qd, *J* = 7.2, 5.1 Hz, 4H), 1.07 (dt, *J* = 30.0, 7.2 Hz, 6H). ^{13}C NMR (126 MHz, $CDCl_3$) δ 157.06, 141.51, 131.04, 126.15, 123.75, 121.16, 118.56, 117.34, 115.97, 96.24, 50.42, 43.64, 14.29, 10.69. ^{19}F NMR (471 MHz, $CDCl_3$) δ -77.75. MASS SPEC NEEDED.

R= CF_3 (orange solid, quant. yield). ^{1}H NMR (500 MHz, Chloroform-*d*) δ 8.07 (s, 1H), 7.51 (dd, *J* = 8.6, 2.0 Hz, 1H), 7.42 (d, 1H), 3.84 (q, *J* = 7.2 Hz, 4H), 1.34 (dt, *J* = 24.0, 7.3 Hz, 6H).

R= H (orange solid, quant. yield). ^{1}H NMR (500 MHz, Chloroform-*d*) δ 7.86 (dd, *J* = 7.9, 1.4 Hz, 1H), 7.38 (dd, *J* = 8.1, 1.6 Hz, 1H), 7.29 (ddd, *J* = 8.3, 7.2, 1.4 Hz, 1H), 6.85 (td, *J* = 7.5, 1.6 Hz, 1H), 3.81 (q, *J* = 7.2 Hz, 4H), 1.34 (t, *J* = 7.2 Hz, 6H).

R= *t*Bu (orange solid, 89% yield). ^{1}H NMR (500 MHz, Chloroform-*d*) δ 7.88 (d, *J* = 2.0 Hz, 1H), 7.60 – 7.01 (m, 2H), 3.80 (q, *J* = 7.2 Hz, 4H), 1.74 – 0.92 (m, 15H).

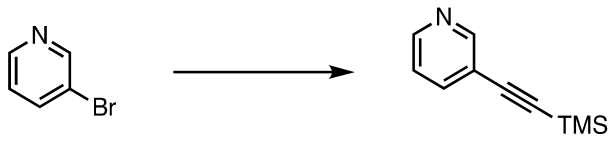

TMS-protected 3-ethynylpyridine.

After a mixture of 10 mL tetrahydrofuran and 10 mL acetonitrile, 3-bromopyridine (0.31 mL, 3.16 mmol), $Pd(PhCN)_2Cl_2$ (0.16 mmol, 5 mol%) and CuI (0.16 mmol, 5 mol%) was outgassed with $N_{2\,(g)}$ for at least 20 minutes, the ligand P(*t*Bu)$_3$ (0.316 mmol, 10 mol%) was added. The alkyne, TMSA (4.74 mmol, 1.5 equiv.) was then added dropwise. The reaction was allowed to stir at room temperature under a steady flow of $N_{2\,(g)}$ overnight. The reaction mixture was run through a silica/celite plug and washed with DCM to afford the crude product that was then purified by column chromatography (gradient from pure hexanes to 2:8, ethylacetate:hexanes) to afford a pure brown oil. (0.549 g, quant. yield). ^{1}H NMR (500 MHz, Chloroform-*d*) δ 8.59 (s, 1H), 8.41 (dd, *J* = 4.9, 1.9 Hz, 1H), 7.62 (dt, *J* = 7.8, 1.8 Hz, 1H), 7.10 (dd, *J* = 7.9, 4.8 Hz, 1H), 0.16 (s, 6H).

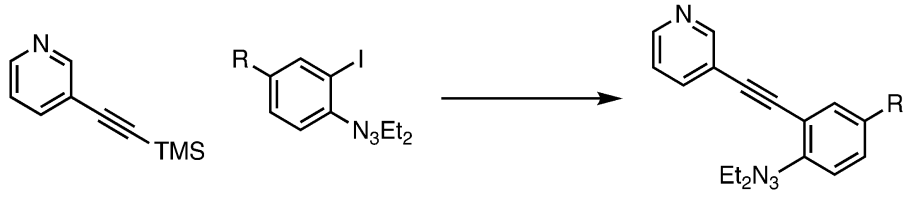

Triazene receptor intermediate, 3a-d.

The 3-ethynylpyridine (1.71 mmols, 1.0 equiv.) was dissolved in Et_2O and set to stir in a flask. Tetrabutylammonium fluoride (TBAF, 2.40 mmols) was then added to the solution and left to stir until the starting material had disappeared by TLC (~ 20 min.). The reaction mixture was quenched with NH_4Cl and extracted with water and brine x2. The organic layer was dried ($NaSO_4$), and the solvent was removed *in vacuo* to furnish 3-ethynylpyridine in quantitative yields. While this was going on a new flask of 50% THF

and 50% DIPA (20 mL total) was outgassed with $N_{2(g)}$ for at least twenty minutes. Once isolated 3-ethynylpyridine (2.28 mmol, 1.3 equiv.) was dissolved in a minimal amount of THF and outgassed for at least 1 min/mL of solvent. After outgassing, the iodotriazene compound (1.76 mmol, 1.0 equiv.), $Pd(PPh_3)_4$ (0.18 mmol, 0.10 equiv.), and CuI (0.11 mmol, 0.06 equiv.) were added to the RBF with the THF/DIPA mixture and set to stir. The separate solution of 3-ethynylpyridine in THF was then cannulated dropwise to the iodotriazene/catalyst mixture and the reaction was left stirring at 45 °C overnight. The next day, the reaction was passed through a silica/celite plug, washed with DCM, and concentrated to afford the crude product that was purified by column chromatography (gradient from 1:9, DCM:hexanes to 100% DCM)

R= SO_2CF_3 (yellow solid, 69% yield). ^{1}H NMR (500 MHz, Chloroform-*d*) δ 8.77 (s, 1H), 8.58 (s, 1H), 8.17 (d, *J* = 2.2 Hz, 1H), 7.85 (dd, *J* = 8.8, 2.2 Hz, 1H), 7.81 (d, *J* = 7.9 Hz, 1H), 7.71 (d, *J* = 8.8 Hz, 1H), 7.31 (dd, *J* = 7.9, 4.8 Hz, 1H), 3.91 (dq, *J* = 11.1, 7.2 Hz, 4H), 1.38 (dt, *J* = 30.4, 7.2 Hz, 6H). ^{13}C NMR (126 MHz, $CDCl_3$) δ 159.95, 153.74, 150.39, 139.86, 137.42, 132.52, 126.79, 125.30, 124.71, 122.71, 120.43, 120.12, 119.17, 117.53, 93.63, 90.41, 51.86, 44.69, 15.84, 12.24. ^{19}F NMR (471 MHz, $CDCl_3$) δ -78.49. HRMS (TOF-MS-ES+) for $C_{18}H_{17}N_4SO_2F_3$ [M+H] +: calcd 410.10, found 410.1024.

R= CF_3 (76% yield). ^{1}H NMR (500 MHz, Acetone-d_6) δ 8.75 (s, 1H), 8.58 (d, *J* = 4.6 Hz, 1H), 7.93 (dt, *J* = 7.9, 1.9 Hz, 1H), 7.85 (d, *J* = 1.9 Hz, 1H), 7.69 – 7.63 (m, 2H), 7.44 (dd, *J* = 7.9, 4.8 Hz, 1H), 3.95 (dq, *J* = 10.6, 7.1 Hz, 4H), 1.36 (dt, *J* = 24.1, 7.1 Hz, 6H). ^{19}F NMR (471 MHz, Acetone) δ -62.61. HRMS (TOF-MS-ES+) for $C_{18}H_{17}N_4F_3$ [M+H] +: calcd 346.14 , found 346.1405.

. HRMS (TOF-MS-ES+) for $C_{18}H_{17}N_4F_3$ [M+H] +: calcd 346.14 , found 346.1405.

R= H (yellow solid, 97% yield). ^{1}H NMR (500 MHz, Chloroform-*d*) δ 8.77 (s, 1H), 8.53 (s, 1H), 7.79 (dd, *J* = 7.8, 1.8 Hz, 1H), 7.54 (dd, *J* = 7.6, 1.5 Hz, 1H), 7.45 (d, *J* = 8.4 Hz, 1H), 7.34 – 7.27 (m, 2H), 7.10 (t, *J* = 7.5 Hz, 1H), 3.82 (q, *J* = 7.2 Hz, 4H), 1.33 (t, *J* = 7.2 Hz, 6H). HRMS (TOF-MS-ES+) for $C_{17}H_{18}N_4$ [M+H] +: calcd 278.15, found 278.1531.

R= *t*Bu (light brown oil, quant. yield). ^{1}H NMR (500 MHz, Chloroform-*d*) δ 7.88 (d, *J* = 2.0 Hz, 1H), 7.60 – 7.01 (m, 2H), 3.80 (q, *J* = 7.2 Hz, 4H), 1.74 – 0.92 (m, 15H). ^{13}C NMR (126 MHz, $CDCl_3$) δ 207.02, 152.31, 150.42, 148.14, 147.85, 147.66, 138.25, 129.58, 127.08, 123.10, 116.83, 116.79, 92.40, 89.24, 34.52, 31.41, 31.04. HRMS (TOF-MS-ES+) for $C_{21}H_{26}N_4$ [M+H] +: calcd 334.22, found 334.2157.

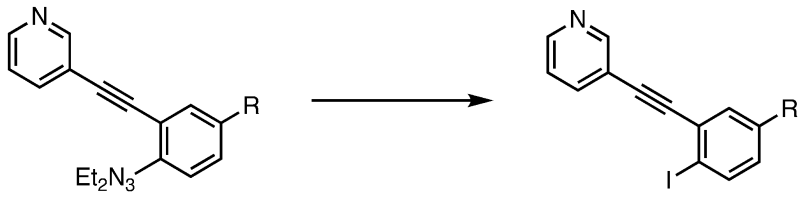

Neutral ethynyl pyridine receptor, 4a-d.

HI (0.54 mmol, 3.0 equiv.) and I_2 (0.54 mmol, 3.0 equiv.) were dissolved in ACN (5 mL) then set to stir at 60 °C. While the first solution was coming up to temperature the triazene (0.18 mmol, 1.0 equiv.) was dissolved in ACN (5 mL), which was then added dropwise into the first flask and stirred at 60 °C while monitoring via TLC. After the starting material was consumed (~40 min), the mixture was extracted with EtOAc and washed with $NaHCO_3$, $Na_2S_2O_3$, and water x2 each. The organic layer was then dried with Na_2SO_4 and concentrated to form an oil which was purified on silica via column chromatography (gradient from 100% hexanes to 3:7 ethylacetate:hexanes).

R= SO_2CF_3 (tan solid, 40% yield). ^{1}H NMR (500 MHz, Acetone-d_6) δ 8.88 (s, 1H), 8.66 (d, *J* = 3.9 Hz, 1H), 8.50 (d, *J* = 8.4 Hz, 1H), 8.23 (d, *J* = 2.3 Hz, 1H), 8.06 (dt, *J* = 7.8, 1.9 Hz, 1H), 7.83 (dd, *J* = 8.4, 2.3 Hz, 1H), 7.50 (dd, *J* = 8.0, 4.8 Hz, 1H).^{13}C NMR (126 MHz, Acetone) δ 152.99, 150.93, 142.45, 139.48, 134.12, 132.75, 132.13, 131.48, 124.46, 121.88, 119.78, 119.29, 116.70, 113.65, 93.60, 92.97. ^{19}F NMR (471 MHz, $CDCl_3$) δ -79.33. HRMS (TOF-MS-ES+) for $C_{14}H_7INSO_2F_3$ [M+H]+: calcd 436.92, found 436.9194.

R= CF_3 (yellow solid, 31% yield). ^{1}H NMR (500 MHz, Chloroform-*d*) δ 8.62 (d, *J* = 2.5 Hz, 1H), 8.42 (dd, *J* = 4.9, 1.7 Hz, 1H), 8.01 (d, *J* = 8.3 Hz, 1H), 7.89 – 7.75 (m, 1H), 7.70 (d, *J* = 2.2 Hz, 1H), 7.35 – 7.13 (m, 2H). ^{19}F NMR (471 MHz, $CDCl_3$) δ -58.44. HRMS (TOF-MS-ES+) for $C_{14}H_7INF_3$ [M+H] +: calcd 372.96, found 372.9575. HRMS (TOF-MS-ES+) for $C_{13}H_8IN$ [M+H] +: calcd 304.97, found 304.970.

R= H (tan solid, 20% yield). ^{1}H NMR (500 MHz, Chloroform-*d*) δ 8.83 (d, *J* = 2.1 Hz, 1H), 8.58 (dd, *J* = 5.0, 1.7 Hz, 1H), 7.92 – 7.85 (m, 2H), 7.54 (dd, *J* = 7.7, 1.7 Hz, 1H), 7.35 (td, *J* = 7.6, 1.2 Hz, 1H), 7.31 (ddd, *J* = 7.8, 4.9, 0.8 Hz, 1H), 7.05 (td, *J* = 7.8, 1.7 Hz, 1H).

R= *t*Bu (yellow solid, 87% yield). ^{1}H NMR (500 MHz, Chloroform-*d*) δ 8.84 (s, 1H), 8.57 (d, *J* = 3.3 Hz, 1H), 7.89 (dt, *J* = 7.9, 2.0 Hz, 1H), 7.79 (d, *J* = 8.4 Hz, 1H), 7.57 (d, *J* = 2.4 Hz, 1H), 7.31 (dd, *J* = 7.9, 4.9 Hz, 1H), 7.09 (dd, *J* = 8.4, 2.4 Hz, 1H), 1.32 (s, 9H). ^{13}C NMR (126 MHz, $CDCl_3$) δ 152.49, 151.68, 149.09, 138.75, 138.72, 130.16, 128.84, 127.96, 123.36, 120.54, 97.64, 95.49, 89.14, 34.89, 31.34. HRMS (TOF-MS-ES+) for $C_{17}H_{16}IN$ [M+H] +: calcd 361.03, found 361.0327.

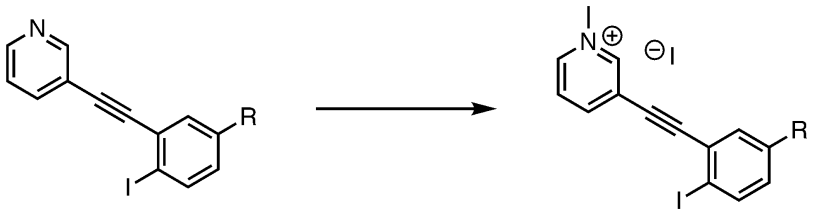

Methylated ethynyl pyridine.

The neutral receptor (0.067 mmol) was added to a bomb flask followed by an excess of MeI (5 mL). The reaction vessel was then sealed and set to stir at 110 °C overnight. Over the next 24 hours, the product would precipitate out of solution. The yellow precipitate was collected and washed with minimal DCM to afford pure product.

R= SO_2CF_3 (yellow solid, quant. yield). ^{1}H NMR (500 MHz, Acetone-d_6) δ 9.65 (s, 1H), 9.30 (d, J = 6.1 Hz, 1H), 8.94 (d, J = 8.1 Hz, 1H), 8.53 (d, J = 8.4 Hz, 1H), 8.42 – 8.32 (m, 1H), 8.26 (d, J = 2.4 Hz, 1H), 7.91 (dd, J = 8.4, 2.3 Hz, 1H). ^{19}F NMR (471 MHz, Acetone) δ -79.27. HRMS (TOF-MS-ES+) for $C_{14}H_7I_2NSO_2F_3$ [M+H] +: calcd 451.94, found 451.9429.

R= CF_3 (yellow solid, quant. yield). ^{1}H NMR (500 MHz, Acetone-d_6) δ 9.62 (s, 1H), 9.30 (d, J = 6.2 Hz, 1H), 8.89 (d, J = 8.1 Hz, 1H), 8.38 (t, J = 7.2 Hz, 1H), 8.29 (d, J = 8.3 Hz, 1H), 8.00 (d, J = 2.2 Hz, 1H), 7.60 (d, J = 8.2 Hz, 1H), 4.76 (s, 3H). ^{19}F NMR (471 MHz, Acetone-d_6) δ -63.70. HRMS (TOF-MS-ES+) for $C_{14}H_7I_2NF_3$ [M+H] +: calcd 387.98, found 387.9810.

R= H (yellow solid, quant. yield). ^{1}H NMR (500 MHz, Acetone-d_6) δ 9.40 (s, 1H), 9.16 (d, J = 6.1 Hz, 1H), 8.84 (d, J = 8.1 Hz, 1H), 8.38 – 8.31 (m, 1H), 8.05 (d, J = 8.0 Hz, 1H), 7.71 (dd, J = 7.9, 1.7 Hz, 1H), 7.59 – 7.52 (m, 1H), 7.30 (td, J = 7.7, 1.5 Hz, 1H), 4.71 (s, 3H). HRMS (TOF-MS-ES+) for $C_{13}H_8I_2N$ [M+H] +: calcd 319.99, found 319.9936.

R= *t*Bu (yellow solid, quant. yield). ^{1}H NMR (500 MHz, Acetone-d_6) δ 9.48 (s, 1H), 9.23 (d, J = 6.1 Hz, 1H), 8.84 (d, J = 8.0 Hz, 1H), 8.39 – 8.32 (m, 1H), 7.94 (d, J = 8.5 Hz, 1H), 7.73 (d, J = 2.4 Hz, 1H), 7.37 (dd, J = 8.5, 2.5 Hz, 1H), 4.74 (s, 3H), 1.34 (s, 9H). NEED CARBON. No peaks shown on ^{19}F NMR. HRMS (TOF-MS-ES+) for $C_{17}H_{16}I_2N$ [M+H] +: calcd 376.06, found 376.0562**.**

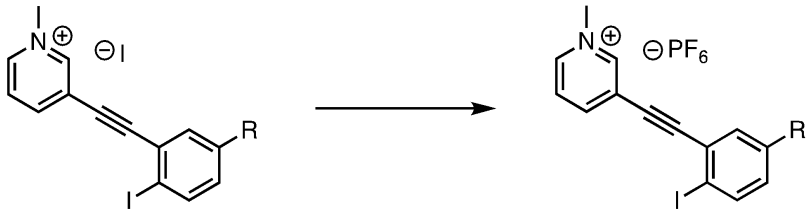

Methylated PF_6 pyridine receptor, 5a-d.

The methylated receptor (0.423 mmol, 1.0 equiv.) was dissolved in 10 mL of acetone and 40 mL of water and set to stir. To this flask, $AgPF_6$ (1.068 mmol, 2.5 equiv.) was added and stirred for about 40 minutes during which time gray precipitate (AgI) formed. This precipitate was filtered off and the filtrate solvent mixture was removed *in vacuo* until only water remained. At this point white precipitate (final product) began to crash out of the water and was collected via filtration and washed with minimal water to give the final pure product.

R= SO_2CF_3 (white solid, quant. yield). ^{1}H NMR (500 MHz, Acetone-d_6) δ 9.52 (s, 1H), 9.24 (d, J = 6.2 Hz, 1H), 8.95 (d, J = 8.2 Hz, 1H), 8.57 (d, J = 8.4 Hz, 1H), 8.41 (t, 1H), 8.27 (d, J = 2.3 Hz, 1H), 7.94 (dd, J = 8.4, 2.3 Hz, 1H), 4.74 (s, 3H). ^{19}F NMR (471 MHz, Acetone) δ -71.74, -73.24, -79.32.

R= CF_3 (white solid, quant. yield). ^{19}F NMR (471 MHz, Acetone-d_6) δ -63.79, -71.90, -73.41.

R= H (white solid, quant. yield). ^{1}H NMR (500 MHz, Acetone-d_6) δ 9.32 (s, 1H), 9.07 (d, J = 6.1 Hz, 1H), 8.80 (d, J = 8.1 Hz, 1H), 8.29 (dd, J = 8.2, 6.2 Hz, 1H), 8.02 (d, J = 8.0 Hz, 1H), 7.71 (dd, J = 7.8, 1.6 Hz, 1H), 7.54 (t, J = 7.6 Hz, 1H), 7.28 (td, J = 7.7, 1.6 Hz, 1H), 4.65 (s, 3H). ^{13}C NMR (126 MHz, Acetone) δ 148.34, 147.55, 145.97, 140.09, 134.29, 132.54, 129.45, 129.12, 128.23, 124.80, 101.12, 99.26, 85.80, 49.52. ^{19}F NMR (471 MHz, Acetone) δ -71.64, -73.14.

R= *t*Bu (white solid, quant. yield). ^{1}H NMR (500 MHz, Acetone-*d*6) δ 9.34 (s, 1H), 9.09 (d, J = 6.1 Hz, 1H), 8.81 (d, J = 8.1 Hz, 1H), 8.33 – 8.25 (m, 1H), 7.93 (d, J = 8.4 Hz, 1H), 7.73 (d, J = 2.5 Hz, 1H), 7.36 (dd, J = 8.5, 2.5 Hz, 1H), 4.67 (s, 3H), 1.33 (s, 9H)). ^{13}C NMR (126 MHz, Acetone) δ 152.86, 148.37, 147.55, 145.95, 139.79, 131.41, 130.25, 129.14, 127.88, 124.92, 99.72, 97.43, 85.30, 49.54, 35.27, 31.12. ^{19}F NMR (471 MHz, Acetone) δ -71.91, -73.41.

Titrations

General Methods. ^{1}H NMR spectra were acquired at room temperature on a Varian Inova 500 MHz spectrometer (500.11 MHz). ^{1}H chemical shifts (δ) are expressed in ppm relative to residual CH_3CN (calibrated to 1.94 ppm) shifts.

General Procedure. A 4.0 mL host solution (0.9-1.5 mM in CD_3CN) was prepared. Of this, 500 μL was added to a septum-sealed NMR tube. A 19-30 mM host/guest (TBAX, where X = I, Br, or Cl) stock solution was prepared using the remaining 3.5 mL of host

solution. Aliquots of the host/guest solution were added to the NMR tube using Hamilton gas-tight syringes, and ^{1}H NMR spectra were recorded at 25 °C after each addition of guest. The Δδ of the CH_{aryl} and CH_{methyl} protons were used to follow the progress of the titration, and association constants were determined using the Thordarson method.

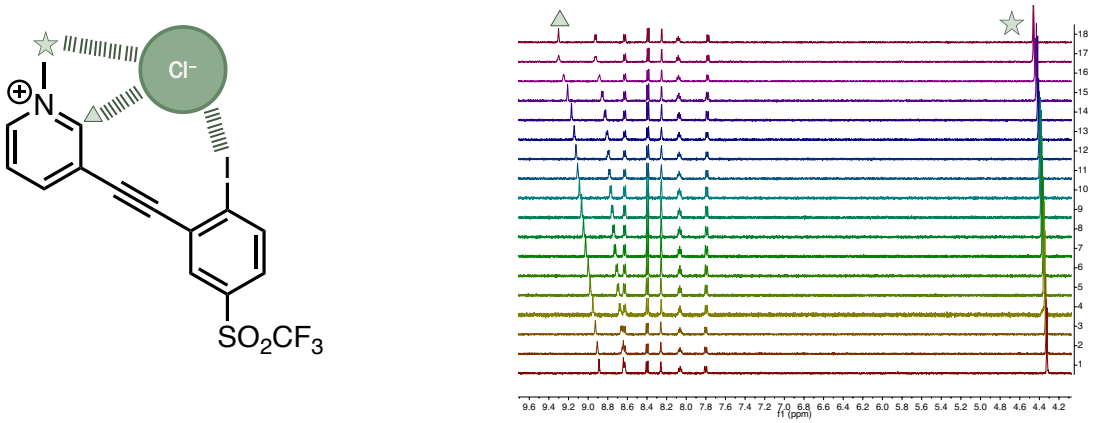

Figure B.1. Representative ^{1}H NMR titration done in CD_3CN with **5a** where participating protons can be seen shifting with increasing chloride concentration.

Table B.1. Representative ^{1}H NMR Titration of **5a • PF6**$^-$ with I^- in CD_3CN at 25 ºC.

Entry	V_{Guest} (µL)	[Host] (M)	[I^-] (M)	Equiv.	δ CH_{aryl}	δ CH_{methyl}
0	0	1.32E-03	0.00E+00	0.00	8.888	4.322
1	5	1.32E-03	2.08E-04	0.16	8.892	4.324
2	5	1.32E-03	4.11E-04	0.31	8.897	4.326
3	10	1.32E-03	8.06E-04	0.61	8.905	4.329
4	10	1.32E-03	1.19E-03	0.90	8.912	4.332
5	10	1.32E-03	1.55E-03	1.18	8.918	4.334
6	15	1.32E-03	2.08E-03	1.58	8.928	4.339
7	15	1.32E-03	2.57E-03	1.95	8.934	4.340
8	15	1.32E-03	3.05E-03	2.31	8.940	4.343

9	20	1.32E-03	3.64E-03	2.76	8.947	4.346
10	20	1.32E-03	4.19E-03	3.18	8.954	4.349
11	20	1.32E-03	4.71E-03	3.57	8.960	4.351
12	30	1.32E-03	5.44E-03	4.12	8.967	4.354
13	50	1.32E-03	6.51E-03	4.93	8.978	4.359
14	100	1.32E-03	8.26E-03	6.26	8.992	4.364
15	200	1.32E-03	1.07E-02	8.14	9.008	4.371
16	500	1.32E-03	1.41E-02	10.68	9.016	4.375
17	500	1.32E-03	1.58E-02	11.97	9.028	4.379
18	500	1.32E-03	1.68E-02	12.75	9.035	4.381

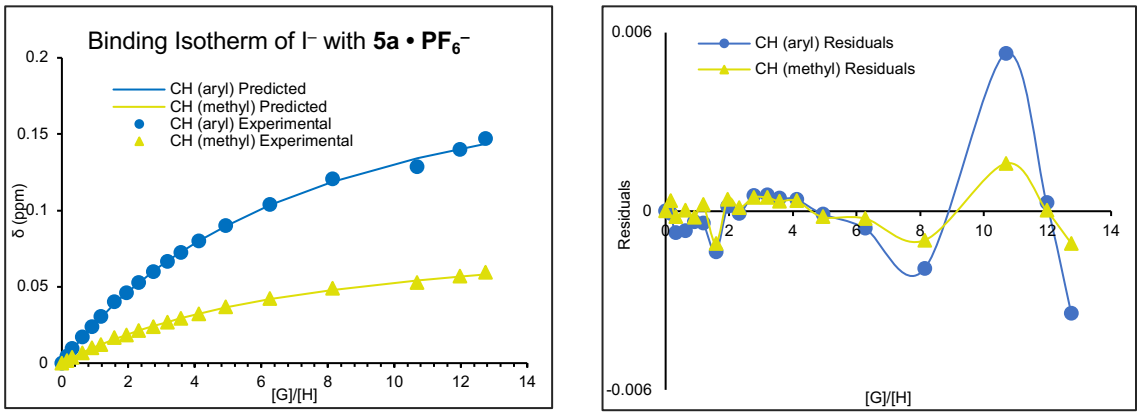

Figure B.2. Representative binding isotherm and residuals for I^- titration of receptor **5a • PF_6^-** in CD_3CN at 25 °C determined by ^1H NMR spectroscopy.

Table B.2. Representative ^1H NMR Titration of **5a • PF6**$^-$ with Br^- in CD_3CN at 25 ºC.

Entry	V_{Guest} (µL)	[Host] (M)	[Br^-] (M)	Equiv.	δ CH_{aryl}	δ CH_{methyl}
0	0	1.25E-03	0.00E+00	0.00	8.888	4.323
1	5	1.25E-03	2.34E-04	0.19	8.896	4.326
2	5	1.25E-03	4.64E-04	0.37	8.905	4.329
3	10	1.25E-03	9.10E-04	0.73	8.922	4.335
4	10	1.25E-03	1.34E-03	1.07	8.938	4.341
5	10	1.25E-03	1.75E-03	1.40	8.951	4.345

6	15	1.25E-03	2.35E-03	1.87	8.967	4.351
7	15	1.25E-03	2.91E-03	2.32	8.982	4.357
8	15	1.25E-03	3.44E-03	2.75	8.994	4.361
9	20	1.25E-03	4.11E-03	3.28	9.008	4.366
10	20	1.25E-03	4.73E-03	3.78	9.022	4.371
11	20	1.25E-03	5.32E-03	4.25	9.033	4.375
12	30	1.25E-03	6.14E-03	4.90	9.047	4.381
13	50	1.25E-03	7.35E-03	5.87	9.065	4.387
14	100	1.25E-03	9.32E-03	7.45	9.093	4.398
15	200	1.25E-03	1.21E-02	9.68	9.124	4.408
16	500	1.25E-03	1.59E-02	12.71	9.157	4.420
17	500	1.25E-03	1.78E-02	14.24	9.160	4.422

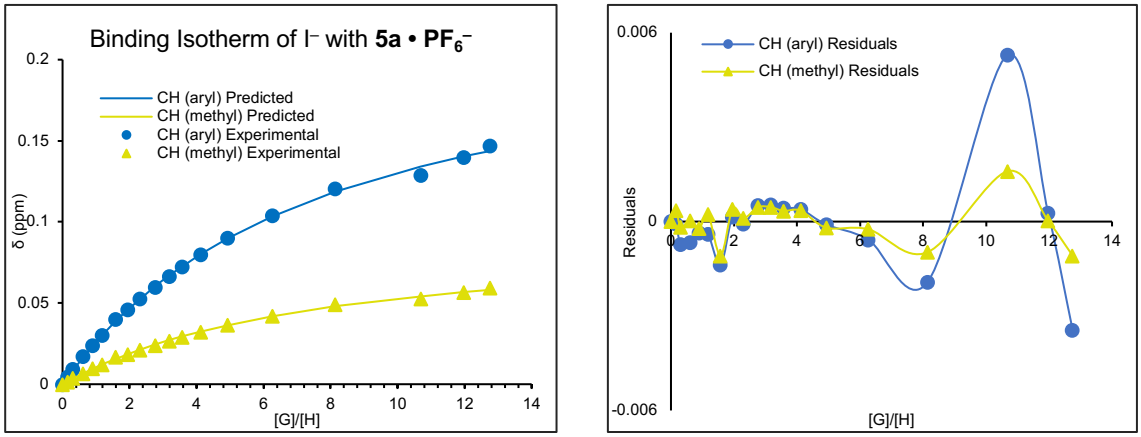

Figure B.3. Representative binding isotherm and residuals for Br^- titration of receptor **5a • PF_6^-** in CD_3CN at 25 °C determined by ^1H NMR spectroscopy.

Table B.3. Representative ^1H NMR Titration of **5a • PF6**$^-$ with Cl^- in CD_3CN at 25 ºC.

Entry	V_{Guest} (µL)	[Host] (M)	[Cl^-] (M)	Equiv.	δ CH_{aryl}	δ CH_{methyl}
0	0	9.58E-04	0.00E+00	0.00	8.887	4.322
1	5	9.58E-04	1.99E-04	0.21	8.905	4.328

2	5	9.58E-04	3.93E-04	0.41	8.911	4.330
3	10	9.58E-04	7.72E-04	0.81	8.941	4.340
4	10	9.58E-04	1.14E-03	1.19	8.957	4.346
5	10	9.58E-04	1.49E-03	1.55	8.972	4.351
6	15	9.58E-04	1.99E-03	2.08	9.006	4.362
7	15	9.58E-04	2.46E-03	2.57	9.019	4.367
8	15	9.58E-04	2.91E-03	3.04	9.037	4.372
9	20	9.58E-04	3.48E-03	3.63	9.057	4.380
10	20	9.58E-04	4.01E-03	4.19	9.079	4.386
11	20	9.58E-04	4.51E-03	4.71	9.090	4.390
12	30	9.58E-04	5.20E-03	5.43	9.108	4.396
13	50	9.58E-04	6.23E-03	6.50	9.134	4.405
14	100	9.58E-04	7.90E-03	8.25	9.170	4.417
15	200	9.58E-04	1.03E-02	10.73	9.205	4.429
16	500	9.58E-04	1.35E-02	14.08	9.262	4.449
17	500	9.58E-04	1.51E-02	15.77	9.263	4.448

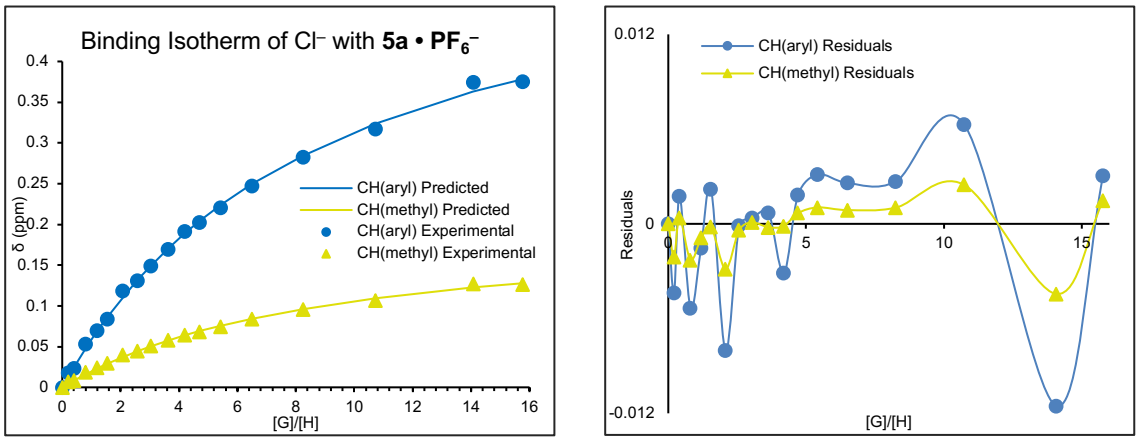

Figure B.4. Representative binding isotherm and residuals for Cl^- titration of receptor **5a** • **PF_6^-** in CD_3CN at 25 °C determined by ^1H NMR spectroscopy.

Table B.4. Representative ^{1}H NMR Titration of **5b • PF6**$^{-}$ with Cl^{-} in CD_3CN at 25 ºC.

Entry	V_{Guest} (μL)	[Host] (M)	[Cl^{-}] (M)	Equiv.	δ CH_{aryl}	δ CH_{methyl}
0	0	1.35E-03	0.00E+00	0.00	8.864	4.318
1	5	1.35E-03	2.46E-04	0.18	8.874	4.322
2	5	1.35E-03	4.88E-04	0.36	8.888	4.327
3	10	1.35E-03	9.57E-04	0.71	8.911	4.335
4	10	1.35E-03	1.41E-03	1.04	8.932	4.342
5	10	1.35E-03	1.84E-03	1.37	8.951	4.349
6	15	1.35E-03	2.47E-03	1.83	8.974	4.357
7	15	1.35E-03	3.06E-03	2.26	8.993	4.364
8	15	1.35E-03	3.62E-03	2.68	9.010	4.370
9	20	1.35E-03	4.32E-03	3.20	9.029	4.376
10	20	1.35E-03	4.98E-03	3.69	9.045	4.382
11	20	1.35E-03	5.59E-03	4.14	9.060	4.387
12	30	1.35E-03	6.45E-03	4.78	9.079	4.394
13	50	1.35E-03	7.72E-03	5.72	9.106	4.403
14	100	1.35E-03	9.80E-03	7.26	9.140	4.415
15	200	1.35E-03	1.27E-02	9.44	9.176	4.428
16	500	1.35E-03	1.67E-02	12.39	9.192	4.434
17	500	1.35E-03	1.87E-02	13.88	9.217	4.442

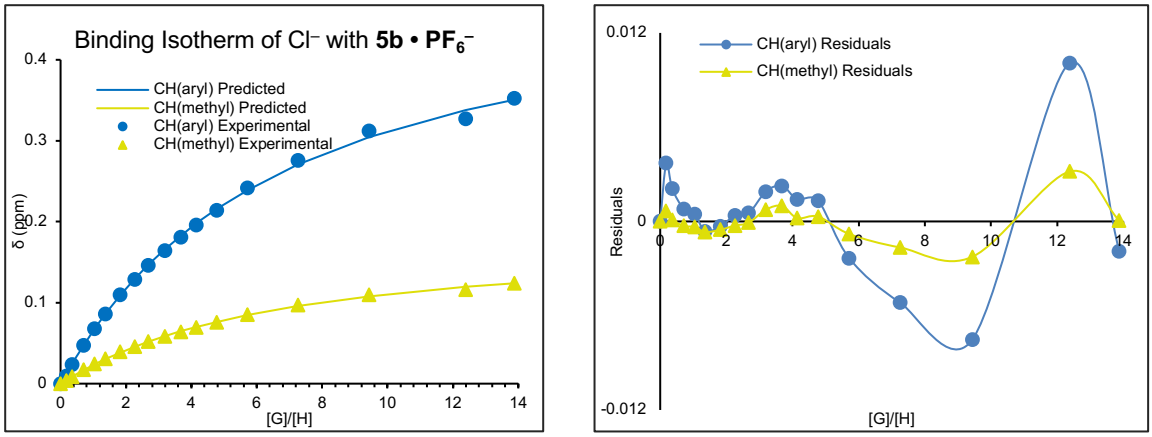

Figure B.5. Representative binding isotherm and residuals for Cl^- titration of receptor **5b • PF_6^-** in CD_3CN at 25 °C determined by ^1H NMR spectroscopy.

Table B.5. Representative ^1H NMR Titration of **5c • PF6⁻** with Cl^- in CD_3CN at 25 ºC.

Entry	V_{Guest} (µL)	[Host] (M)	[Cl^-] (M)	Equiv.	δ CH_{aryl}	δ CH_{methyl}
0	0	1.36E-03	0.00E+00	0.00	8.838	4.309
1	5	1.36E-03	2.45E-04	0.18	8.847	4.312
2	5	1.36E-03	4.85E-04	0.36	8.857	4.316
3	10	1.36E-03	9.52E-04	0.70	8.877	4.324
4	10	1.36E-03	1.40E-03	1.03	8.891	4.330
5	10	1.36E-03	1.83E-03	1.35	8.907	4.336
6	15	1.36E-03	2.45E-03	1.80	8.918	4.340
7	15	1.36E-03	3.04E-03	2.23	8.941	4.348
8	15	1.36E-03	3.60E-03	2.64	8.954	4.354
9	20	1.36E-03	4.29E-03	3.16	8.969	4.359
10	20	1.36E-03	4.95E-03	3.64	8.982	4.363
11	20	1.36E-03	5.56E-03	4.09	8.997	4.371
12	30	1.36E-03	6.41E-03	4.72	9.013	4.377
13	50	1.36E-03	7.68E-03	5.65	9.034	4.384
14	100	1.36E-03	9.75E-03	7.17	9.064	4.397
15	200	1.36E-03	1.27E-02	9.32	9.094	4.405

16	500	1.36E-03	1.66E-02	12.23	9.138	4.424
17	500	1.36E-03	1.86E-02	13.70	9.142	4.425

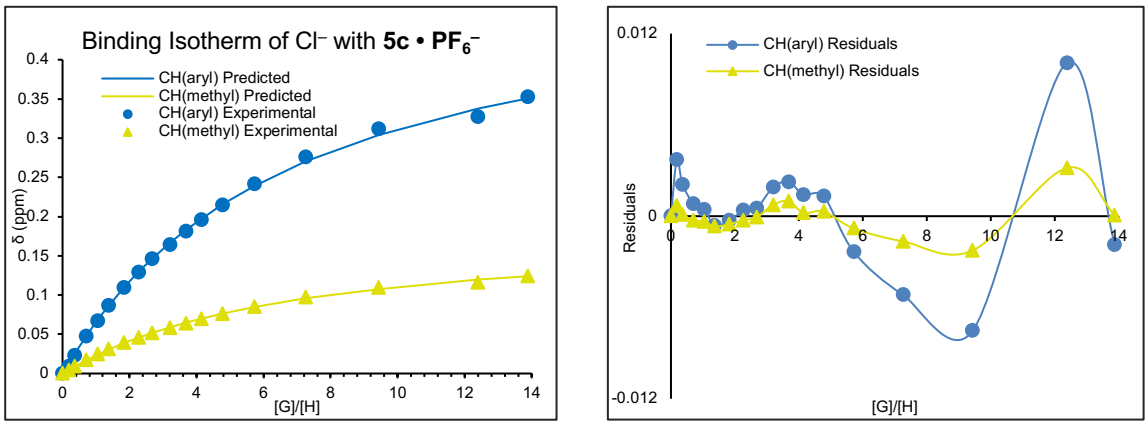

Figure B.6. Representative binding isotherm and residuals for Cl^- titration of receptor **5c • PF_6^-** in CD_3CN at 25 °C determined by ^1H NMR spectroscopy.

Table B.6. Representative ^1H NMR Titration of **5d • PF6⁻** with Cl^- in CD_3CN at 25 ºC.

Entry	V_{Guest} (µL)	[Host] (M)	[Cl^-] (M)	Equiv.	δ CH_{aryl}	δ CH_{methyl}
0	0	1.73E-03	0.00E+00	0.00	8.828	4.310
1	5	1.73E-03	2.33E-04	0.14	8.834	4.312
2	5	1.73E-03	4.62E-04	0.27	8.843	4.316
3	10	1.73E-03	9.07E-04	0.53	8.859	4.322
4	10	1.73E-03	1.33E-03	0.77	8.873	4.328
5	10	1.73E-03	1.75E-03	1.01	8.885	4.333
6	15	1.73E-03	2.34E-03	1.35	8.903	4.340
7	15	1.73E-03	2.90E-03	1.68	8.917	4.345
8	15	1.73E-03	3.43E-03	1.98	8.929	4.350
9	20	1.73E-03	4.09E-03	2.37	8.944	4.356
10	20	1.73E-03	4.72E-03	2.73	8.958	4.361
11	20	1.73E-03	5.30E-03	3.07	8.970	4.366
12	30	1.73E-03	6.11E-03	3.54	8.985	4.372
13	50	1.73E-03	7.32E-03	4.24	9.006	4.380

14	100	1.73E-03	9.29E-03	5.38	9.037	4.392
15	200	1.73E-03	1.21E-02	6.99	9.078	4.407
16	500	1.73E-03	1.58E-02	9.18	9.106	4.418
17	500	1.73E-03	1.78E-02	10.28	9.110	4.419

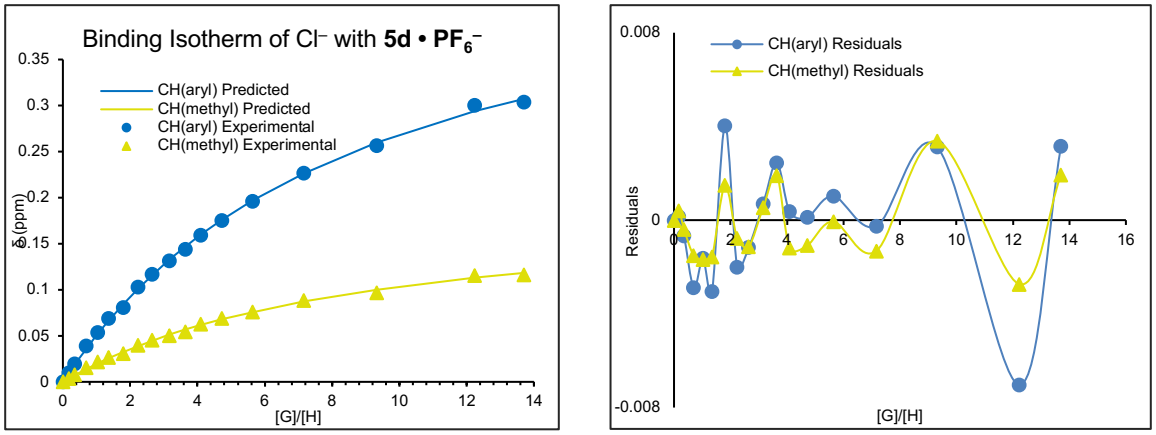

Figure B.7. Representative binding isotherm and residuals for Cl^- titration of receptor **5d** • $\mathbf{PF_6^-}$ in CD_3CN at 25 °C determined by ^1H NMR spectroscopy.

Linear Regression Fitting and Statistics of log(KaR/KaH) and σ_p

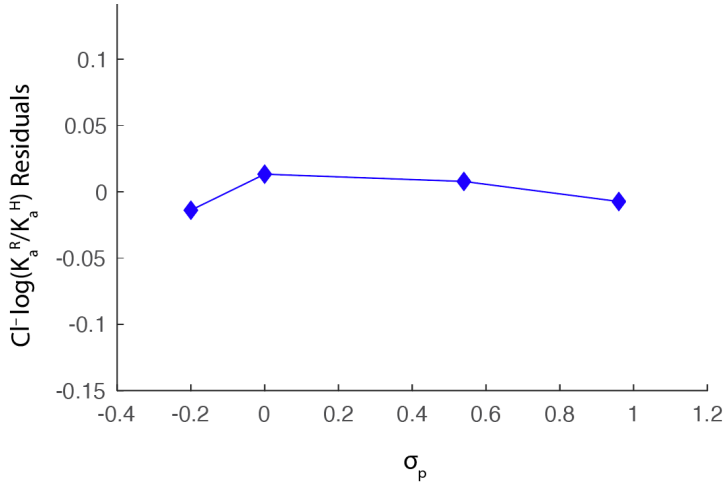

Figure B.8. Linear regression residuals of $\log(K_a^R/K_a^H)$ of Cl^- and σ_p.

X-Ray Crystallography

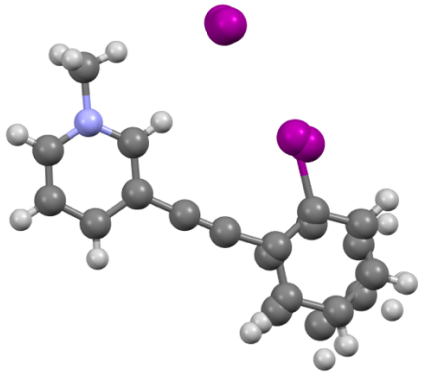

Figure B.9. Disordered crystal structure of **5c** binding to $\mathbf{I}^-$. C–H_{aryl} -- I^- bond distance is 3.172 Å; C–H_{methyl} -- I^- bond distance is 3.098 Å; C–I -- I^- bond distance is 3.656 Å.

X-ray Crystallography. X-ray diffraction intensities for **5a • Cl**$^-$, **5d • I**$^-$, **5c • I**$^-$, **5b • I**$^-$ and **5a • I**$^-$ were collected at 173 K on a Bruker Apex2 CCD DUO diffractometer using CuKα and MoKα (**5a • I**$^-$) radiation, 1.54178 Å and 0.71073 Å, respectively. Space groups were determined based on systematic absences. Absorption corrections were applied by SADABS.[1] Structures were solved by direct methods and Fourier techniques and refined on F^2 using full matrix least-squares procedures. All non-H atoms were refined with anisotropic thermal parameters except of the C atoms in the disordered C_6-ring in **5c • I**$^-$ which were refined with isotropic thermal parameters. H atoms in **5a • Cl**$^-$ were found on the residual density map. H atoms in other structures were refined in calculated positions in a rigid group model. The crystal structure of **5a • Cl**$^-$ includes an additional solvent water molecule. The cation in **5c • I**$^-$ is located on a mirror plane and its C_6H_4I fragment is disordered over two positions in ratio 0.5507/0.4493. This fragment was refined with restriction on its geometry; it was refined as a flat group and the value of 1.39 Å was used as the target for C-C bonds in this group in refinement. The I atom in this group was refined with anisotropic thermal parameters and the C atoms were refined with isotropic thermal parameters. The isolated anion I(-) is also disordered over three positions; one is located on a mirror plane and two others are slightly out of the mirror plane. Refinement shown that occupation factor for the I(-) located on the mirror plane is close to 0.3 and occupation factor for two other positions is close to 0.2. Occupation

factors for the I atom in these positions have been fixed at these values in the final refinement. Refinement of **5c • I**$^{-}$ doesn't show good convergence and it indicates that above-mentioned fragments seem to be disordered not over two or three positions but inside small areas in the structure. Cations and anions in all structures are connected in the packing via extended network of H-bonds. All calculations were performed by the Bruker SHELXL-2014/7 package.[2]

Crystallographic Data for ***5a • I***$^{-}$: $C_{15}H_{10}F_3I_2NO_2S$, M = 579.10, 0.20 x 0.06 x 0.01 mm, T = 173(2) K, Monolinic, space group $P2_1/c$, a = 6.0579(6) Å, b = 37.243(4) Å, c = 8.0583(8) Å, β = 90.834(2)°, V = 1817.9(3) Å^3, Z = 4, Dc = 2.116 Mg/m^3, μ(Mo) = 3.611 mm^{-1}, F(000) = 1088, $2\theta_{max}$ = 50.0°, 16280 reflections, 3196 independent reflections [R_{int} = 0.0729], R1 = 0.0410, wR2 = 0.1125 and GOF = 1.007 for 3196 reflections (217 parameters) with I>2σ(I), R1 = 0.0477, wR2 = 0.1173 and GOF = 1.007 for all reflections, max/min residual electron density +1.790/-1.405 eÅ^{-3}.

Crystallographic Data for ***5a • Cl***$^{-}$: $C_{15}H_{12}ClF_3INO_3S$, M = 505.67, 0.09 x 0.04 x 0.03 mm, T = 173(2) K, Monolinic, space group $P2_1/n$, a = 7.7083(3) Å, b = 5.9634(3) Å, c = 39.0065(15) Å, β = 93.725(2)°, V = 1789.25(13) Å^3, Z = 4, Dc = 1.877 Mg/m^3, μ(Cu) = 16.956 mm^{-1}, F(000) = 984, $2\theta_{max}$ = 133.56°, 10598 reflections, 3156 independent reflections [R_{int} = 0.0398], R1 = 0.0326, wR2 = 0.0832 and GOF = 1.096 for 3156 reflections (274 parameters) with I>2σ(I), R1 = 0.0332, wR2 = 0.0837 and GOF = 1.096 for all reflections, max/min residual electron density +1.013/-0.767 eÅ^{-3}.

Crystallographic Data for ***5d • I***$^{-}$: $C_{18}H_{19}I_2N$, M = 503.14, 0.11 x 0.02 x 0.01 mm, T = 173(2) K, Orthorhombic, space group $Pna2_1$, a = 8.2589(3) Å, b = 37.1653(14) Å, c = 6.0428(2) Å, V = 1854.80(11) Å^3, Z = 4, Dc = 1.802 Mg/m^3, μ(Cu) = 26.570 mm^{-1}, F(000) = 960, $2\theta_{max}$ = 133.84°, 10517 reflections, 3183 independent reflections [R_{int} = 0.0571], R1 = 0.0410, wR2 = 0.1006 and GOF = 1.021 for 3183 reflections (190 parameters) with I>2σ(I), R1 = 0.0472, wR2 = 0.1038 and GOF = 1.021 for all reflections, Flack = 0.034(13), max/min residual electron density +1.215/-0.505 eÅ^{-3}.

Crystallographic Data for ***5c • I***$^{-}$: $C_{14}H_{11}I_2N$, M = 447.04, 0.06 x 0.04 x 0.03 mm, T = 173(2) K, Orthorhombic, space group *Pnma*, *a* = 17.2706(9) Å, *b* = 6.5898(6) Å, *c* = 12.9492(9) Å, *V* = 1473.75(19) Å^3, *Z* = 4, *D*c = 2.015 Mg/m^3, μ(Cu) = 33.341 mm^{-1}, F(000) = 832, $2\theta_{max}$ = 133.24°, 8134 reflections, 1413 independent reflections [R_{int} = 0.0551], R1 = 0.0374, wR2 = 0.0976 and GOF = 1.072 for 1413 reflections (138 parameters) with I>2σ(I), R1 = 0.0416, wR2 = 0.1005 and GOF = 1.091 for all reflections, max/min residual electron density +1.436/-0.526 eÅ^{-3}.

Crystallographic Data for ***5b • I***$^{-}$: $C_{15}H_{10}F_3I_2N$, M = 515.04, 0.08 x 0.05 x 0.01 mm, T = 173(2) K, Monolinic, space group $P2_1/n$, *a* = 7.2021(2) Å, *b* = 22.8379(7) Å, *c* = 10.2666(3) Å, β = 102.938(2)°, *V* = 1645.79(8) Å^3, *Z* = 4, *D*c = 2.079 Mg/m^3, μ(Cu) = 30.240 mm^{-1}, F(000) = 960, $2\theta_{max}$ = 133.71°, 8804 reflections, 2924 independent reflections [R_{int} = 0.0585], R1 = 0.0454, wR2 = 0.1143 and GOF = 1.080 for 2924 reflections (190 parameters) with I>2σ(I), R1 = 0.0479, wR2 = 0.1165 and GOF = 1.080 for all reflections, max/min residual electron density +1.709/-1.022 eÅ^{-3}.

Computational Details

General. Gas phase optimization and frequency analyses were performed for structures **4a-d** and **5a-d** via Gaussian 09.[3] All computations were ran using B97-D3 density functional theory[4] with a Def2-TZVP basis set.[5] This work utilized the resources of the University of Oregon's high-performance computer, Talapas. Electrostatic potential surface (ESP) maps and figures were generated using Gaussian 09. The σ–hole values ($V_{S,max}$) were assessed using Multiwfn, an open-source software.[6]

Table B.7. Cartesian coordinates for **5a**.

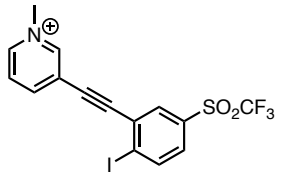

	X	Y	Z
H	0.56677	3.82829	-1.70301
C	0.47593	2.87918	-1.18175
C	0.35303	0.46906	0.15123
C	-0.729	2.18606	-1.13094
C	-0.7917	0.97061	-0.45739
C	1.5382	1.19649	0.07591
H	-1.61602	2.58904	-1.61598
H	-1.73203	0.42135	-0.415
C	0.3235	-0.77869	0.84392
C	0.32554	-1.82742	1.43
C	0.34676	-3.08209	2.12455
C	0.31521	-5.58703	3.40306
C	-0.70468	-3.97748	1.89278
C	1.37881	-3.44364	3.00595
C	1.36104	-4.69326	3.64051
C	-0.71983	-5.21743	2.54135
H	-1.50099	-3.71063	1.19888
H	2.16216	-4.9904	4.31555
H	0.32672	-6.56422	3.88476
I	3.00298	-2.17607	3.42256
S	-2.03813	-6.37912	2.20256
O	-2.68494	-5.90191	0.98831
O	-1.41507	-7.69345	2.21649
C	-3.12485	-6.14675	3.64653

F	-4.24422	-6.91894	3.59412
F	-2.49414	-6.44563	4.81836
F	-3.54626	-4.85335	3.76174
N	1.57981	2.38196	-0.57785
C	2.85121	3.122	-0.65002
H	3.38779	2.99487	0.29388
H	2.64531	4.18346	-0.80889
H	3.42333	2.70879	-1.4843
H	2.46056	0.84427	0.53021

Table B.8. Cartesian coordinates for **5b**.

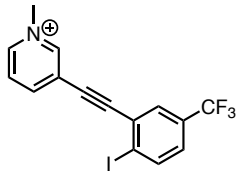

	X	Y	Z
H	-1.53275	3.76493	-1.78037
C	-1.38771	2.79981	-1.30259
C	-1.01487	0.40151	0.00457
C	-1.15997	1.64474	-2.04358
C	-0.97322	0.43414	-1.38441
C	-1.24573	1.58185	0.70669
H	-1.12618	1.68659	-3.13058
H	-0.79381	-0.47476	-1.9582
C	-0.82222	-0.8228	0.71243
C	-0.66365	-1.83578	1.33849
C	-0.47692	-3.03151	2.10796
C	-0.10428	-5.43182	3.51025
C	-0.25728	-4.23164	1.41783
C	-0.50752	-3.04179	3.50985

C	-0.32245	-4.24067	4.2072
C	-0.06163	-5.43967	2.10936
H	-0.23499	-4.23489	0.32754
H	-0.34636	-4.26692	5.29513
H	0.03456	-6.35798	4.06876
I	-0.82882	-1.30413	4.64765
N	-1.43308	2.75067	0.04866
C	-1.66487	3.9834	0.82046
H	-2.27816	3.74318	1.69296
H	-2.19203	4.70953	0.19661
H	-0.688	4.36885	1.12262
C	0.15158	-6.72706	1.34718
F	0.87956	-6.54656	0.21043
F	-1.02302	-7.28983	0.95554
F	0.80825	-7.67594	2.06716
H	-1.2821	1.60883	1.7926

Table B.9. Cartesian coordinates for **5c**.

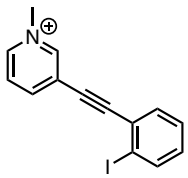

	X	**Y**	**Z**
H	-0.50817	4.43527	-1.02704
C	-0.48071	3.41393	-0.65688
C	-0.29988	0.84185	0.31428
C	-1.55026	2.54177	-0.82891
C	-1.45968	1.24356	-0.33803
C	0.74749	1.74798	0.46379
H	-2.45066	2.87027	-1.3443

H	-2.29234	0.553	-0.46944
C	-0.17051	-0.48405	0.82552
C	-0.01911	-1.59256	1.26293
C	0.19677	-2.90886	1.78928
C	0.50705	-5.50189	2.8093
C	-0.91261	-3.75041	1.94049
C	1.46802	-3.37775	2.155
C	1.62015	-4.67304	2.66367
C	-0.75745	-5.0417	2.44871
H	-1.90818	-3.40942	1.66417
H	2.59794	-5.05314	2.9514
H	0.62686	-6.50848	3.20466
I	3.20272	-2.2032	1.9755
N	0.64043	3.00945	-0.01598
C	1.75685	3.95646	0.14343
H	2.49346	3.55124	0.84114
H	1.35543	4.89386	0.53772
H	2.20639	4.10522	-0.84168
H	-1.62362	-5.68993	2.56328
H	1.67384	1.47574	0.96261

Table B.10. Cartesian coordinates for **5d**.

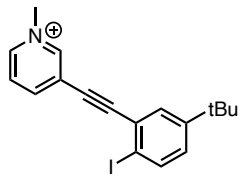

	X	**Y**	**Z**
H	-0.54887	4.16441	-0.7044
C	-0.51057	3.13011	-0.3736

C	-0.31151	0.52189	0.49514
C	-1.654	2.34004	-0.31213
C	-1.55373	1.02329	0.12489
C	0.80703	1.34771	0.41795
H	-2.62042	2.74803	-0.6018
H	-2.44459	0.39789	0.17638
C	-0.17184	-0.8223	0.9528
C	-0.01105	-1.94687	1.34322
C	0.21552	-3.28282	1.81312
C	0.52861	-5.91198	2.71504
C	-0.88599	-4.14825	1.90275
C	1.48227	-3.74708	2.18082
C	1.63549	-5.05929	2.63044
C	-0.75653	-5.47874	2.35418
H	-1.86683	-3.77401	1.61326
H	2.61127	-5.44248	2.92192
H	0.7066	-6.9238	3.07203
I	3.20389	-2.5473	2.09002
N	0.69275	2.6251	-0.01688
C	1.89375	3.47511	-0.07706
H	2.06597	3.87004	0.9272
H	1.73022	4.28734	-0.78969
H	2.73915	2.86676	-0.40925
C	-1.9942	-6.39185	2.43575
C	-2.62474	-6.53738	1.03391
H	-1.90222	-6.94502	0.31692
H	-2.97777	-5.57963	0.63624
H	-3.48855	-7.21207	1.05718
C	-3.03161	-5.77468	3.39845
H	-2.6044	-5.62872	4.39768

H	-3.90929	-6.42335	3.50238
H	-3.39314	-4.801	3.05015
C	-1.6871	-7.81715	2.94834
H	-1.26652	-7.80011	3.96056
H	-0.97955	-8.33808	2.29277
H	-2.59754	-8.42723	2.98847
H	1.79828	1.0032	0.70098

Table B.11. Cartesian coordinates for **4a**.

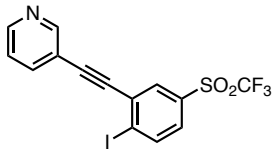

	X	Y	Z
H	0.12833	4.06952	-1.50739
C	0.09491	3.1812	-0.8827
C	0.03654	0.8788	0.59272
C	-0.17191	3.27212	0.47482
C	-0.20114	2.0976	1.22376
C	0.29564	0.89081	-0.77145
H	-0.3525	4.23526	0.93901
H	-0.40727	2.13987	2.28997
N	0.32942	2.01632	-1.52557
C	0.01373	-0.34359	1.33028
C	-0.00662	-1.36417	1.96397
C	-0.03199	-2.58061	2.72196
C	-0.07289	-5.02761	4.1081
C	-0.0645	-3.79005	2.01574
C	-0.0238	-2.60209	4.12583
C	-0.04077	-3.82364	4.81352
C	-0.09988	-5.0029	2.71216

H	-0.05583	-3.77896	0.92616
H	-0.02193	-3.8516	5.90152
H	-0.06927	-5.96817	4.65676
I	0.02064	-0.85142	5.2863
S	-0.11451	-6.54016	1.8013
O	0.52307	-6.25747	0.52367
O	0.46727	-7.53929	2.68596
C	-1.8991	-6.82928	1.58524
F	-2.16671	-7.97659	0.90112
F	-2.55334	-6.92652	2.7788
F	-2.50587	-5.81711	0.90043
H	0.48998	-0.02813	-1.31777

Table B.12. Cartesian coordinates for **4b**.

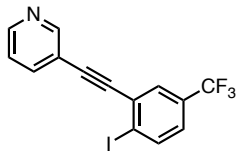

	X	**Y**	**Z**
H	-0.61441	3.63972	-1.96172
C	-0.53895	2.79105	-1.28756
C	-0.36464	0.58185	0.31563
C	-0.33555	2.97446	0.07163
C	-0.24718	1.84722	0.88575
C	-0.56718	0.50125	-1.05576
H	-0.24789	3.97198	0.48754
H	-0.08809	1.96166	1.95474
N	-0.65718	1.57898	-1.87258
C	-0.27887	-0.59429	1.12059
C	-0.20507	-1.57517	1.81055
C	-0.11666	-2.74377	2.63628

C	0.05041	-5.10381	4.14315
C	-0.18469	-3.99616	2.00876
C	0.03487	-2.68174	4.02822
C	0.11909	-3.86099	4.7776
C	-0.11009	-5.18559	2.7531
H	-0.29901	-4.04976	0.92543
H	0.24008	-3.82845	5.85847
H	0.12133	-6.01176	4.74169
I	0.14907	-0.86677	5.07889
C	-0.16172	-6.5257	2.05983
F	-0.94596	-6.51885	0.94655
F	1.06761	-6.94205	1.65112
F	-0.65058	-7.51908	2.853
H	-0.66647	-0.45794	-1.55648

Table B.13. Cartesian coordinates for **4c**.

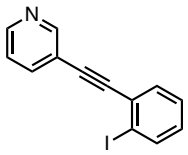

	X	**Y**	**Z**
H	-0.25865	3.86017	-1.8606
C	-0.23302	2.99815	-1.19981
C	-0.15813	0.75799	0.3676
C	-0.31725	3.15014	0.17583
C	-0.27884	2.00716	0.97164
C	-0.08068	0.70888	-1.01796
H	-0.41053	4.1356	0.61829
H	-0.34277	2.0964	2.05291
N	-0.11545	1.80251	-1.81792

C	-0.11516	-0.43375	1.15264
C	-0.07923	-1.42898	1.82488
C	-0.03577	-2.6154	2.6287
C	0.05698	-5.00698	4.09191
C	0.0479	-3.8504	1.97172
C	-0.07296	-2.58755	4.03035
C	-0.02645	-3.78348	4.75821
C	0.09408	-5.04084	2.70004
H	0.07779	-3.89261	0.88475
H	-0.0543	-3.77786	5.84527
H	0.093	-5.93357	4.65986
I	-0.19811	-0.80048	5.12778
H	0.15904	-5.9935	2.17987
H	0.01453	-0.23682	-1.54442

Table B.14. Cartesian coordinates for **4d**.

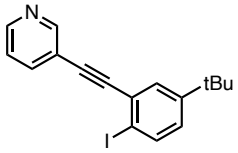

	X	**Y**	**Z**
H	-0.03841	3.62563	-1.89212
C	-0.03046	2.78586	-1.20288
C	-0.04513	0.60119	0.44255
C	0.31885	2.95765	0.12793
C	0.31043	1.84289	0.96365
C	-0.37971	0.53078	-0.90328
H	0.59119	3.93671	0.50593
H	0.57942	1.94808	2.01141
N	-0.3803	1.59676	-1.74051

C	-0.06423	-0.56177	1.27045
C	-0.07811	-1.53237	1.97848
C	-0.09364	-2.6899	2.82471
C	-0.13067	-5.03315	4.35472
C	-0.15686	-3.95149	2.21089
C	-0.0484	-2.6109	4.21911
C	-0.06724	-3.78194	4.97962
C	-0.17676	-5.1487	2.95721
H	-0.19087	-3.99424	1.12298
H	-0.033	-3.74219	6.06609
H	-0.1425	-5.90975	4.9973
I	0.04936	-0.78885	5.25586
C	-0.24619	-6.5068	2.23602
C	-1.534	-6.57894	1.38733
H	-1.5567	-5.8155	0.60201
H	-2.4252	-6.43685	2.0101
H	-1.62591	-7.55187	0.89045
C	0.98089	-6.66774	1.31281
H	1.01089	-5.90612	0.52599
H	0.97446	-7.64367	0.81337
H	1.91516	-6.59015	1.88152
C	-0.26077	-7.7213	3.19174
H	0.64495	-7.7607	3.80811
H	-0.3107	-8.66344	2.63263
H	-1.12885	-7.69792	3.86082
H	-0.66609	-0.41026	-1.36486

References

(1) Sheldrick, G. M. *Bruker/Siemens Area Detector Absorption Correction Program*.

Bruker AXS, Madison, WI, 1998.

(2) Sheldrick, G. M. Crystal Structure Refinement with SHELXL. *Acta Crystallogr. Sect. C Struct. Chem.* **2015**, *71*, 3–8.

(3) Frisch, M. J.; Trucks, G. W.; Schlegel, H. B.; Scuseria, G. E.; Robb, M. A.; Cheeseman, R. J.; Scalmani, G.; Barone, V.; Mennucci, B.; Petersson, G. A.; et al. Gaussian 09, Revision E.01. Wallingford, CT 2013.

(4) Grimme, S.; Ehrlich, S.; Goerigk, L. Effect of the Damping Function in Dispersion Corrected Density Functional Theory. *J. Comput. Chem.* **2011**, *32*, 1456–1465.

(5) Weigend, F.; Ahlrichs, R. Balanced Basis Sets of Split Valence, Triple Zeta Valence and Quadruple Zeta Valence Quality for H to Rn: Design and Assessment of Accuracy. *Phys. Chem. Chem. Phys.* **2005**, *7*, 3297–3305.

(6) Lu, T.; Chen, F. Multiwfn: A Multifunctional Wavefunction Analyzer. *J. Comput. Chem.* **2012**, *33*, 580–592.

NMR Spectra

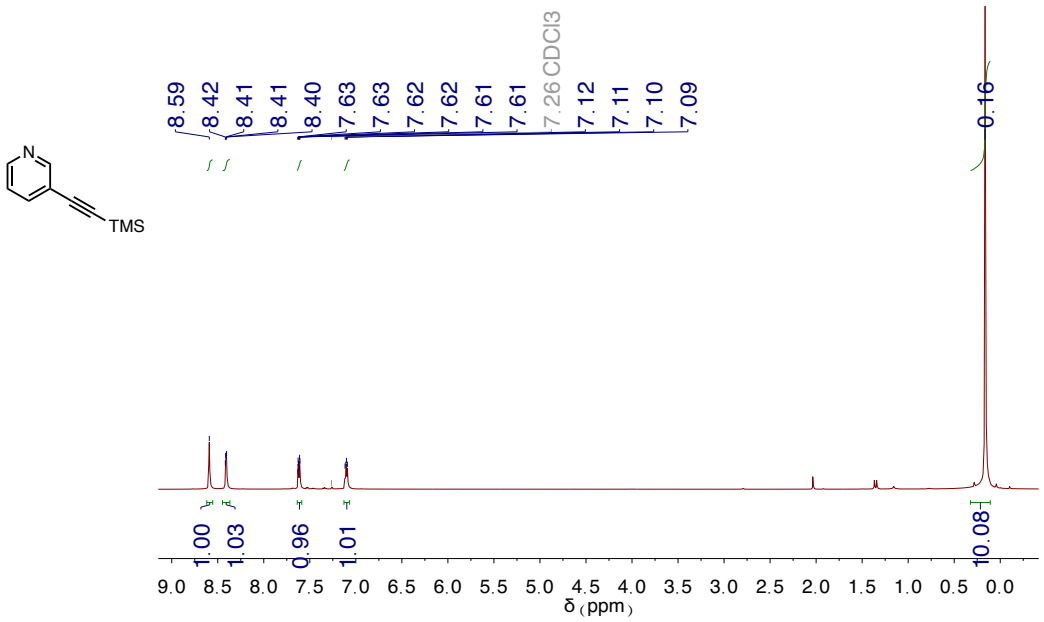

Figure B.10. ^{1}H NMR spectrum of TMS-protected 3-ethynylpyridine.

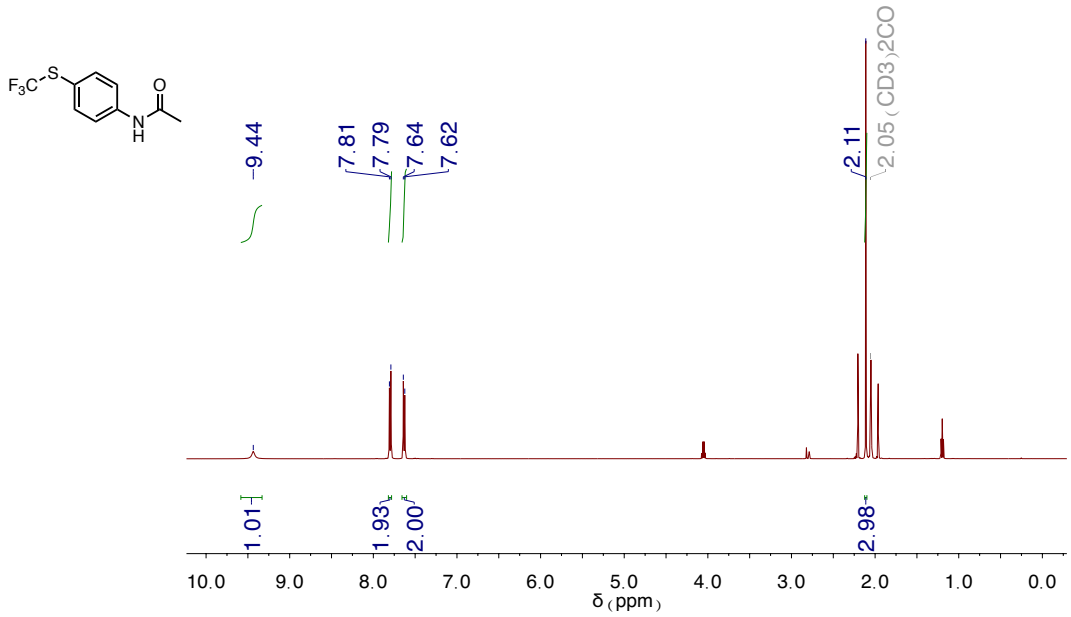

Figure B.11. [1]H NMR spectrum of 4-(trifluoromethylthio)acetamide. Wet with water and ethyl acetate.

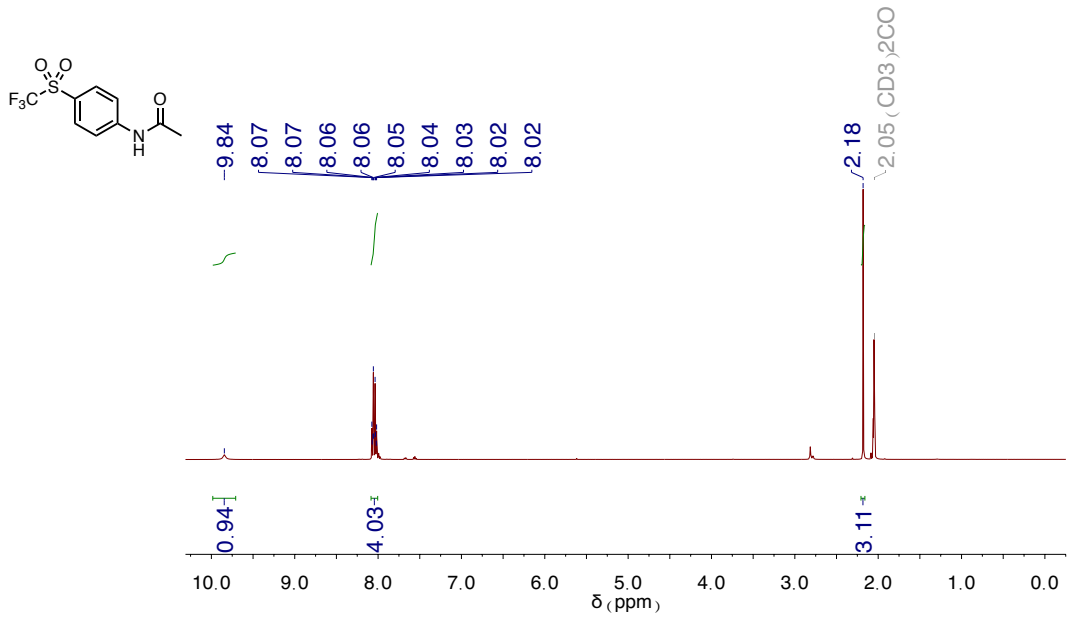

Figure B.12. [1]H NMR spectrum of N-[4-[(trifluoromethyl)sulfonyl]phenyl]acetamide.

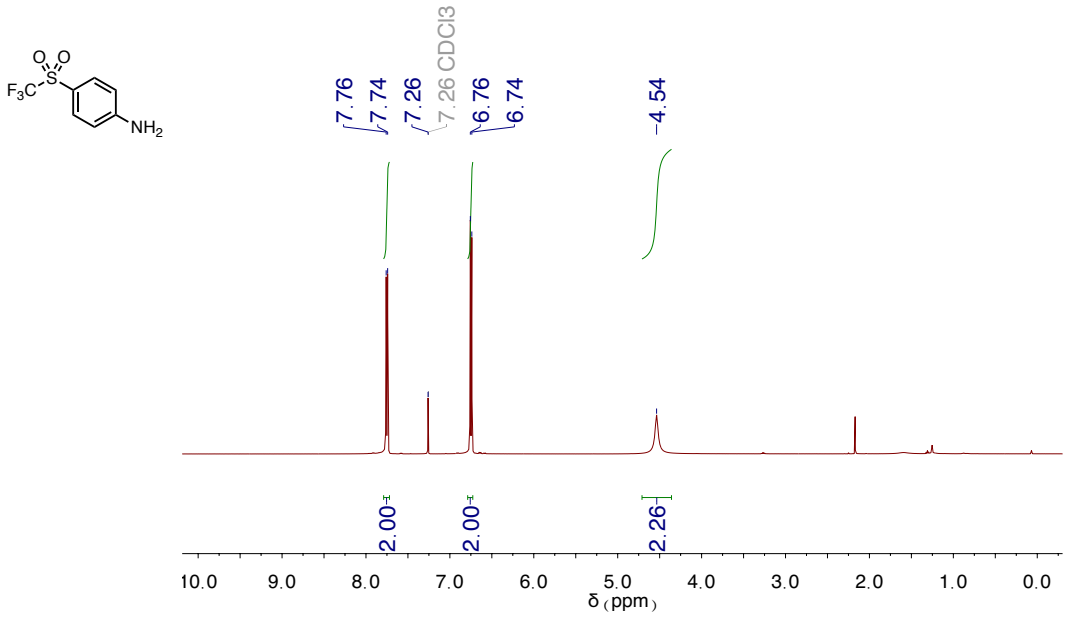

Figure B.13. ^{1}H NMR spectrum of N-[4-[(Trifluoromethyl)sulfonyl]phenyl]aniline.

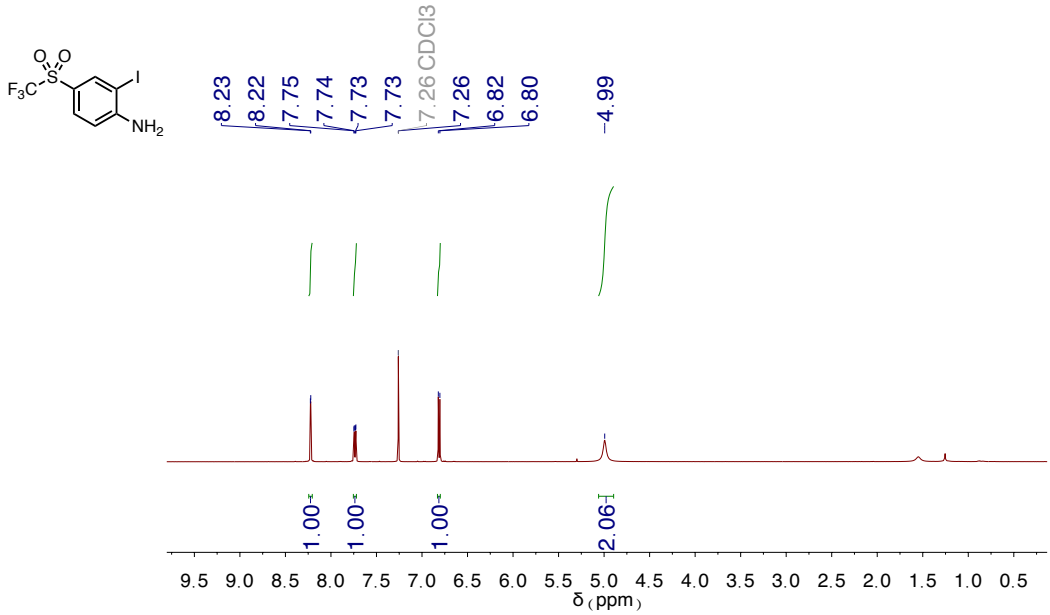

Figure B.14. ^{1}H NMR spectrum of **1a**.

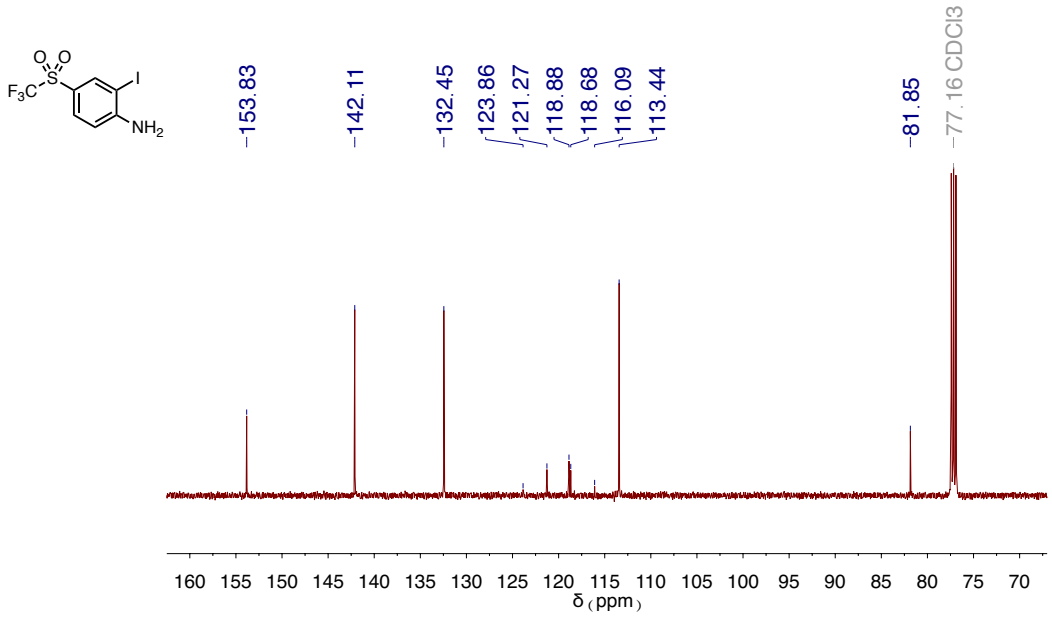

Figure B.15. ^{13}C NMR spectrum of **1a**.

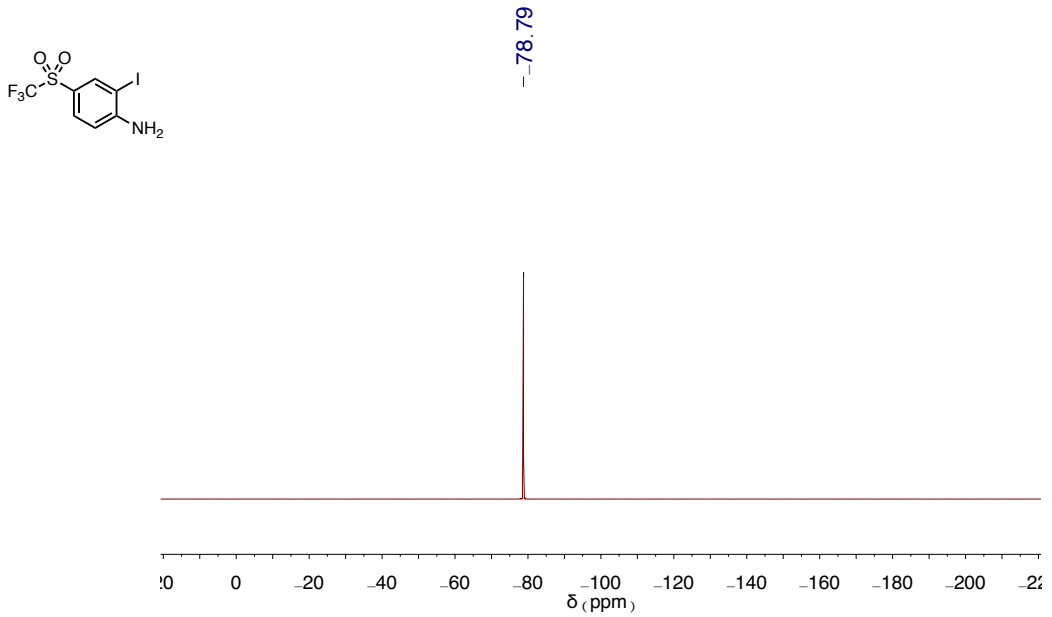

Figure B.16. ^{19}F NMR spectrum of **1a**.

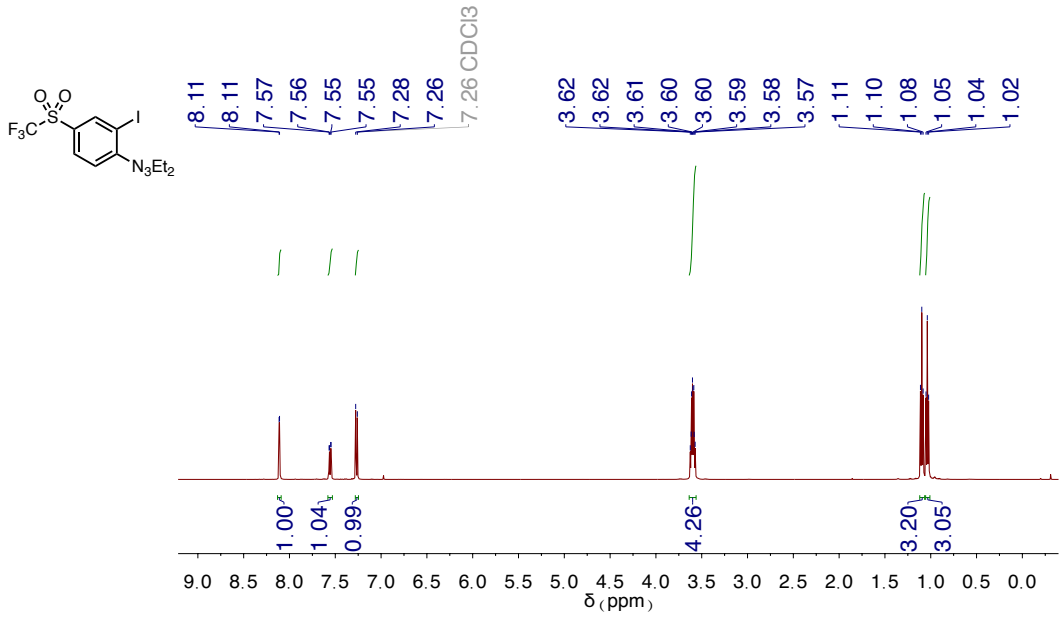

Figure B.17. ^{1}H NMR spectrum of **2a**.

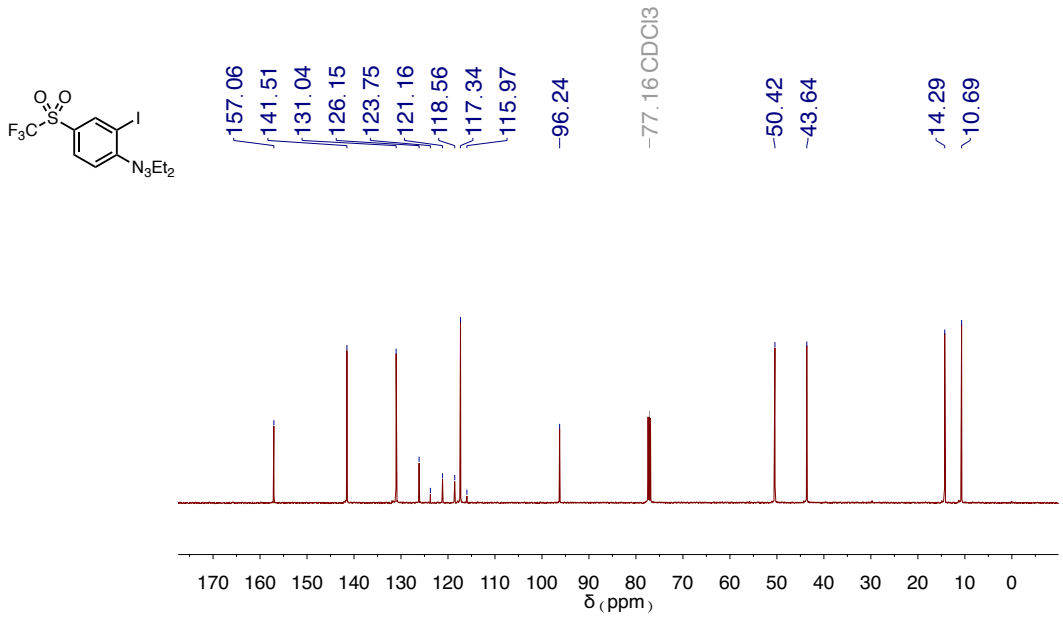

Figure B.18. ^{13}C NMR spectrum of **2a**.

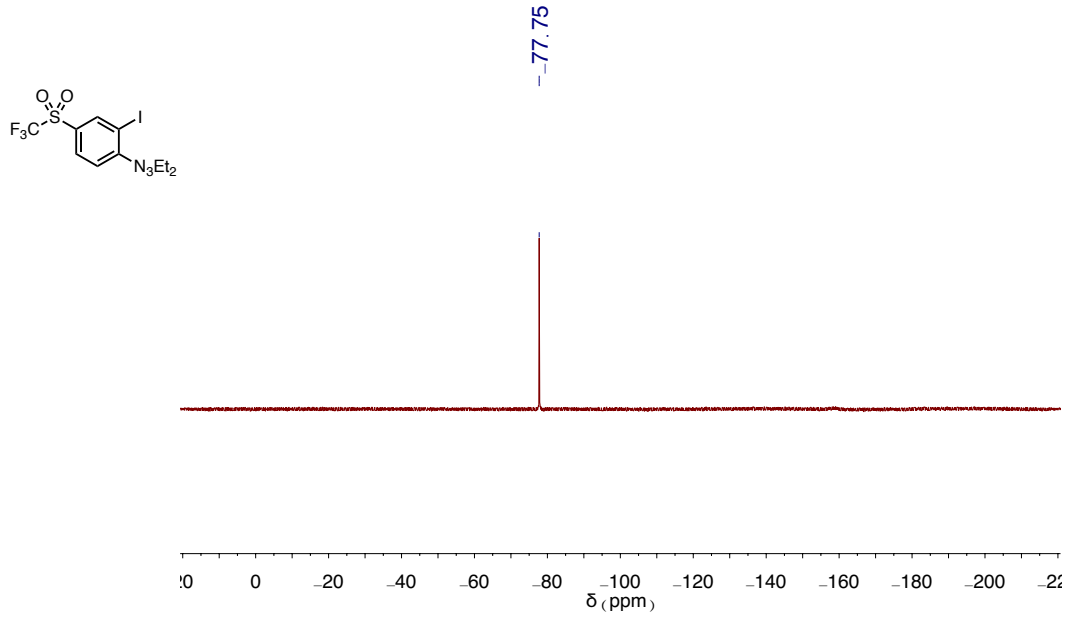

Figure B.19. ^{19}F NMR spectrum of **2a**.

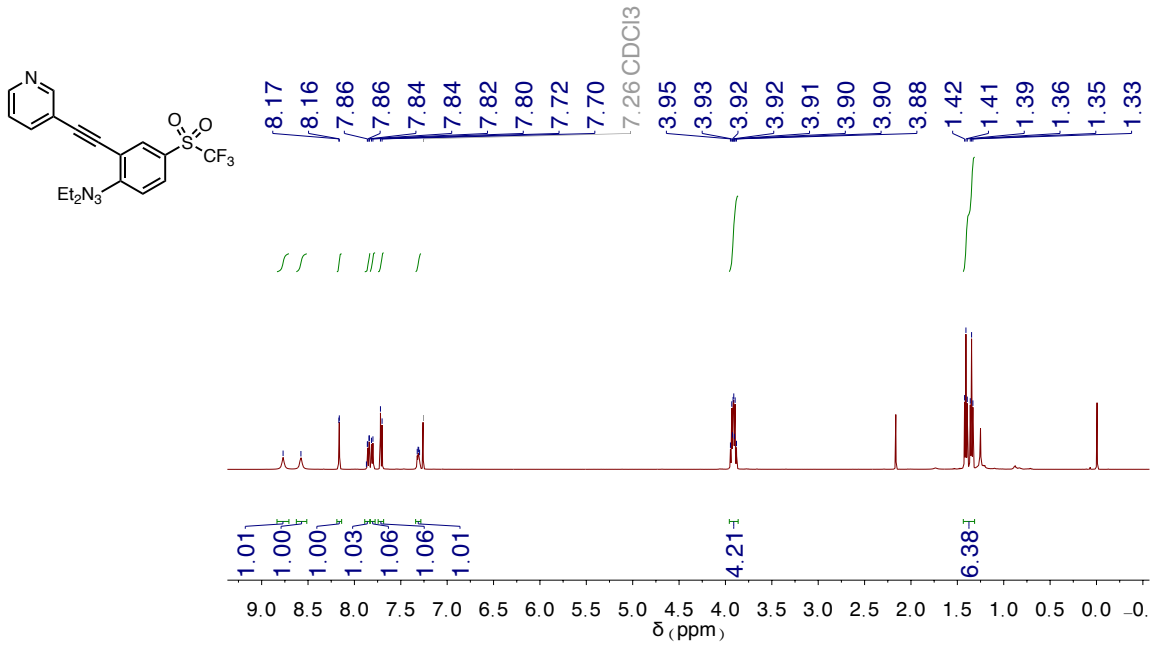

Figure B.20. ^{1}H NMR spectrum of **3a**. Wet with water and grease.

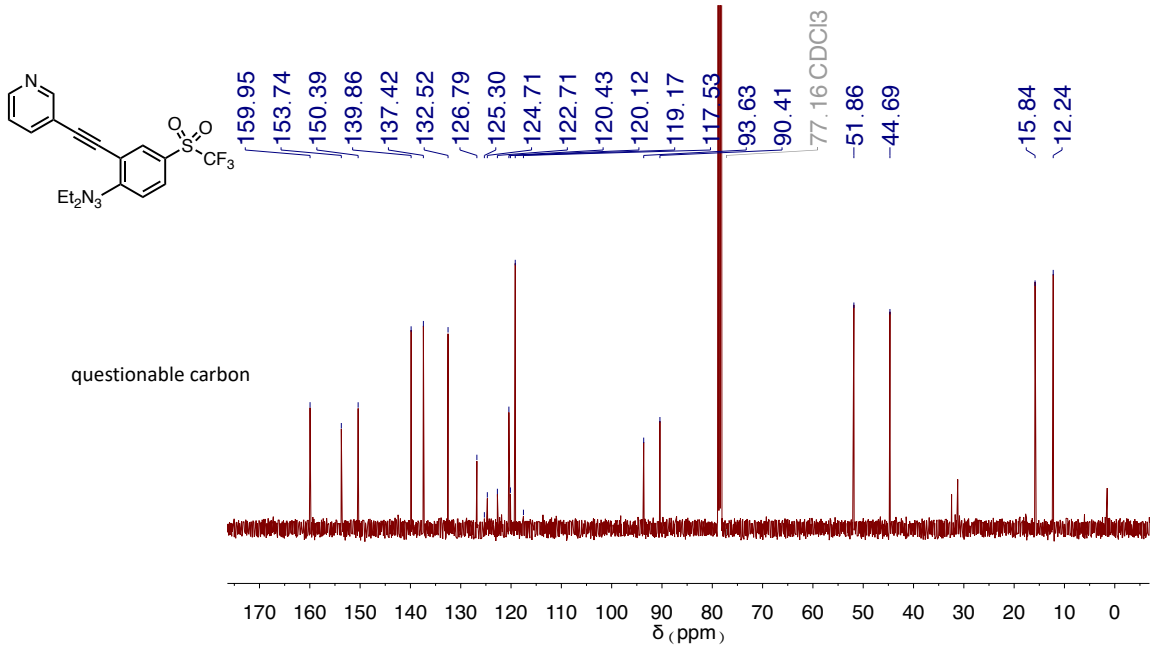

Figure B.21. ^{13}C NMR spectrum of **3a**. Contains grease.

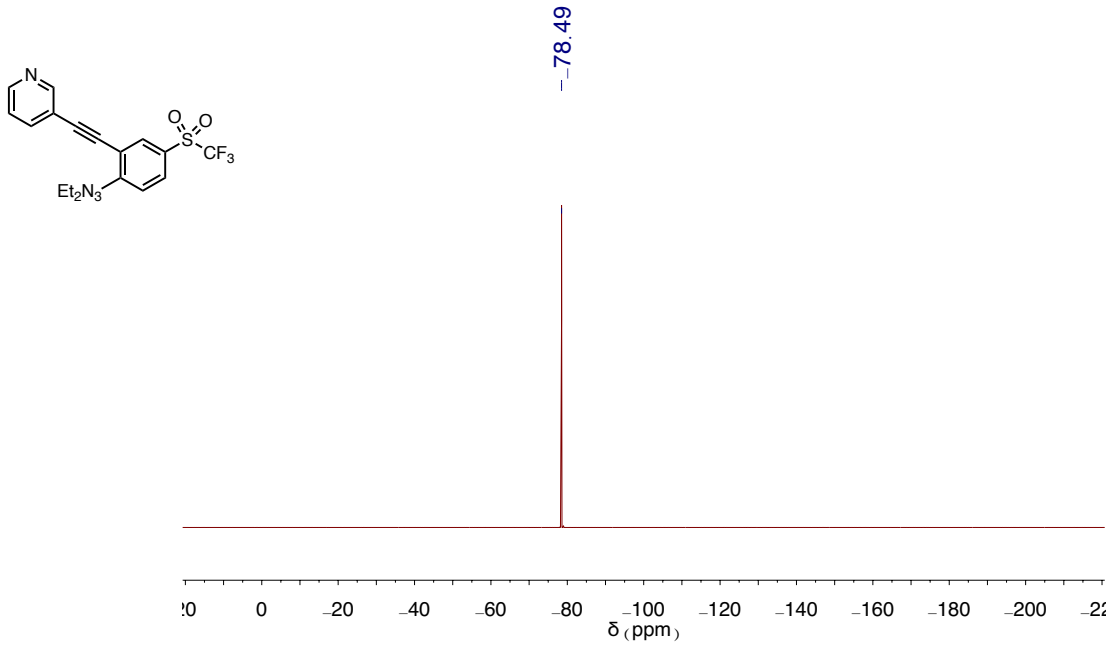

Figure B.22. ^{19}F NMR spectrum of **3a**.

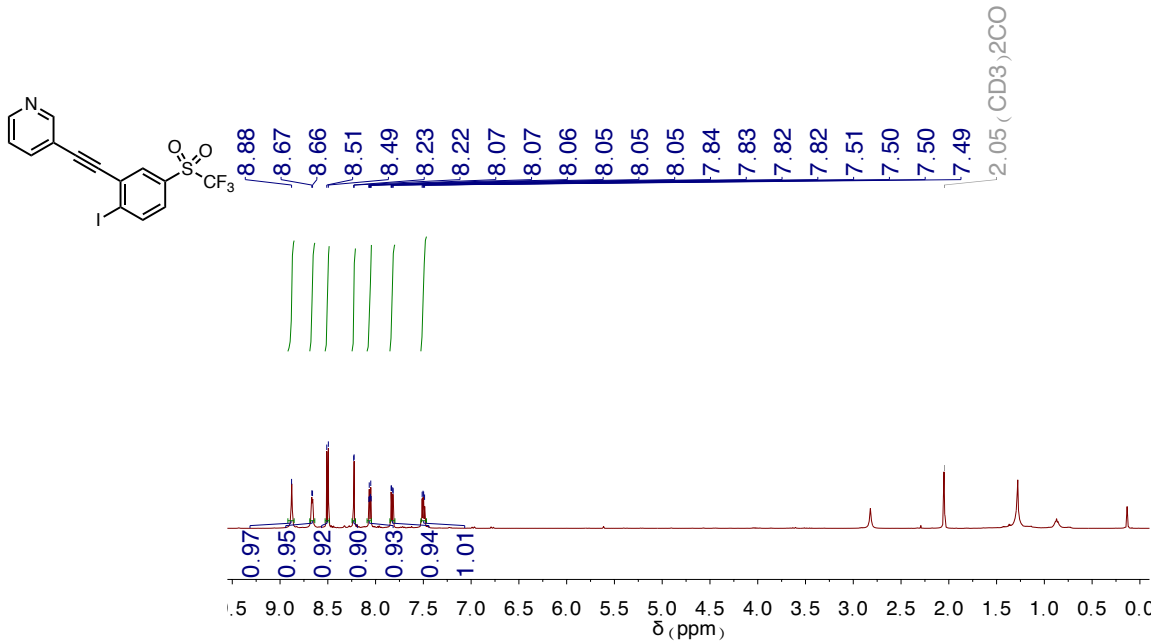

Figure B.23. ^{1}H NMR spectrum of **4a**. Wet with water and grease.

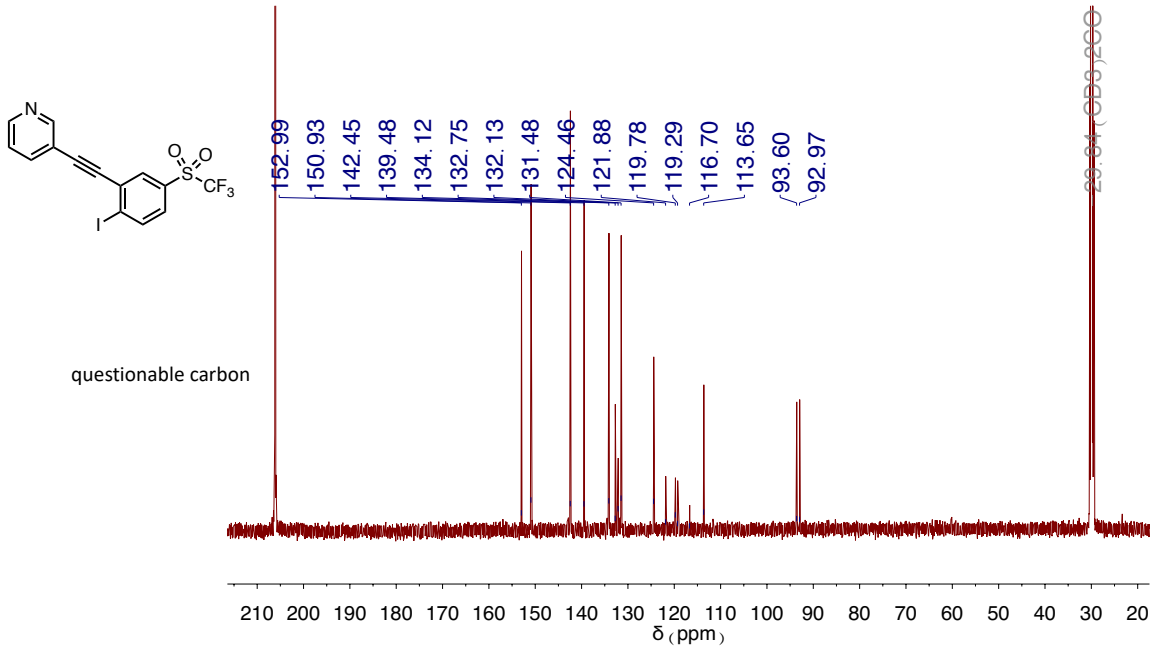

Figure B.24. ^{13}C NMR spectrum of **4a**.

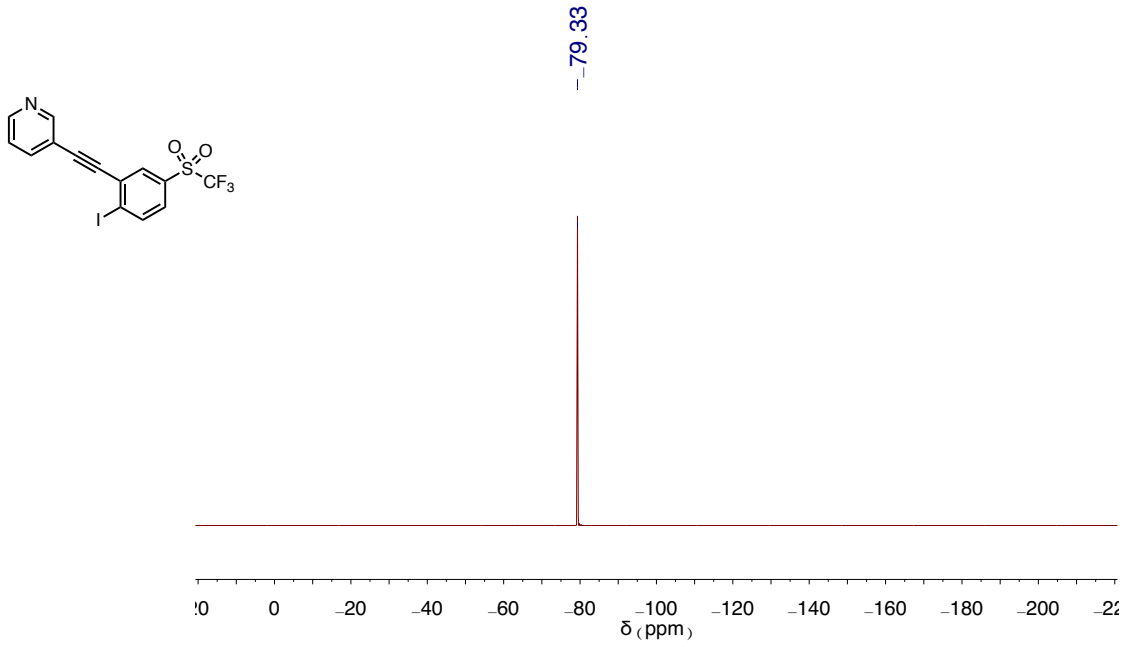

Figure B.25. ^{19}F NMR spectrum of **4a**.

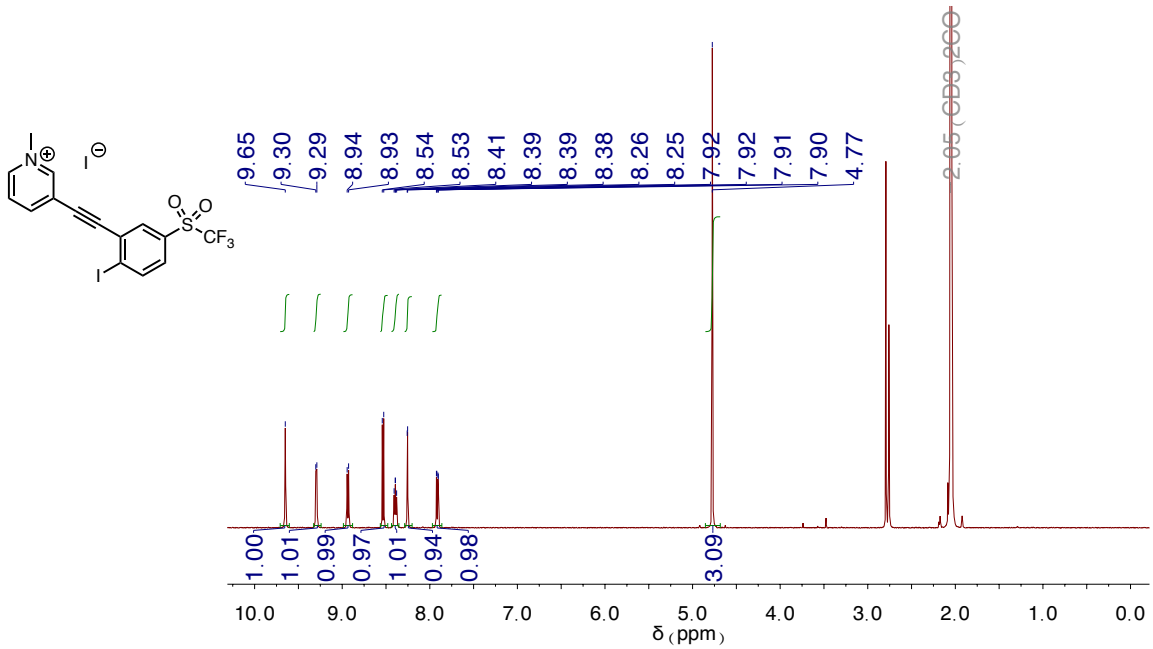

Figure B.26. ^{1}H NMR spectrum of **5a • I**$^{-}$. Wet with water.

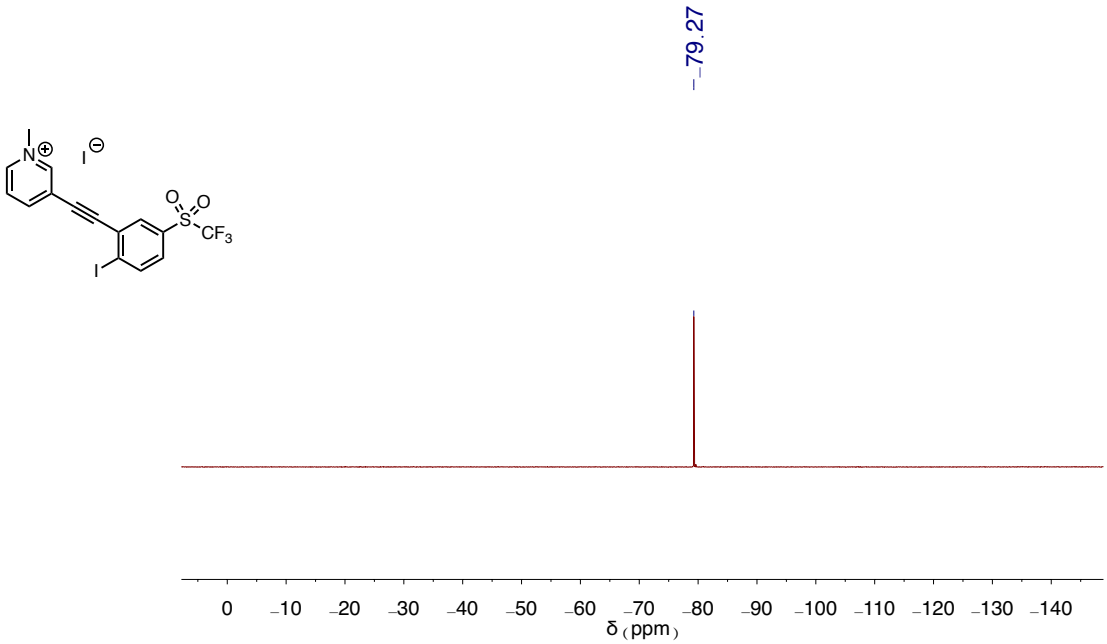

Figure B.27. ^{19}F NMR spectrum of **5a • I**$^{-}$.

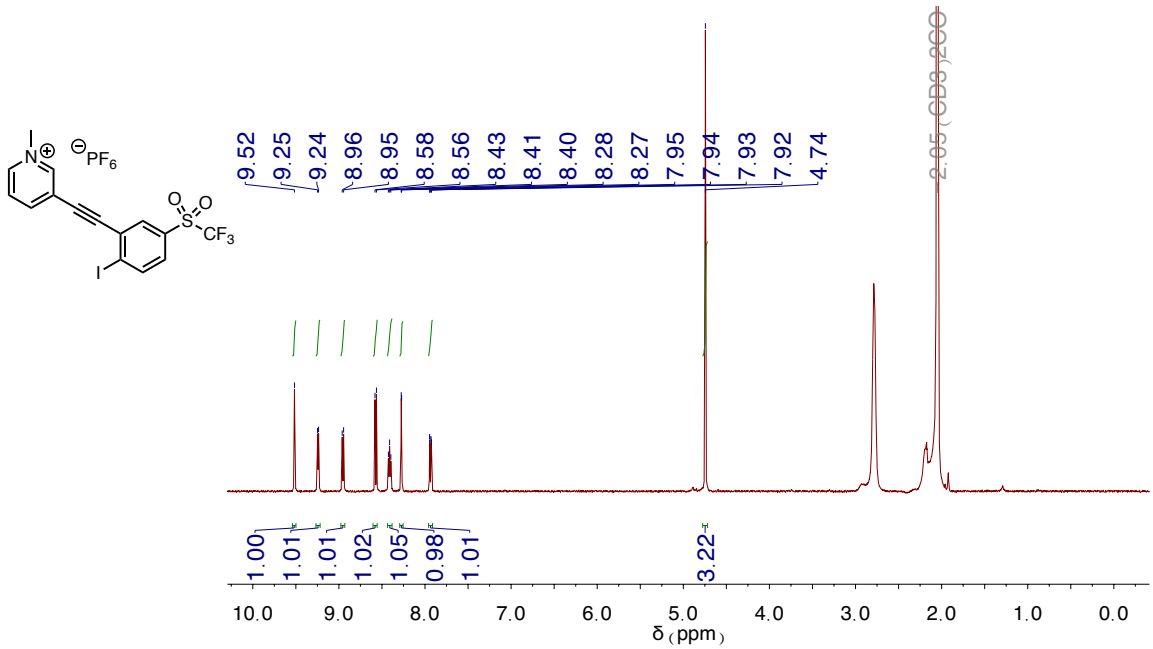

Figure B.28. ^{1}H NMR spectrum of **5a • PF_6**$^{-}$.

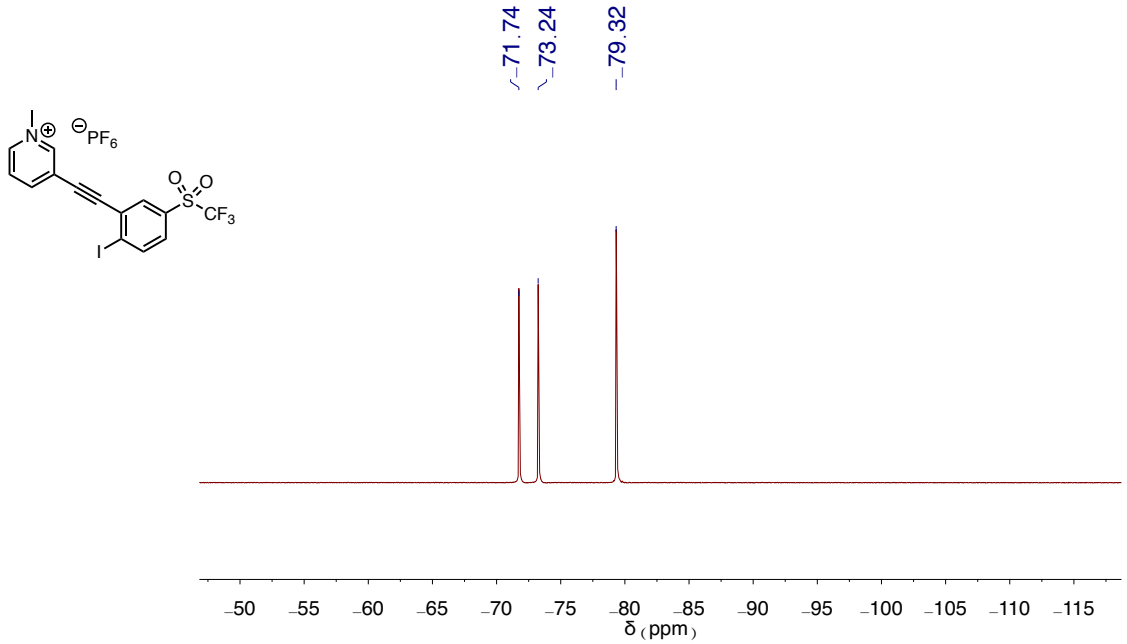

Figure B.29. ^{19}F NMR spectrum of **5a • PF_6^-**.

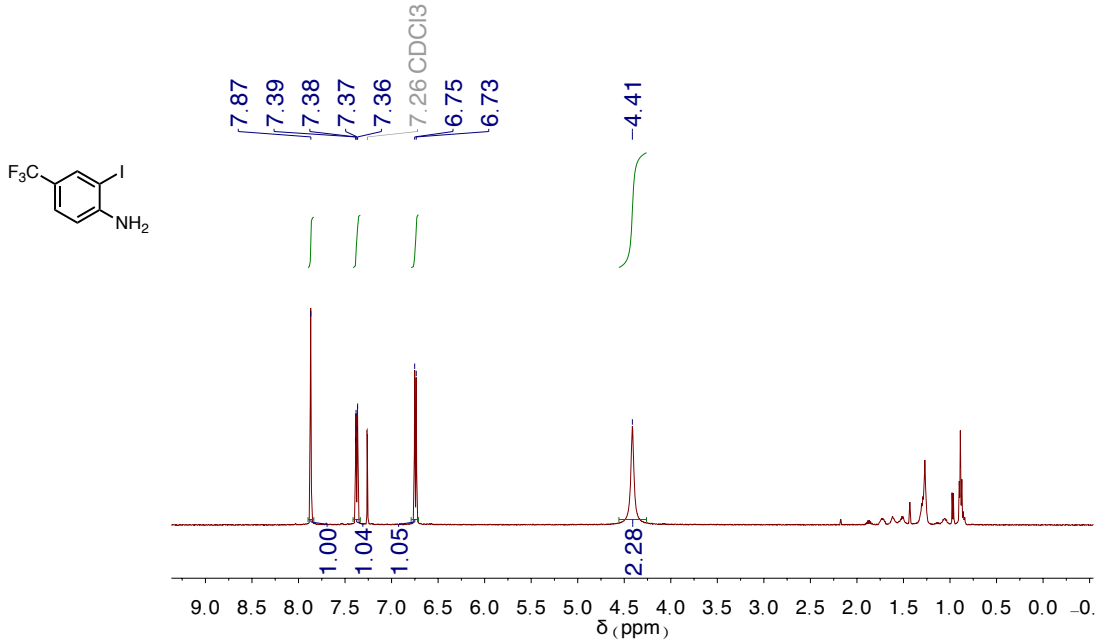

Figure B.30. ^{1}H NMR spectrum of **1b**.

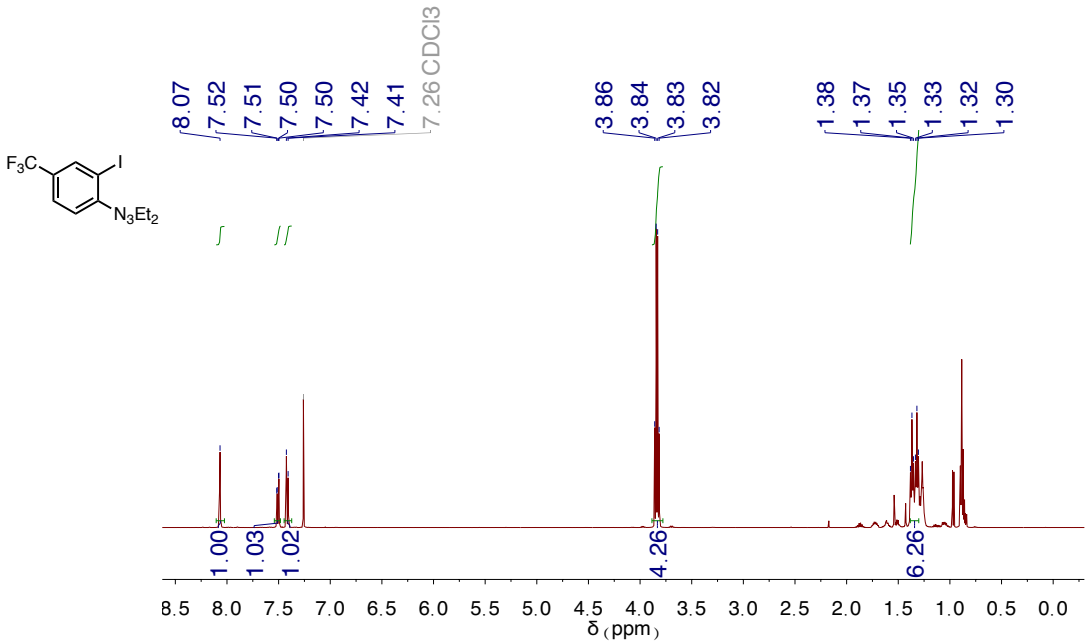

Figure B.31. [1]H NMR spectrum of **2b**.

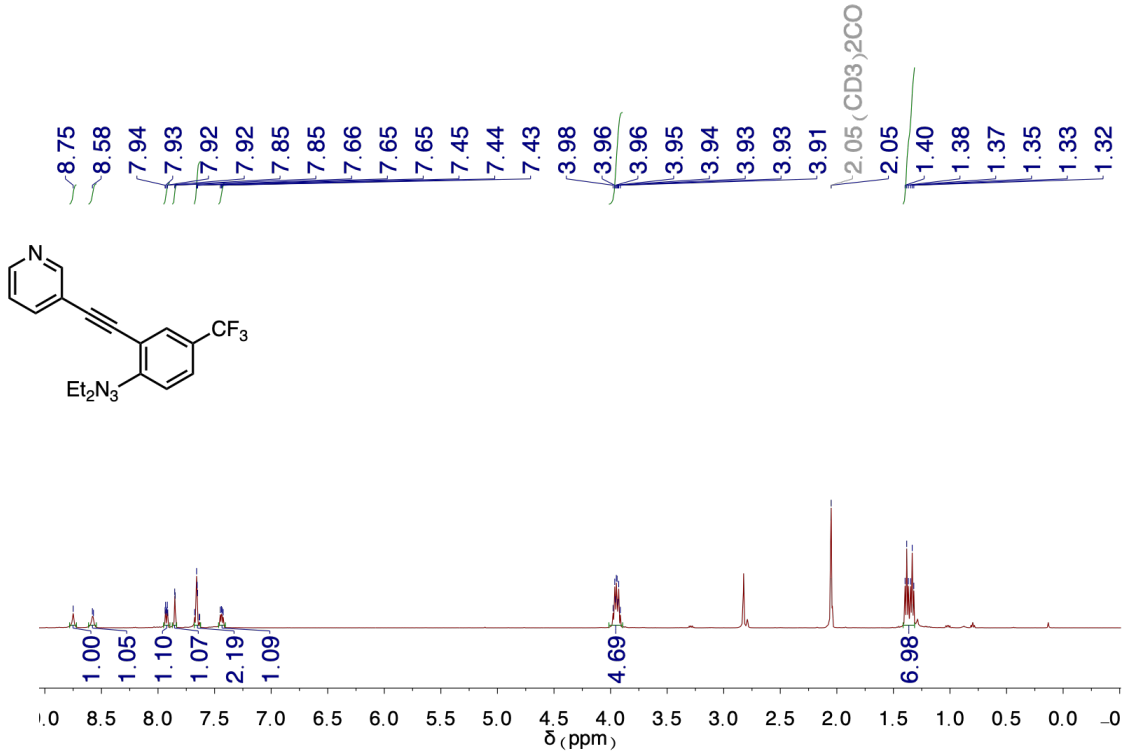

Figure B.32. [1]H NMR spectrum of **3b**.

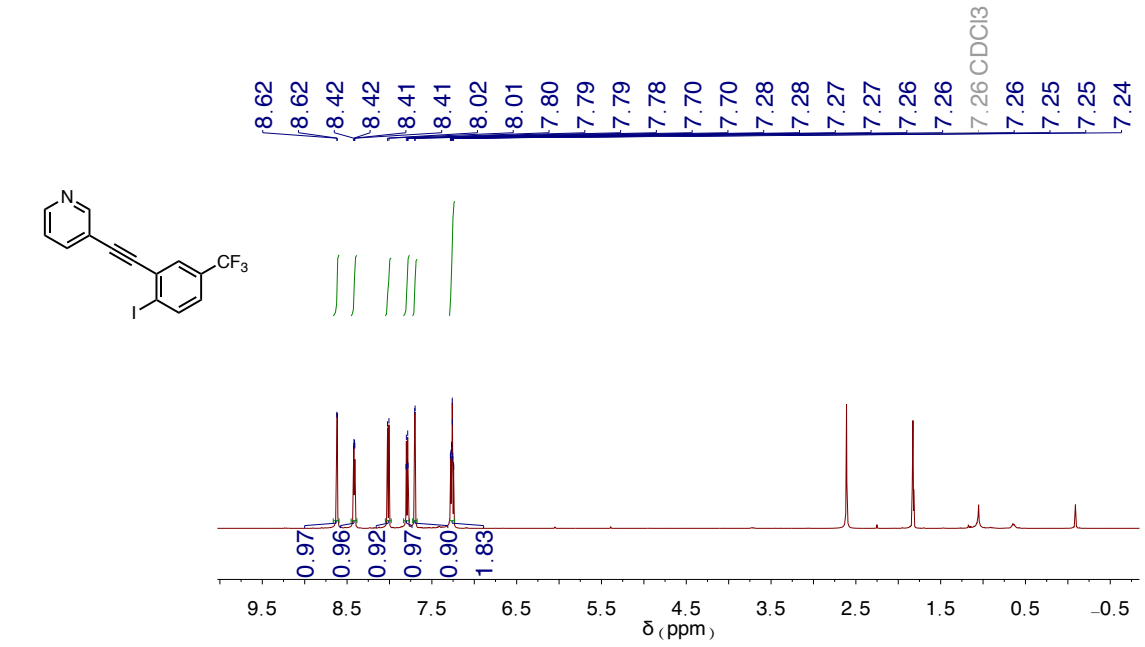

Figure B.33. ^{1}H NMR spectrum of **4b**.

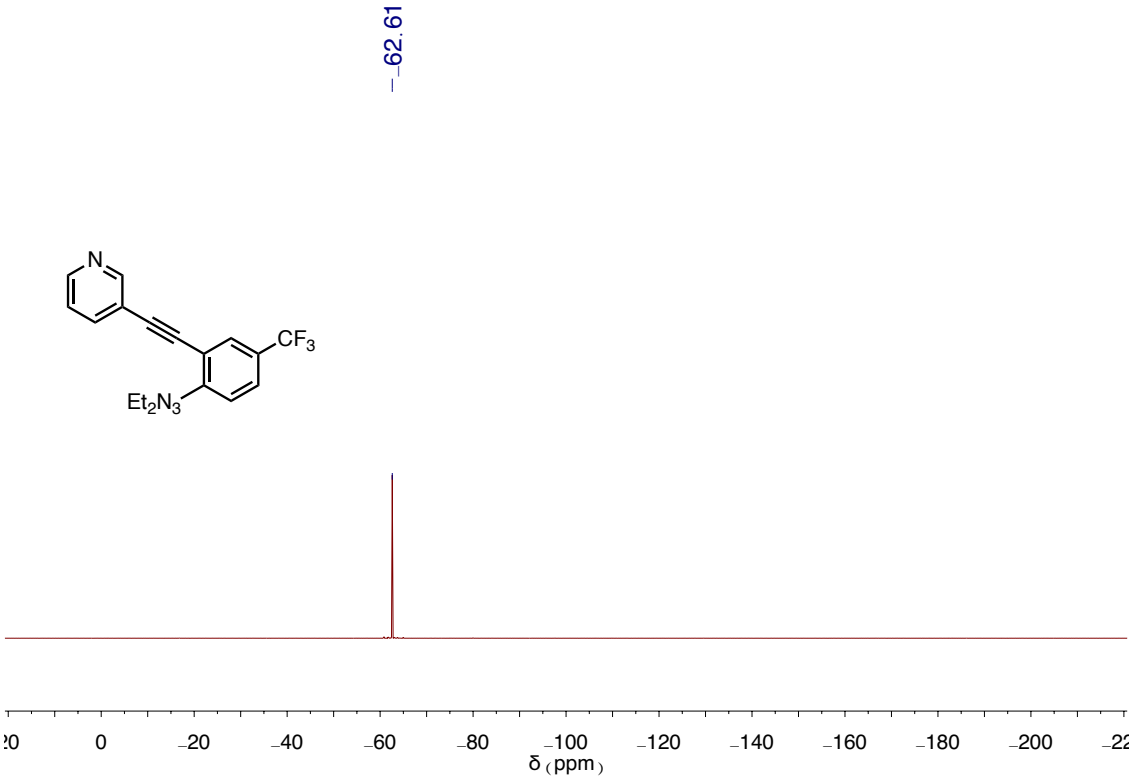

Figure B.34. ^{19}F NMR spectrum of **3b**.

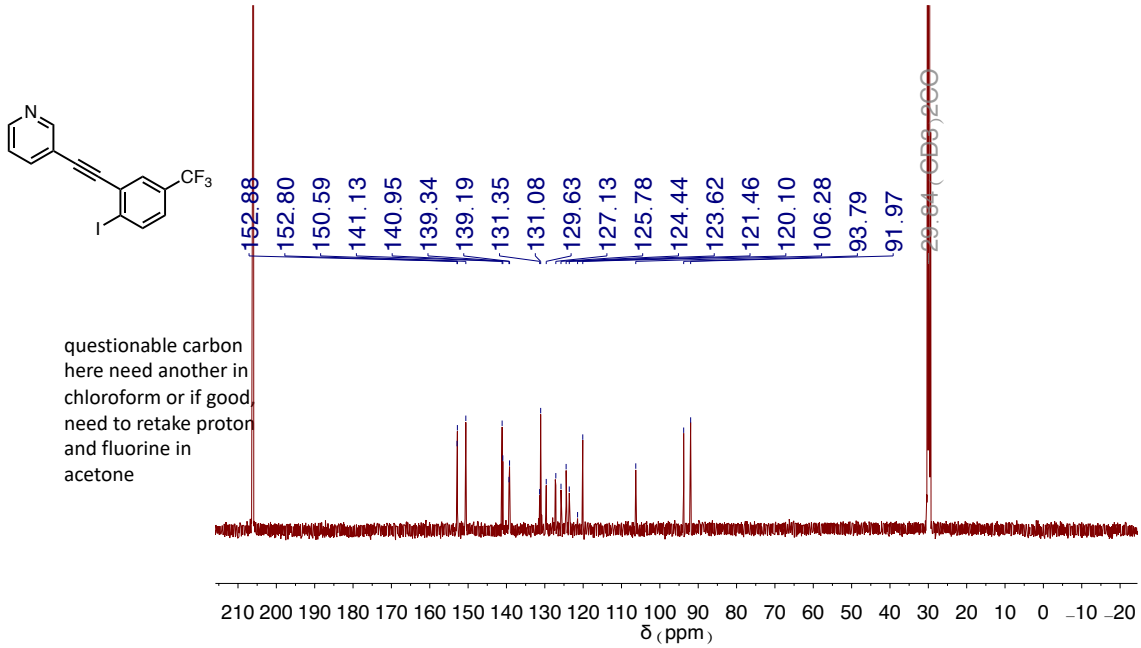

Figure B.35. ^{13}C NMR spectrum of **4b**.

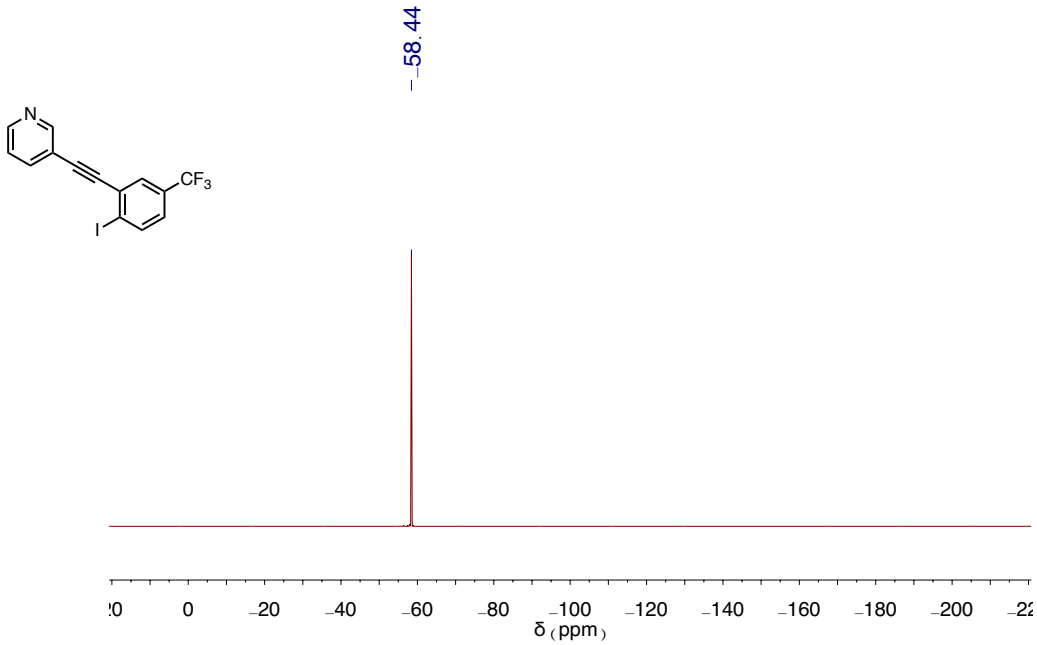

Figure B.36. ^{19}F NMR spectrum of **4b**.

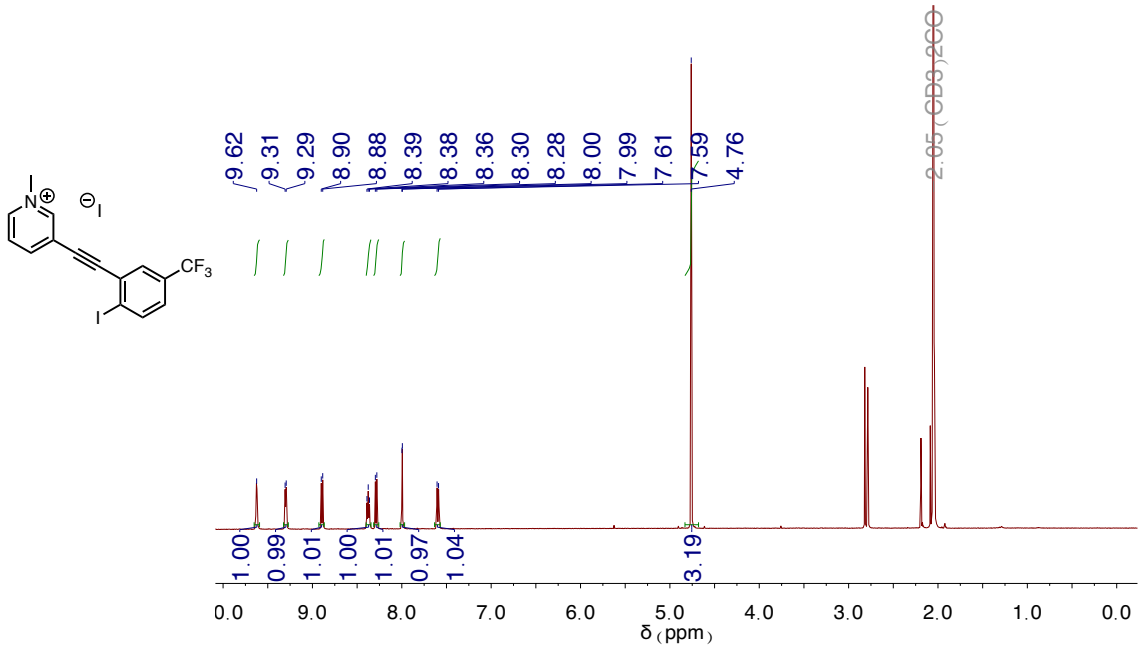

Figure B.37. ^{1}H NMR spectrum of **5b • I**$^{-}$.

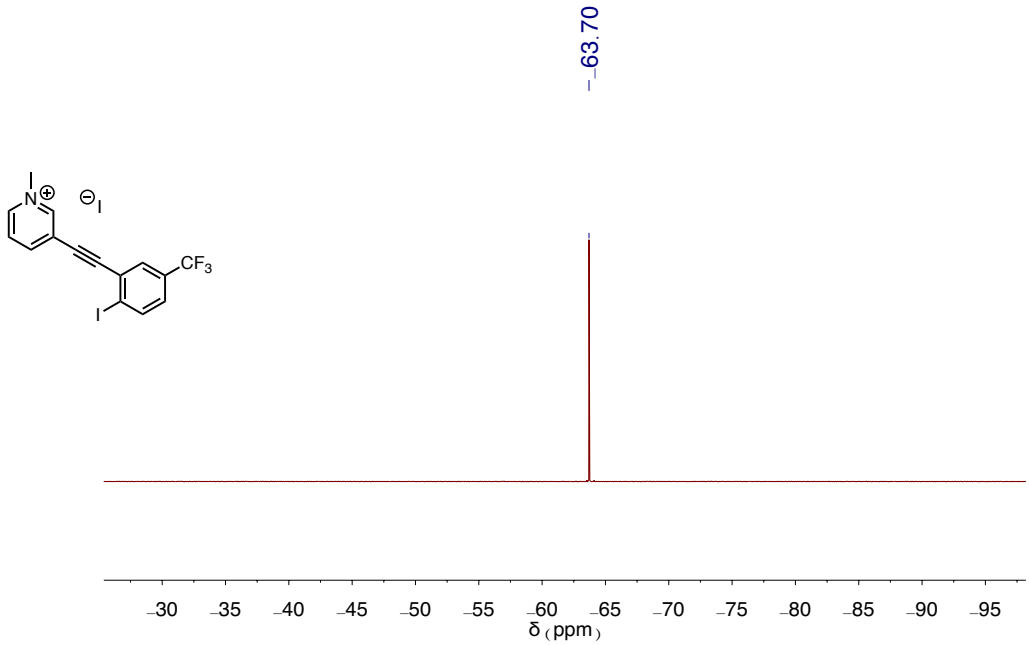

Figure B.38. ^{19}F NMR spectrum of **5b • I**$^{-}$.

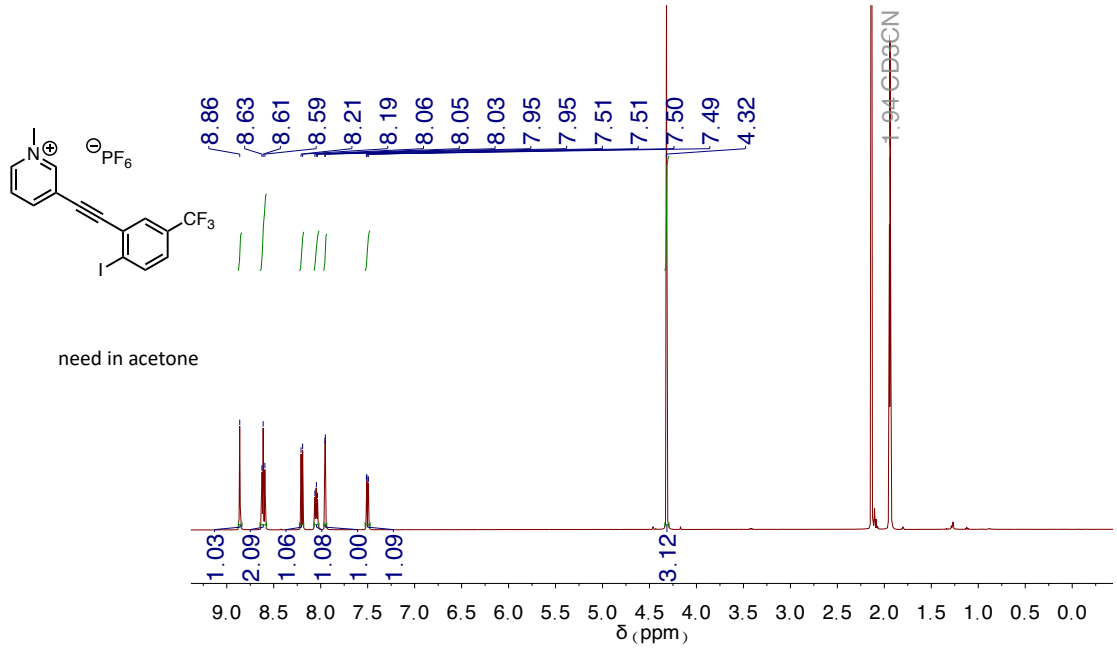

Figure B.39. ^{1}H NMR spectrum of **5b • PF_6^-**.

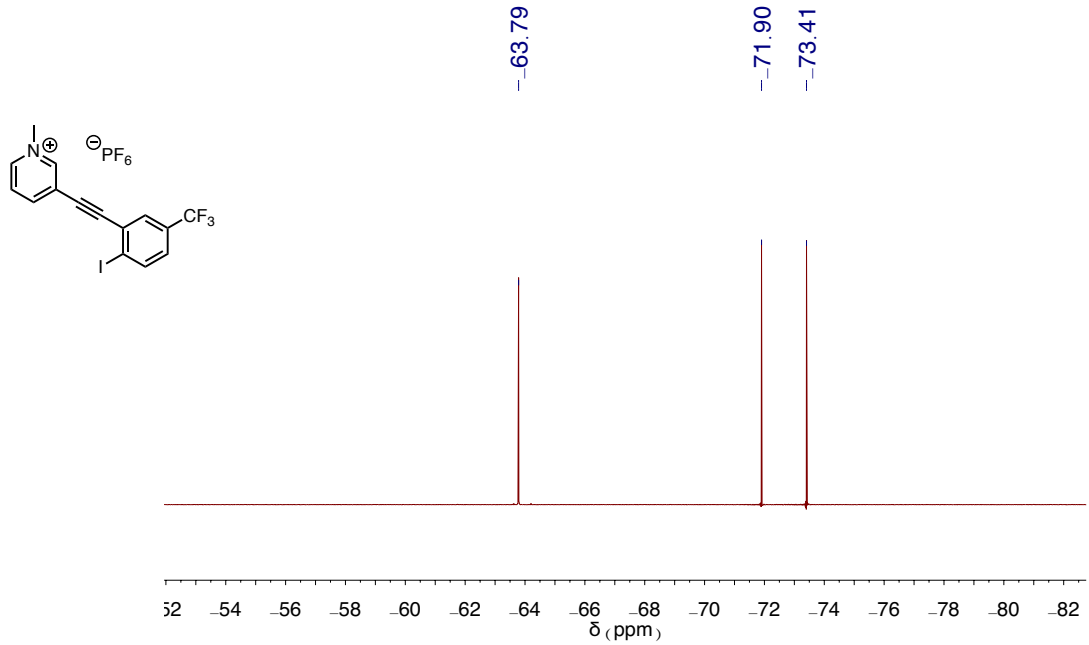

Figure B.40. ^{19}F NMR spectrum of **5b • PF_6^-**.

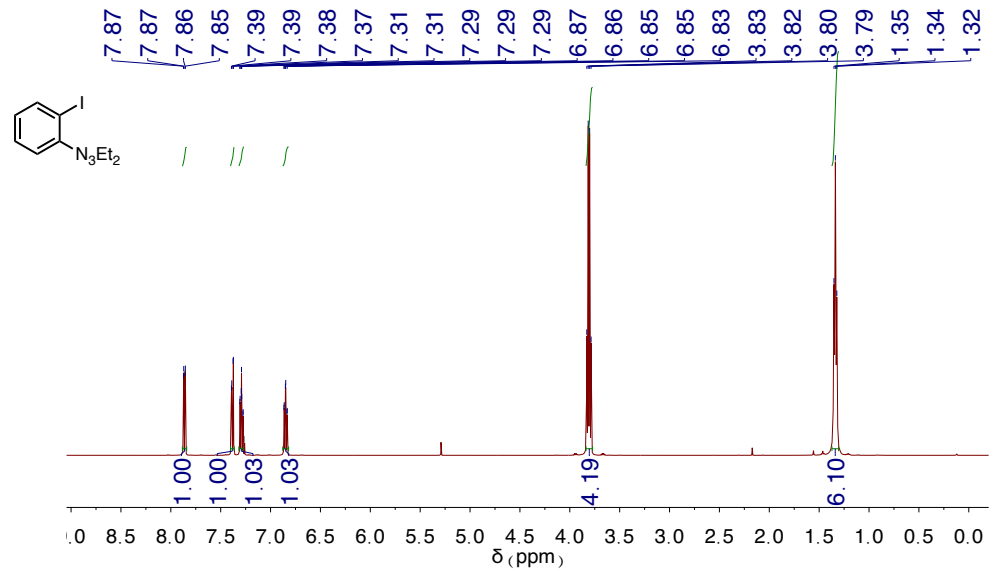

Figure B.41. [1]H NMR spectrum of **2c**.

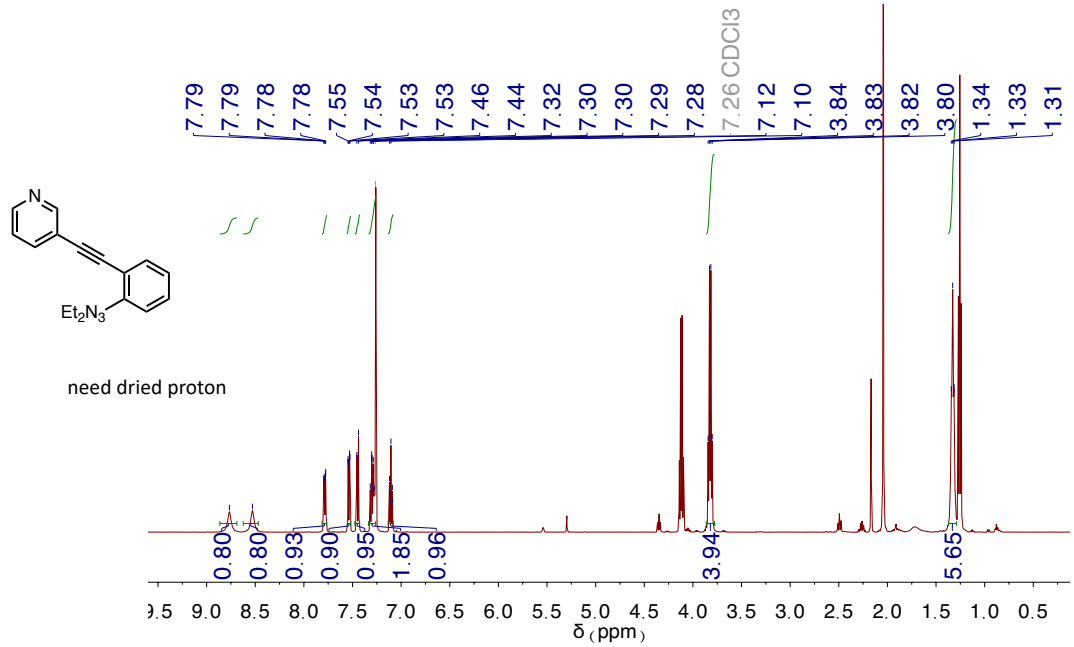

Figure B.42. [1]H NMR spectrum of **3c**.

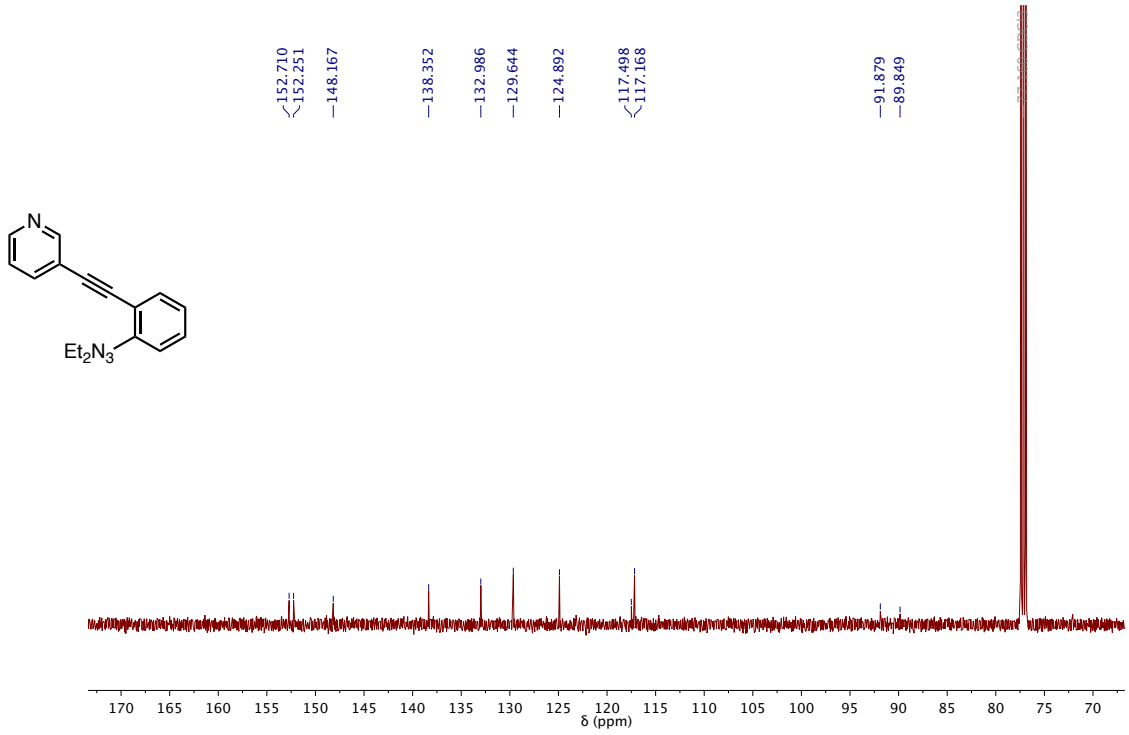

Figure B.43. ^{13}C NMR spectrum of **3c**.

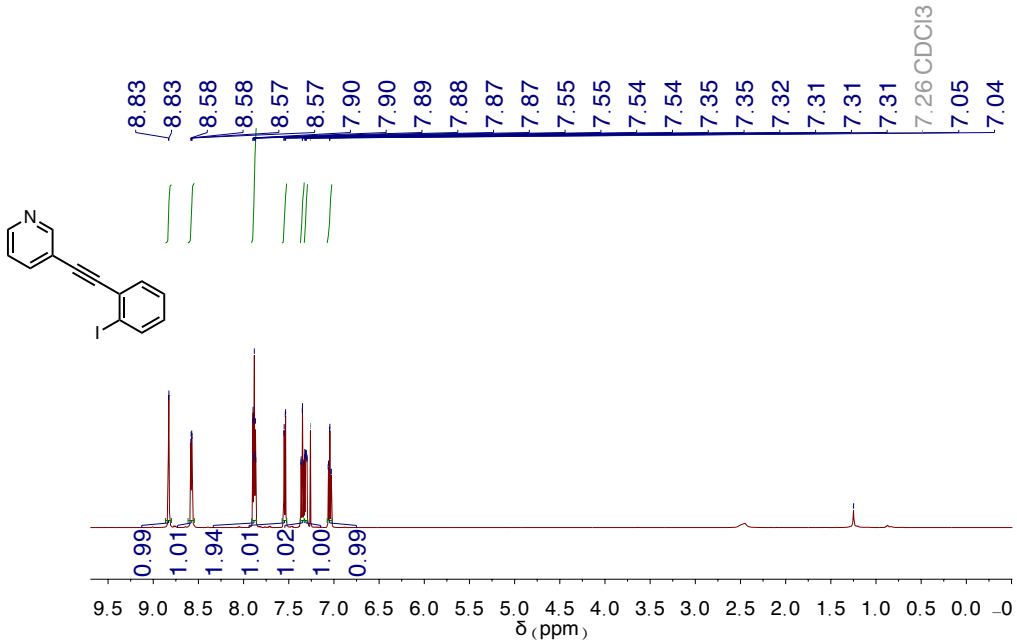

Figure B.44. ^{1}H NMR spectrum of **4c**.

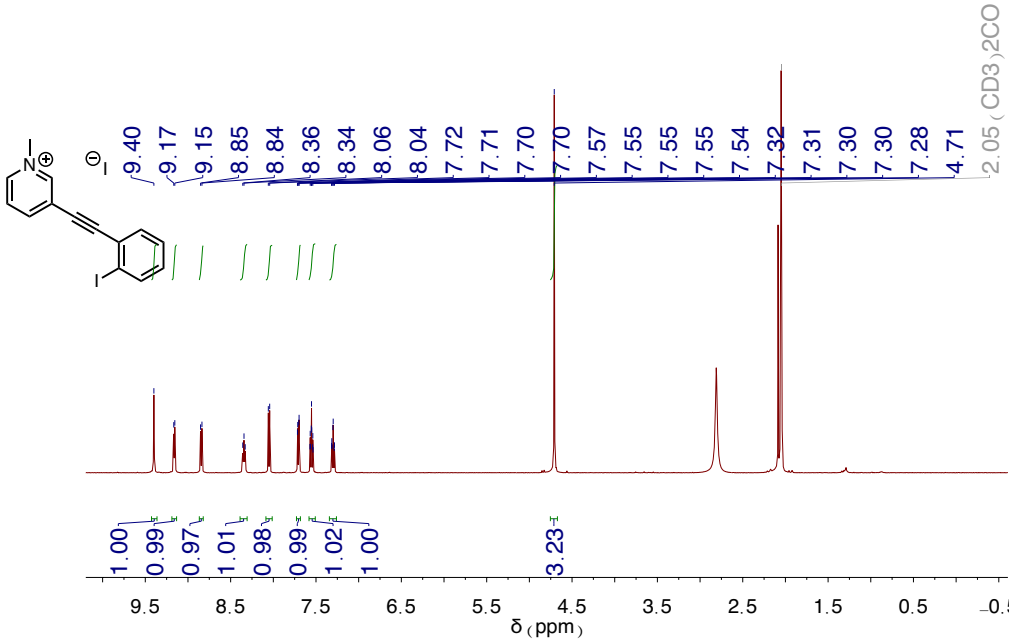

Figure B.45. ^{1}H NMR spectrum of **5c • I**$^{-}$.

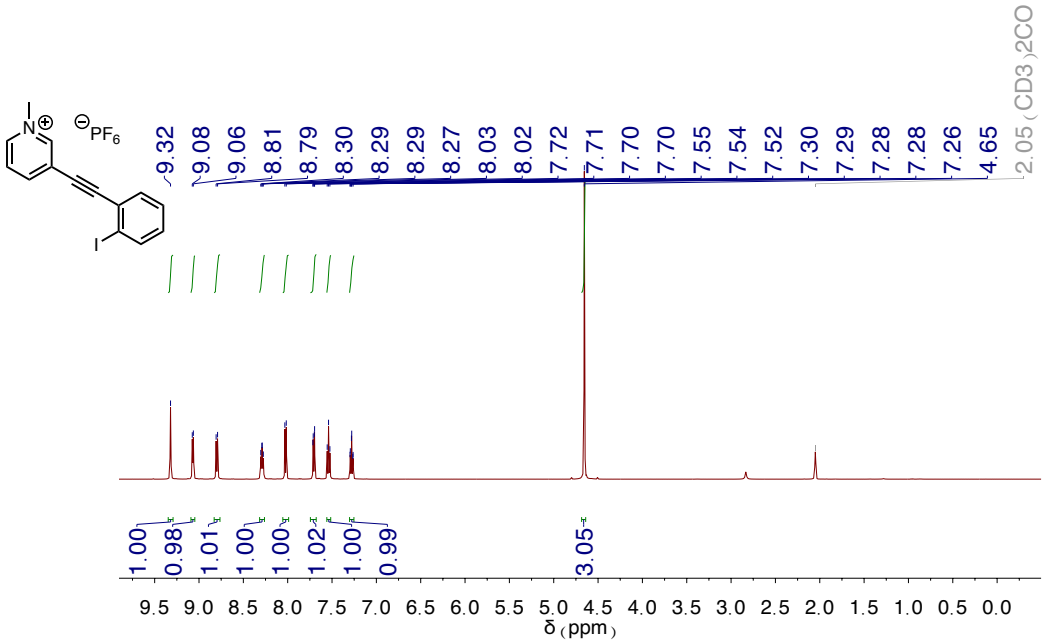

Figure B.46. ^{1}H NMR spectrum of **5c • PF_6**$^{-}$.

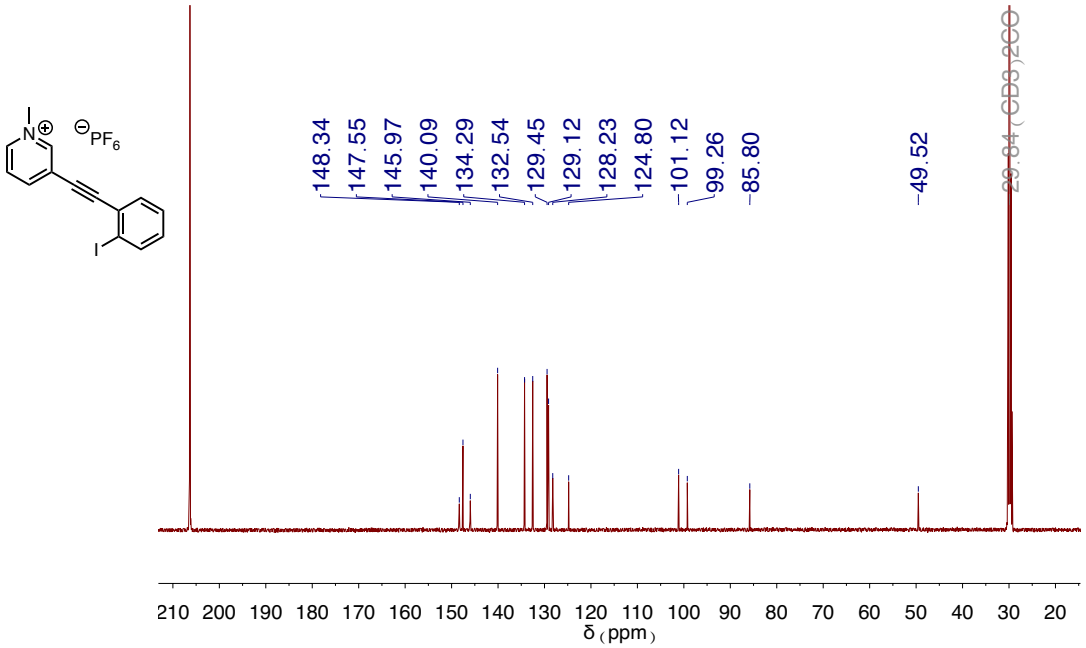

Figure B.47. ^{13}C NMR spectrum of **5c • PF_6^-**.

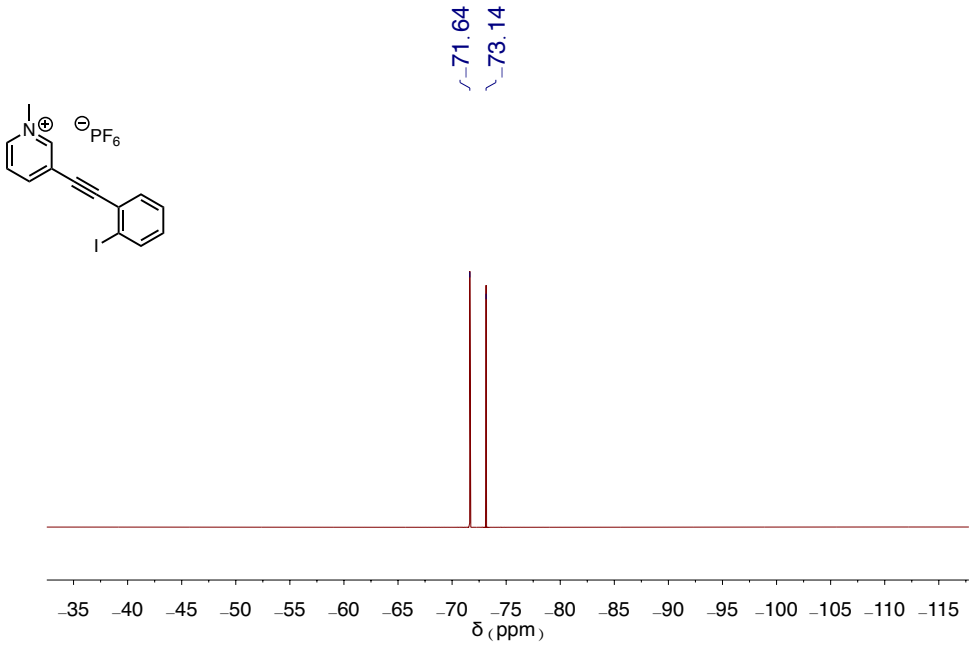

Figure B.48. ^{19}F NMR spectrum of **5c • PF_6^-**.

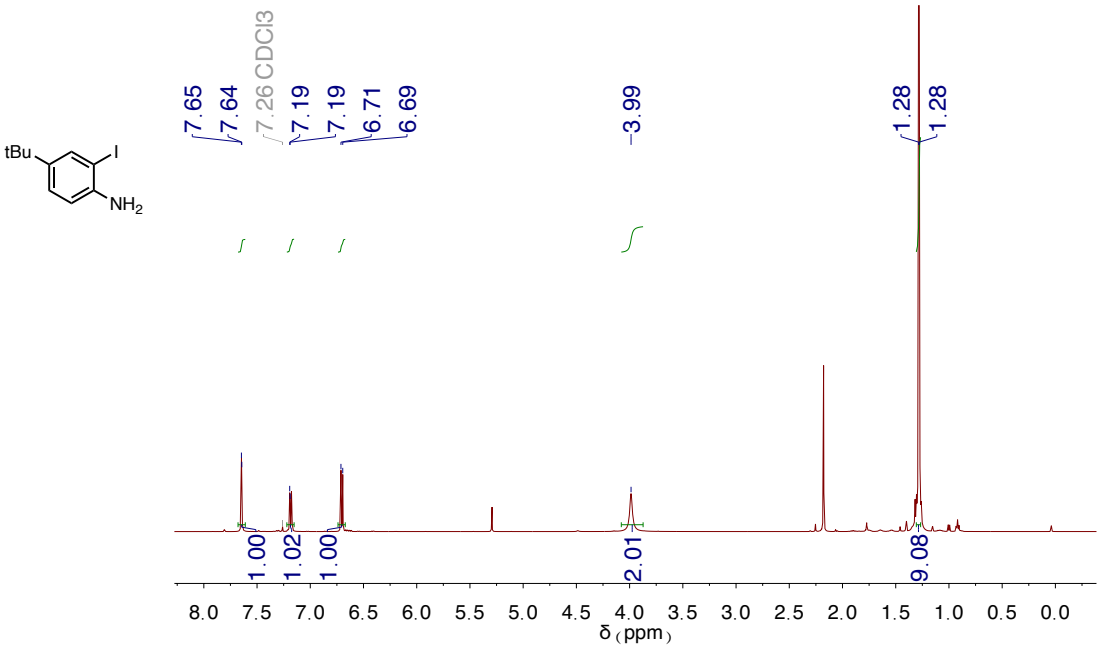

Figure B.49. [1]H NMR spectrum of **1d**. Wet with DCM and water.

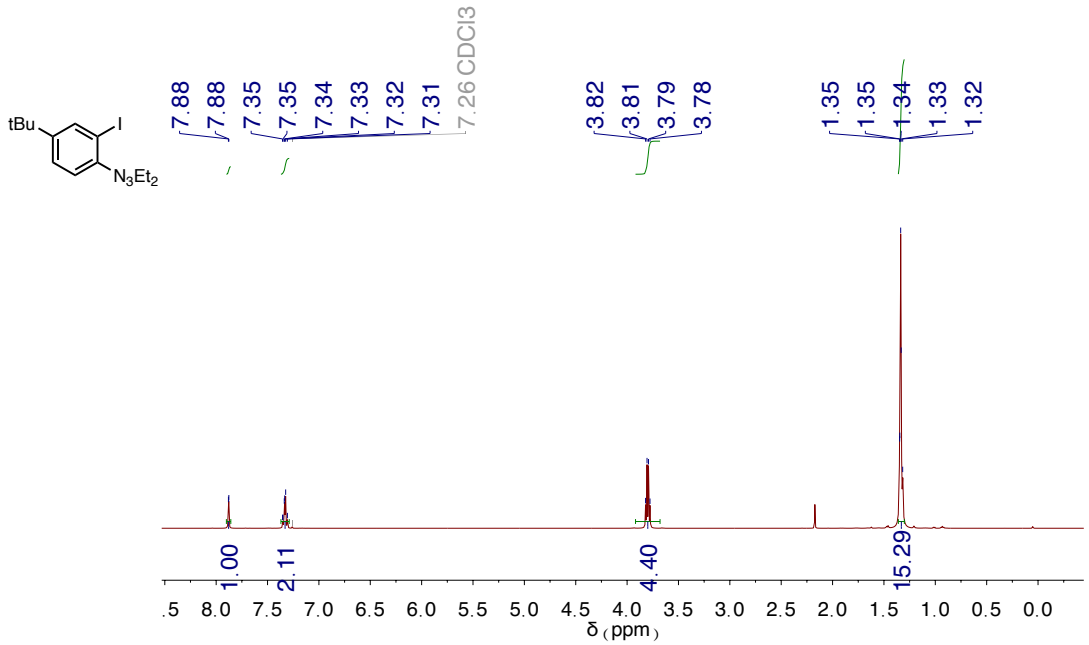

Figure B.50. [1]H NMR spectrum of **2d**.

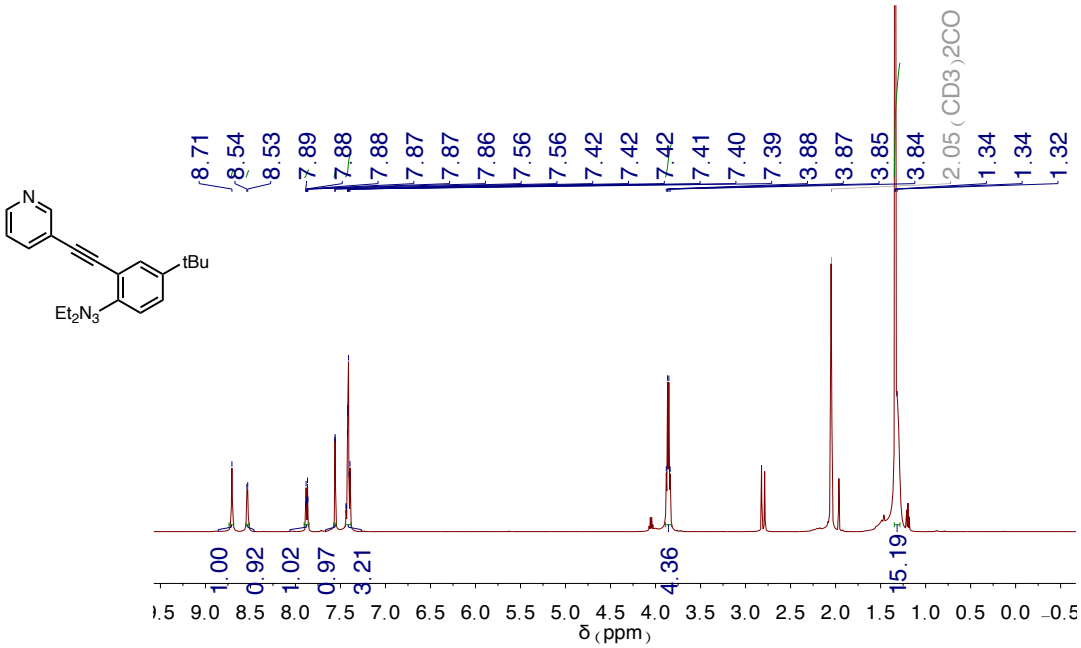

Figure B.51. [1]H NMR spectrum of **3d**. Wet with water and ethyl acetate.

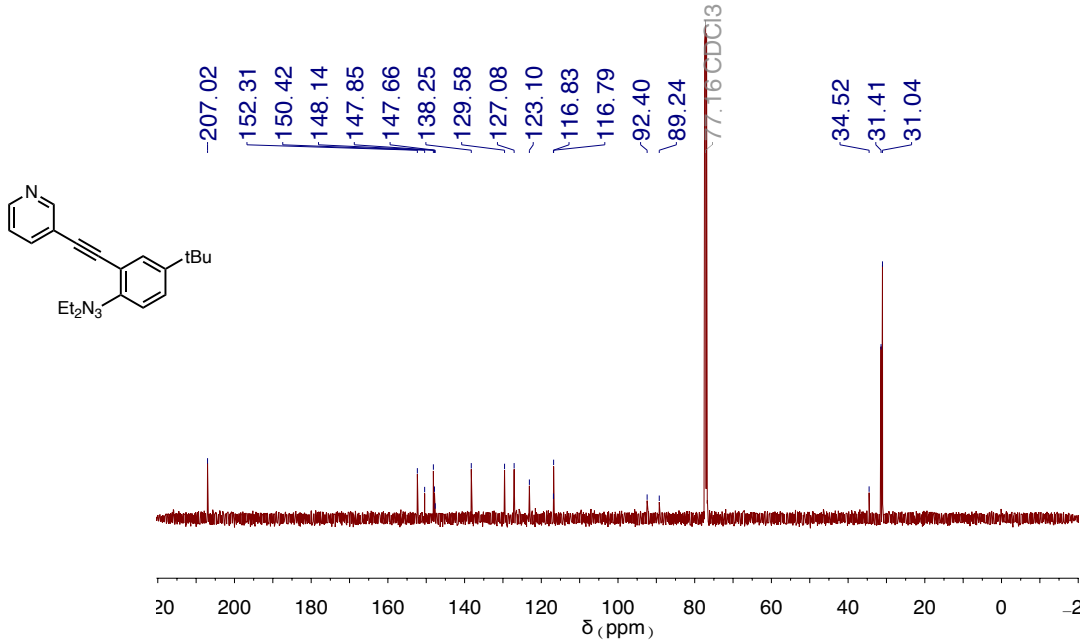

Figure B.52. [13]C NMR spectrum of **3d**.

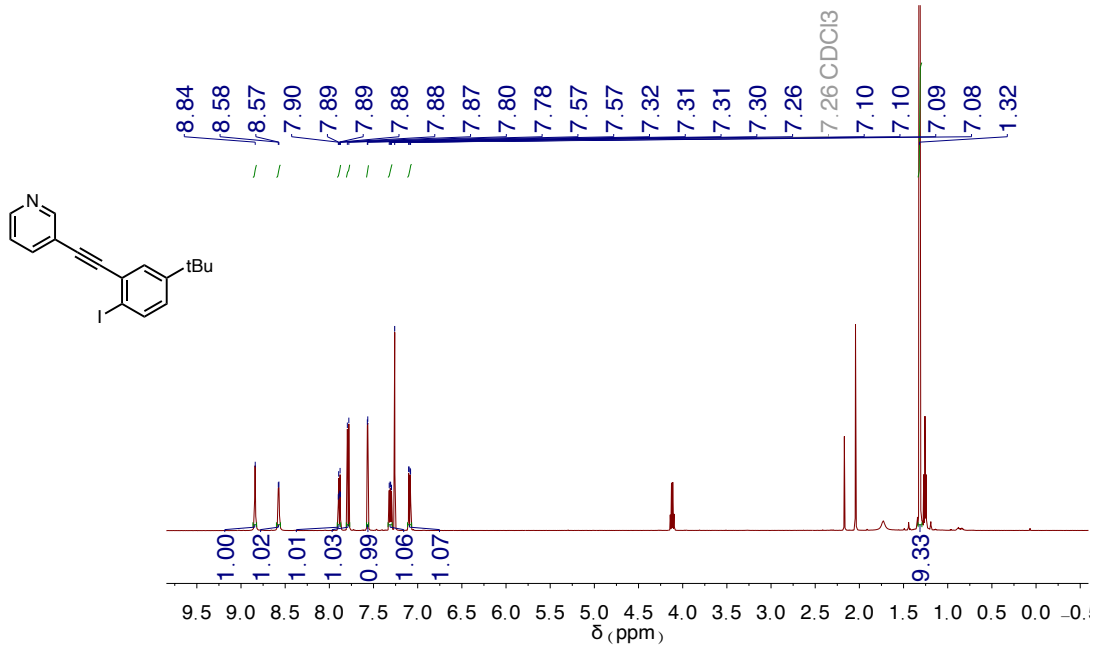

Figure B.53. ^{1}H NMR spectrum of **4d**. Wet with water and ethyl acetate.

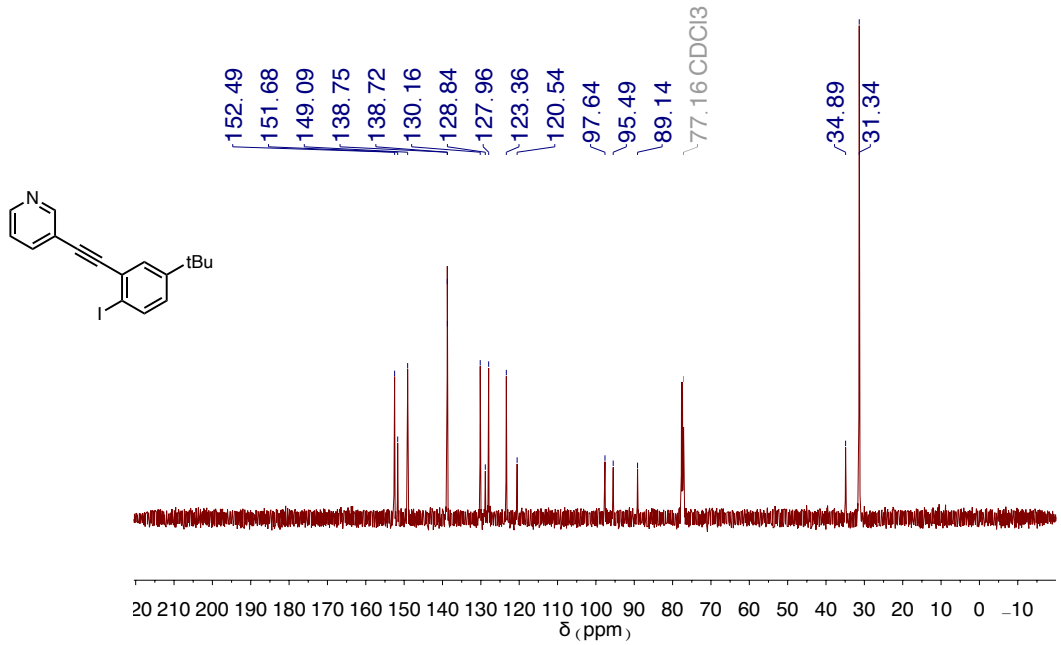

Figure B.54. ^{13}C NMR spectrum of **4d**.

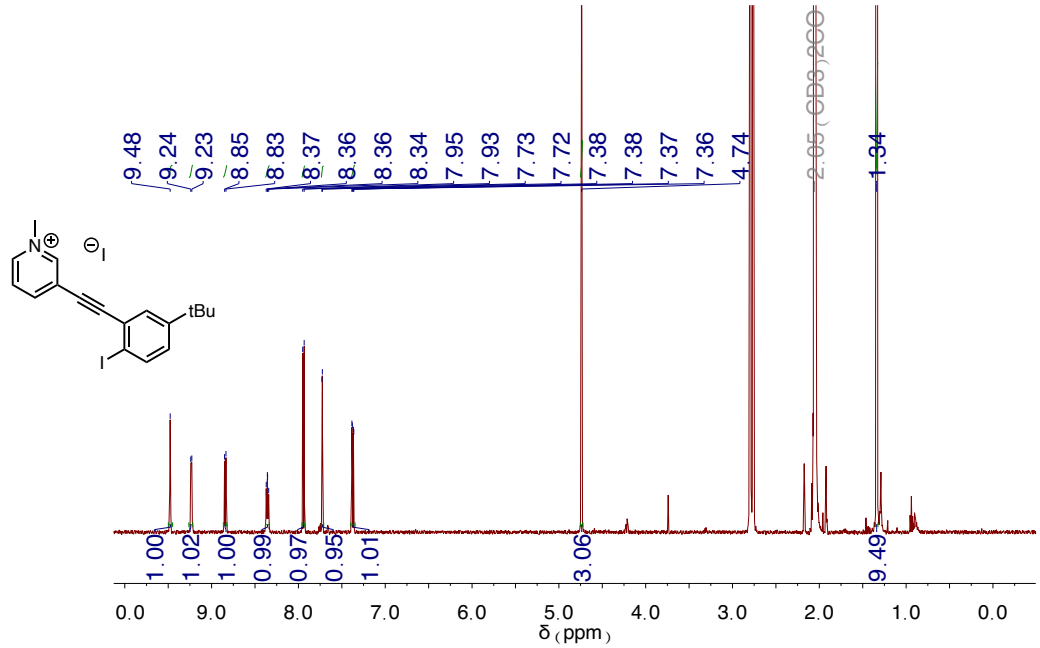

Figure B.55. ^{1}H NMR spectrum of **5d • I**$^{-}$. Wet with water.

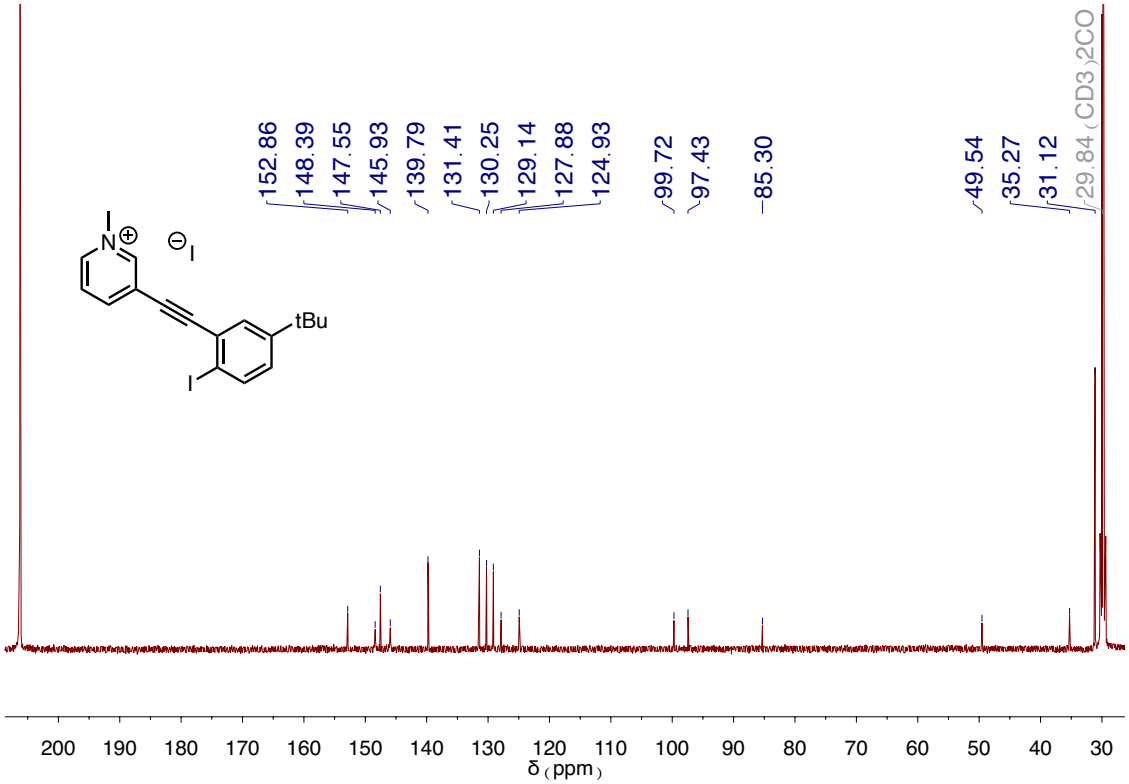

Figure B.56. ^{13}C NMR spectrum of **5d • I**$^{-}$.

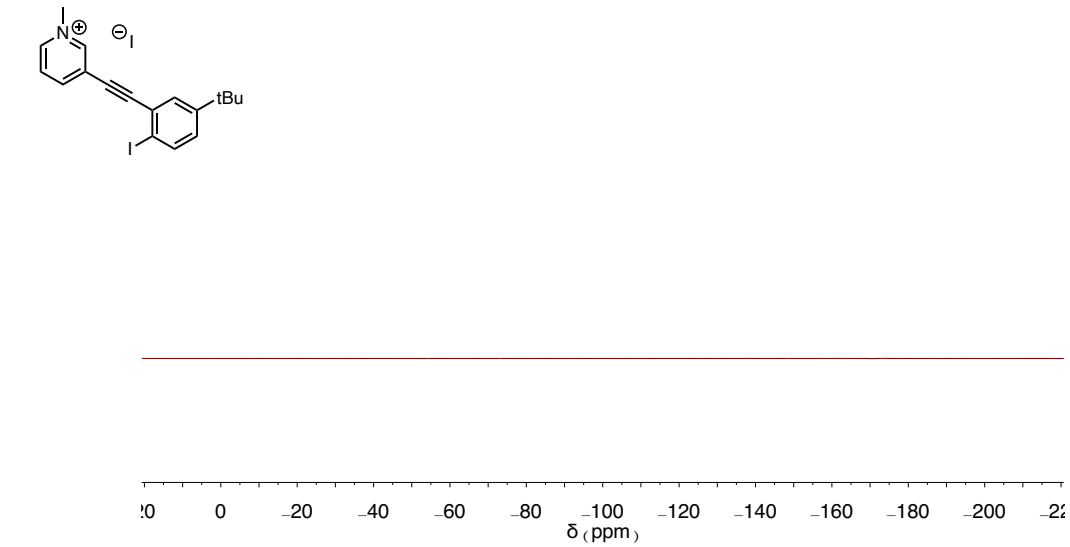

Figure B.57. ^{19}F NMR spectrum of **5d • I**$^{-}$.

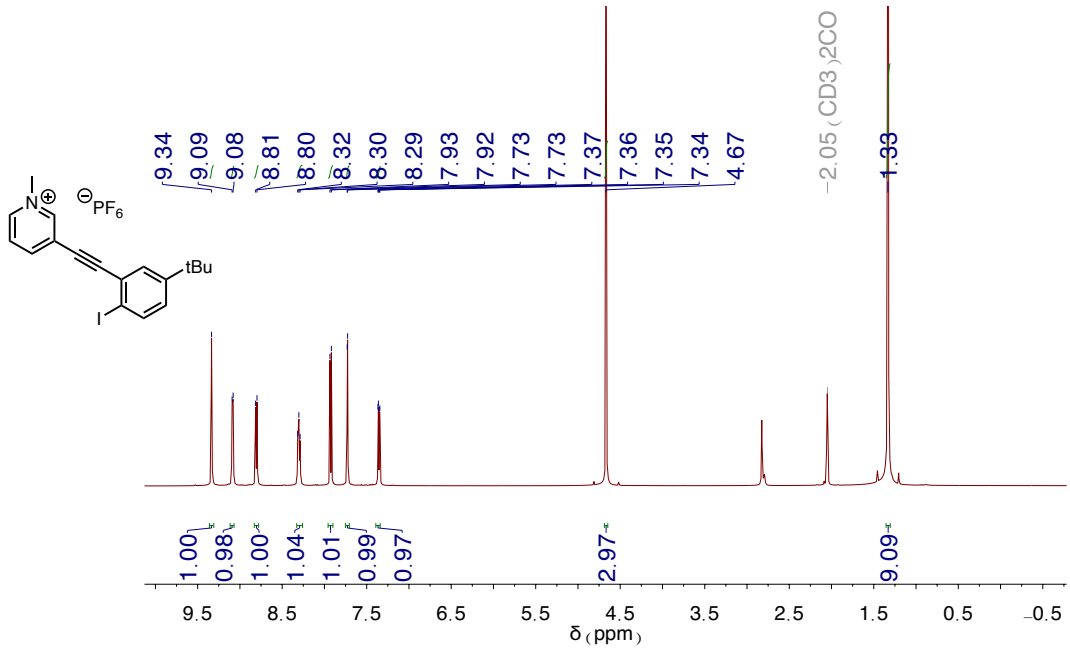

Figure B.58. ^{1}H NMR spectrum of **5d • PF_6^-**.

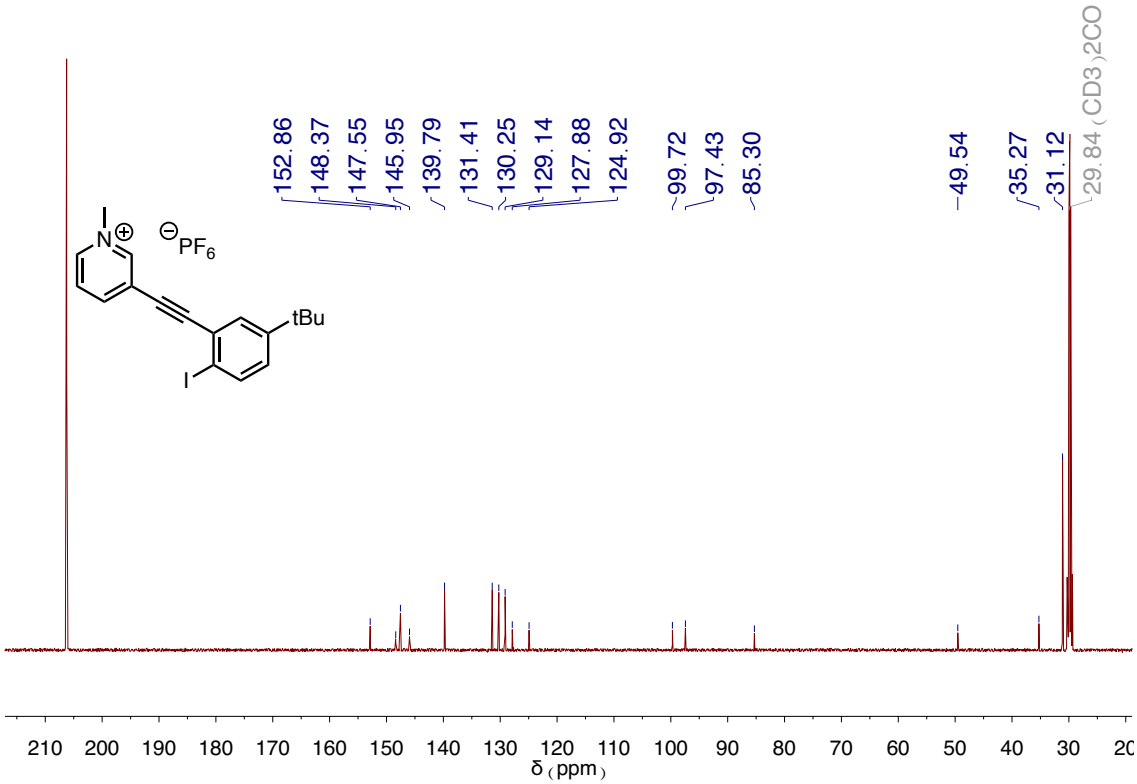

Figure B.59. ^{13}C NMR spectrum of **5d • PF_6^-**.

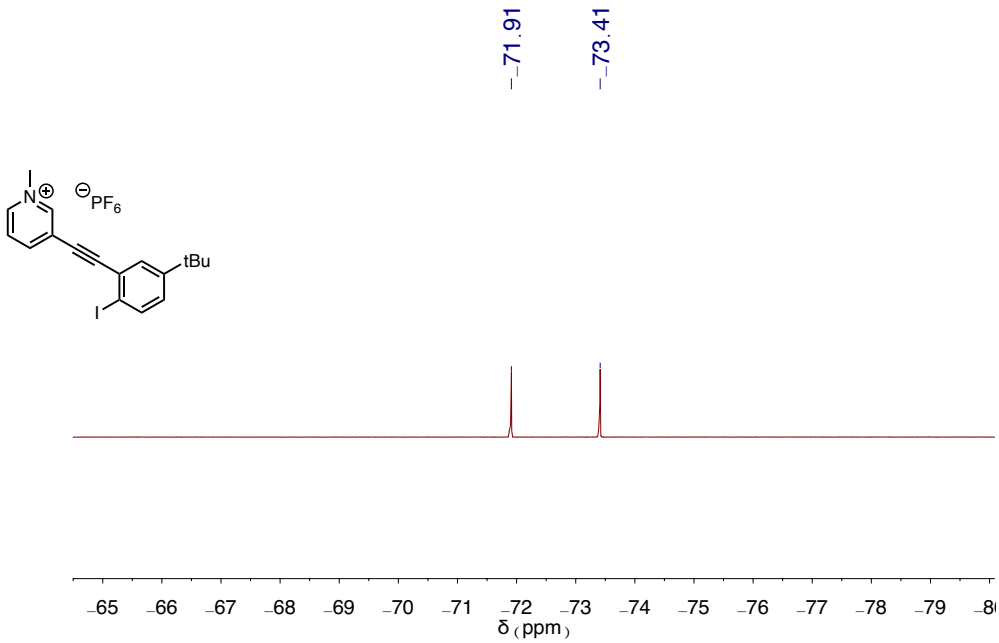

Figure B.60. ^{19}F NMR spectrum of **5d • PF_6^-**.

APPENDIX C

SUPPLEMENTARY CONTENT FOR CHAPTER IV

Experimental Details

Materials and Methods.

Unless otherwise noted all reactions were run open to the atmosphere and consequently were exposed to air and water. All reagents were used as purchased from commercial sources. The ^{1}H NMR, ^{13}C NMR, and ^{19}F spectra were obtained using a Bruker 500 MHz spectrometer (^{1}H 500 MHz, ^{13}C 126 MHz, ^{19}F 471 MHz), and the ^{1}H NMR titrations were performed on a Varian 500 MHz spectrometer (^{1}H 500.10 MHz). All ^{1}H NMR and ^{13}C NMR chemical shifts (δ) are reported in parts per million and referenced to residual solvent peaks ($CHCl_3$: ^{1}H 7.26 ppm, ^{13}C 77.16 ppm; $(CH_3)_2CO$: ^{1}H 2.05ppm, ^{13}C 29.84 and 206.26 ppm; CH_3CN ^{1}H 1.94 ppm, ^{13}C 118.26 and 1.32 ppm).

Masses for novel compounds were determined with a Waters Xevo G2-XS ToF spectrometer.

Full Receptor Synthesis.

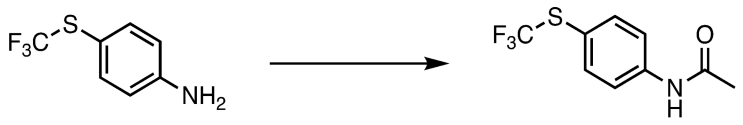

4-(trifluoromethylthio)acetamide, 2.

4-(trifluoromethylthio)aniline (7.4 mL, 71.8 mmol) was added under N_2 to an oven-dried, vacuum-cooled round bottom flask. Acetic anhydride (10.2 mL, 108 mmol) was added to the flask dropwise and a white precipitate crashed out upon addition. The mixture was stirred at room temperature for one hour. Afterwards, the solid was dissolved using ethyl acetate and washed with water and brine. The organic layer was dried (Na_2SO_4), filtered, and concentrated to give the crude protected aniline. The white powdered product was purified by running the crude product through a plug with dichloromethane. (12 g, 71% yield). ^{1}H NMR (500 MHz, Acetone-d_6) δ 9.44 (s, 1H), 7.80 (d, J = 8.7 Hz, 2H), 7.63 (d, J = 8.7 Hz, 2H), 2.11 (s, 3H).

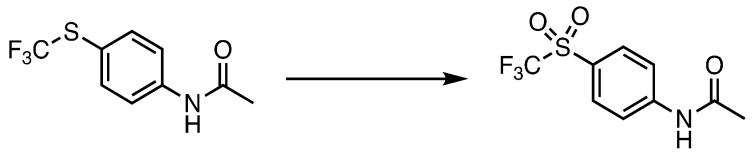

N-[4-[(trifluoromethyl)sulfonyl]phenyl]acetamide, 3.

In an oven-dried, vacuum-cooled round bottom flask, the 4-(trifluoromethyl)thio phenyl acetamide (12 g, 51.0 mmol) was dissolved in 200 mL of dry dichloromethane and cooled to 0 ºC. mCPBA (26 g, 153 mmol) was added in 4 portions under a heavy $N_{2\,(g)}$ flow. The reaction was allowed to warm up to room temperature while stirring overnight. The

reaction mixture was diluted with more dichloromethane and $Na_2S_2O_3$ was used to quench any excess mCPBA. The mixture was extracted with dichloromethane and the combined organic layers were washed with $Na_2S_2O_3$, $NaHCO_3$, water and brine, then dried (Na_2SO_4) and concentrated to afford a white precipitate (11.4 g, 84% yield). ^{1}H NMR (500 MHz, Acetone-d_6) δ 9.84 (s, 1H), 8.08 – 8.00 (m, 4H), 2.18 (s, 3H).

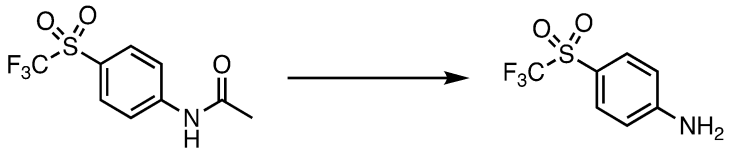

N-[4-[(trifluoromethyl)sulfonyl]phenyl]aniline, 4.

N-[4-[(trifluoromethyl)sulfonyl]phenyl]acetamide (6.2 g, 23.15 mmol) was dissolved in 200 mL of EtOH; KOH (1.43 g, 25.46 mmol) was added, and the reaction mixture was set to 60 ºC and allowed to stir. After 3 hours, the mixture was concentrated to afford a crude solid which was then dissolved in water. White precipitate formed and collected via vacuum filtration to afford pure product (4.7 g, 90% yield). ^{1}H NMR (500 MHz, Chloroform-*d*) δ 7.75 (d, *J* = 8.8 Hz, 2H), 6.75 (d, *J* = 8.8 Hz, 2H), 4.54 (s, 2H).

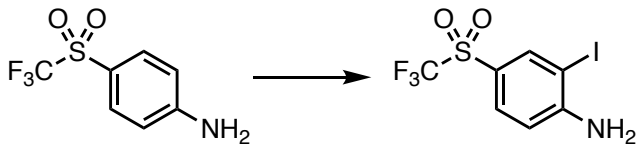

Iodoaniline, 5.

The aniline (4.68 g, 20.76 mmol) was dissolved in 40 mL methanol. In another flask, KIO_3 (1.56 g, 7.27 mmol) and KI (2.28 g, 13.70 mmol) were dissolved in 100 mL water. The aqueous solution was added to the solution containing the aniline then 1 M HCl (23 mL) was added dropwise. After the reaction stirred at room temperature overnight, the mixture

was extracted with ethyl acetate. The combined organic layers were then washed with $Na_2S_2O_3$, $NaHCO_3$, water, and brine, then dried (Na_2SO_4) and concentrated to afford crude product which was then purified by flash chromatography (gradient from 100% hexanes to 2:8 ethylacetate: hexanes) to afford a pure red/brown solid (6.72 g, 92% yield). ^{1}H NMR (500 MHz, Chloroform-*d*) δ 8.22 (d, *J* = 2.1 Hz, 1H), 7.74 (dd, *J* = 8.6, 2.1 Hz, 1H), 6.81 (d, *J* = 8.6 Hz, 1H), 4.99 (s, 2H). ^{13}C NMR (126 MHz, $CDCl_3$) δ 153.83, 142.11, 132.45, 123.86, 121.27, 118.88, 118.68, 116.09, 113.44, 81.85, 77.16. ^{19}F NMR (471 MHz, $CDCl_3$) δ -78.79.

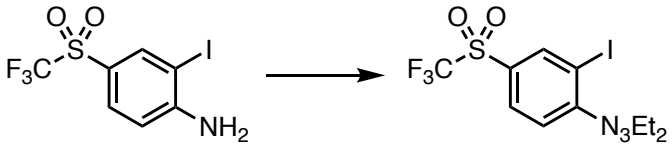

Iodotriazene, 6.

The iodoaniline (1.6 g, 4.56 mmol) was dissolved in 30 mL acetonitrile and set to cool at -10 ºC. Concentrated HCl (3.04 mL) was added to the flask. In another flask, a solution of $NaNO_2$ (0.755 g, 10.94 mmol) in 30 mL water was prepared. The aqueous $NaNO_2$ solution was added dropwise to the solution with the iodoaniline and left to stir at -10 ºC. This reaction mixture was monitored by TLC for consumption of starting material. Once consumed, the reaction mixture was added to a quench solution of: $HNEt_2$ (4.71 mL, 45.47 mmol) and K_2CO_3 (3.65 g, 26.43 mmol) in 50 mL of acetonitrile and 100 mL of water at -10 ºC. This quenched reaction mixture was allowed to warm up to room temperature while continuously stirring overnight. The reaction was extracted with ether and the combined organic layers were washed with $Na_2S_2O_3$, $NaHCO_3$, water, and brine. The organic layer was collected and dried (Na_2SO_4) and concentrated to afford the crude iodotriazene that

was purified by column chromatography (gradient from pure hexanes to 1:9, dichloromethane:hexanes) to afford pure orange solid. (0.55 g, 28% yield.) ^{1}H NMR (500 MHz, Chloroform-*d*) δ 8.11 (d, *J* = 2.2 Hz, 1H), 7.56 (dd, *J* = 8.6, 1.9 Hz, 1H), 7.27 (d, *J* = 8.7 Hz, 1H), 3.60 (qd, *J* = 7.2, 5.1 Hz, 4H), 1.07 (dt, *J* = 30.0, 7.2 Hz, 6H). ^{13}C NMR (126 MHz, $CDCl_3$) δ 157.06, 141.51, 131.04, 126.15, 123.75, 121.16, 118.56, 117.34, 115.97, 96.24, 50.42, 43.64, 14.29, 10.69. ^{19}F NMR (471 MHz, $CDCl_3$) δ -77.75.

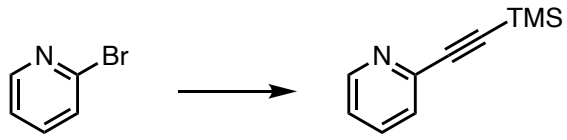

TMS-protected 2-ethynylpyridine.

After a mixture of 10 mL tetrahydrofuran and 10 mL acetonitrile, 2-bromopyridine (0.30 mL, 3.16 mmol), $Pd(PhCN)_2Cl_2$ (0.061g, 0.158 mmol) and CuI (0.030 g, 0.158 mmol) was outgassed with $N_{2\,(g)}$ for 20 minutes, the ligand P(*t*Bu)$_3$ (0.09 mL, 0.316 mmol) was added. The alkyne, TMSA (0.68 mL, 4.74 mmol) was then added dropwise. The reaction was allowed to stir at room temperature under a steady flow of $N_{2\,(g)}$ overnight. The reaction mixture was run through a silica/celite plug and washed with DCM to afford the crude product that was then purified by column chromatography (gradient from pure hexanes to 2:8, ethylacetate:hexanes) to afford a pure brown oil. (0.527 g, 95% yield). ^{1}H NMR (500 MHz, Chloroform-d) δ 8.57 (ddd, J = 5.0, 1.8, 1.0 Hz, 1H), 7.63 (td, J = 7.7, 1.8 Hz, 1H), 7.45 (dt, J = 7.8, 1.1 Hz, 1H), 7.22 (ddd, J = 7.6, 4.9, 1.2 Hz, 1H), 0.27 (s, 9H).

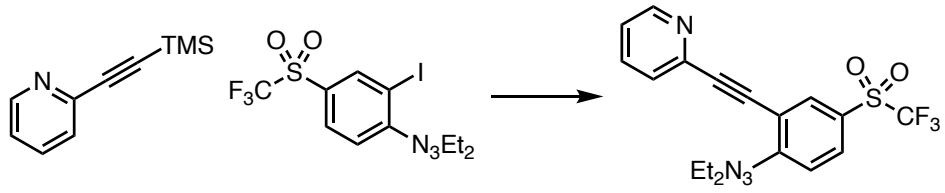

Triazene receptor intermediate, 7.

The 2-ethynylpyridine (0.30 g, 1.71 mmol) was dissolved in Et_2O and set stirring in a flask. Tetrabutylammonium fluoride (TBAF, 2.4 mL, 2.40 mmol) was then added to the solution and left stirring until the SM had disappeared by TLC (~ 20 min.). Then, the solution was quenched with NH_4Cl and extracted with water and brine x2. This solution was then dried, and solvent was removed *in vacuo* to furnish 2-ethynylpyridine in quantitative yields. While this was going on, another flask of 50% THF and 50% DIPA (20 mL total) was outgassed with N_2 for at least twenty minutes. While that was occurring, isolated 2-ethynylpyridine (0.15 g, 1.46 mmol) was dissolved in a minimal amount of THF and outgassed–for at least 1 min./mL of solvent–in a separate flask. After outgassing, the iodotriazene (0.488 g, 1.12 mmol), $Pd(PPh_3)_2$ (0.130 g, 0.112 mmol) and CuI (0.013 g, 0.067 mmol) were added to the RBF with the THF/DIPA mixture and set to stir under N_2(g). The separate solution of 2-ethynylpyridine in THF was then cannulated dropwise to the iodotriazene/catalyst mixture and the reaction was left stirring at 55 °C overnight. The next day, the reaction was passed through a silica/celite plug, washed with DCM, and concentrated to afford the crude product that was purified by column chromatography (gradient from 1:9, DCM:hexanes to 100% DCM) to give a pure amber oil (0.207 g, 45% yield). ^{1}H NMR (500 MHz, Chloroform-d) δ 8.64 (d, J = 4.4 Hz, 1H), 8.24 (d, J = 2.2 Hz, 1H), 7.85 (dd, J = 8.8, 2.2 Hz, 1H), 7.69 (dd, J = 8.2, 6.0 Hz, 2H), 7.50 (d, J = 7.8 Hz, 1H), 7.29 – 7.23 (m, 1H), 3.92 (dq, J = 17.6, 7.2 Hz, 4H), 1.37 (dt, J = 32.5, 7.1 Hz, 6H).

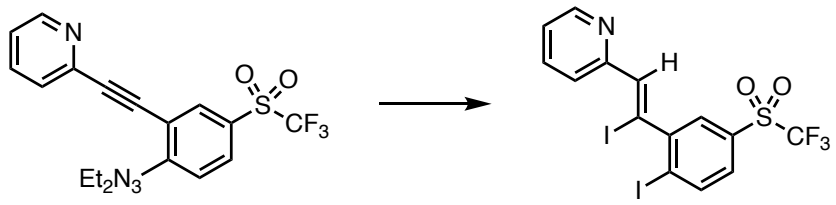

Vinylic iodo receptor intermediate, 8.

HI (0.14 mL, 1.07 mmol) and I_2 (0.272 g, 1.07 mmol) were dissolved in CH_3CN (30 mL) then set to stir at 60 °C. While the first solution was coming up to temperature the triazene (0.22 g, 0.54 mmol) was dissolved in CH_3CN (10 mL). The triazene solution was then added dropwise into the first flask and stirred at 60 °C while monitoring via TLC. After the SM was consumed then the mixture was extracted with EtOAc and washed with $NaHCO_3$, $Na_2S_2O_3$, and water x2 each. The EtOAc was then dried with Na_2SO_4 and concentrated to form an oil which was purified on silica via column chromatography (gradient from 100% hexanes to 1:9 ethylacetate:hexanes) to get pure product (0.218 g, 72% yield). ^{1}H NMR (500 MHz, Chloroform-d) δ 8.72 (dt, J = 4.8, 1.4 Hz, 1H), 8.23 (d, J = 8.4 Hz, 1H), 7.98 (d, J = 2.3 Hz, 1H), 7.85 – 7.76 (m, 2H), 7.57 (dd, J = 8.3, 2.2 Hz, 1H), 7.32 (ddd, J = 6.7, 4.7, 1.6 Hz, 1H), 7.01 (s, 1H). ^{13}C NMR (126 MHz, Chloroform-*d*) δ 154.57, 151.08, 149.81, 141.73, 140.84, 136.41, 131.80, 130.49, 130.22, 124.04, 123.65, 119.70 (q, J = 326.0 Hz), 109.99, 99.92.

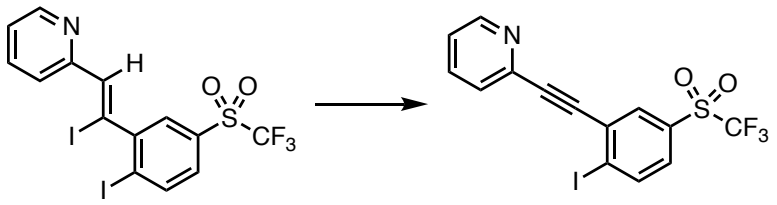

Neutral *ortho* receptor, 9.

In a round bottomed flask, the alkene (0.100 g, 0.18 mmol) was refluxed with triethylamine (10 mL) overnight. The crude reaction mixture was run through a silica plug and washed down with dichloromethane and acetone. The organic mixture was concentrated to afford a pure amber oil product (0.077 g, quant. yield). ^{1}H NMR (500 MHz, Chloroform-*d*) δ 8.69 (ddd, *J* = 4.9, 1.8, 1.0 Hz, 1H), 8.22 (d, *J* = 8.4 Hz, 1H), 8.17 (d, *J* = 2.3 Hz, 1H), 7.75 (td, *J* = 7.7, 1.8 Hz, 1H), 7.66 – 7.60 (m, 2H), 7.34 (ddd, *J* = 7.7, 4.9, 1.2 Hz, 1H).

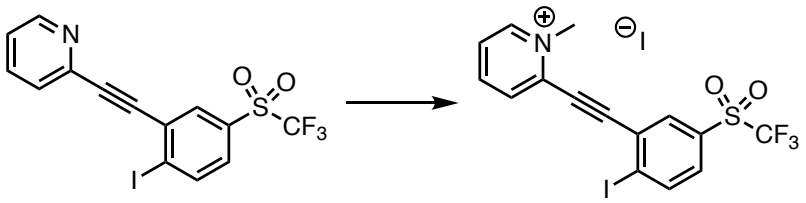

Methylated ethynyl pyridine, 10.

The neutral receptor (0.05 g, 0.11 mmol) was added to a bomb flask followed by an excess of MeI (5 mL). The reaction vessel was then sealed and set stirring at 110 °C overnight. Over the next 24 hours the product would precipitate out of solution. The yellow precipitate was collected and washed with minimal DCM to afford pure yellow solid (0.065 g, quant. yield). ^{1}H NMR (500 MHz, Acetone-d_6) δ 9.41 (d, *J* = 6.2 Hz, 1H), 8.82 (t, *J* = 7.9 Hz, 1H), 8.68 – 8.63 (m, 1H), 8.59 (d, *J* = 8.4 Hz, 1H), 8.49 (d, *J* = 2.2 Hz, 1H), 8.37 – 8.30 (m, 1H), 8.00 (dd, *J* = 8.4, 2.2 Hz, 1H), 4.87 (s, 3H). ^{19}F NMR (471 MHz, Acetone) δ -79.32.

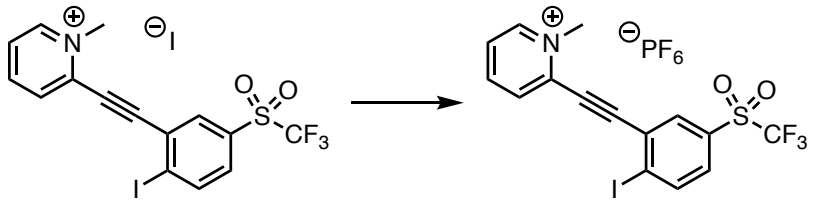

Methylated PF_6 pyridine receptor, 10.

The methylated receptor (0.065 g, 0.11 mmol) was then dissolved in 10 mL of acetone and 40 mL of water and set to stir. To this flask, $AgPF_6$ (0.071 g, 0.28 mmol) was added and stirred for about 40 minutes during which time gray ppt (AgI) formed. This ppt was filtered off and the filtrate solvent was removed *in vacuo* until only water remained. At this point white ppt (final product) began to crash out of the water and was collected via filtration and washed with minimal water to give the final pure white powder (0.066 g, quant. yield). ^{1}H NMR (500 MHz, Acetone-d_6) δ 9.32 (d, J = 6.2 Hz, 1H), 8.82 (td, J = 7.9, 1.4 Hz, 1H), 8.67 – 8.61 (m, 2H), 8.52 (d, J = 2.3 Hz, 1H), 8.34 (ddd, J = 7.8, 6.2, 1.6 Hz, 1H), 8.02 (dd, J = 8.4, 2.3 Hz, 1H), 4.87 (s, 3H). ^{19}F NMR (471 MHz, Acetone) δ -71.91, -73.42, -79.28.

Titrations

General Methods. ^{1}H NMR spectra were acquired at room temperature on a Varian Inova 500 MHz spectrometer (500.11 MHz). ^{1}H chemical shifts (δ) are expressed in ppm relative to residual CH_3CN (calibrated to 1.94 ppm) shifts.

General Procedure. A 4.0 mL host solution (0.9-1.5 mM in CD_3CN) was prepared. Of this, 500 μL was added to a septum-sealed NMR tube. A 19-30 mM host/guest (TBAX, where X = I, Br, or Cl) stock solution was prepared using the remaining 3.5 mL of host solution. Aliquots of the host/guest solution were added to the NMR tube using Hamilton gas-tight syringes, and ^1H NMR spectra were recorded at 25 °C after each addition of guest. The Δδ of the CH_{aryl} and CH_{methyl} protons were used to follow the progress of the titration, and association constants were determined using the Thordarson method.

Table C.1. Representative ^1H NMR Titration of **10 • PF6**$^-$ with Cl^- in CD_3CN at 25 ºC.

Entry	V_{Guest} (μL)	[Host] (M)	[Cl^-] (M)	Equiv.	δ CH_{aryl}	δ CH_{methyl}
0	0	1.27E-03	0.00E+00	0.00	8.727	4.482
1	5	1.27E-03	2.09E-04	0.16	8.742	4.487
2	5	1.27E-03	4.14E-04	0.33	8.756	4.491
3	10	1.27E-03	8.12E-04	0.64	8.777	4.496
4	10	1.27E-03	1.19E-03	0.94	8.796	4.501
5	10	1.27E-03	1.56E-03	1.23	8.813	4.506
6	15	1.27E-03	2.09E-03	1.65	8.834	4.511
7	15	1.27E-03	2.59E-03	2.04	8.852	4.515
8	15	1.27E-03	3.07E-03	2.42	8.868	4.520
9	20	1.27E-03	3.66E-03	2.89	8.887	4.525
10	20	1.27E-03	4.22E-03	3.33	8.903	4.529
11	20	1.27E-03	4.75E-03	3.74	8.917	4.533
12	30	1.27E-03	5.47E-03	4.31	8.935	4.537
13	50	1.27E-03	6.55E-03	5.16	8.958	4.543
14	100	1.27E-03	8.32E-03	6.56	8.993	4.552

15	200	1.27E-03	1.08E-02	8.52	9.032	4.561
16	500	1.27E-03	1.42E-02	11.19	9.065	4.570
17	500	1.27E-03	1.59E-02	12.53	9.071	4.571

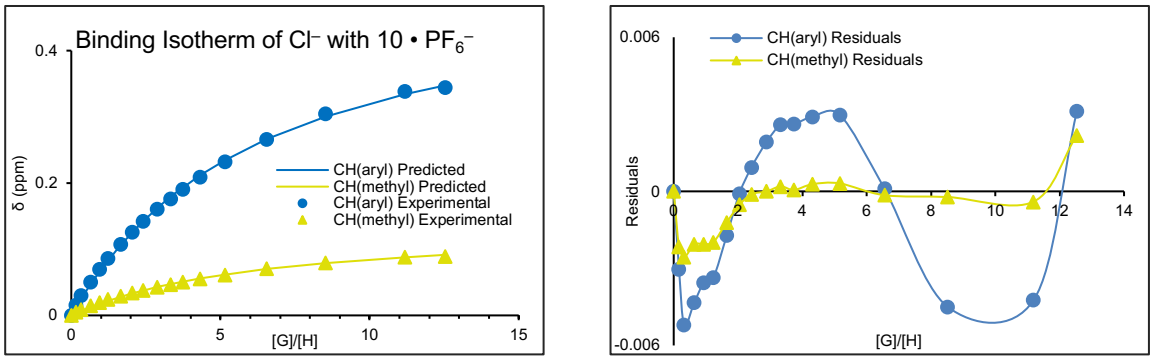

Figure C.1. Representative binding isotherm and residuals for Cl^- titration of receptor **10 • PF_6^-** in CD_3CN at 25 °C determined by ^1H NMR spectroscopy.

Table C.2. Representative ^1H NMR Titration of **10 • PF6**$^-$ with Br^- in CD_3CN at 25 ºC.

Entry	V_{Guest} (µL)	[Host] (M)	[Br^-] (M)	Equiv.	δ CH_{aryl}	δ CH_{methyl}
0	0	1.06E-03	0.00E+00	0.00	8.727	4.483
1	5	1.06E-03	2.09E-04	0.20	8.735	4.486
2	5	1.06E-03	4.15E-04	0.39	8.743	4.488
3	10	1.06E-03	8.13E-04	0.77	8.755	4.493
4	10	1.06E-03	1.20E-03	1.13	8.766	4.496
5	10	1.06E-03	1.57E-03	1.48	8.775	4.500
6	15	1.06E-03	2.09E-03	1.98	8.787	4.504
7	15	1.06E-03	2.60E-03	2.45	8.798	4.508
8	15	1.06E-03	3.07E-03	2.90	8.807	4.511
9	20	1.06E-03	3.67E-03	3.46	8.818	4.515

10	20	1.06E-03	4.23E-03	3.99	8.826	4.517
11	20	1.06E-03	4.75E-03	4.48	8.834	4.520
12	30	1.06E-03	5.48E-03	5.17	8.845	4.524
13	50	1.06E-03	6.56E-03	6.19	8.858	4.529
14	100	1.06E-03	8.33E-03	7.85	8.879	4.535
15	200	1.06E-03	1.08E-02	10.21	8.902	4.543
16	500	1.06E-03	1.42E-02	13.40	8.929	4.551
17	500	1.06E-03	1.59E-02	15.01	8.935	4.553

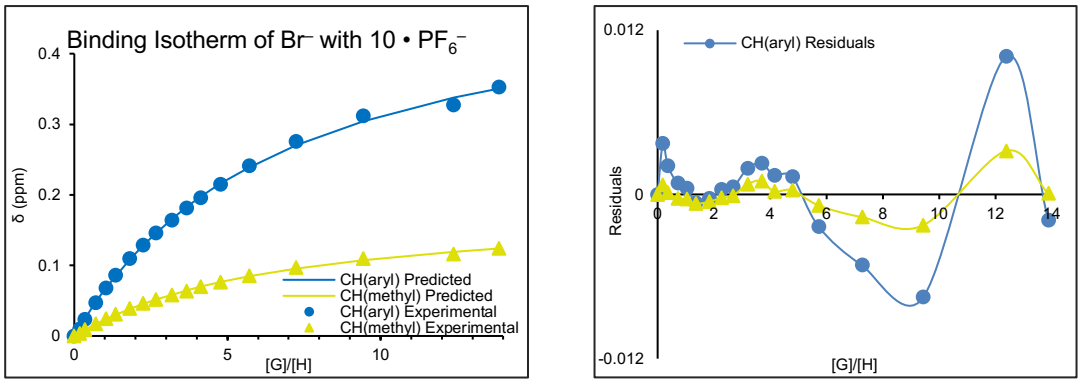

Figure C.2. Representative binding isotherm and residuals for Br^- titration of receptor **10 • PF_6^-** in CD_3CN at 25 °C determined by ^1H NMR spectroscopy.

Table C.3. Representative ^1H NMR Titration of **10 • PF6**$^-$ with I^- in CD_3CN at 25 ºC.

Entry	V_{Guest} (μL)	[Host] (M)	[I^-] (M)	Equiv.	δ CH_{aryl}	δ CH_{methyl}
0	0	1.34E-03	0.00E+00	0.00	8.730	4.487
1	5	1.34E-03	3.11E-04	0.23	8.735	4.489
2	5	1.34E-03	6.16E-04	0.46	8.739	4.491
3	10	1.34E-03	1.21E-03	0.90	8.746	4.495
4	10	1.34E-03	1.78E-03	1.32	8.752	4.498

5	10	1.34E-03	2.33E-03	1.73	8.757	4.501
6	15	1.34E-03	3.12E-03	2.32	8.765	4.504
7	15	1.34E-03	3.86E-03	2.87	8.768	4.507
8	15	1.34E-03	4.57E-03	3.40	8.774	4.509
9	20	1.34E-03	5.46E-03	4.06	8.780	4.512
10	20	1.34E-03	6.29E-03	4.68	8.785	4.515
11	20	1.34E-03	7.07E-03	5.26	8.789	4.517
12	30	1.34E-03	8.15E-03	6.06	8.795	4.520
13	50	1.34E-03	9.76E-03	7.26	8.804	4.524
14	100	1.34E-03	1.24E-02	9.22	8.815	4.530
15	200	1.34E-03	1.61E-02	11.98	8.828	4.536
16	500	1.34E-03	2.11E-02	15.72	8.845	4.544
17	500	1.34E-03	2.37E-02	17.62	8.845	4.544

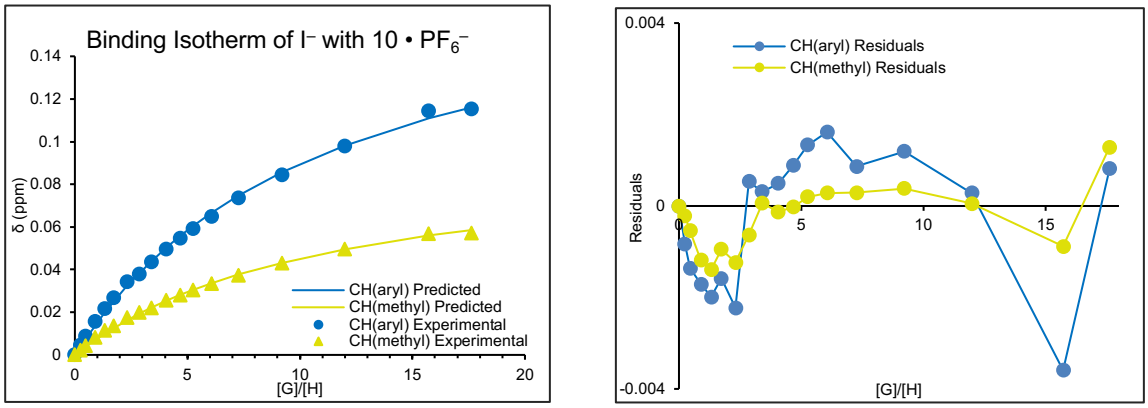

Figure C.3. Representative binding isotherm and residuals for I^- titration of receptor **10 • PF_6^-** in CD_3CN at 25 °C determined by ^1H NMR spectroscopy.

X-Ray Crystallography

Waiting on Lev for crystal Day

NMR Spectra

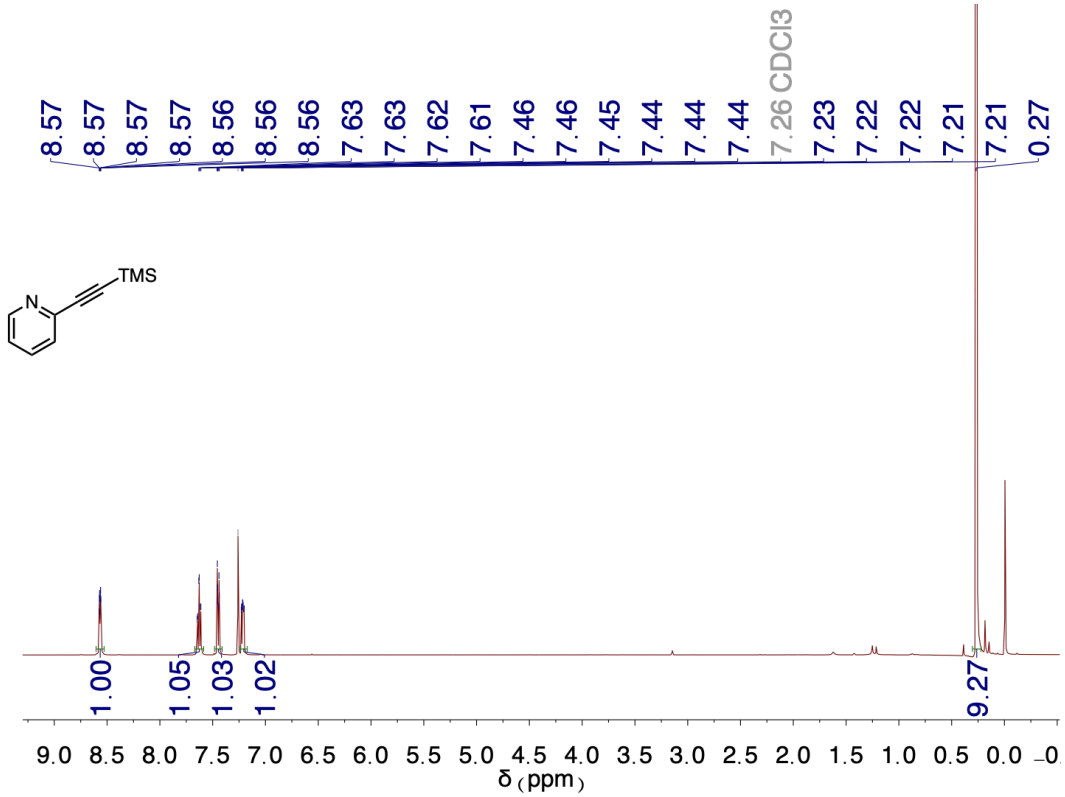

Figure C.4. ^{1}H NMR spectrum of TMS-protected 2-ethynylpyridine.

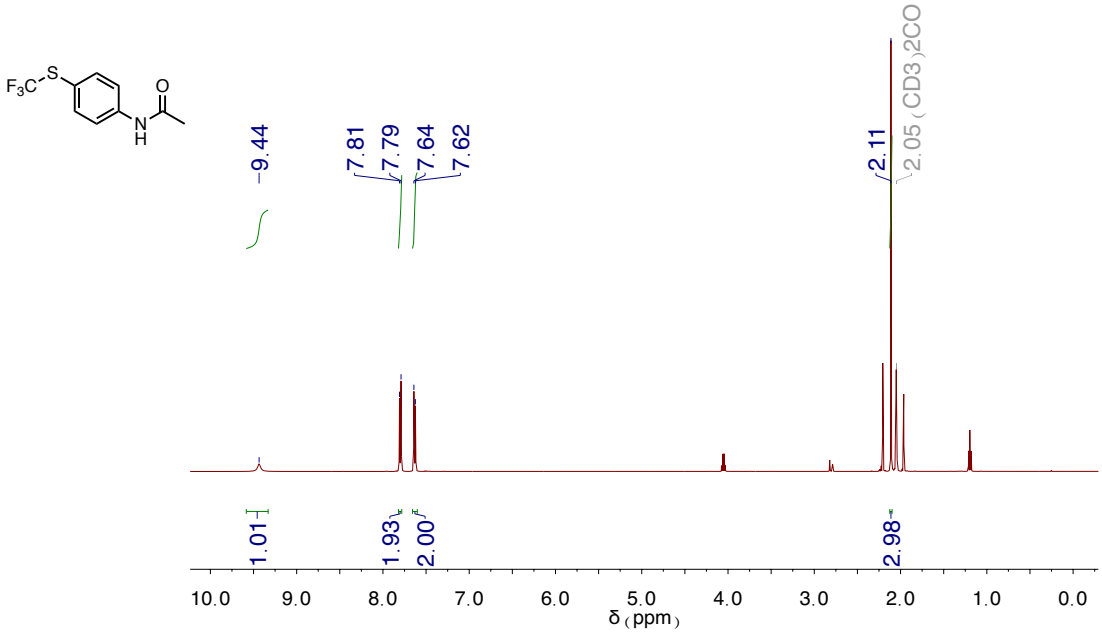

Figure C.5. ^{1}H NMR spectrum of **2**. Wet with water and ethyl acetate.

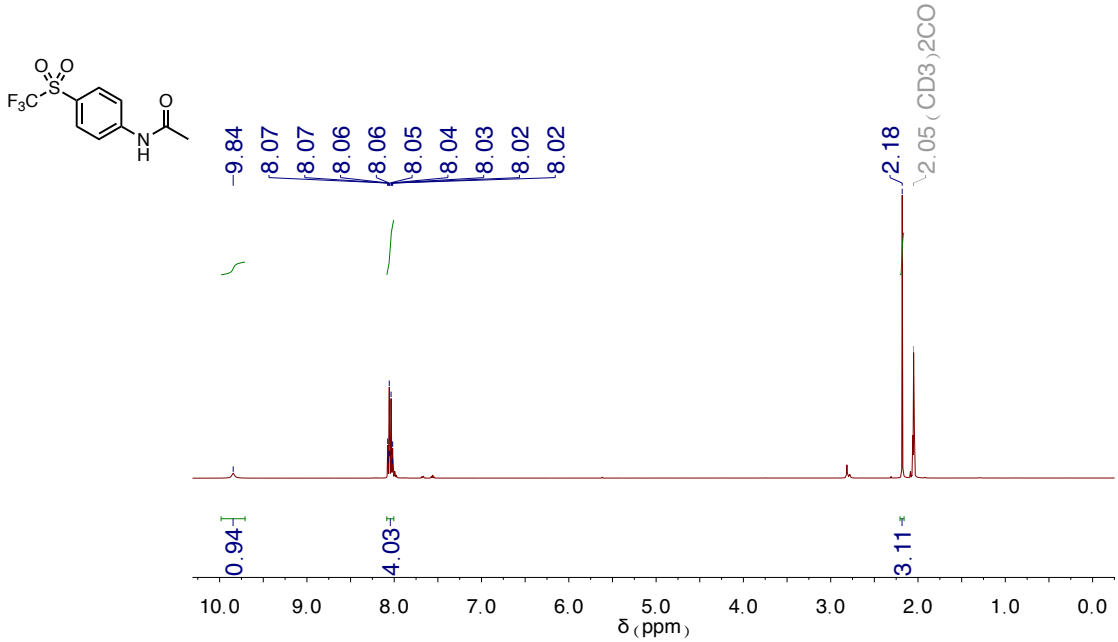

Figure C.6. ^{1}H NMR spectrum of **3**.

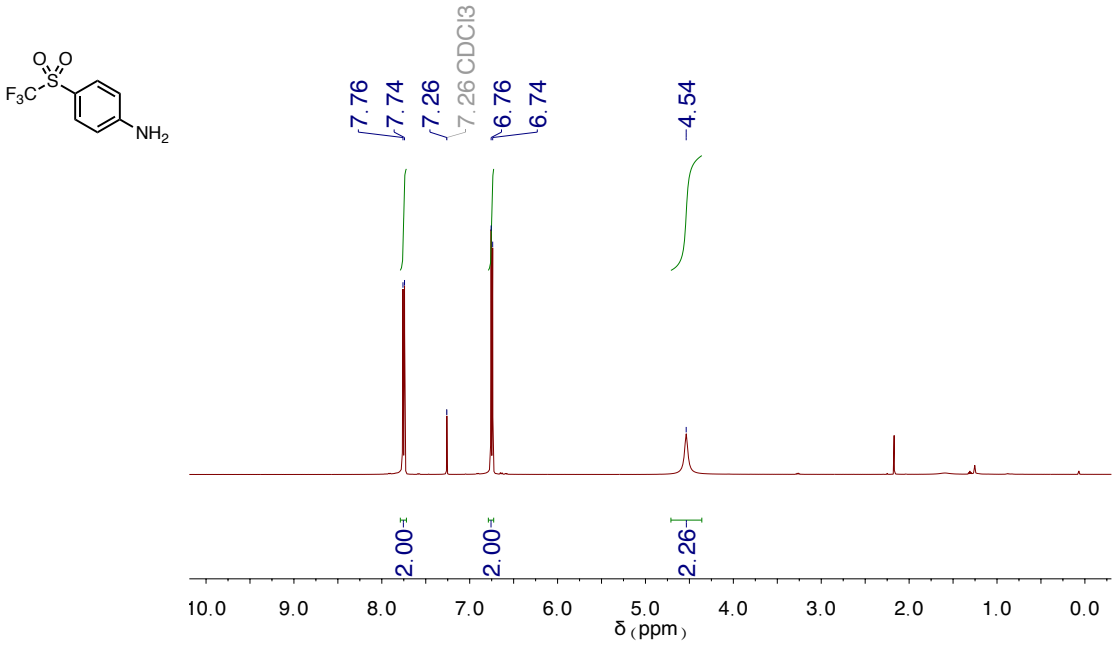

Figure C.7. ^{1}H NMR spectrum of **4**.

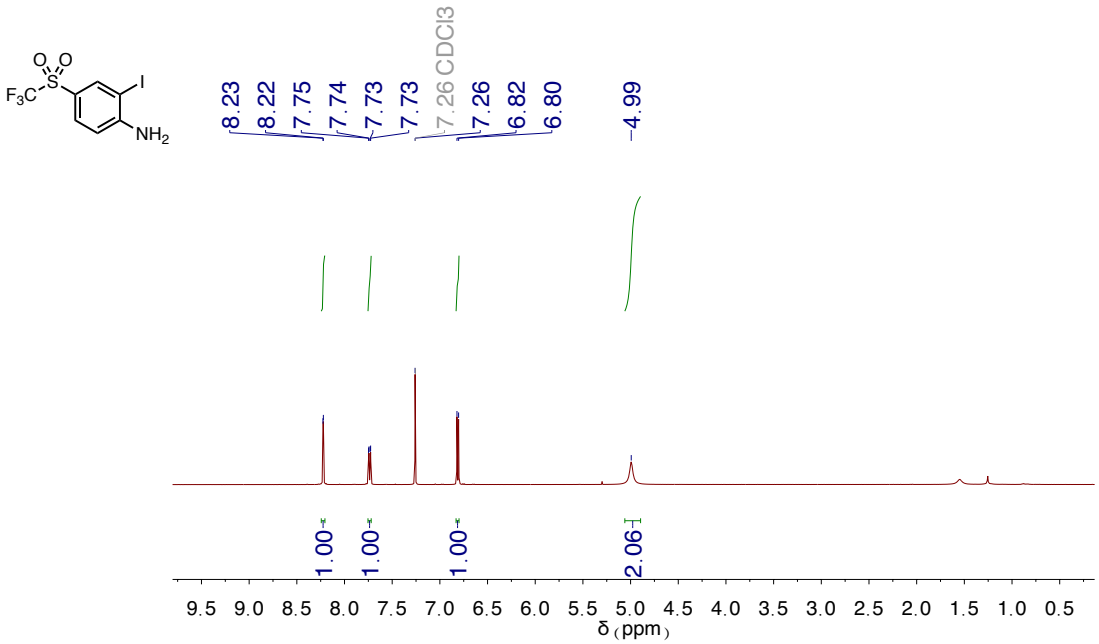

Figure C.8. ^{1}H NMR spectrum of **5**.

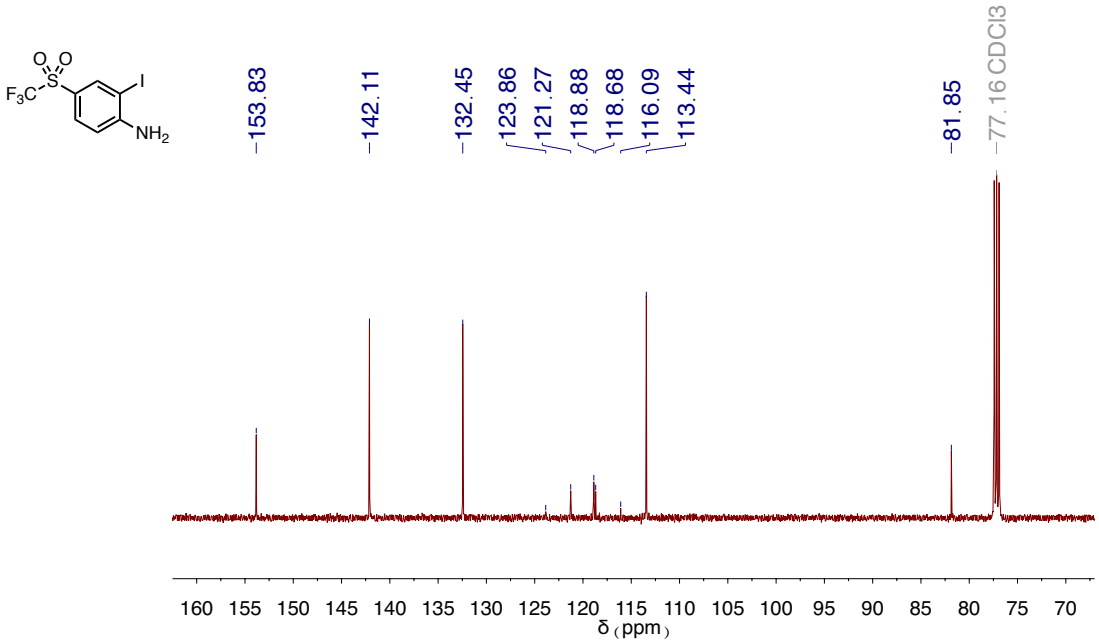

Figure C.9. ^{13}C NMR spectrum of **5**.

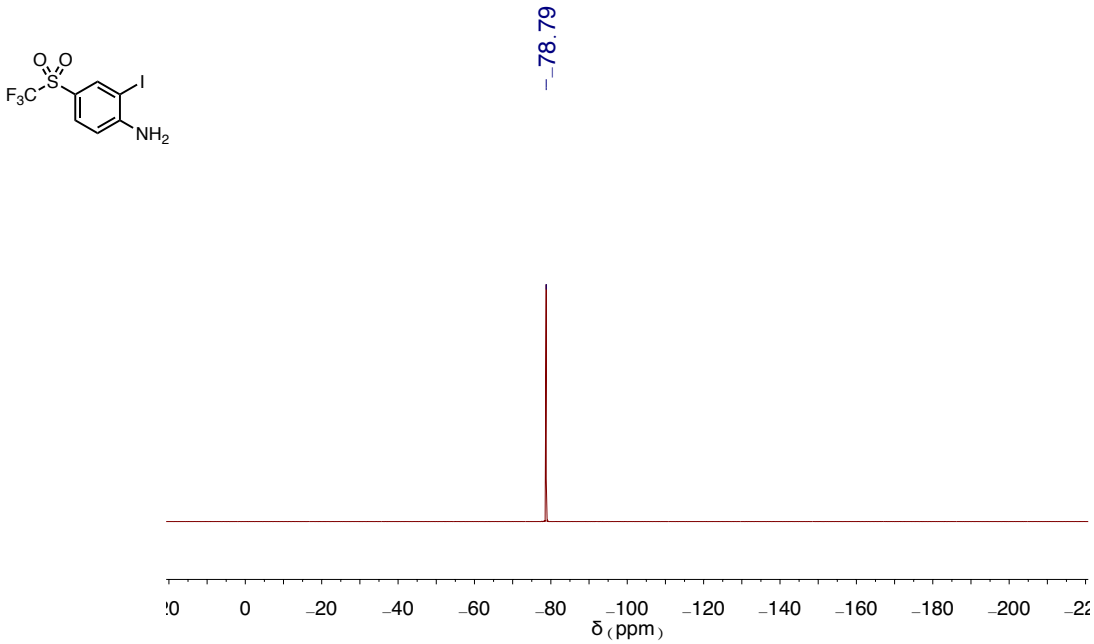

Figure C.10. ^{19}F NMR spectrum of **5**.

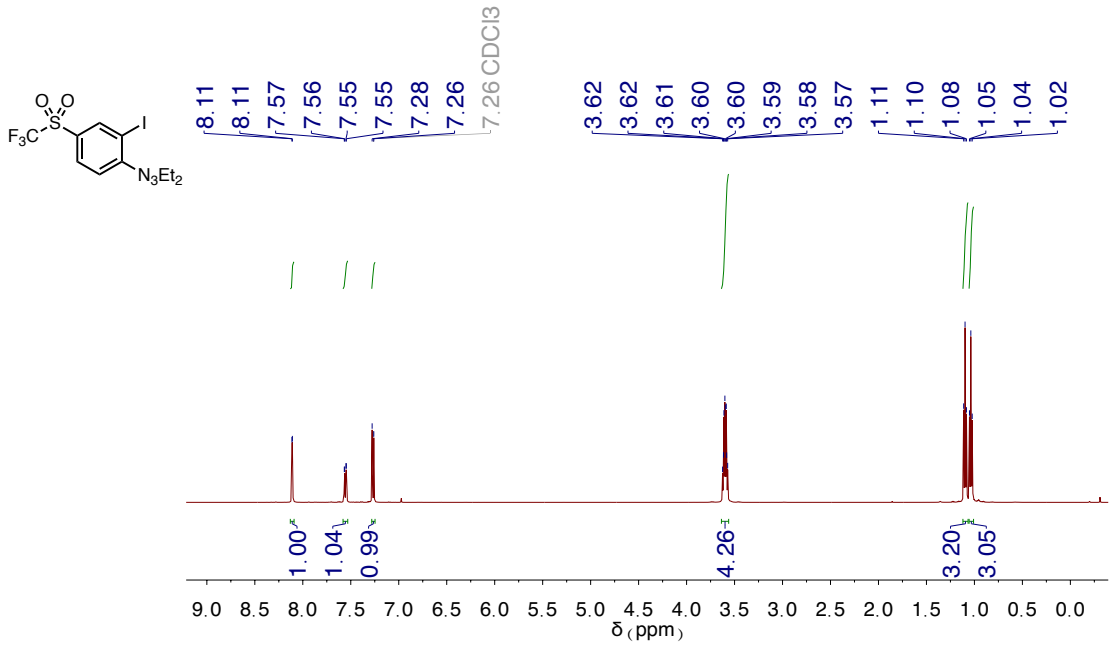

Figure C.11. ^{1}H NMR spectrum of **6**.

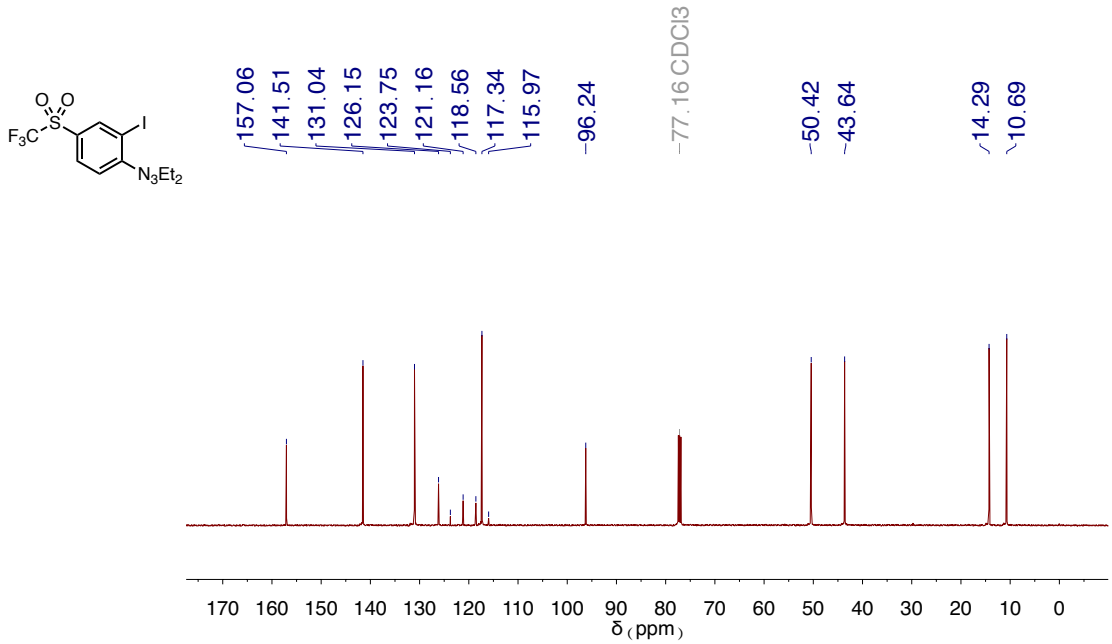

Figure C.12. ^{13}C NMR spectrum of **6**.

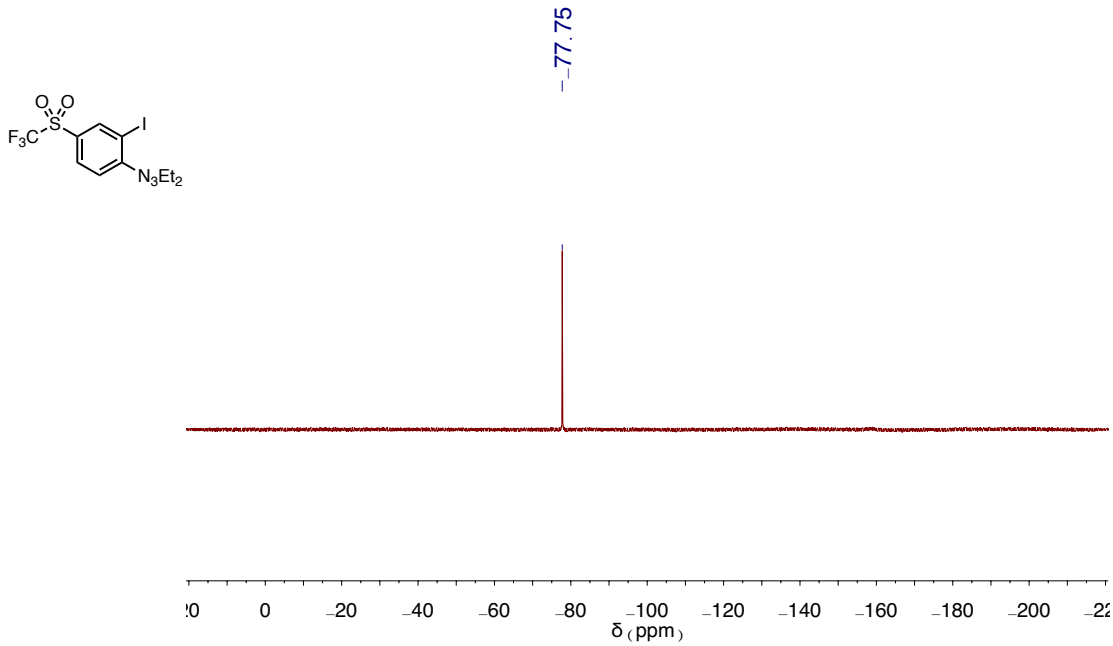

Figure C.13. ^{19}F NMR spectrum of **6**.

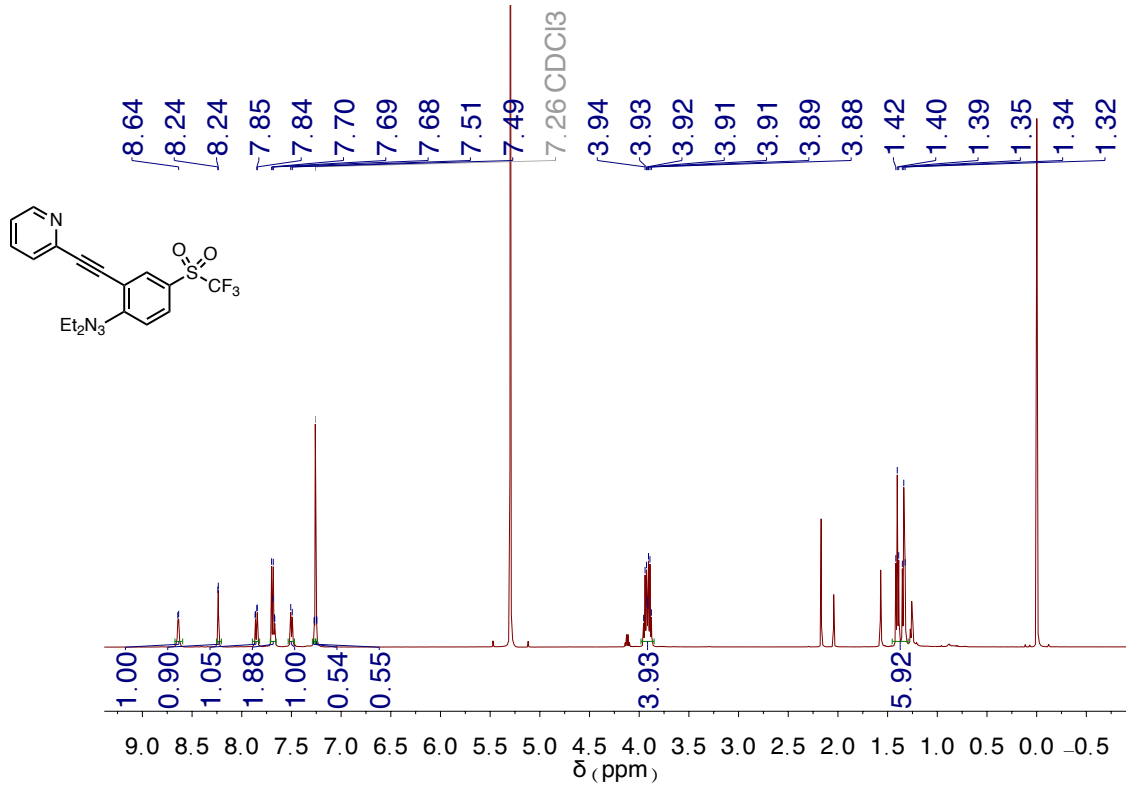

Figure C.14. [1]H NMR spectrum of **7**. Wet with dichloromethane and acetone.

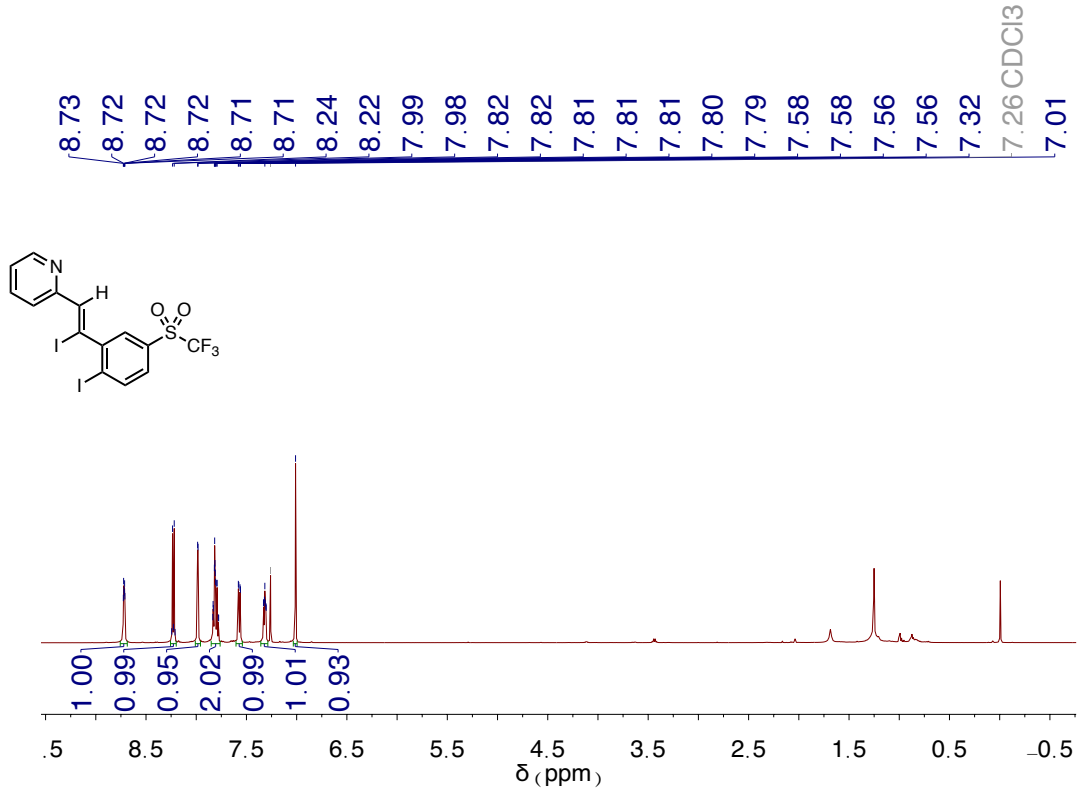

Figure C.15. [1]H NMR spectrum of **8**. Wet with water.

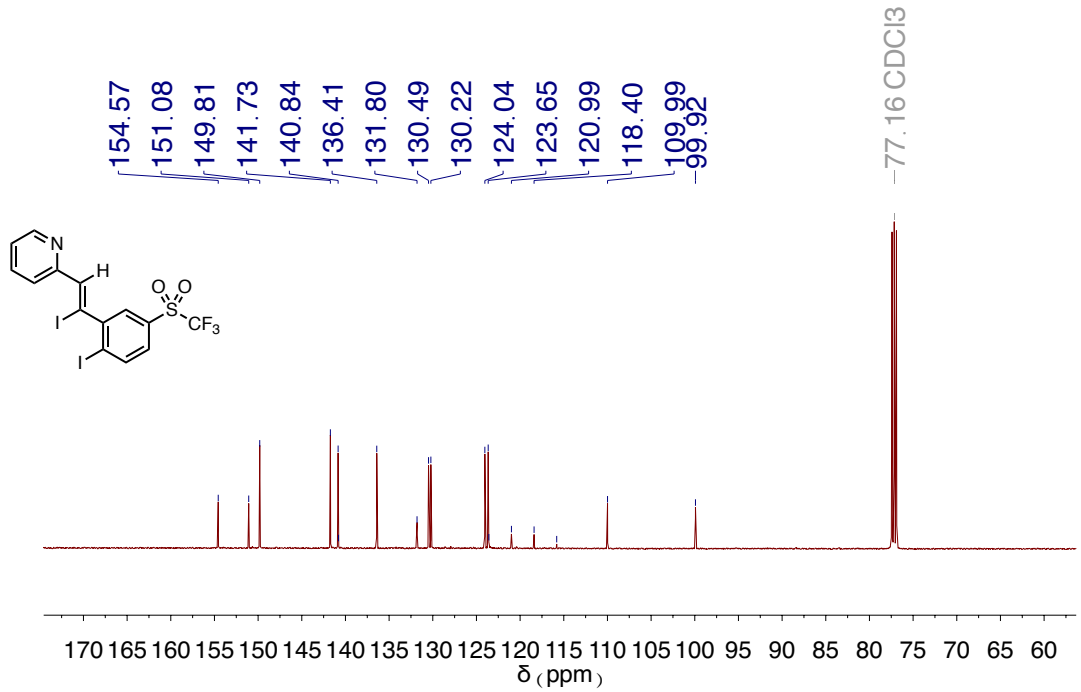

Figure C.16. ^{13}C NMR spectrum of **8**.

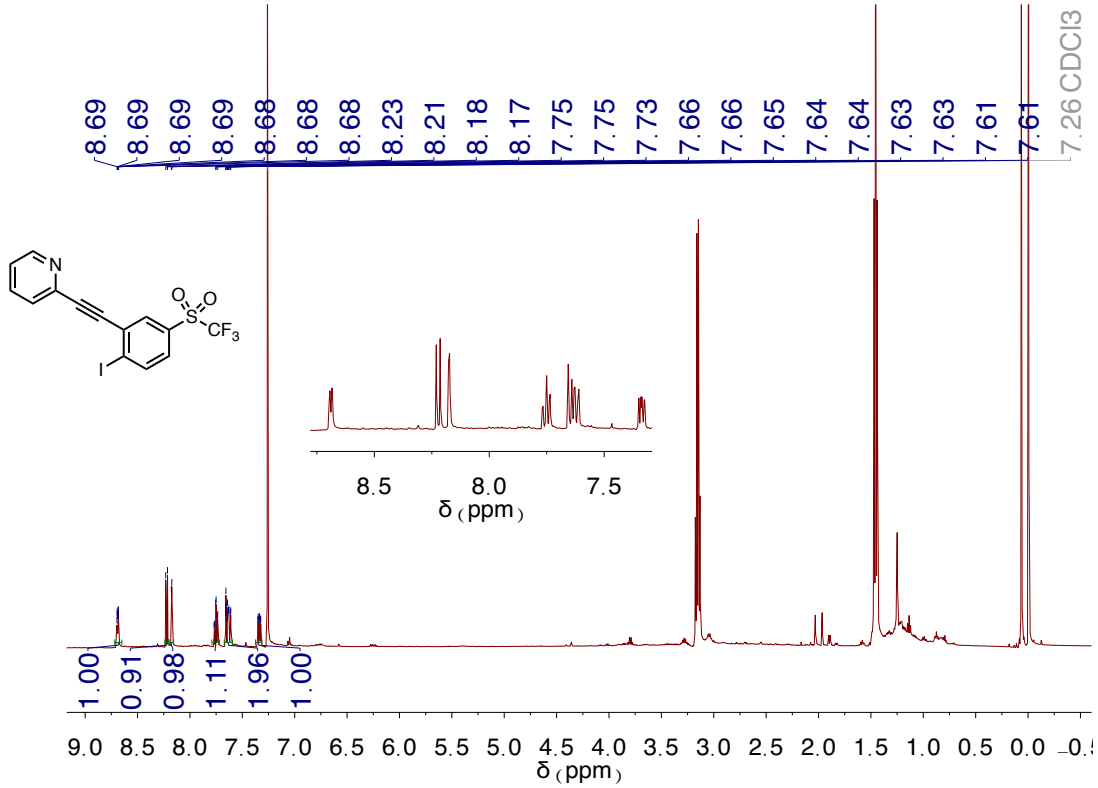

Figure C.17. ^{1}H NMR spectrum of **9**. Wet with ethyl acetate.

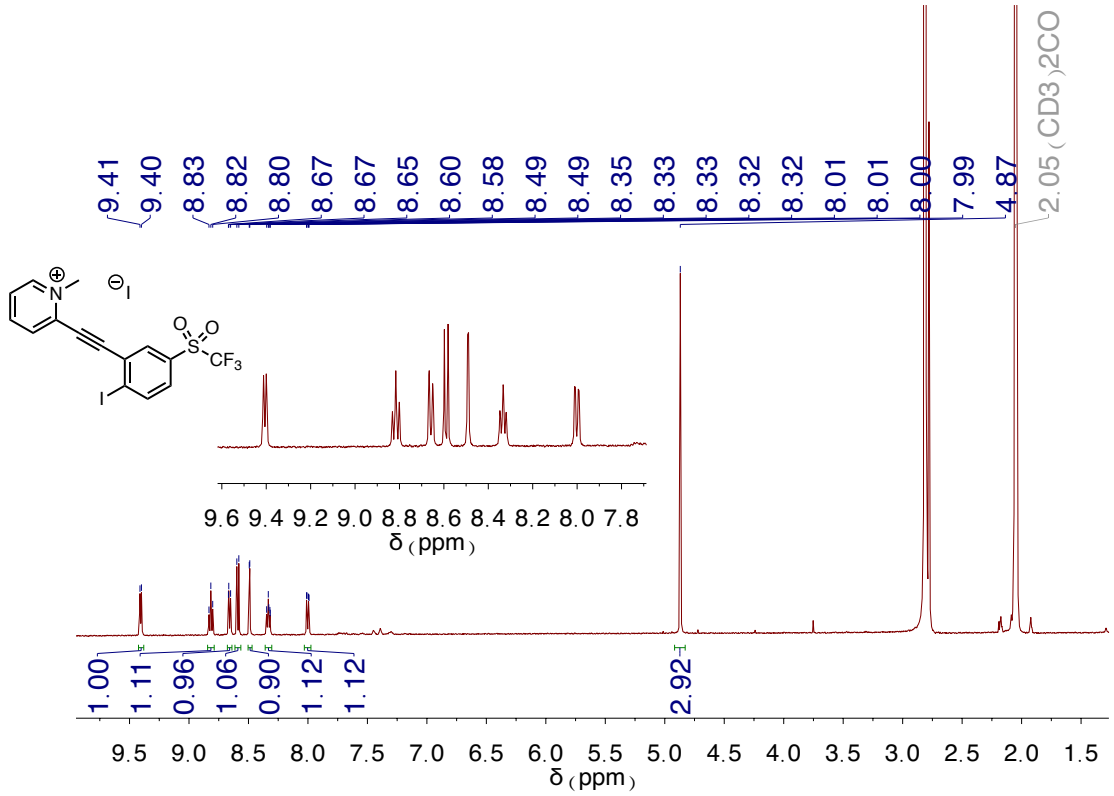

Figure C.18. ^{1}H NMR spectrum of **10 • I**$^{-}$. Wet with water.

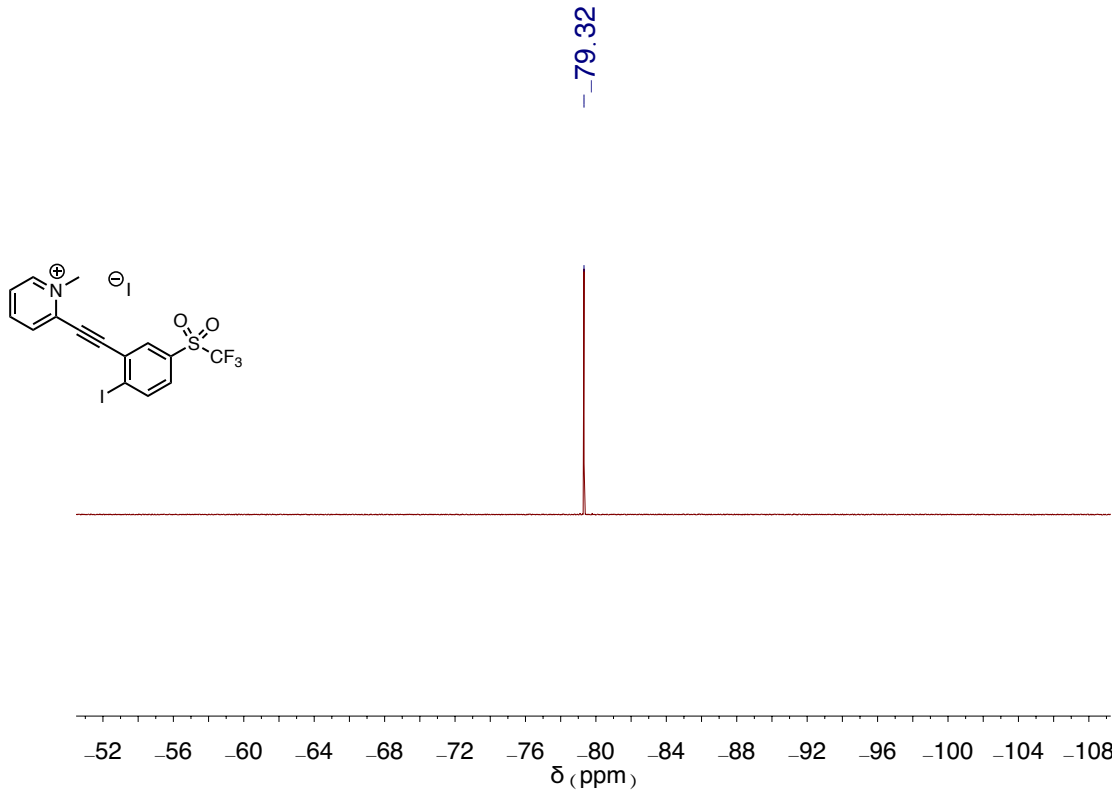

Figure C.19. ^{19}F NMR spectrum of **10 • I**$^{-}$.

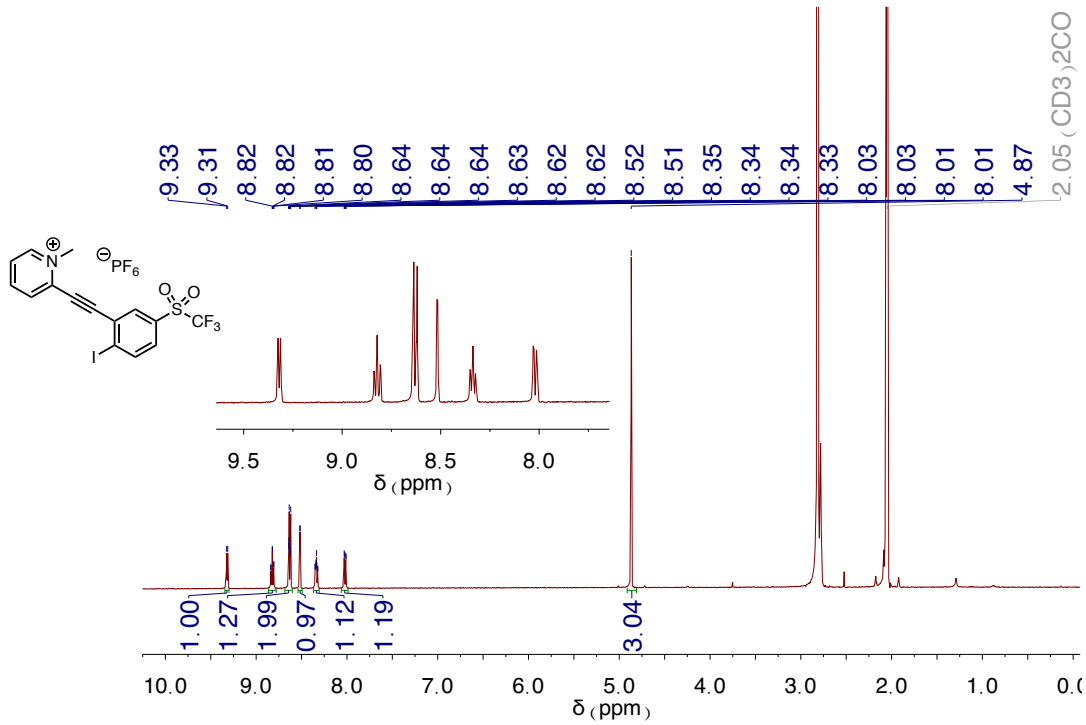

Figure C.20. ^{1}H NMR spectrum of **10 • PF_6^-**.

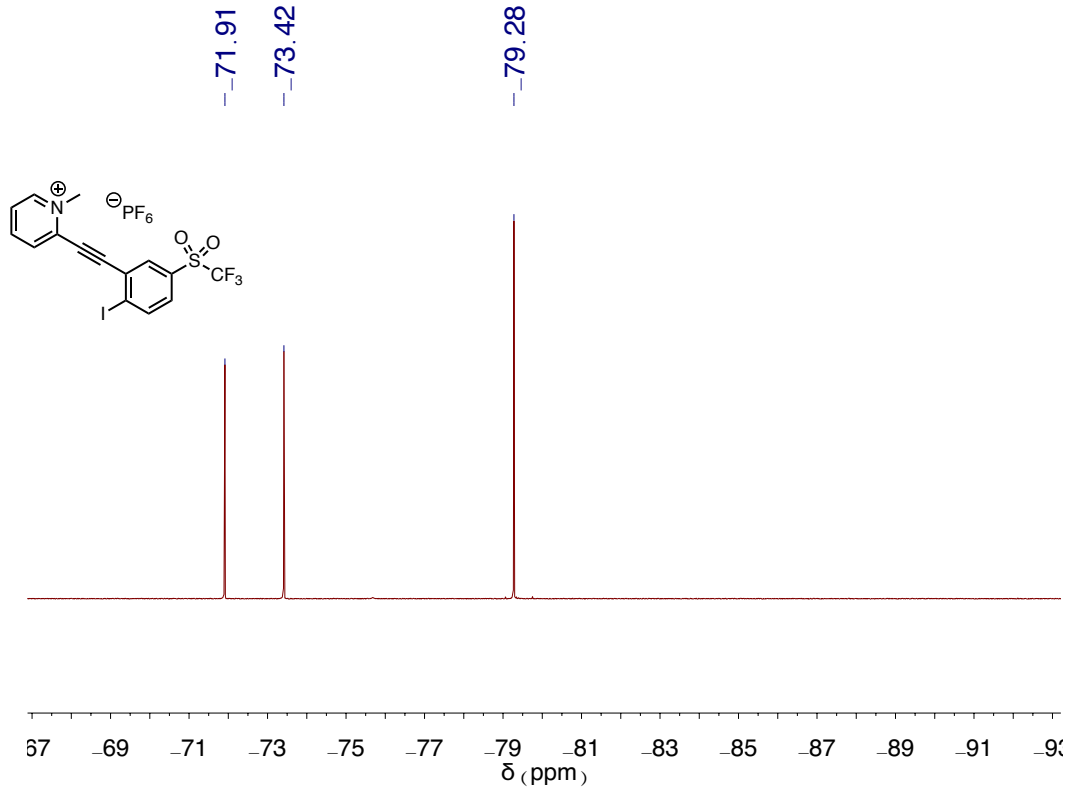

Figure C.21. ^{19}F NMR spectrum of **10 • PF_6^-**.

APPENDIX D

DEUTERIUM EQUILIBRIUM ISOTOPE EFFECTS IN A SUPRAMOLECULAR RECEPTOR FOR THE HYDROCHALCOGENIDE AND HALIDE ANIONS

This appendix includes previously published and co-authored material from Fargher, H.A.; Nickels, R.A.; de Faria, T.P.; Haley, M.M.; Pluth, D.W.; Johnson, D.W. *RSC Adv.* **2021**, *11*, 26581–26585. This manuscript was written by Hazel A. Fargher with editorial support from Professors Michael M. Haley, Michael D. Pluth, and Darren W. Johnson. The project in this chapter was developed by Hazel A. Fargher and Professors Michael M. Haley, Michael D. Pluth, and Darren W. Johnson. Synthesis in this chapter was performed by Russell A. Nickels. Analytical work and data analysis was performed by Hazel A. Fargher. Mass spectra were obtained by Thaís P. de Faria.

Introduction

Molecular recognition and host-guest binding in both biological and synthetic systems are often driven by a mixture of competitive and additive primarily non-covalent interactions. Understanding the role of each of these forces in a host-guest system can reveal insights into the driving forces behind binding and help inform in the molecular design of future hosts.[1–3] Equilibrium isotope effects (EIE), also referred to as binding isotope effects (BIE) in structural molecular biology,[4] measure the effect of isotopic substitution on supramolecular interactions through changes in the vibrational energy of

the substituted bond. These studies can be used to elucidate the complex non-covalent forces involved in host conformational changes and host-guest binding.[5–8]

Examples from structural molecular biology have demonstrated that EIEs can reveal mechanistic information in enzyme-ligand binding events.[4,9] Isotopic substitution in synthetic supramolecular systems has been used both for labelling purposes and for studying individual non-covalent interactions. For example, Bergman, Raymond, and coworkers used deuterium equilibrium isotope effects (DEIE) to study benzylphosphonium cation guest binding in a self-assembled supramolecular complex in aqueous solution.[10] From these DEIE studies, the authors found that attractive cation···π interactions in the interior of the host were important for promoting guest binding, and that C–H···π and π···π interactions were relatively small contributors. In another example, Shimizu and coworkers studied the DEIE on the strength of C–H···π interactions in their molecular balances.[11] Both computational and experimental results showed that the strength of C–H···π and C–D···π interactions were about equal, settling the debate on which interaction is stronger and easing concerns about using deuteration for spectroscopic and labelling applications.

Previously, we used a DEIE to study Cl^- binding with the arylethynyl bisurea anion receptor **4.1$^{H/D}$** (**Figure D.1**) in DMSO-d_6.[12] We found an experimental DEIE of 1.019 ± 0.010, which matched the computationally-predicted DEIE of 1.020. Further computational analysis determined that the DEIE was due to a distorted N–H···Cl^- hydrogen bond geometry, which lead to changes in the C–H/D bond vibrational energy in the host-guest complex. In addition, Paneth and coworkers performed a computational study with **4.1^{H}** and other hydrogen bonding supramolecular Cl^- receptors to determine

the EIE of $^{35/37}$Cl binding in these hosts.[13] Because isotope effects, both equilibrium and kinetic, originate solely from changes in the vibrational energy of the isotopically labelled bond, the EIE arising from this study came from changes in the vibrational energies of the bonds in the supramolecular hosts when participating in hydrogen bonding with Cl^- isotopes. Indeed, a linear relationship was observed between the hydrogen bond donor (D) D–H bond lengths in the host-guest complex and the computed $^{35/37}$Cl EIE.

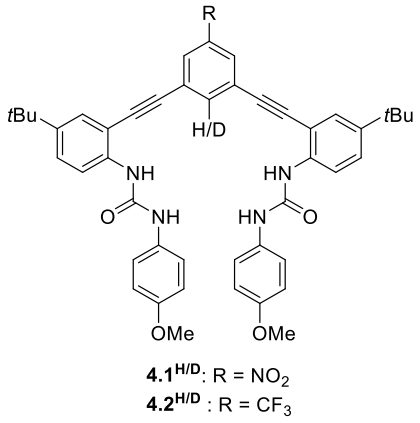

Figure D.1. Arylethynyl bisurea receptors **4.1^{H}** and **4.1^{D}** used in our previous DEIE study of Cl^- binding. Related receptors **4.2^{H}** and **4.2^{D}** are used in the current study to avoid reaction with HS^-.[14]

Previous EIE studies with receptor **4.1$^{H/D}$** have focused on Cl^- binding; however, to the best of our knowledge, no work has yet investigated the EIE of hydrosulfide (HS^-) binding in this or other systems. HS^- is a highly reactive anion that plays crucial roles in biology. At physiological pH, HS^- is favored in solution by a 3:1 ratio over its conjugate acid, hydrogen sulfide (H_2S). H_2S has been identified as the third physiological gasotransmitter alongside CO and NO and plays essential roles in physiological systems.[15] Despite its high nucleophilicity and reducing potential, HS^- has been observed

to be bound through non-covalent interactions in the protein crystal structure of a bacterial ion channel[16] and in the turn-over state of vanadium-containing nitrogenase.[17] The supramolecular chemistry of HS^- is under-studied in synthetic supramolecular receptors, likely due to the inherent high reactivity of HS^-. Indeed, we are aware of only three families of receptors that have been shown to reversibly bind HS^-.[14,18–20]

Recently, we used a series of arylethynyl bisurea anion receptors to investigate and demonstrate a linear free energy relationship between the polarity of a non-traditional C–H hydrogen bond donor and the solution binding energy of HS^-, HSe^-, Cl^-, and Br^-.[14] A major and unexpected finding of this study was that HS^- demonstrated a significant increase in sensitivity towards the polarity of the C–H hydrogen donor over HSe^-, Cl^-, and Br^-. Although increasing the polarity of the C–H hydrogen bond donor did not lead to changes in selectivity between HSe^-, Cl^-, and Br^-, we observed a 9-fold increase in selectivity for HS^- over Cl^-, suggesting a fresh approach to selective HS^- recognition using non-covalent interactions. In this current study, we label the C–H hydrogen bond donor in an arylethynyl bisurea receptor with a deuterium atom (**$4.2^{H/D}$, Figure D.1**) to further investigate this apparent preference of polar C–H hydrogen bond donors for HS^- over Cl^- and Br^- through DEIE.

Methods

Receptor **4.2^{H}** is a previously reported anion receptor for HS^-, Cl^-, and Br^- and was prepared by established methods.[14] Deuterium labelling of the isotopologue **4.2^{D}** was achieved by selective monodeuteration of intermediates through methods similar to those reported in the literature (**Scheme D.1**).[21] The diazonium salt **4.3** was synthesized in a

71% yield from 2,6-diiodo-4-trifluoromethylaniline.[22] Dediazonation in DMF-d_7 is catalyzed by $FeSO_4$ and allows for selective synthesis of monodeuterated intermediate **4.4^{D}**. The deuteration step proceeds through a radical pathway that uses DMF-d_7 as the deuterium source. This deuteration reaction provides efficient deuterium incorporation even with up to 50% by volume H_2O in the reaction solution due to the differential bond strengths in DMF and H_2O.[21] Sonogashira cross-coupling reaction of **4.4^{D}** and 4-*t*-butyl-2-ethynylaniline[23] afforded **4.5^{D}** in 45% yield. Subsequent addition with 4-methoxyphenyl isocyanate gave **4.2^{D}** in 34% yield. Compound **4.2^{D}** and intermediates were characterized through ^{1}H, ^{2}H, $^{13}C\{^{1}H\}$, and ^{19}F NMR spectroscopy and high-resolution mass spectrometry (see Supporting Information at the end of Appendix D).

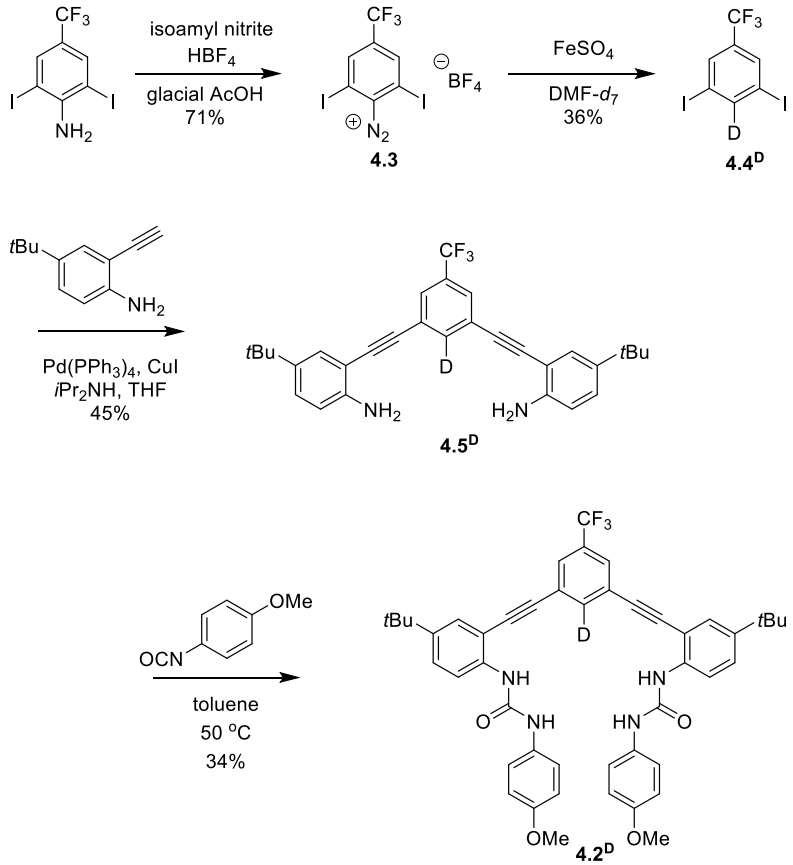

Scheme D.1. Synthetic route for the selective deuteration of anion receptor **4.2^{D}**.

Previous work on the DEIE of Cl^- binding with **4.1$^{H/D}$** in DMSO revealed an experimental isotope effect of 1.019 ± 0.010. Therefore, we expected similar small DEIEs for HS^-, Cl^-, and Br^- binding with **4.2$^{H/D}$**. Typical methods to determine binding constants (K_a) in supramolecular systems use non-linear regression fitting of titration data. Results from this method can be affected by small errors in the known initial host and guest concentration, quality of the titration isotherm, and subsequent data fitting, which when taken together often results in 2-15% errors in K_a. To increase the precision in K_a^H/K_a^D data for this study, we used the Perrin method of competitive titrations,[24] which has been shown previously to reduce errors in EIE values significantly with errors as small as 0.0004.[25] In this method, a linearized plot of the chemical shifts of **4.2^{H}** (δ_H) and **4.2^{D}** (δ_D) in fast exchange with an anionic guest is fit by linear regression to **Equation D.1**. The slope of the linear regression is equal to the DEIE of the system. Because the linear regression only relies on chemical shift values and is independent of host and guest concentration, the precision of the method is limited to the precision of the NMR instrument and quality of data fitting.

$$(\delta_H^0 - \delta_H)(\delta_D - \delta_D^f) = DEIE(\delta_D^0 - \delta_D)(\delta_H - \delta_H^f) \quad \textbf{(D.1)}$$

In addition, ^{13}C NMR spectroscopy is sensitive to isotopic labelling and can show changes in chemical shifts between isotopomers. We were able to differentiate between the ^{13}C NMR signals for C^{ab}, C^1, and C^2 for free and bound **4.2^{H}** and **4.2^{D}** (**Figure D.2a**) in 10% DMSO-d_6/CD_3CN, which were similar to those reported for **4.1$^{H/D}$** in DMSO.[12] Competitive ^{13}C NMR spectroscopy titrations were performed in anaerobic and anhydrous 10% DMSO-d_6/CD_3CN at 25 °C with mixtures of **4.2^{H}** and **4.2^{D}** in combined concentrations between 5.71 and 13.46 mM. Aliquots of the tetrabutylammonium (TBA)

salts of HS^-, Cl^-, and Br^- were added until the system had reached saturation. In an effort to decrease reactivity of HS^- with **4.2$^{H/D}$** and DMSO over long periods of time and decrease oxygen and water contaminations, some titrations with HS^- were performed by splitting the host solution of **4.2$^{H/D}$** between four J-young NMR tubes. For each point in the competitive titration, TBASH was added to a new solution of **4.2$^{H/D}$** inside an N_2-glovebox shortly before obtaining a ^{13}C NMR spectra. The C^{ab}, C^1, and C^2 ^{13}C NMR signals were tracked for **4.2^{H}** and **4.2^{D}** in each titration for each anion. A representative competitive titration and linearized plots for Cl^- binding is shown in **Figure D.2**.

Results and Discussion

The DEIE calculated from tracking the chemical shifts of the C^{ab}, C^1, and C^2 ^{13}C NMR signals from Cl^- and Br^- binding are summarized in **Table D.1**. The results shown are an average of three trials. Analysis of the data for competitive titrations of **4.2$^{H/D}$** with Cl^- reveals a normal DEIE of 1.014 ± 0.002, calculated from monitoring the C^2 ^{13}C NMR signal. The C^{ab} and C^1 ^{13}C NMR signals have the largest percent error in the calculated DEIE and show no statistically significant DEIE (i.e., DEIE = 1) for Cl^- binding; however, because there is only one DEIE in the system, these positions must not be sensitive enough to the vibrational energy of the C–H/D bond in the free host and the host-guest complex to reveal the normal DEIE.

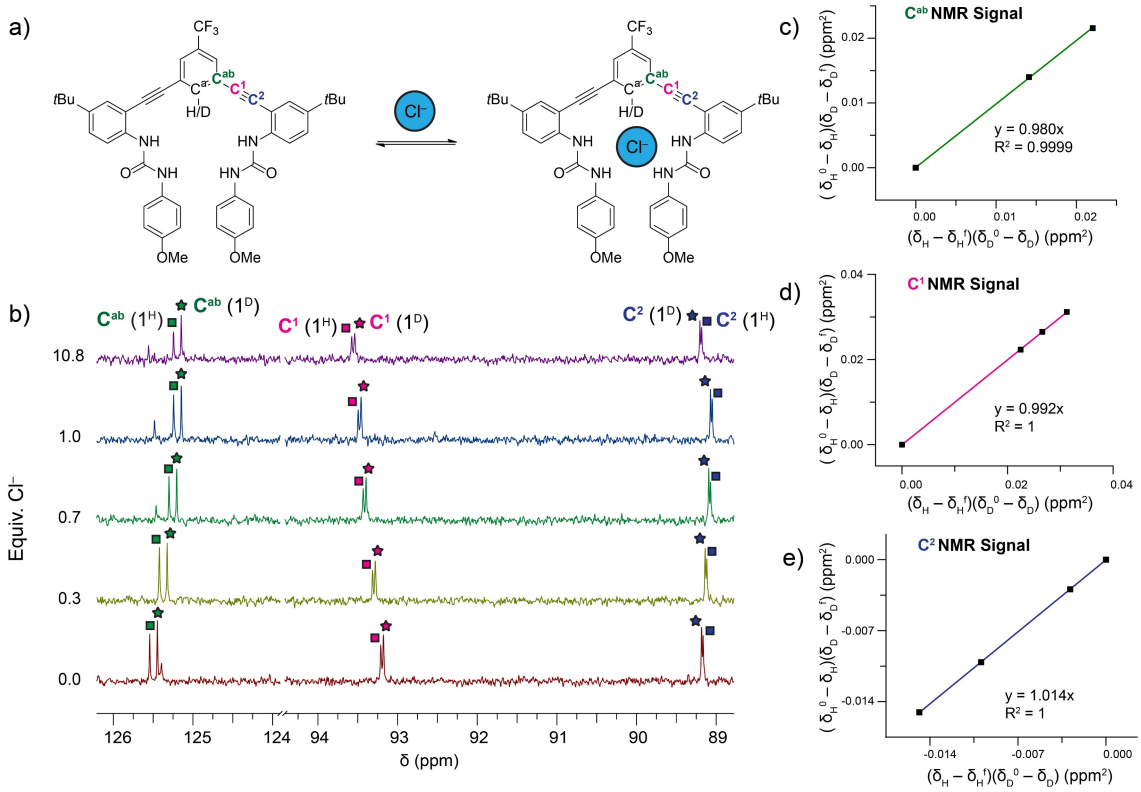

Figure D.2. Representation of the host-guest equilibrium between **4.2$^{H/D}$** and Cl^-. Differences in the chemical shifts between the **4.2^{H}** and **4.2^{D}** isotopologues are observed in the ^{13}C NMR signals for the C^{ab}, C^1, and C^2 carbons. b) ^{13}C NMR signals for the C^{ab}, C^1, and C^2 carbons in **4.2^{H}** and **4.2^{D}** are tracked throughout a titration. c-e) Linearized plots from fitting the chemical shifts of the C^{ab}, C^1, and C^2 throughout a titration to Equation D.1.

Table D.1. Calculated DEIE for Cl^- and Br^- binding. Goodness of fit (R^2) of the titration data to Equation 4.1 through linear regression is included in parentheses.

^{13}C NMR Signal	DEIE (R^2)	
	Cl^-	Br^-
C^{ab}	0.983 ± 0.017 (0.997)	1.006 ± 0.010 (0.999)
C^1	1.006 ± 0.007 (0.999)	1.009 ± 0.018 (0.997)
C^2	1.014 ± 0.002 (1.00)	0.990 ± 0.046 (0.981)

Notably, our experimental DEIE value for Cl^- binding with **4.2$^{H/D}$** in 10% DMSO-d_6/CD_3CN is smaller than the computed value of 1.020 for Cl^- binding with **4.1$^{H/D}$** in DMSO-d_6.[12] Our previously published computational study revealed that the DEIE of Cl^- binding resulted from distorted urea N–H···Cl^- hydrogen bonding geometry affecting the

vibrational frequency of the C–H/D bond in the host-guest complex. Replacing the NO_2 functional group in **4.1$^{H/D}$** (σ_p = 0.78) with a CF_3 functional group (σ_p = 0.54) in **4.2$^{H/D}$** decreases the polarization of the C–H/D bond and subsequently makes it a slightly poorer hydrogen bond donor. In addition, the DEIE of Cl^- binding in this current study is in a less polar solvent system (10% DMSO/CH_3CN, ε ~ 42) compared to the previous study (DMSO, ε = 47). We hypothesize that the decreased polarization of the C–H/D bond and the lower solvent polarity either relieve the distorted N–H···Cl^- hydrogen bonding geometry or decreases its influence on the vibrational frequency of the C–H/D bond in the host-guest complex. To deconvolute and better understand the role of both C–H/D hydrogen bond donor polarity and solvent on the DEIE of Cl^- binding in these receptors, a systematic study of these two variables would be required, similar to those previously reported.[14,26,27]

Analysis of the data for competitive titrations of **4.2$^{H/D}$** with Br^- revealed no DEIE at any of the tracked ^{13}C NMR signals; however, each calculated DEIE has a relatively large percent error (0.99 – 4.64%, compared to 0.20% for the DEIE of Cl^- binding), which could potentially obscure small DEIEs. We attribute these large percent errors to a limitation in the Perrin method that assumes that the hosts are fully bound by guest at saturation. This limitation can potentially decrease the precision of this method for weakly bound guests with low K_a, such as Br^- which has a K_a of 173 ± 9 with **4.2^{H}** in 10% DMSO-d_6/CD_3CN at 25 °C.[14]

Using the combined data from 11 experiments, we were unable to determine the DEIE for HS^- binding. The C^1 ^{13}C NMR signal appeared to be the most sensitive to the change in vibrational energy of the C–H/D bond in the free host and the host-guest

complex; however, in over half these trials, data from the C^1 ^{13}C NMR signal showed a poor linear fit ($R^2 < 0.99$). In addition, we were unable to triplicate any DEIE from the data which showed a good linear fit ($R^2 > 0.99$). We hypothesize that the high nucleophilicity and air and water sensitivity of HS^- made it incompatible with the long experiment times needed for ^{13}C NMR spectroscopy titrations. In addition, HS^- is the only protic guest investigated in these studies, and it is also possible that vibrational coupling between the S–H motif and the receptor may further complicate the measurement of these small EIEs. Such coupling between S–H and other motifs has been implicated previously in the IR inactivity of S–H stretching modes in many metal-sulfhydryl complexes.[28]

Conclusion

Deuterium equilibrium isotope effects (DEIE) can be used to elucidate non-covalent driving forces behind anion binding in our arylethynyl bisurea receptors. We endeavored to use DEIE studies to further investigate a preference of polarized C–H hydrogen bond donors for HS^- over Cl^- and Br^- which we reported previously.[14] In this current work, we highlight a convenient method to selectively and completely deuterate the aryl C–H hydrogen bond donor in our supramolecular anion receptors. We then found a DEIE of 1.014 ± 0.002 for Cl^- binding with $\mathbf{4.2^{H/D}}$. This DEIE was smaller than the computed DEIE of Cl^- binding with $\mathbf{4.1^{H/D}}$ which features a more polarized C–H hydrogen bond donor and in a more polar solvent. Finally, we reveal challenges in using

the Perrin method and ^{13}C NMR spectroscopy titrations in determining small and precise EIE for weakly binding or highly reactive guests.

From this work, we have highlighted several areas that need further research. The first is to study how solvent and hydrogen bond donor polarity affect EIE of guest binding. A computational study from Paneth and coworkers suggest that both these variables can be used to influence $^{35/37}Cl$ EIE in supramolecular hosts.[13] We also were unable to determine a DEIE of HS^- binding in our receptors, likely due to its high reactivity. A new method to determine small, precise EIE of reactive species such as HS^- is needed in order to learn more about the supramolecular chemistry of this biologically relevant anion.

Supplementary Information

Synthesis.

General Methods. All reagents were purchased from commercial sources and used as received, unless otherwise noted. NMR spectra were acquired at room temperature on a Bruker Avance-III-HD 600 MHz (^1H 600 MHz, ^{13}C 151 MHz, ^{19}F 565 MHz, ^2H 76.75 MHz) spectrometer with a Prodigy multinuclear broadband BBO CryoProbe. ^1H and ^{13}C chemical shifts (δ) are reported in ppm relative to residual $CHCl_3$ (^1H: 7.26 ppm, ^{13}C: 77.16 ppm), CH_3CN (^1H: 1.94 ppm, ^{13}C: 118.26 ppm), or DMSO (^1H: 2.50 ppm, ^{13}C: 39.52 ppm) shifts. ^{19}F chemical shifts are referenced to $CFCl_3$ (δ = 0 ppm) as an external standard. ^2H chemical shifts are reported in ppm relative to residual $CDCl_3$ (7.26 ppm), CD_3CN (1.94), or DMSO-d_6 (2.50 ppm). High-resolution mass spectra (HRMS) were

recorded on a Waters XEVO G2-SX mass spectrometer. Tetrabutylammonium hydrosulfide (TBASH),[29] 2,6-diiodo-4-trifluoromethylaniline,[22] 4-tertbutyl-2-((trimethylsilyl)ethynyl)aniline,[23] and host **4.2**$^{\mathbf{H}}$[14] were synthesized according to previous reports. *Note*: Hydrogen sulfide and related salts are highly toxic and should be handled carefully to avoid exposure.

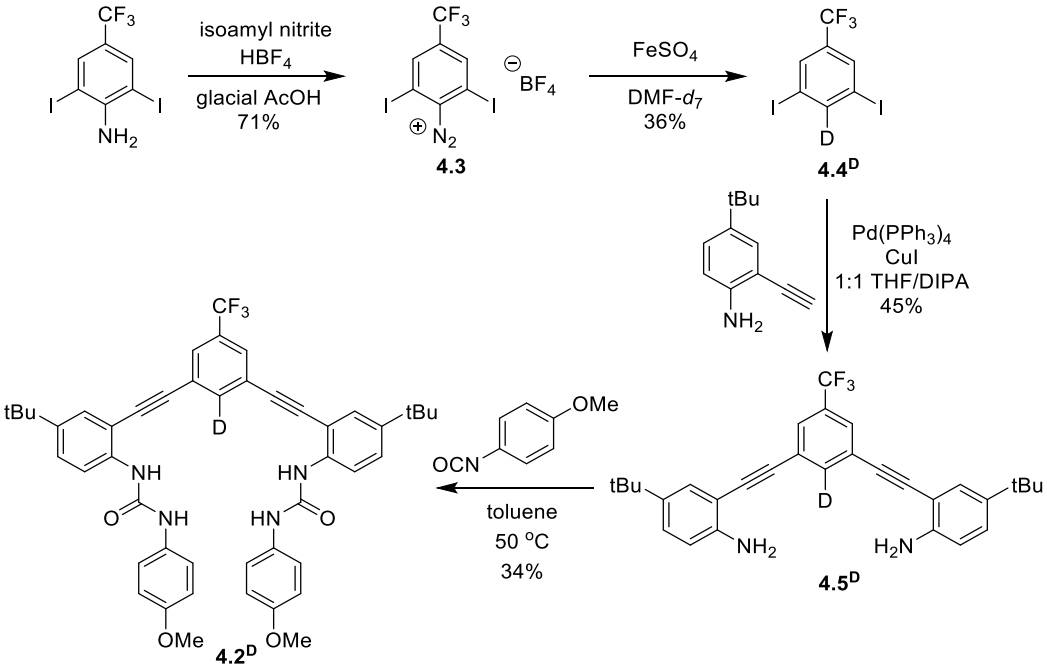

Scheme D.1.1 Synthetic pathway to the selective deuteration of anion receptor **4.2**$^{\mathbf{D}}$.

2,6-Diiodo-4-trifluoromethyldiazonium tetrafluoroborate (4.3). This preparation was adapted from previous reports.[12] A solution of 2,6-diiodo-4-trifluoromethylaniline[22] (0.25 g, 0.61 mmol), glacial AcOH (1.0 mL), and 48% HBF_4 (0.18 mL) was stirred at 25 °C. Isoamyl nitrite (0.14 mL) was combined with glacial AcOH (2.0 mL) and added dropwise over 5 min to produce a bright yellow solution. After stirring the reaction mixture at 25 °C for 15 min, diethyl ether (2.0 mL) was slowly added. The resulting liquid was placed in a -20 °C freezer for 16 h, and the solid product was isolated by

vacuum filtration and washed with diethyl ether to afford **4.3** (0.25 g, 0.48 mmol, 71%) as a bright yellow solid. *Note*: Caution should be observed when working with isoamyl nitrite or isolating diazonium salts as a solid as these compounds are known to be shock sensitive and explosive.[30,31] ^{1}H NMR (600 MHz, CD_3CN) δ: 8.59 (s, 2H). ^{13}C NMR (151 MHz, CD_3CN) δ: 140.2 (q, J = 34.7), 139.7 (q, J = 3.0), 133.1, 121.4 (q, J = 274.8), 102.9. ^{19}F (565 MHz, CD_3CN) δ: 4.7, -151.8.

1,3-Diiodo-2-duetero-5-trifluoromethylbenzene (4.4^{D}). This preparation was adapted from previous reports.[21] A solution of $FeSO_4$ (0.54 g, 2.0 mmol) and DMF-d_7 (10 mL) was allowed to stir for 15 min. A separate solution containing **4.3** (1.0 g, 2.0 mmol) dissolved in DMF-d_7 (4 mL) was added dropwise over 10 min to the stirring solution. The solution was allowed to stir for an additional 15 min before adding water to precipitate a solid. The precipitate was isolated by vacuum filtration and washed with water to afford **4.4^{D}** (0.28 g, 0.71 mmol, 36%) as a tan solid. ^{1}H NMR (600 MHz, $CDCl_3$) δ: 7.91 (s, 2H). ^{13}C NMR (151 MHz, $CDCl_3$) δ: 148.3 (t, J = 27.2), δ 133.7 (q, J = 33.7), δ 133.7 (q, J = 1.5), δ 121.9 (q, J = 273.8), δ 94.6. ^{19}F (565 MHz, $CDCl_3$) δ -63.0. ^{2}H (76.75 MHz, $CDCl_3$) δ 8.29. HRMS (TOF-MS-ASAP) $[M]^+$ calc'd for $C_7H_2DF_3I_2$ 398.8339, found 398.8317.

Deuterated dianiline intermediate (4.5^{D}). This preparation was adapted from previous reports.[14] A suspension of 4-tertbutyl-2-((trimethylsilyl)ethynyl)aniline[23] (0.68 g, 2.4 mmol), K_2CO_3 (1.90 g, 13.8 mmol), MeOH (20 mL), and Et_2O (10 mL) was stirred at 25

°C for 3 h. The suspension was diluted with water and extracted with CH_2Cl_2 (15 mL, x3) and washed with brine (15 mL, x2). The organic layer was dried (Na_2SO_4) and concentrated *in vacuo* to afford a dark brown oil. The oil was dissolved in THF (20 mL) and DIPA (20 mL) and purged with N_2 for 40 min. The solution was cannulated into an N_2-purged solution of **4.4^{D}** (0.36 g, 0.92 mmol), $Pd(PPh_3)_4$ (0.032 g, 0.046 mmol), CuI (0.0017 g, 0.0092 mmol), THF (20 mL), and i-$PrNH_2$ (20 mL). The solution was stirred for 18 h at 50 °C, cooled, and concentrated *in vacuo*. The resulting oil was dissolved in CH_2Cl_2 and filtered through a 3 cm silica plug, which was washed with additional CH_2Cl_2. The filtrate was concentrated *in vacuo* and the resulting brown oil was purified by column chromatography (5:1 hexanes/EtOAc) to afford **5^{D}** (0.20 g, 0.41 mmol, 45%) as a brown solid. ^{1}H NMR (600 MHz, $CDCl_3$) δ: 7.71 (s, 2H), 7.40, (d, *J* = 2.0, 2H), 7.24 (dd, *J* = 8.4, 2H), 6.70 (d, *J* = 8.4, 2H), 4.19 (s, 4H), 1.30 (s, 18H). ^{13}C NMR (151 MHz, $CDCl_3$) δ: 145.8, 141.2, 136.7 (t, *J* = 25.7), 131.5 (q, *J* = 33.2), 129.0, 128.0, 127.4 (q, *J* = 3), 124.9, 124.6 (q, *J* = 273.3), 114.6, 106.6, 92.1, 89.1, 34.1, 31.5. ^{19}F (565 MHz, $CDCl_3$) -63.1. ^{2}H (76.75 MHz, $CDCl_3$) δ: 7.90. HRMS (TOF-MS-ASAP) $[M+H]^+$ calc'd for $C_{31}H_{31}DN_2F_3$ 490.2580, found 490.2549.

Deuterated arylethynyl bisurea host (4.2^{D}). This preparation was adapted from previous reports.[14] All glassware was dried in a 110 °C oven overnight. A round bottom flask was charged with dry toluene (100 mL) and 4.**5^{D}** (0.20 g, 0.41 mmol). 4-Methoxyphenyl isocyanate (0.16 mL, 1.2 mmol) was added dropwise, and the solution was stirred for 46 h at 50 °C. The reaction became cloudy upon completion, and the precipitate was collected by vacuum filtration to afford **4.2^{D}** (0.11 g, 0.14 mmol,

34%). ^{1}H NMR (600 MHz, 10% DMSO-d_6/CD_3CN) δ: 8.87 (s, 2H), 8.08 (d, J = 8.8, 2H), 7.99 (s, 2H), 7.96 (s, 2H), 7.56 (d, J = 2.2, 2H), 7.45 (dd, J = 8.8, 2H), 7.38 (d, J = 8.9, 4H), 6.84 (d, J = 8.9, 4H), 3.72 (s, 6H), 1.31 (s, 18H). ^{13}C NMR (151 MHz, 10% DMSO-d_6/CD_3CN) δ: 156.2, 153.9, 145.9, 139.5, 133.5, 131.8 (q, J = 32.2), 129.8, 128.7 (q, J = 3.6), 128.3, 125.4, 124.5 (q, J = 272.8), 121.8, 120.7, 114.9, 111.6, 93.2, 89.2, 55.9, 34.8, 31.4. ^{19}F (565 MHz, 10% DMSO-d_6/CD_3CN) δ: -63.2. ^{2}H (76.75 MHz, 10% DMSO-d_6/CD_3CN) δ: 8.28. HRMS (TOF-MS-ASAP) $[M+H]^+$ calc'd for $C_{47}H_{45}DN_4O_4F_3$ 788.3534, found 788.3543.

NMR Spectra.

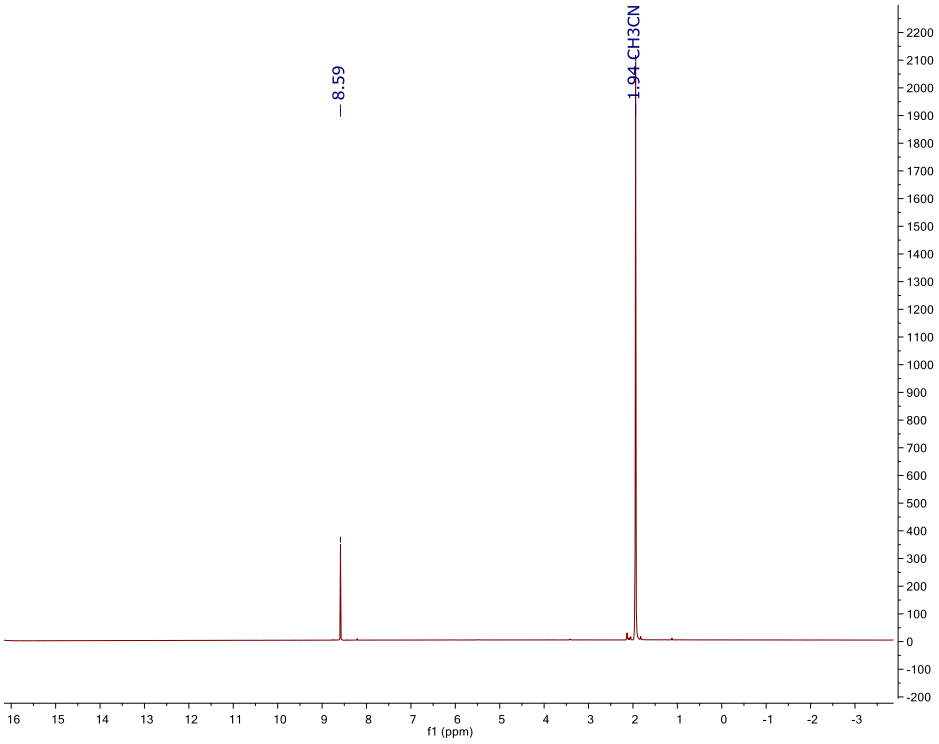

Figure D.1.1. ^{1}H NMR spectrum of **4.3** in CD_3CN.

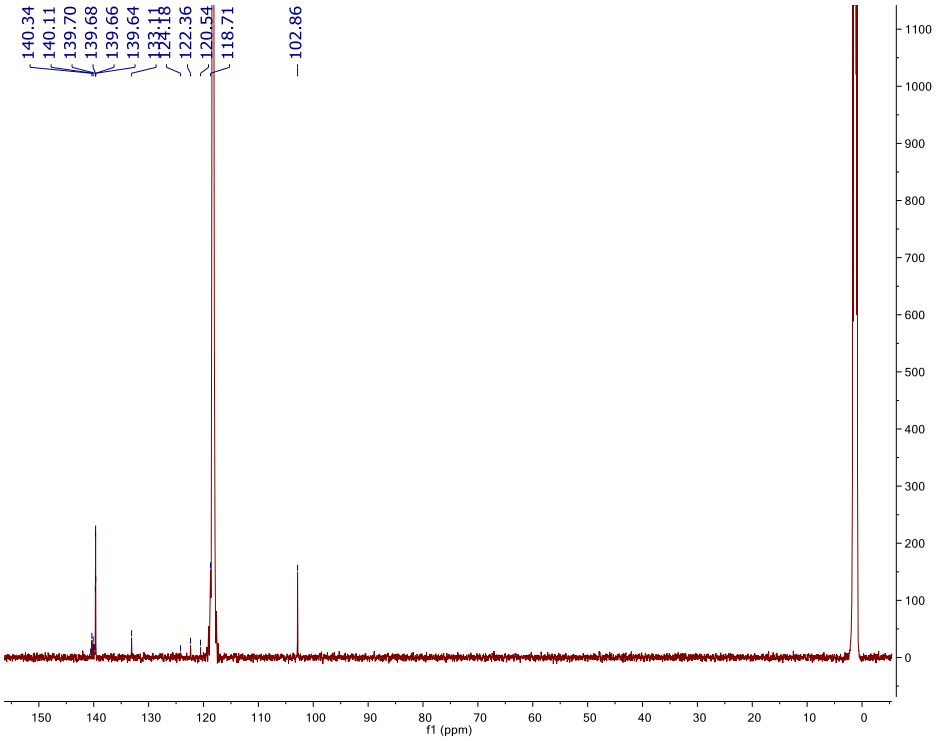

Figure D.1.2. $^{13}C\{^{1}H\}$ NMR spectrum of **4.3** in CD_3CN.

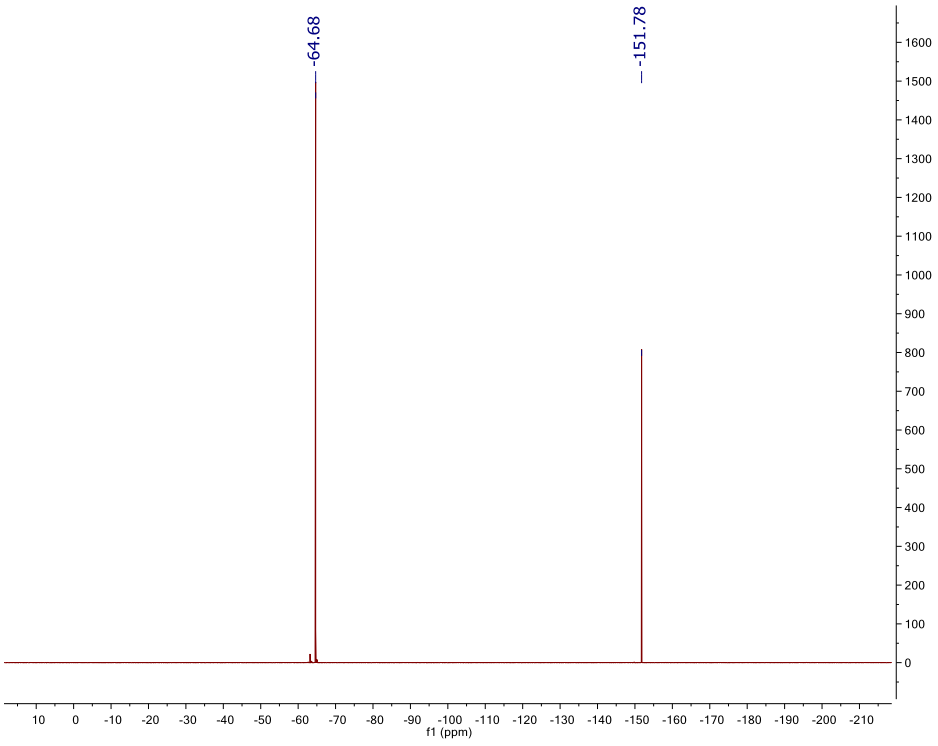

Figure D.1.3. ^{19}F NMR spectrum of **4.3** in CD_3CN.

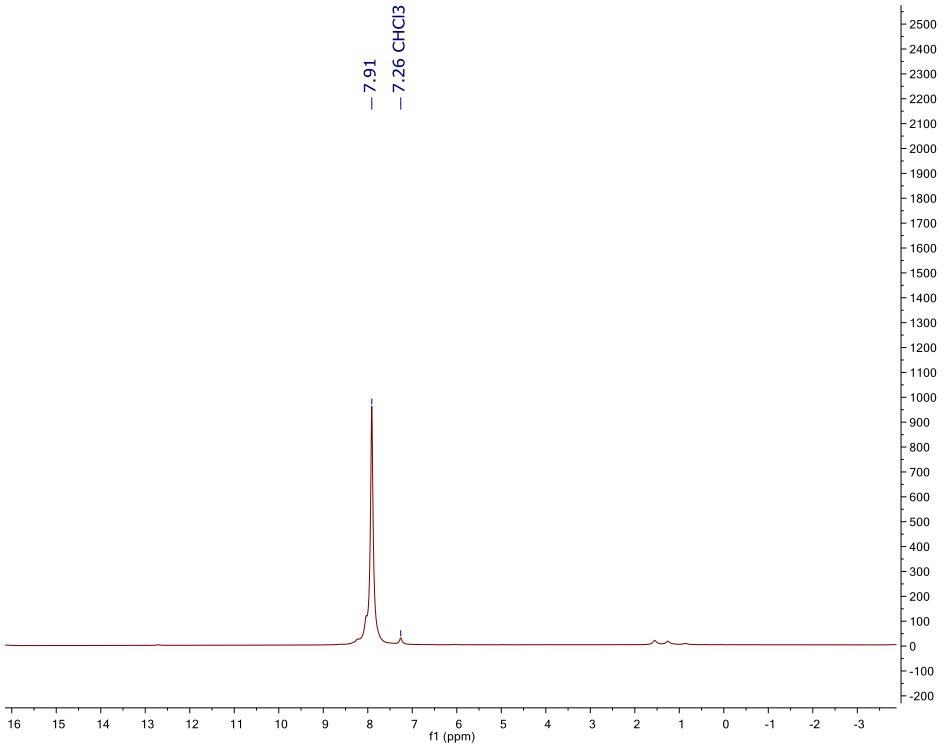

Figure D.1.4. ^{1}H NMR spectrum of **4.4^{D}** in $CDCl_3$.

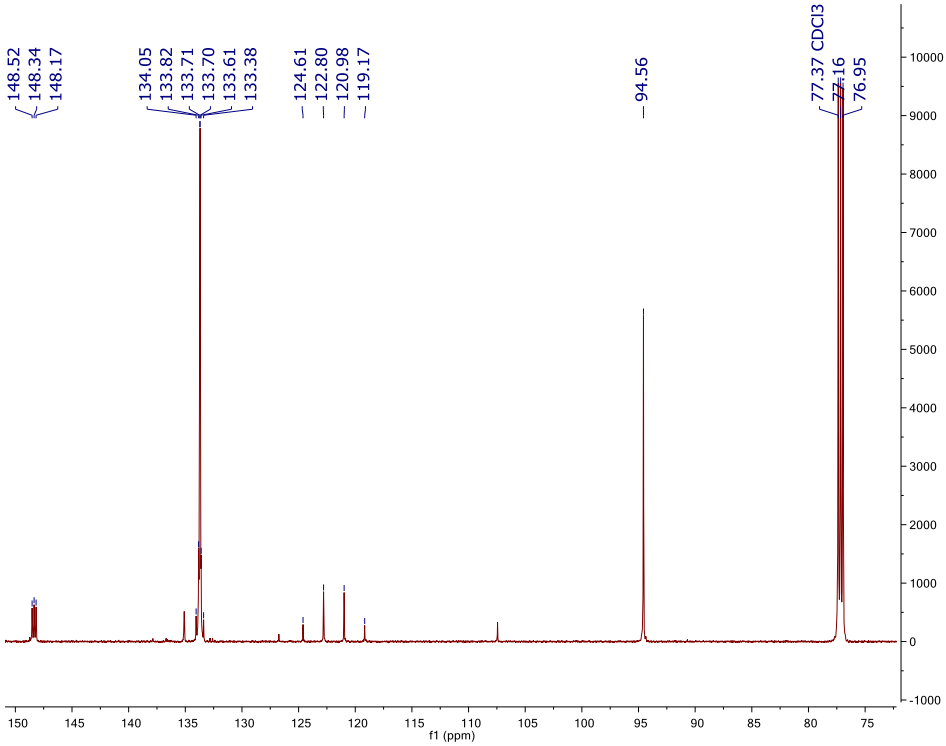

Figure D.1.5. $^{13}C\{^{1}H\}$ NMR spectrum of **4.4^{D}** in $CDCl_3$.

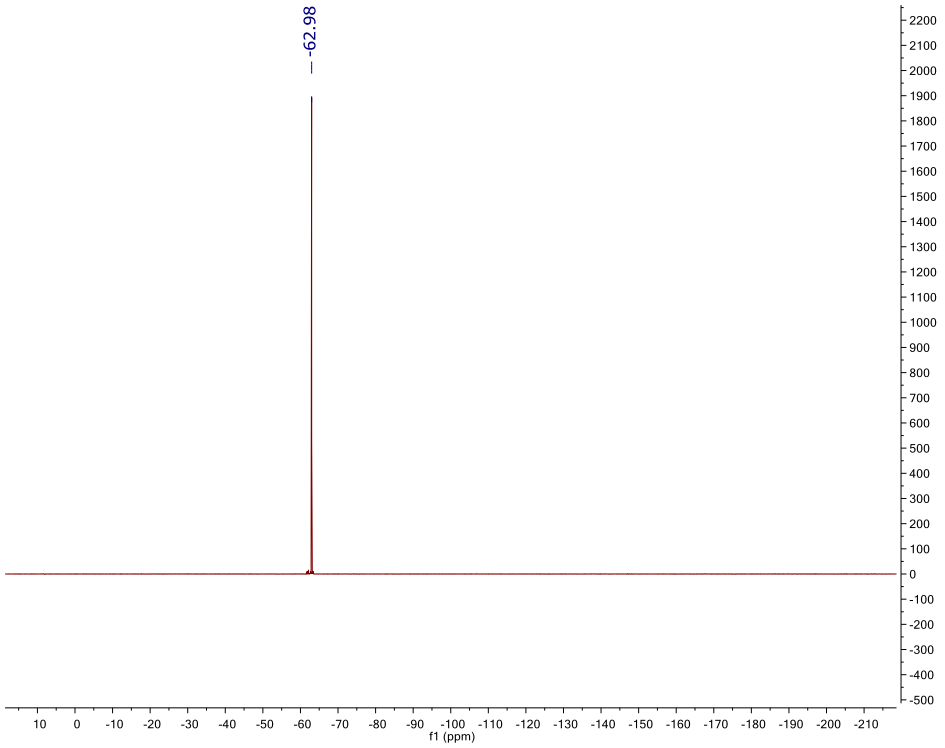

Figure D.1.6. ^{19}F NMR spectrum of **4.4^{D}** in $CDCl_3$.

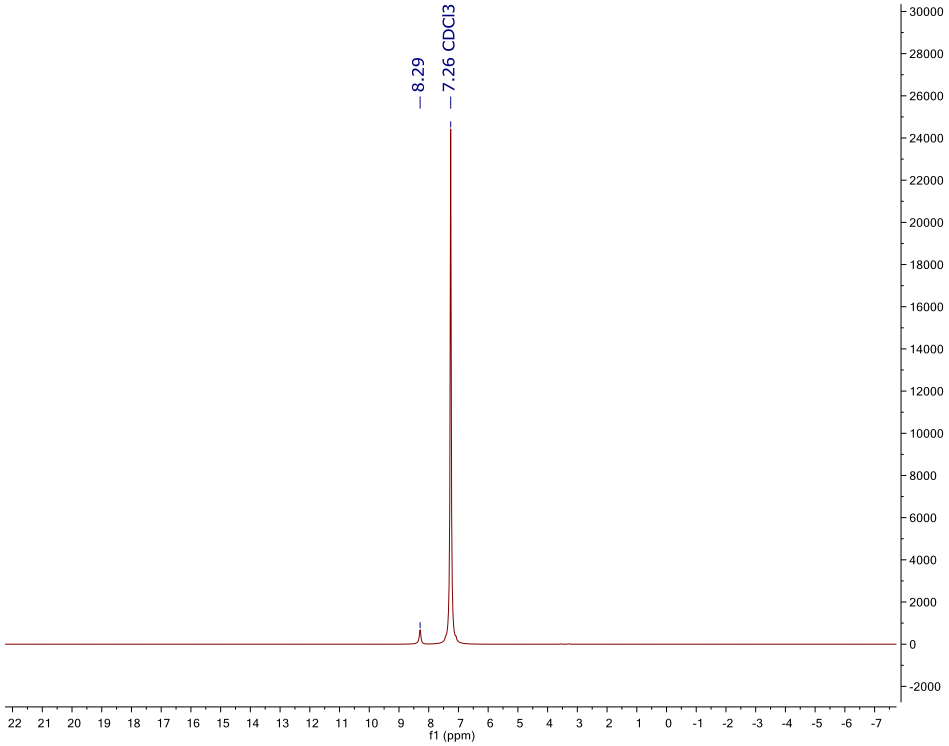

Figure D.1.7. ^{2}H NMR spectrum of **4.4^{D}** in $CHCl_3$.

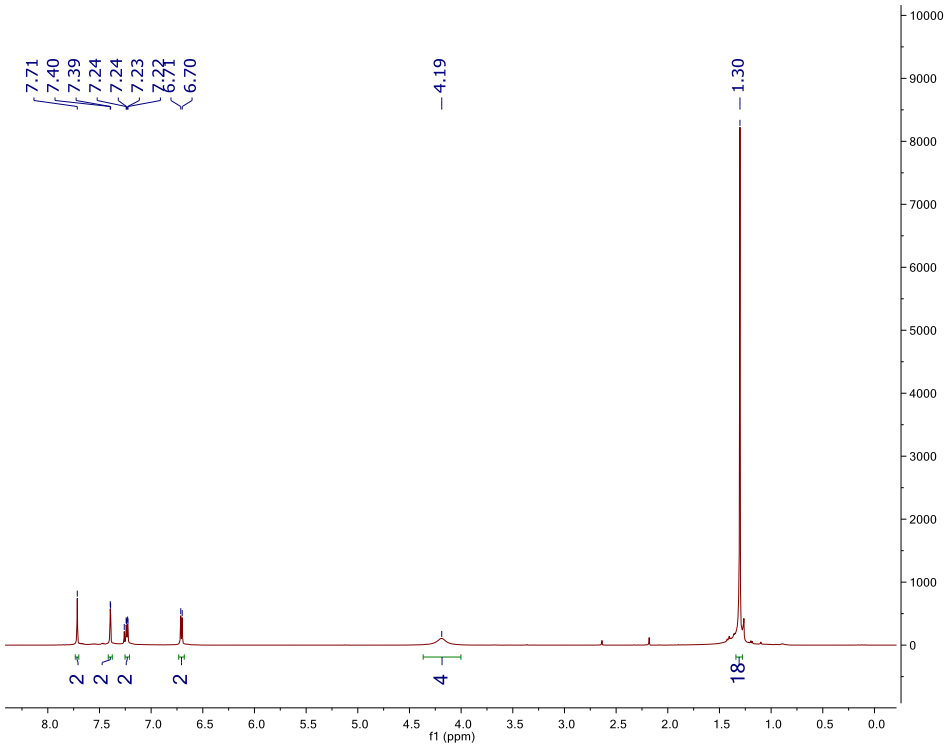

Figure D.1.8. ^{1}H NMR spectrum of **4.5^{D}** in $CDCl_3$.

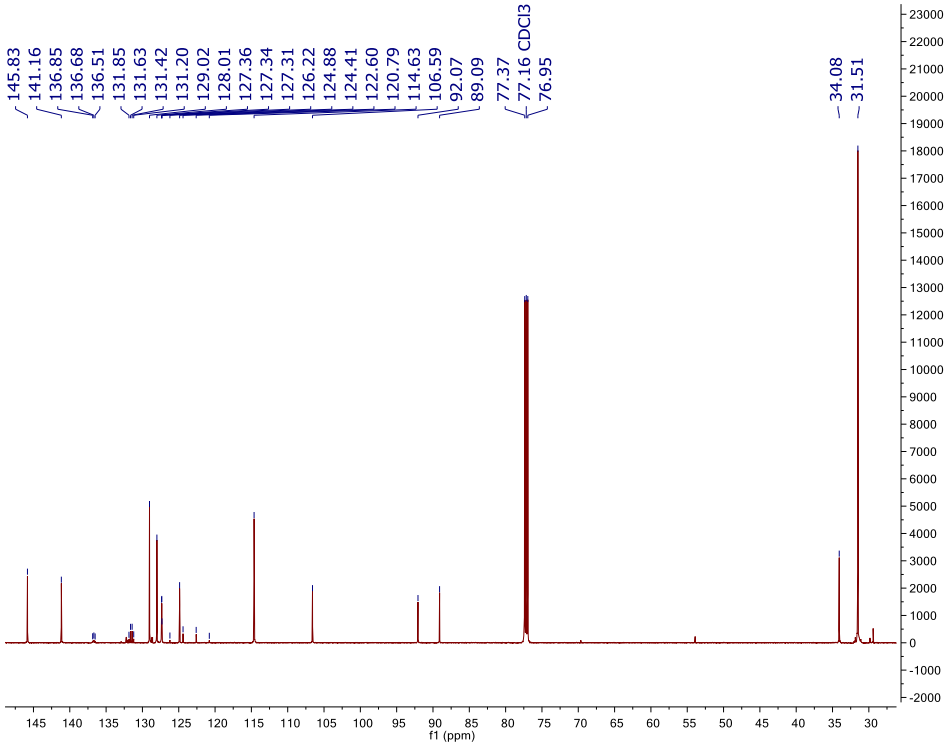

Figure D.1.9. $^{13}C\{^{1}H\}$ NMR spectrum of **4.5^{D}** in $CDCl_3$.

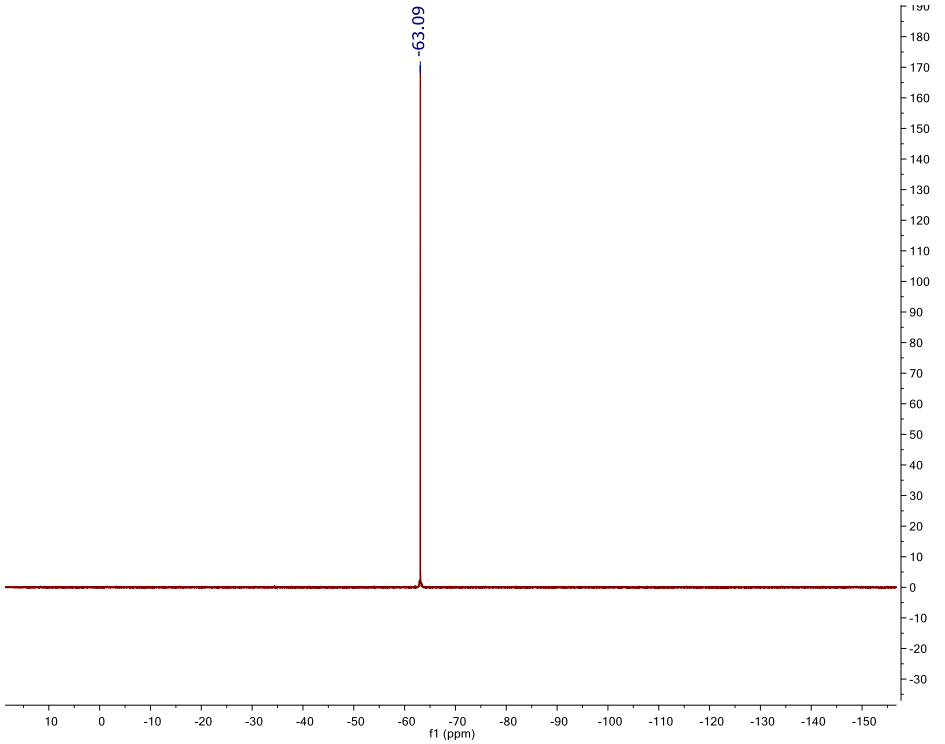

Figure D.1.10. ^{19}F NMR spectrum of **4.5^{D}** in $CDCl_3$.

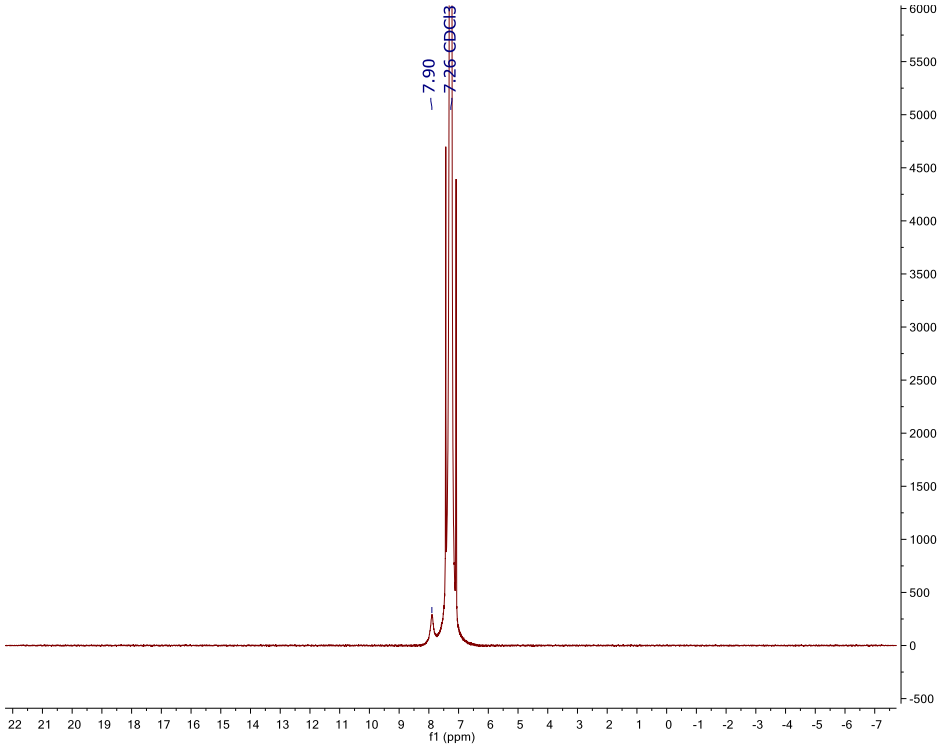

Figure D.1.11. ^{2}H NMR spectrum of **4.5^{D}** in $CHCl_3$.

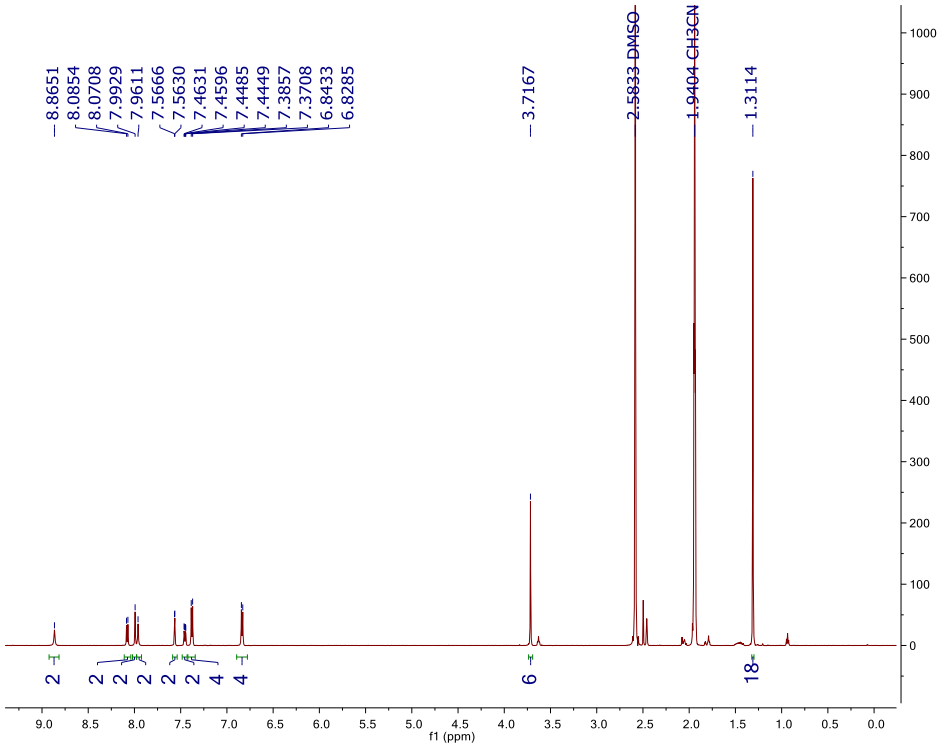

Figure D.1.12. ^{1}H NMR spectrum of **4.2^{D}** in 10% DMSO-d_6/CD_3CN.

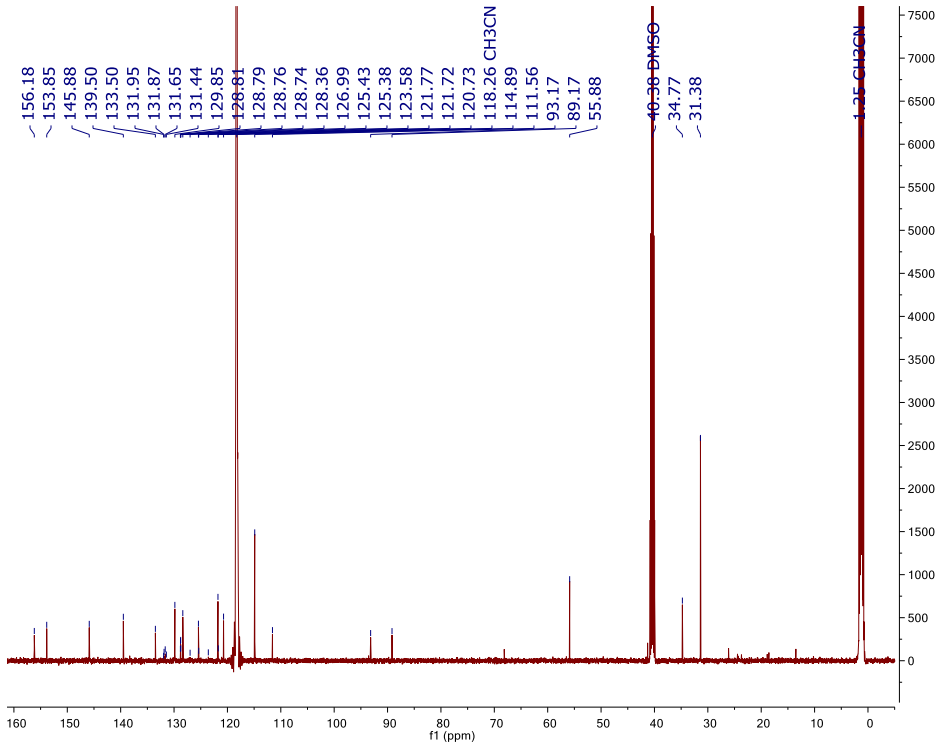

Figure D.1.13. ^{13}C{^{1}H} NMR spectrum of **4.2^{D}** in 10% DMSO-d_6/CD_3CN.

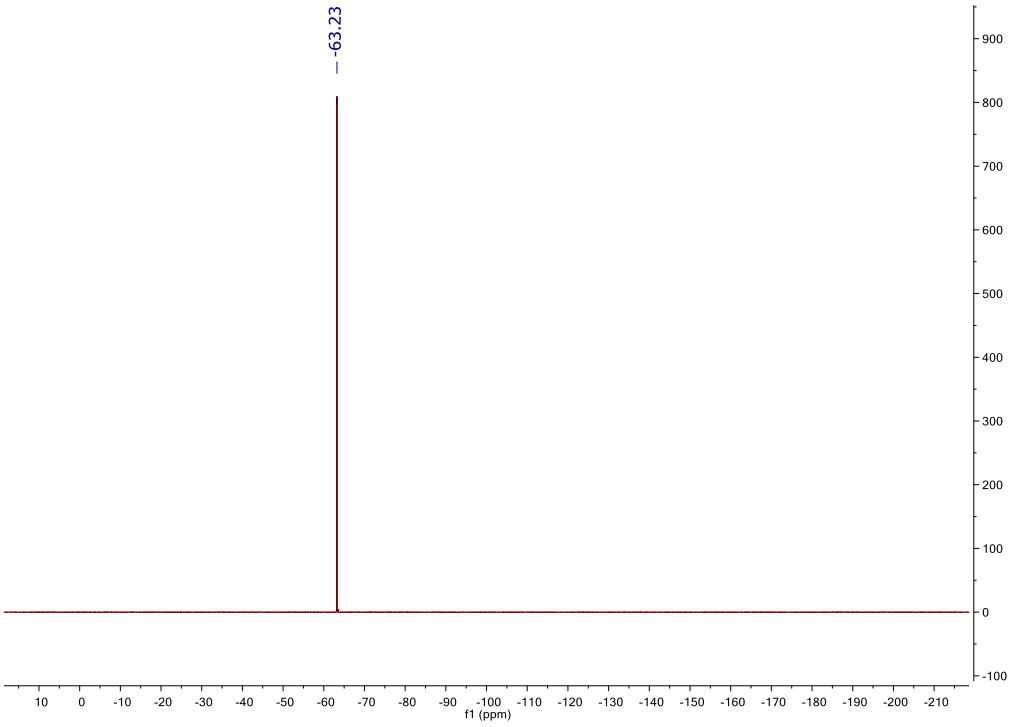

Figure D.1.14. ^{19}F NMR spectrum of **4.2^{D}** in 10% DMSO-d_6/CD_3CN.

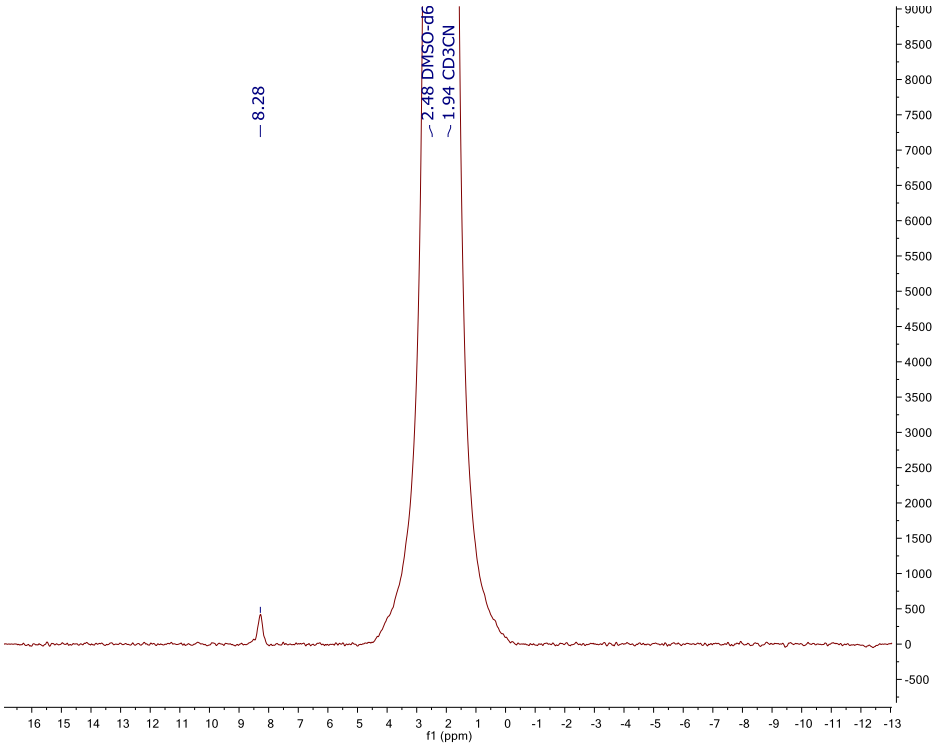

Figure D.1.15. ^{2}H NMR spectrum of **4.2^{D}** in 10% DMSO/CH_3CN.

Competitive Titration of $\mathbf{4.2^H}$ and $\mathbf{4.2^D}$.

General Methods. Samples were prepared under an inert atmosphere using an Innovative Atmospheres N_2-filled glovebox. CD_3CN and DMSO-d_6 were distilled from calcium hydride under reduced pressure, deoxygenated by purging with N_2 and stored over 4 Å molecular sieves in an inert atmosphere glove box. Tetrabutylammonium chloride (TBACl) and tetrabutylammonium bromide (TBABr) were recrystallized by layering an anhydrous THF solution under anhydrous Et_2O. Tetrabutylammonium hydrosulfide (TBASH) was synthesized according to previous reports.[29] *Note*: Hydrogen sulfide and related salts are highly toxic and should be handled carefully to avoid exposure.

General Procedure for NMR Titrations.

Method A. A solution of $\mathbf{4.2^H}$ and $\mathbf{4.2^D}$ in 10% DMSO-d_6/CD_3CN (combined concentration between 5.71 and 13.46 mM) was prepared and 500 μL was added to a septum-sealed NMR tube. A stock solution of guest (TBASH, TBACl, or TBABr) was prepared in 10% DMSO-d_6/CD_3CN (54.69 – 223.09 mM). Aliquots of the guest solution were added to the NMR tube using Hamilton gas-tight syringes, and ^{13}C NMR spectra were recorded at 25°C after each addition of guest. The Δδ of the C^{ab}, C^1, and C^2 of $\mathbf{4.2^H}$ and $\mathbf{4.2^D}$ were used to follow the progress of the titration, and DEIE were determined using the Perrin method.[24]

Method B. A solution of **4.2^{H}** and **4.2^{D}** in 10% DMSO-d_6/CD_3CN (combined concentration between 4.65 and 6.04 mM) was prepared and 500 μL aliquots were added to four J-young NMR tubes. A stock solution of TBASH was prepared in CD_3CN (47.18 – 81.29 mM). For each point in the titration, TBASH stock solution and DMSO-d_6 were added to a new solution of **2^{H}** and **2^{D}** inside an N_2-glovebox shortly before obtaining a ^{13}C NMR spectra. The Δδ of the C^{ab}, C^1, and C^2 of **4.2^{H}** and **4.2^{D}** were used to follow the progress of the titration, and DEIE were determined using the Perrin method.[24]

Competitive ^{13}C NMR Titration Representative Data.

Table D.1.1. Representative competitive titration between **4.2^{H}** and **4.2^{D}** with Cl^- in 10% DMSO-d_6/CD_3CN at 25°C.

Entry	V_{Guest} (µL)	[4.2^{H}] (mM)	[4.2^{D}] (mM)	[Cl^-] (mM)	δ C^{ab} (4.2^{H}) (ppm)	δ C^{ab} (4.2^{D}) (ppm)	δ C^{1} (4.2^{H}) (ppm)	δ C^{1} (4.2^{D}) (ppm)	δ C^{2} (4.2^{H}) (ppm)	δ C^{2} (4.2^{D}) (ppm)
1	0	7.4	2.8	0	125.5158	125.4206	93.2006	93.1679	89.1431	89.1625
2	10	7.2	2.7	1.5	125.4586	125.3627	93.2448	93.2117	89.210	89.1440
3	50	6.5	2.5	8.0	125.2459	125.1484	93.4583	93.4213	89.0492	89.0715
4	60	5.8	2.2	14.4	125.1863	125.0894	93.5353	93.4970	89.0370	89.0597
5	200	4.3	1.3	28.4	125.1896	125.0942	93.5570	93.5180	89.0795	89.1019

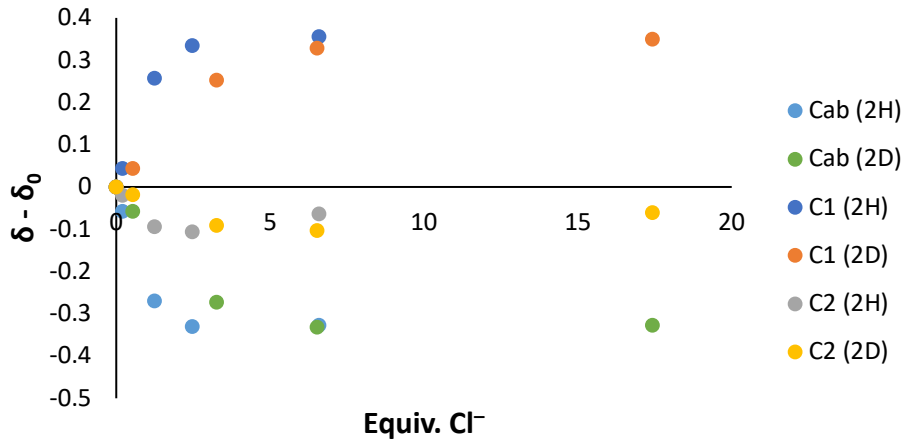

Figure D.1.16. Binding isotherm for Cl^- binding with a mixture of **4.2^{H}** and **4.2^{D}** in 10% DMSO-d_6/CD_3CN at 25°C.

Table D.1.2. Representative competitive titration between **4.2^{H}** and **4.2^{D}** with Br^- in 10% DMSO-d_6/CD_3CN at 25°C.

Entry	V_{Guest} (µL)	[4.2^{H}] (mM)	[4.2^{D}] (mM)	[Br^-] (mM)	δ C^{ab} (4.2^{H}) (ppm)	δ C^{ab} (4.2^{D}) (ppm)	δ C^{1} (4.2^{H}) (ppm)	δ C^{1} (4.2^{D}) (ppm)	δ C^{2} (4.2^{H}) (ppm)	δ C^{2} (4.2^{D}) (ppm)
1	0	9.4	4.1	0	125.5253	125.4301	93.2145	93.1818	89.1588	89.1780
2	5	9.3	4.0	1.1	125.4977	125.4008	93.2280	93.1959	89.1571	89.1772
3	10	9.1	3.9	3.2	125.4451	125.3496	93.2538	93.2223	89.1546	89.1743
4	60	8.1	3.5	14.1	125.2864	125.1897	93.3491	93.3152	89.1485	89.1692
5	200	5.8	2.5	37.5	125.1987	125.1029	93.4268	93.3909	89.1687	89.1896
6	500	3.5	1.5	62.6	125.1856	125.0898	93.4606	93.4253	89.2015	89.2217

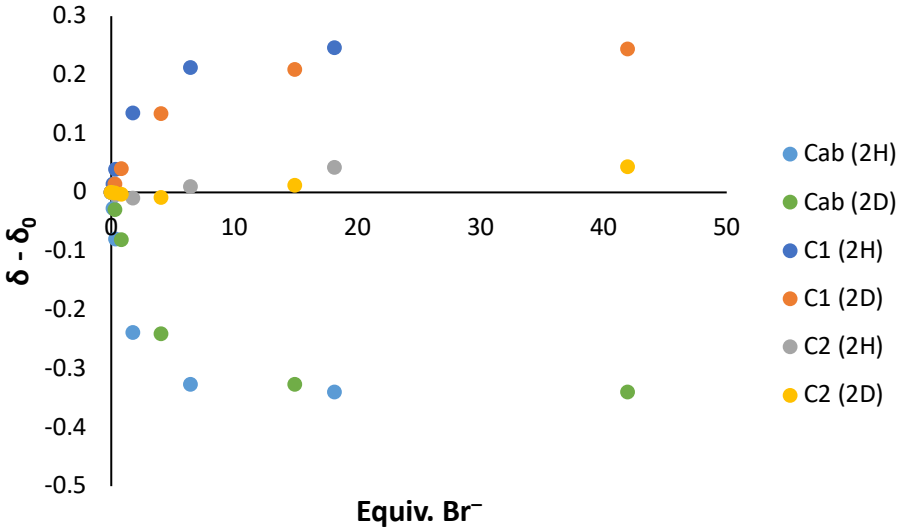

Figure D.1.17. Binding isotherm for Br^- binding with a mixture of **4.2^{H}** and **2^{D}** in 10% DMSO-d_6/CD_3CN at 25°C.

References Cited.

(1) Schneider, H. J. Limitations and Extensions of the Lock-and-Key Principle: Differences between Gas State, Solution and Solid State Structures. *Int. J. Mol. Sci.* **2015**, *16* (4), 6694–6717.

(2) Antonisse, M. M. G.; Reinhoudt, D. N. Neutral Anion Receptors: Design and Application. *Chem. Commun.* **1998**, No. 4, 443–448.

(3) Smulders, M. M. J.; Zarra, S.; Nitschke, J. R. Quantitative Understanding of Guest Binding Enables the Design of Complex Host-Guest Behavior. *J. Am. Chem. Soc.* **2013**, *135* (18), 7039–7046.

(4) Swiderek, K.; Paneth, P. Binding Isotope Effects. *Chem. Rev.* **2013**, *113*, 7851–7879.

(5) Laughrey, Z. R.; Upton, T. G.; Gibb, B. C. A Deuterated Deep-Cavity Cavitand Confirms the Importance of C-H···X-R Hydrogen Bonds in Guest Binding. *Chem. Commun.* **2006**, No. 9, 970–972.

(6) Rechavi, D.; Scarso, A.; Rebek, J. Isotopomer Encapsulation in a Cylindrical Molecular Capsule: A Probe for Understanding Noncovalent Isotope Effects on a Molecular Level. *J. Am. Chem. Soc.* **2004**, *126* (25), 7738–7739.

(7) Zhao, Y. L.; Houk, K. N.; Rechavi, D.; Scarso, A.; Rebek, J. Equilibrium Isotope Effects as a Probe of Nonbonding Attractions. *J. Am. Chem. Soc.* **2004**, *126* (37), 11428–11429.

(8) Haino, T.; Fukuta, K.; Iwamoto, H.; Iwata, S. Noncovalent Isotope Effect for Guest Encapsulation in Self-Assembled Molecular Capsules. *Chem. Eur. J.* **2009**, *15* (48), 13286–13290.

(9) Wade, D. Deuterium Isotope Effects on Noncovalent Interactions between Molecules. *Chem. Biol. Interact.* **1999**, *117* (3), 191–217.

(10) Mugridge, J. S.; Bergman, R. G.; Raymond, K. N. Equilibrium Isotope Effects on Noncovalent Interactions in a Supramolecular Host-Guest System. *J. Am. Chem. Soc.* **2012**, *134* (4), 2057–2066.

(11) Zhao, C.; Parrish, R. M.; Smith, M. D.; Pellechia, P. J.; Sherrill, C. D.; Shimizu, K. D. Do Deuteriums Form Stronger CH-π Interactions? *J. Am. Chem. Soc.* **2012**, *134* (35), 14306–14309.

(12) Tresca, B. W.; Brueckner, A. C.; Haley, M. M.; Cheong, P. H. Y.; Johnson, D. W. Computational and Experimental Evidence of Emergent Equilibrium Isotope Effects in Anion Receptor Complexes. *J. Am. Chem. Soc.* **2017**, *139* (11), 3962–3965.

(13) Paneth, A.; Paneth, P. Isotopic Consequences of Host-Guest Interactions; Noncovalent Chlorine Isotope Effects. *J. Phys. Chem. B* **2021**, *125* (7), 1874–1880.

(14) Fargher, H. A.; Lau, N.; Richardson, H. C.; Cheong, P. H. Y.; Haley, M. M.; Pluth, M. D.; Johnson, D. W. Tuning Supramolecular Selectivity for Hydrosulfide: Linear Free Energy Relationships Reveal Preferential C-H Hydrogen Bond Interactions. *J. Am. Chem. Soc.* **2020**, *142* (18), 8243–8251.

(15) Wang, R. Physiological Implications of Hydrogen Sulfide: A Whiff Exploration That Blossomed. *Physiol. Rev.* **2012**, *92* (2), 791–896.

(16) Czyzewski, B. K.; Wang, D.-N. Identification and Characterization of Bacterial

Hydrosulfide Ion Channel. *Nature* **2013**, *483* (7390), 494–497.

(17) Sippel, D.; Rohde, M.; Netzer, J.; Trncik, C.; Gies, J.; Grunau, K.; Djurdjevic, I.; Decamps, L.; Andrade, S. L. A.; Einsle, O. A Bound Reaction Intermediate Sheds Light on the Mechanism of Nitrogenase. *Science* **2018**, *359* (6383), 1484–1489.

(18) Hartle, M. D.; Hansen, R. J.; Tresca, B. W.; Prakel, S. S.; Zakharov, L. N.; Haley, M. M.; Pluth, M. D.; Johnson, D. W. A Synthetic Supramolecular Receptor for the Hydrosulfide Anion. *Angew. Chem. Int. Ed.* **2016**, *55* (38), 11480–11484.

(19) Lau, N.; Zakharov, L. N.; Pluth, M. D. Modular Tripodal Receptors for the Hydrosulfide (HS-) Anion. *Chem. Commun.* **2018**, *54* (19), 2337–2340.

(20) Weekley, C. M.; Harris, H. H. Which Form Is That? The Importance of Selenium Speciation and Metabolism in the Prevention and Treatment of Disease. *Chem. Soc. Rev.* **2013**, *42* (23), 8870–8894.

(21) Wassmundt, F. W.; Kiesman, W. F. Efficient Catalysis of Hydrodediazoniations in Dimethylformamide1. *J. Org. Chem.* **1995**, *60* (6), 1713–1719.

(22) Lindsay, D. M.; Dohle, W.; Jensen, A. E.; Kopp, F.; Knochel, P. Preparation of Polyfunctional Heterocycles Using Highly Functionalized Aminated Arylmagnesium Reagents as Versatile Scaffolds. *Org. Lett.* **2002**, *4* (11), 1819–1822.

(23) Carroll, C. N.; Berryman, O. B.; Johnson, C. A.; Zakharov, L. N.; Haley, M. M.; Johnson, D. W. Protonation Activates Anion Binding and Alters Binding Selectivity in New Inherently Fluorescent 2,6-Bis(2-Anilinoethynyl)Pyridine Bisureas. *Chem. Commun.* **2009**, No. 18, 2520–2522.

(24) Perrin, C. L.; Fabian, M. A. Multicomponent NMR Titration for Simultaneous Measurement of Relative PKas. *Anal. Chem.* **1996**, *68* (13), 2127–2134.

(25) Perrin, C. L.; Karri, P. Position-Specific Secondary Deuterium Isotope Effects on Basicity of Pyridine. *J. Am. Chem. Soc.* **2010**, *132* (34), 12145–12149.

(26) Haley, M. M.; Pluth, M. D.; Johnson, D. W.; Sherbow, T. J.; Fargher, H. A. Solvent-Dependent Linear Free-Energy Relationship in a Flexible Host-Guest System. *J. Org. Chem.* **2020**, *85* (19), 12367–12373.

(27) Tresca, B. W.; Hansen, R. J.; Chau, C. V.; Hay, B. P.; Zakharov, L. N.; Haley, M. M.; Johnson, D. W. Substituent Effects in CH Hydrogen Bond Interactions: Linear Free Energy Relationships and Influence of Anions. *J. Am. Chem. Soc.* **2015**, *137* (47), 14959–14967.

(28) Pluth, M. D.; Tonzetich, Z. J. Hydrosulfide Complexes of the Transition Elements: Diverse Roles in Bioinorganic, Cluster, Coordination, and Organometallic Chemistry. *Chem. Soc. Rev.* **2020**, *49* (12), 4070–4134.

(29) Hartle, M. D.; Meininger, D. J.; Zakharov, L. N.; Tonzetich, Z. J.; Pluth, M. D. NBu4SH Provides a Convenient Source of HS- Soluble in Organic Solution for H2S and Anion-Binding Research. *Dalt. Trans.* **2015**, *44* (46), 19782–19785.

(30) Bernard, M. K. Isoamyl Nitrite Can Cause Serious Explosions. *J. Chem. Educ.* **2010**, *87* (6), 583.

(31) Firth, J. D.; Fairlamb, I. J. S. A Need for Caution in the Preparation and Application of Synthetically Versatile Aryl Diazonium Tetrafluoroborate Salts. *Org. Lett.* **2020**, *22* (18), 7057–7059.

APPENDIX E

UTILIZATION OF THE 2-Λ^5-PHOSPHAQUINOLIN-2-ONE SCAFFOLD AS A NON-CYTOTOXIC, PH-STABLE, AND LYSOSOME TARGETING CELL IMAGING REAGENT

The material in this appendix is taken from a manuscript *in preparation* by Jeremy P. Bard, Sarah G. Bolton, Holden J. Howard, J. Nolan McNeill, Thaís P. de Faria, Lev N. Zakharov, Michael D. Pluth, Darren W. Johnson, and Michael M. Haley. Jeremy P. Bard and Holden J. Howard performed all of the synthesis and characterization of the molecules; Sarah G. Bolton performed all of the cell growth and imaging, and Thaís P. de Faria assisted in the pH stability studies and photophysical characterization of the molecules herein.

Introduction

Advancements in cell/tissue imaging has benefited the understanding of biological systems and mechanisms enormously, thus the development of new imaging methods, higher power scopes, and more diverse chemical dyes remain as active areas of chemical biology research. While there has been significant progress in all of these areas, the development of chemical chromophores and fluorophores stands out as one of the most well-studied and broadly understood.[1–10] A variety of fluorophores exist that span a

series of brightnesses and emission colors, yet many are based on only a few "core" molecular scaffolds, including coumarins, xanthenes, cyanines, and BODIPY (**Figure E.1**).

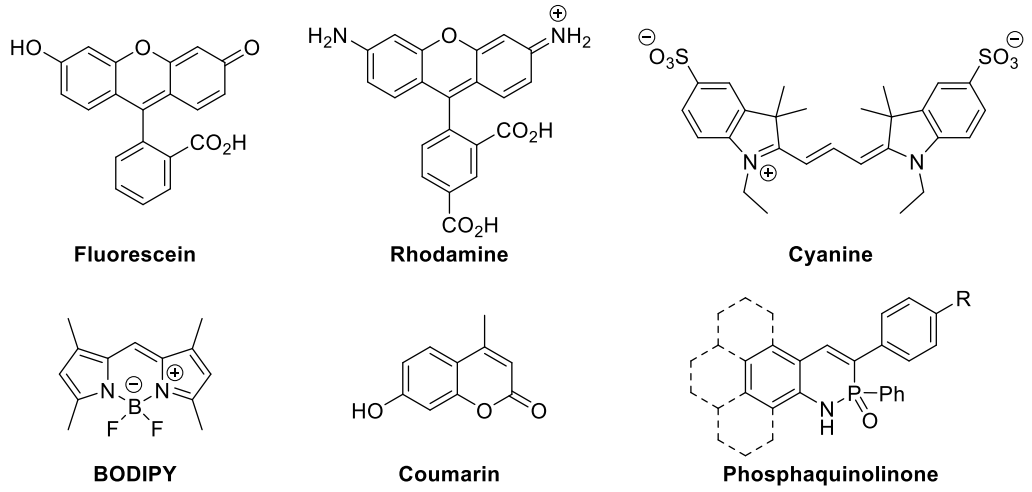

Figure E.1. Examples of core fluorophore scaffolds and the phosphaquinolinone scaffold.

Many structure-property relationships focusing on substituent group placement, heteroatom insertion, and backbone modification have been built for these compounds, which have led to a thorough understanding of their capabilities and limitations.[11–18] Examples of such limitations include pH-sensitivity, low brightnesses, chemical instability, cytotoxicity, and photobleaching. The development of unique chemical structures is paramount to further expanding the toolkit of cell imaging reagents available to chemical biologists.

Recently, a new phosphorus- and nitrogen-containing (PN) coumarin-like scaffold, the 2-λ^5-phosphaquinolin-2-one framework, has been reported and has been shown to exhibit interesting photophysical properties (**Figure E.1**).[19,20] While a variety of P-containing heterocycles exist, relatively few contain the phosphonamidate moiety

owing to difficulties in synthesis and purification, thus making this PN framework structurally unique and poised for potentially promising physicochemical properties. Primarily, this PN scaffold shows coumarin-like fluorescence, structural modularity, and very good Stokes shifts. In addition to a variety of studies examining the effects of arene core modification[19] and integration of heteroatoms into the scaffold,[21,22] several structure-property relationships have been drawn for the substituent group placement along both the pendent aryl group, as well as the 6-position of the PN-naphthalene system. It was found that having electron-withdrawing groups (EWG) on the pendant aryl ring upon the carbon in the three position and/or electron-donating groups (EDG) upon the carbon in the 6-position both led to increased Stokes shifts and red shifted emissions.[23] Additionally, placement of the more rigid phenyl group in place of the original phenoxy group on the phosphorus center leads to a 3- to 4-fold increase in the quantum yield of the scaffold.[24]

Furthermore, a vast majority of the prepared PN systems are compatible with Lipinski's Rule of Five (Ro5), as they have less than five hydrogen bond donors, less than ten hydrogen bond acceptors, weigh less than 500 amu, and have a low octanol-water partition coeffient,[25] suggesting that the scaffold should be able to permeate cell membranes. With these promising characteristics, the 2-λ^5-phosphaquinolin-2-one scaffold warrants investigation as a cell imaging reagent.

Results and discussion

While this system holds promise for cell imaging, several proof-of-principle studies need to be performed first to ensure that the photophysical properties seen in organic solvents hold when in more cell-like solvents, that the phosphonamidate is non-cytotoxic, and that the dyes can enter cells as suggested by the Ro5 compatibility.

To first test the viability of this PN system in cell imaging applications, non-substituted PN derivative **1** was prepared through cyclization of 2-(2-phenylethynyl)-benzenamine **2** with $PhP(OPh)_2$ following the standard cyclization procedure (Scheme 1). This initial derivative was chosen due to its relatively low molecular weight, simple molecular structure, and minimal number of H-bond donors and acceptors to promote potential cell permeability.

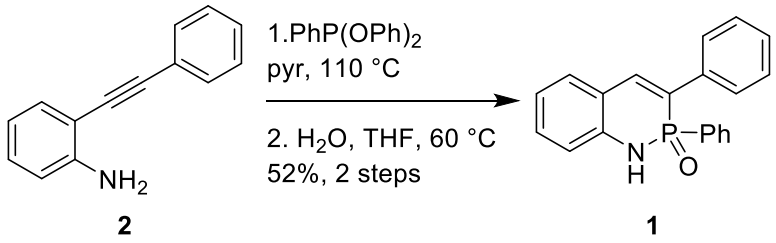

Scheme E.1. Synthesis of heterocycle **1**.

Upon isolation, we first examined the photophysical properties of **1** in $CHCl_3$ (**Figures E.1.3** and **E.1.4**, **Table E.1**). Two absorbance events can be observed at 293 nm and 338 nm, with absorption coefficients of 18000 $M^{-1}cm^{-1}$ and 11000 $M^{-1}cm^{-1}$. The emission is seen at 441 nm with a 44% quantum yield and a monoexponential fluorescence lifetime of 3.7 ns. These values are in line with previously reported P-Ph

heterocycles, showing a moderate quantum yield likely due to the structural rigidification caused by placing the phenyl group upon the phosphorus center instead of the traditional phenoxy.

Table E.1. Photophysical properties in $CHCl_3$ at 298 K[a]

cmpd	$\lambda_{abs,max}$ (nm)	λ_{abs} (nm)	$\varepsilon_{abs,max}$ ($M^{-1}cm^{-1}$)	ε_{abs}[b] ($M^{-1}cm^{-1}$)	λ_{em} (nm)	Stokes shift (nm/cm^{-1})	Φ[c] (%)	τ[d] (ns)
1	293	338	18000	11000	441	103/6910	44	3.7
3	307	369	16200	7520	487	118/6567	24	6.1
7	306	357	24200	11900	471	114/6780	24	4.9
8	306	367	16700	7500	486	119/6671	63	5.9
9	305	368	14500	6650	487	119/6640	77	6.1

[a]All values collected in $CHCl_3$ with ca. 10^{-5} M solutions. [b]Lowest energy absorbance maximum. [c]Collected using a quinine sulfate in 0.1 M H_2SO_4 solution. [d]Decay curves fitted with a monoexponential model.

To better represent the photophysical properties of **1** in an environment closer to that found in cellular environments, we next collected photophysical data in a ca. 5% DMSO in pH 7.4 PBS a buffer mixture (**Figures E.1.3** and **E.1.4**, **Table E.2**). Comparable photophysical properties are observed with absorption peaks at 290 nm (ε = 17500 $M^{-1}cm^{-1}$) and 336 nm (ε = 9140 $M^{-1}cm^{-1}$) and slightly lower energy emission at 452 nm (Φ = 23%, τ = 3.6 ns). These shifts in the emission properties were expected due to the shift to the more polar solvent mixture.

Table E.2. Photophysical properties in ca. 5% DMSO in pH 7.4 PBS Buffer at 298 K[a]

cmpd	$\lambda_{abs,max}$ (nm)	λ_{abs} (nm)	$\varepsilon_{abs,max}$ ($M^{-1}cm^{-1}$)	ε_{abs}[b] ($M^{-1}cm^{-1}$)	$\varepsilon_{abs,405}$ ($M^{-1}cm^{-1}$)	λ_{em} (nm)	Stokes shift (nm/cm^{-1})	Φ[c] (%)	τ[d] (ns)
1	290	336	17500	9140	183	452	116/7638	23	3.6
3	313	382	17500	10100	7190	499	117/6138	17	5.9
7	314	375	10700	7790	6040	485	110/6049	16	5.2
8	304	359	21000	9200	2300	500	141/7855	50	6.2
9	303	359	13000	5810	1120	493	134/7572	61	5.9

[a]All values collected in approx. 5% DMSO in pH 7.4 PBS Buffer with ca. 10^{-5} M solutions. [b]Lowest energy absorbance maximum. [c]Collected using a quinine sulfate in 0.1 M H_2SO_4 solution. [d]Decay curves fitted with a monoexponential model.

With these properties, we wanted to see how **1** performed as a cell imaging reagent. For this, we first determined cell permeability of **1**, which was studied through treatment of HeLa cells with ca. 1×10^5 M solutions of our dye in 0.5% DMSO in PBS buffer for 30 minutes and imaging them on a confocal microscope. The PN dye was excited at 405 nm and imaged on the GFP channel (**Figure E.2**). While the attained images were relatively dull based upon the minimal absorbance of **1** at 405 nm (**Table E.2**), they still showed evidence for cell permeation and integration of the dye into the cytosol of the cell.

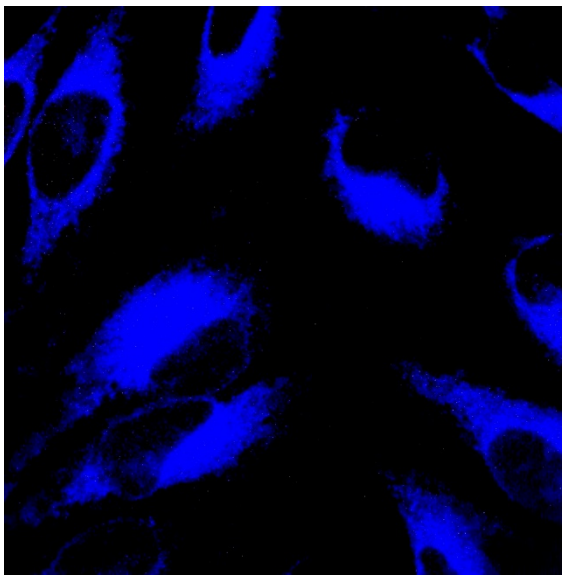

Figure E.2. Initial images of HeLa cells upon treatment with a 25 μM solution of **1** and incubation for 30 minutes.

This proof-of-principle experiment indeed showed promise for the use of our PN derivatives for cell imaging, so our next steps were to optimize the physicochemical

properties of the dye and broaden our understanding of the interactions with cells. For this, we designed heterocycle **3** (**Scheme E.2**). Not only does **3** retain the P-Ph substitution for improved quantum yield, but it also contains an EWG on the 3 position and an EDG on the 6-position, which leads to redshifted absorptions and emissions in these types of fluorophores. Additionally, **3** contains a methyl group upon the phosphonamide nitrogen, which removes the protic hydrogen and should impart base-insensitivity to the scaffold in addition to its inherent acid-stability.

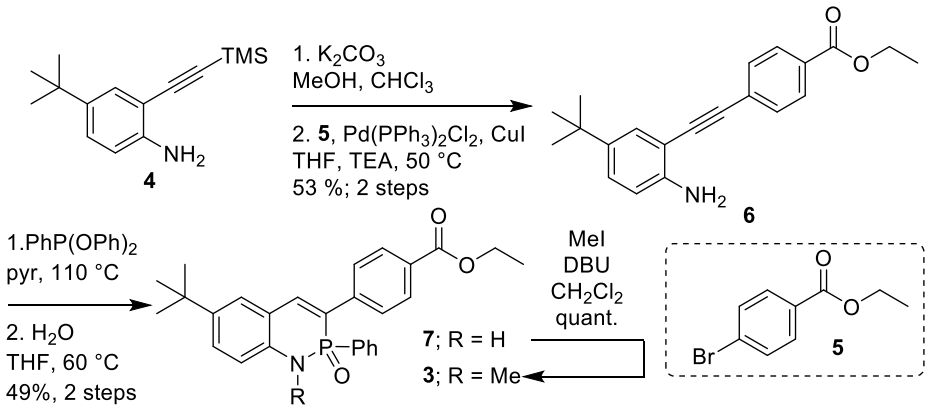

Scheme E.2. Synthesis of methylated PN **3**.

For this synthesis of **3**, 4-tert-butyl-2-((trimethylsilyl)ethynyl)aniline **4** was first protodesilylated with K_2CO_3 before the resultant terminal acetylene was formed by Sonogashira cross-coupling with ethyl 4-bromobenzoate **5** to afford ethynyl aniline **6**. **6** was then cyclized following standard protocol with $PhP(OPh)_2$ to give heterocycle **7** in good yield. Next, **7** was treated with MeI and DBU to afford fluorophore **3** in quantitative yield after only minimal aqueous washing.

When examining the photophysical properties of heterocycle **3** in $CHCl_3$, absorbances of 307 nm and 369 nm with absorption coefficients of 16200 $M^{-1}cm^{-1}$ and

7520 $M^{-1}cm^{-1}$, respectively, are seen (**Figures E.1.3** and **E.1.4**, **Table E.1**). Emission is observed at 487 nm (Φ = 24%, τ = 6.1 ns), giving the desired red-shift in emission energy. In a comparable DMSO/PBS mixture, absorbances at 313 nm (ε = 17500 $M^{-1}cm^{-1}$) and 382 nm (ε = 10100 $M^{-1}cm^{-1}$) and emission at 499 nm (Φ = 17%, τ = 5.9 ns) are observed (**Figures E.1.3** and **E.1.4**, **Table E.2**). Interestingly, when comparing these properties to those of the unmethylated heterocycle **7** (**Figures E.1.3** and **E.1.4**, **Tables E.1** and **E.2**), a slight redshift in both the lowest energy absorbance peak and the emission peak are present, suggesting electron donation into the aromatic system from the attached methyl group. Gratifyingly, the redshift in the absorption spectrum of **3** also leads to an absorption coefficient of 7190 $M^{-1}cm^{-1}$ at 405 nm in the DMSO/PBS mixture, which is significantly higher than that of **1** (**Table E.2**). While the quantum yield of **3** is slightly lower owing in part to the added degrees of freedom in the ester and alkyl groups, this large increase in absorptivity suggests that brighter images may be attainable using heterocycle **3**. To test this imaging capability, HeLa cells were treated with the same procedure outlined for **1** (**Figure E.3**). Gratifyingly, images of **3** were much brighter than those of **1**, likely due to the increased absorbance at 405 nm. Cytotoxicity of **3** was measured using a CCK-8 cell assay, which showed no cytotoxicity even up to 150 μM dye concentration (**Figure E.4**). These results suggest that the PN scaffold is indeed compatible with cells and is suitable for general cell imaging applications.

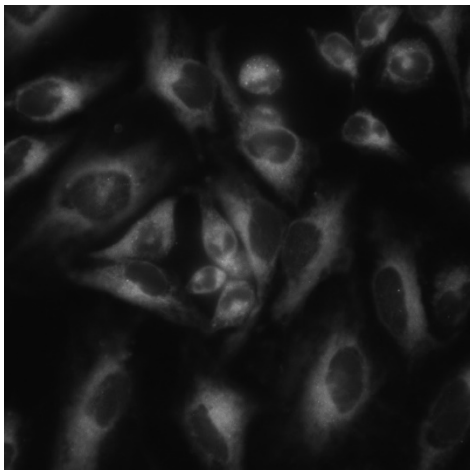

Figure E.3. Initial images of HeLa cells upon treatment with a 25 μM solution of **3** and incubation for 30 minutes.

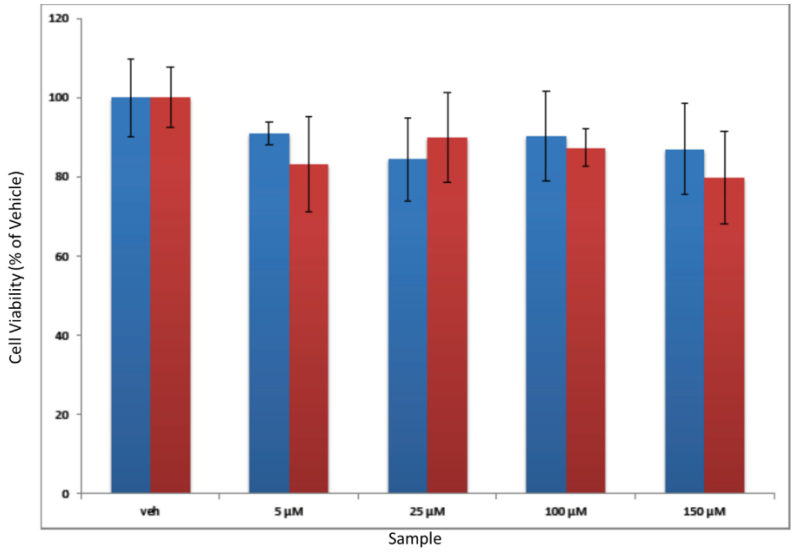

Figure E.4. Cytotoxicity studies on heterocycle **3** showing minimal cytotoxicity up to 150 μM.

With this confirmation, we wanted to see if this new fluorophore scaffold could be further functionalized such that it could be appended to different subcellular location targeting groups. For this we designed heterocycle **8**, integrating the well-known lysosome-targeting morpholine unit.[26] To access **8**, we first hydrolyzed the ester group of

3 to give the respective carboxylic acid **9**. Peptide coupling with HBTU and 4-(2-aminoethyl)morpholine **10** is then used to afford **8** in moderate yields (**Scheme E.3**). Slow diffusion of pentane into a concentrated solution of **8** in $CHCl_3$ was used to grow single crystals suitable for x-ray diffraction (**Figures E.1.1** and **E.1.2**). In this structure, the P–N bond distance is 1.674(3) Å, the P=O bond distance is 1.478(3) Å, the P-C bond distance is 1.784(3) Å, and the isolated C=C bond distance is (1.341(5) Å, all of which are in line with previously reported parameters.[19] Without the traditional phosphonamide N-H, however, hydrogen bonding is instead seen between amide groups and the phosphonamide P=O, with an N···O intermolecular distance is 2.832(4) Å

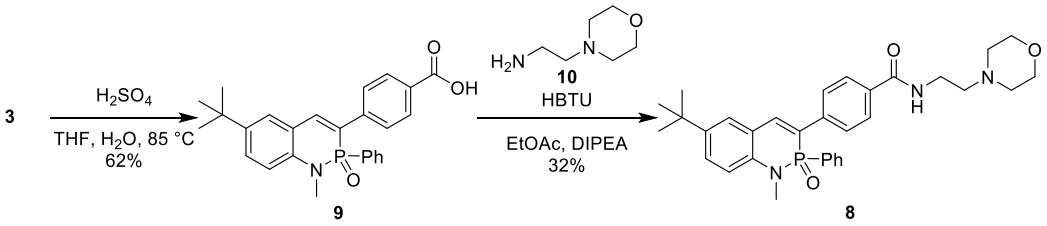

Scheme E.3. synthesis of heterocycle **8**.

The photophysical properties of **8** are nearly identical to those of heterocycle **3** in $CHCl_3$ with absorbances of 306 nm (ε = 16700 $M^{-1}cm^{-1}$) and 367 nm (ε = 7500 $M^{-1}cm^{-1}$) and emission at 486 nm (Φ = 63%, τ = 5.9 ns) (Figures S3 and S4, Table 1). The key difference is the significant increase of the quantum yield of **8**, potentially owing to interactions between the morpholine subunit and the solvent hindering vibrational relaxations caused by the substituent group. In DMSO/PBS, however, a slight blue-shift can be seen in the absorbance of **8**, with the lowest energy absorbance peak at 359 nm

(**Figures E.1.3** and **E.1.4**, **Table E.2**). Consequently, this leads to a moderate decrease in the absorption of 405 nm light, given a 2300$M^{-1}cm^{-1}$ absorption coefficient. Gratifyingly, the more polar solvent and polar solvent mixture leads to both a much larger Stokes shift of 141 nm (7855 cm^{-1}) in **8**, leading to an emission at 500 nm and a good quantum yield of 50%, suggesting that the brightness of the dye when exciting at 405 nm will still remain bright enough for cell imaging purposes.

Having shown the lack of cytotoxicity, the cell permeability, and the potential for bright cell images of the PN scaffold upon structural optimization, we wanted to explore the effects of the methylation on the acid- and base-sensitivity for the heterocycle **8**. For this, a ca. 1×10^4 M solution of **8** in 5% DMSO in deionized H_2O was prepared and separated into three portions. Absorption and emission spectra were collected using a plate reader for each sample before concentrated NaOH and concentrated HCl were used to adjust the pH of separate samples to ca. 10 and 2, respectively (Figure 5). Absorption and emission spectra were collected both immediately following these pH adjustments as well as 18 hours after.

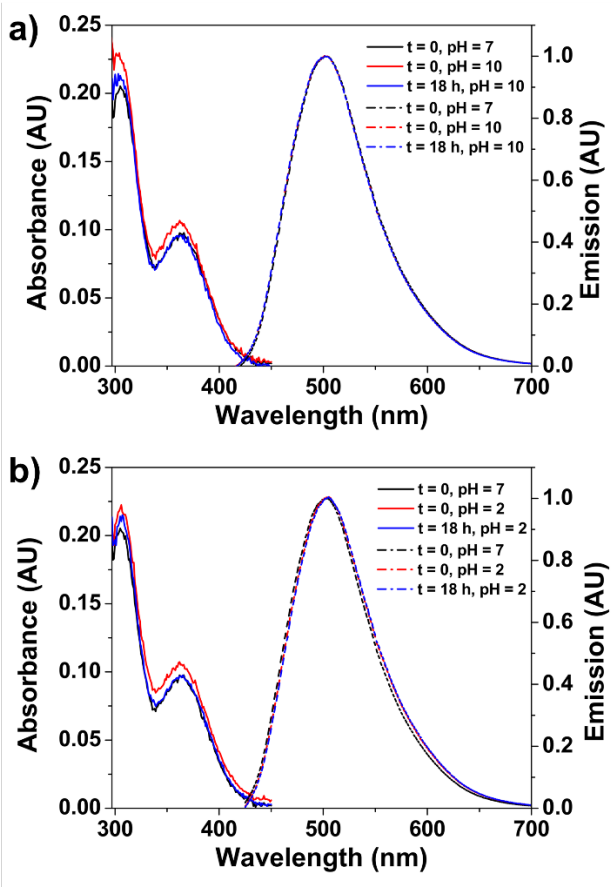

Figure E.5. Absorption (solid) and emission (dashed) of **8** in ca. 5% DMSO in H_2O before and after addition of (a) NaOH and (b) HCl.

As **Figure E.5a** shows, the photophysical properties of **8** show negligible changes after treatment with the NaOH solution. This supports the hypothesis that the methylation of the phosphonamidate nitrogen removes the base-sensitivity that is typically observed with these heterocycles.[20] However, the emission of the acidic solution decreases immediately upon addition of the acid and remains that way after the 18-hour period, yet the absorption spectrum remains virtually unchanged (**Figure E.5b**). This behavior suggests that the heterocycle structure remains unchanged, yet a quenching pathway like donor-excited Photoinduced Electron Transfer is occurring.[27,28] While this partial

quenching may not be ideal, **8** will likely still be emissive enough to afford suitable images of cells.

Lastly, with **8** being well-characterized and evidence suggesting cell compatibility of the PN scaffold, both the imaging and lysosome targeting capabilities of **8** were tested using co-localization studies with LysoTracker deep red in HeLa cell plates. Cells were incubated for 45 minutes individually for both **8** and the lysotracker dye in 0.5% DMSO in pH = 7.4 buffer. For trials with only one of the dyes, the second 45-minute incubation was performed with 0.5% DMSO in in buffer instead. Then, cells were rinsed with FluoroBrite media and imaged on a Leica widefield scope. The probe was imaged with the DAPI long pass cube, and LysoTracker is imaged with Cy5 channel. The images are all colored with a Red-Hot filter (**Figure E.6**).

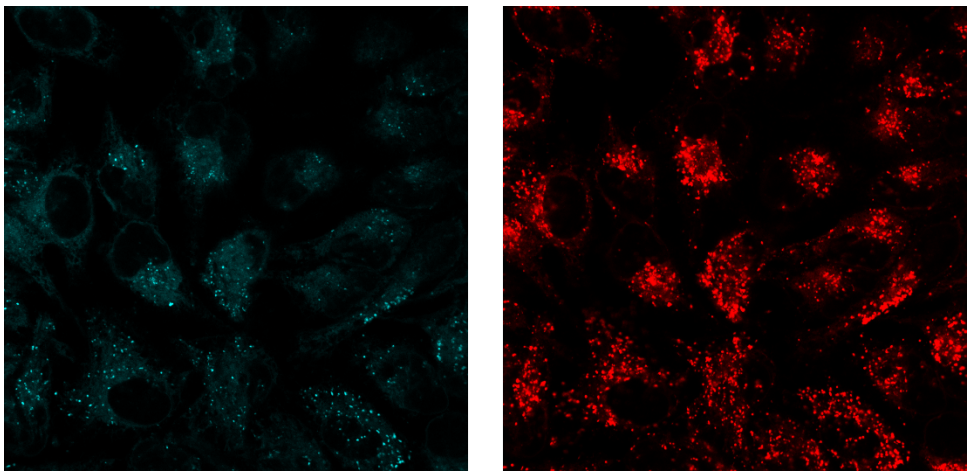

Figure E.6. Colocalization of 5 μM **8** (left) and 50 nM LysoTracker Deep Red (right) in HeLa Cells.

Five sets of images were collected with the following dye concentrations: 1) 5 μM heterocycle **8** alone, 2) 50 nM LysoTracker alone, 3) 1 μM heterocycle **8** + 50 nM LysoTracker, 4) 3 μM heterocycle **8** + 50 nM LysoTracker, 5) 5 μM heterocycle **8** + 50

nM LysoTracker (**Figures E.6. and E.1.5-E.1.9**). These experiments show moderate colocalization at every concentration, with average Pearson Correlation coefficients of 0.49 for the 1 μM heterocycle **8** + 50 nM LysoTracker trials, 0.61 for the 3 μM heterocycle **8** + 50 nM LysoTracker trials, and 0.65 for the 5 μM heterocycle **8** + 50 nM LysoTracker trials.[29] These results, suggest that heterocycle **8** can give suitable cell images at relatively low concentrations.

Conclusions and Future Works

We have prepared a series of cell imaging reagents based upon the coumarin-like phosphaquinolinone scaffold. With good solubilities, excellent Stokes shift, and moderate brightnesses in DMSO/PBS mixtures, this PN framework is poised to expand the toolkit available to both chemists and chemical biologists for live cell imaging applications. A morpholine-appended PN derivative has been prepared, and we have shown very good compatibility between this class of dye and living HeLa cells including minimal cytotoxicity, bright images, pH-stability, and localization of the fluorophore within the lysosomes of cells. Additionally, these results set the precedent for future derivations of the phosphaquinolinone moiety within cell imaging, as the penultimate carboxylic acid-containing heterocycle may be attached to several other functional groups with the goal of targeting other sub-cellular locations including the mitochondria, Golgi apparatus, or nucleus. Furthermore, with the promising imaging presented by these simple naphthalene-like PN scaffolds, it could be beneficial to explore the larger acene backbone PN derivatives that have been developed in these imaging experiments as well. While the

increased size of the scaffold may inhibit cell permeation, the inherently brighter fluorophores would give much brighter images of cells at lower concentrations if they were able to enter cells.

Experimental Section

General. All oxygen- and water-free reactions were performed under an N_2 atmosphere using Schlenk technique. Column chromatography was performed using silica gel (240–300 mesh), with solvent systems being referenced to the most abundant solvent. NMR spectra were acquired at room temperature on a Varian Inova 500 (^{1}H: 500 MHz, ^{13}C: 126 MHz, ^{31}P: 202 MHz) or a Bruker Avance III HD 500 equipped with a Prodigy multinuclear cryoprobe (^{1}H: 500 MHz, ^{13}C: 126 MHz, ^{31}P: 202 MHz). ^{1}H and ^{13}C NMR chemical shifts (δ) are expressed in ppm relative to residual $CHCl_3$ (^{1}H: 7.26 ppm, ^{13}C: 77.16 ppm) or DMSO (^{1}H: 2.50 ppm, ^{13}C: 39.52 ppm) shifts. ^{31}P NMR shifts are referenced to 85% H_3PO_4 (δ 0 ppm) as an external reference. ^{19}F NMR shifts are referenced to $CFCl_3$ (δ 0 ppm) as an external reference. UV-vis spectra were recorded using an Agilent Technologies Cary 60 UV-vis spectrophotometer. Fluorescence emission spectra were recorded using a Horiba Jobin Yvon FluoroMax-4 fluorimeter exciting at 365 nm. Quantum yields (ϕ) were determined through comparison of the emission and absorption intensities of the analyte to those of a 0.1M H_2SO_4 quinine sulfate solution.[30] Fluorescence lifetime measurements were recorded using a Horiba FluoroHub Single Photon Counting Controller with a TemPro Fluorescence Lifetime System attachment. Acid- and base-stability studies were performed using a Tecan Spark

20 M plate reader. High-resolution mass spectra (HRMS) were recorded on a Waters XEVO G2-XS mass spectrometer. Compounds **2**,[20], **4**,[31] and **10**[r32] were prepared as previously described.

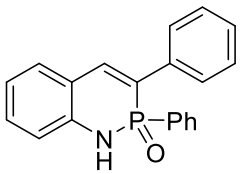

Unfunctionalized heterocycle **1** was prepared by treating 2-(2-phenylethynyl)-benzenamine **2** (665 mg, 3.4 mmol, 1 equiv.) with $P(Ph)(OPh)_2$ (2.0 g, 6.9 mmol, 2 equiv.) in pyridine (4 mL) and heating in a sand bath to 110 °C for 48 h. The reaction mixture was then cooled to room temperature before *ca*. 20 mL of toluene was added and the solvent was removed *in vacuo*. Two more analogous toluene washes were performed to fully remove pyridine from the mixture. The crude residue was then dissolved in minimal THF and 5 drops of water were added before the solution was heated to 60 °C for 1 h in a water bath. The mixture was then dried (Na_2SO_4), filtered, and concentrated *in vacuo*. Column chromatography (2:1:1 hexanes:EtOAc:CH_2Cl_2, R_f = 0.15) and subsequent recrystallization from CH_2Cl_2 and hexanes was used to give heterocycle **1** (565 mg, 52%) as a yellow solid: mp > 250 °C; ^{1}H NMR (500 MHz, Chloroform-*d*) δ 7.66 (d, *J* = 7.1 Hz, 1H), 7.65 – 7.61 (m, 1H), 7.62 (d, *J* = 32.7 Hz, 1H), 7.61 – 7.56 (m, 3H), 7.38 (t, *J* = 8.0 Hz, 2H), 7.33 – 7.17 (m, 6H), 7.01 (d, *J* = 8.1 Hz, 1H), 6.99 (t, *J* = 7.4 Hz, 1H). ^{13}C NMR (126 MHz, Chloroform-*d*) δ 139.6 (d, *J* = 3.6 Hz), 139.0 (d, *J* = 4.0 Hz), 136.9 (d, *J* = 11.5 Hz), 133.2 (d, *J* = 138.6 Hz), 132.6 (d, *J* = 10.6 Hz), 132.0 (d, *J* = 2.8 Hz), 130.6, 130.5, 128.7, 128.3, 128.2, 127.9 (d, *J* = 5.9 Hz), 127.3 (d, *J* = 117.7 Hz), 120.8, 119.6 (d, *J* = 12.3 Hz), 117.2 (d, *J* = 7.7 Hz). ^{31}P NMR (202 MHz,

Chloroform-*d*) δ 11.99; HRMS (ASAP) $[M + H]^+$ calcd for $C_{20}H_{17}NOP$ 318.1048, found 318.1032.

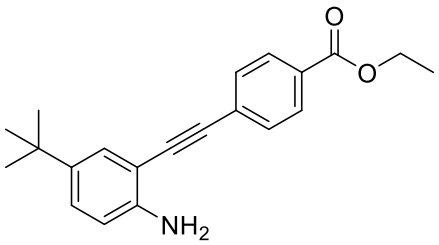

Aniline **6** was prepared by first dissolving 4-tert-Butyl-2-((trimethylsilyl)ethynyl)aniline **4** (2.18 g, 8.9 mmol, 1.0 equiv.) and K_2CO_3 (3.70 g, 26.7 mmol, 3.0 equiv.) in 70 mL of 1:1 MeOH:$CHCl_3$ and stirring at room temperature for 1.5 h. Once the protodesilylation reaction was complete by TLC, the reaction mixture was reduced *in vacuo*. The crude mixture was then suspended in ca. 20 mL CH_2Cl_2 and washed 3× with H_2O. The organic layer was collected, dried (Na_2SO_4), and concentrated *in vacuo*. The crude terminal acetylene was then carried forward to the next step.

Sonogashira cross-coupling was then performed by adding Ethyl 4-bromobenzoate **5** (2.04 g, 8.9 mmol, 1.0 equiv.), CuI (119 mg, 0.623 mmol, 0.07 equiv.), and $Pd(PPh_3)_2Cl_2$ (437 mg, 0.623 mmol, 0.07 equiv.) to the crude terminal acetylene. This mixture was then dissolved in THF (30 mL) and the solution was made air-free using four rounds of atmosphere exchange with N_2. TEA (30 mL) was then added via syringe before the reaction was heated to 50 °C and stirred for 48 h. The reaction mixture was then cooled to room temperature and concentrated *in vacuo*. Three 20 mL portions of EtOAc were added to the reaction mixture and subsequently removed *in vacuo* to remove the residual TEA. Column chromatography (16:1:1 hexanes:EtOAc:CH_2Cl_2, R_f = 0.20) was used to give aniline **6** (1.53 g, 53%) as an orange solid: mp > 97.5-98.8 °C; NMR ^{1}H NMR (500 MHz, Chloroform-*d*) δ 8.03 (d, *J* = 8.4 Hz, 2H), 7.58 (d, *J* = 8.4 Hz, 2H), 7.39 (d, *J* = 2.4

Hz, 1H), 7.21 (dd, J = 8.5, 2.3 Hz, 1H), 6.69 (d, J = 8.5 Hz, 1H), 4.39 (q, J = 7.1 Hz, 2H), 4.18 (s, 2H), 1.41 (t, J = 7.2 Hz, 3H), 1.29 (s, 9H). ^{13}C NMR (126 MHz, Chloroform-*d*) δ 166.1, 145.6, 141.0, 131.3, 129.7, 129.5, 128.8, 128.1, 127.7, 114.4, 106.9, 93.6, 89.6, 61.1, 33.9, 31.4, 14.3; HRMS (ASAP) $[M + H]^+$ calcd for $C_{21}H_{24}NO_2$ 322.1807, found 322.1816.

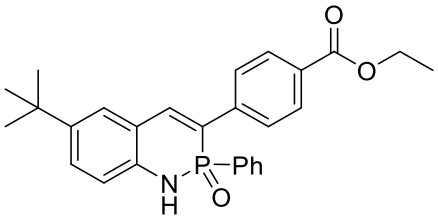

Heterocycle **7** was prepared by treating aniline **6** (960 mg, 2.98 mmol, 1.0 equiv.) with $P(Ph)(OPh)_2$ (1.76 g, 5.96 mmol, 2.0 equiv.) in pyridine (5 mL) and heating in a sand bath to 110 °C for 48 h. The reaction mixture was then cooled to room temperature before *ca*. 20 mL of toluene was added and the solvent was removed *in vacuo*. Two more analogous toluene washes were performed to fully remove pyridine from the mixture. The crude residue was then dissolved in minimal THF and 5 drops of water were added before the solution was heated to 60 °C for 1 h in a water bath. The mixture was then dried (Na_2SO_4), filtered, and concentrated *in vacuo*. Column chromatography (5:1:1 → 1:1:1 hexanes:EtOAc:CH_2Cl_2, R_f = 0.15 in 3:1:1) and subsequent recrystallization from CH_2Cl_2 and hexanes was used to give heterocycle **7** (652 mg, 49%) as a yellow solid: mp > 250 °C; NMR ^{1}H NMR (500 MHz, Chloroform-*d*) δ 7.90 (d, J = 8.4 Hz, 2H), 7.77 (d, J = 3.0 Hz, 1H), 7.68 (d, J = 31.1 Hz, 1H), 7.67 (d, J = 8.1 Hz, 2H), 7.63 (d, J = 7.3 Hz, 1H), 7.60 (d, J = 7.3 Hz, 1H), 7.40 (d, J = 2.3 Hz, 1H), 7.38 – 7.31 (m, 2H), 7.24 (dt, J = 7.5, 3.9 Hz, 2H), 6.99 (d, J = 8.5 Hz, 1H), 4.32 (q, J = 7.1 Hz, 2H), 1.36 (t, J = 7.2 Hz, 3H), 1.34 (s, 9H). ^{13}C NMR (126 MHz, Chloroform-*d*) δ 166.4, 143.6, 141.5 (d, J = 11.6

Hz), 140.9 (d, J = 3.2 Hz), 132.8 (d, J = 139.4 Hz), 132.5 (d, J = 10.8 Hz), 131.9 (d, J = 2.7 Hz), 129.7, 129.4, 128.5, 128.2, 128.1, 127.6 (d, J = 6.2 Hz), 127.1, 126.0 (d, J = 119.1 Hz), 118.7 (d, J = 12.1 Hz), 117.0 (d, J = 7.6 Hz), 61.0, 34.2, 31.4, 14.3. ^{31}P NMR (202 MHz, Chloroform-*d*) δ 11.79; HRMS (ASAP) $[M + H]^+$ calcd for $C_{27}H_{29}NO_3P$ 446.1888, found 446.1885.

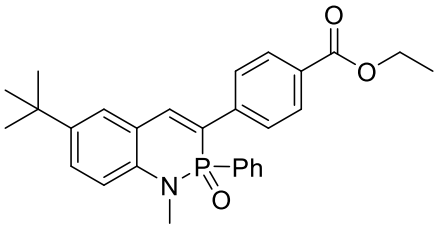

Methylated heterocycle **3** was prepared by dissolving **7** (78 mg, 0.175 mmol, 1.0 equiv.) in dry CH_2Cl_2 and the mixture was put under N_2 via atmosphere exchange. MeI (0.9 mL, 3.95 mmol, 22.5 equiv.) was then added before DBU (0.4 mL, 1.75 mmol, 10 equiv.) was added dropwise, which induced an immediate red-shift in both the color of solution and the emission color of the solution. The solution was let stir for 16 h, at which point the solution had returned to its original color and the reaction was complete via TLC. The reaction mixture was then reduced *in vacuo*, before being dissolved in CH_2Cl_2, washed 3 × with an aqueous $NaHCO_3$ solution to remove excess DBU. After drying (K_2CO_3), filtering, and concentration *in vacuo*, methylated PN heterocycle **3** was afforded as a yellow solid (79 mg, 98% yield) in an excellent yield: mp = 125.4-126.8 °C; NMR ^{1}H NMR (500 MHz, Chloroform-*d*) δ 7.91 (d, J = 8.1 Hz, 2H), 7.83 – 7.61 (m, 5H), 7.50 (d, J = 8.7 Hz, 1H), 7.46 (s, 1H), 7.39 (t, J = 6.7 Hz, 1H), 7.34 (td, J = 7.5, 3.2 Hz, 2H), 7.04 (d, J = 8.7 Hz, 1H), 4.33 (q, J = 7.1 Hz, 2H), 3.12 (d, J = 7.7 Hz, 3H), 1.37 (s, 9H), 1.35 (t, J = 7.0 Hz, 3H). ^{13}C NMR (126 MHz, Chloroform-*d*) δ 166.4, 143.3, 141.4 (d, J = 11.7 Hz), 141.0 (d, J = 3.0 Hz), 139.5, 132.4 (d, J = 10.5 Hz), 132.2 (d, J = 138.1 Hz),

132.0 (d, J = 2.8 Hz), 129.7, 129.5, 128.7, 128.5, 128.4, 127.7 (d, J = 6.2 Hz), 125.7 (d, J = 117.8 Hz), 120.0 (d, J = 11.5 Hz), 112.9 (d, J = 5.0 Hz), 61.0, 34.1, 31.5 (d, J = 4.0 Hz), 31.4, 14.3. ^{31}P NMR (202 MHz, Chloroform-*d*) δ 16.75; HRMS (ASAP) $[M + H]^+$ calcd for $C_{28}H_{31}NO_3P$ 460.2042, found 460.2068.

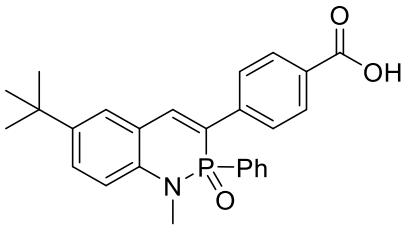

Acid heterocycle **9** was prepared by dissolving methylated heterocycle **3** (200 mg; 0.435 mmol, 1.0 equiv.) in 20 mL THF and 20 mL H_2SO_4 (30% v:v in H_2O) and heating to 85 °C under a reflux condenser for 24 hr. The reaction mixture was then cooled to room temperature before the organic layer was extracted with 5 × rounds of ca. 40 mL EtOAc. The organic layer was the dried (K_2CO_3), filtered and concentrated *in vacuo*. Several round of recrystallization from CH_2Cl_2 and pentanes was used to remove residual EtOAc and afford carboxylic acid **9** (117 mg, 62%) as a yellow solid: mp > 250 °C; NMR ^{1}H NMR (500 MHz, DMSO-d_6) δ 8.06 (d, J = 31.2 Hz, 1H), 7.83 (d, J = 8.2 Hz, 2H), 7.79 (d, J = 8.1 Hz, 2H), 7.71 (s, 1H), 7.63 – 7.52 (m, 3H), 7.44 (dt, J = 15.9, 7.5 Hz, 3H), 7.14 (d, J = 8.8 Hz, 1H), 2.99 (d, J = 7.6 Hz, 3H), 1.33 (s, 9H). ^{13}C NMR (126 MHz, DMSO-d_6) δ 166.9, 142.6, 141.1, 141.0, 139.1, 132.3 (d, J = 134.5 Hz), 132.1, 131.8 (d, J = 10.8 Hz), 129.4, 129.3 (d, J = 105.0 Hz), 128.7, 128.6 (d, J = 8.9 Hz), 127.4 (d, J = 6.1 Hz), 124.9, 123.9, 119.5 (d, J = 11.2 Hz), 113.1, 33.8, 31.2, 31.1. ^{31}P NMR (202 MHz, DMSO-d_6) δ 15.7; HRMS (ASAP) $[M + H]^+$ calcd for $C_{26}H_{27}NO_3P$ 432.1729, found 432.1758.

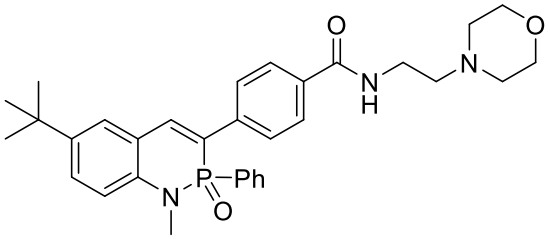

Morpholine-containing PN heterocycle **8** was prepared via peptide coupling conditions. Carboxylic acid PN **9** (314 mg; 0.730 mmol, 1.0 equiv.) and HBTU (554 mg; 1.46 mmol, 2.0 equiv.) were added to a round-bottom flask, which was then put under an N_2 atmosphere via atmosphere exchange. This mixture was then dissolved in dry CH_2Cl_2 (18 mL) before 4-(2-aminoethyl)morpholine **10** (0.38 mL, 2.92 mmol, 4.0 equiv.) was added. Lastly, DIPEA (0.140 mL; 0.82 mmol, 1.0 equiv.) was added via Hamilton syringe. The reaction was stirred for 1 hour, at which point it showed complete conversion of starting material. The reaction mixture was then concentrated *in vacuo* before being suspended in MeCN and cooled in an ice bath for 1 h. Salt byproducts then crashed out and were filtered off. The organic solution was then reduced to dryness *in vacuo* and redissolved in minimal DCM. Pentanes was slow-layered and left overnight. This initial process led to a brown oil coating the bottom of the flask, which allowed for a cleaner product solution to be decanted, reconcentrated, and set up for another round of recrystallization following the same procedure. This led to a fluorescent, yellow oil suspending on the bottom of the flask with crystalline yellow solids dotted throughout. The organic layer was removed, and the oil/solid mixture was dried *in vacuo* to afford **8** (126 mg; 32% yield) as a yellow solid: mp = 234.5-235.9 °C. It is expected that the reaction yield is higher than this, however, due to structural similarities between the product and the coupling side-products, the isolation of more product presents a significant challenge. ^{1}H NMR (500 MHz, DMSO-d_6) δ 8.35 (t, J = 5.7 Hz, 1H), 8.04 (d, J = 31.4 Hz, 1H), 7.80 – 7.66 (m,

5H), 7.64 – 7.51 (m, 3H), 7.48 (td, J = 7.3, 1.5 Hz, 1H), 7.43 (td, J = 7.1, 3.3 Hz, 2H), 7.13 (d, J = 8.7 Hz, 1H), 3.55 (t, J = 4.6 Hz, 4H), 3.35 (d, J = 6.7 Hz, 2H), 2.99 (d, J = 7.6 Hz, 3H), 2.42 (t, J = 7.0 Hz, 2H), 2.39 (t, J = 4.0 Hz, 4H), 1.34 (s, 9H). ^{13}C NMR (126 MHz, DMSO-d_6) δ 165.6, 142.5, 140.6, 139.2 (d, J = 12.0 Hz), 139.0, 133.5, 132.4 (d, J = 134.8 Hz), 132.0, 132.0, 131.7 (d, J = 10.3 Hz), 128.6 (d, J = 13.1 Hz), 128.4, 127.3, 127.1 (d, J = 6.2 Hz), 124.5 (d, J = 116.9 Hz), 119.5 (d, J = 11.3 Hz), 113.0, 66.2, 57.3, 53.3, 36.5, 33.8, 31.2, 31.0 (d, J = 3.7 Hz). ^{31}P NMR (202 MHz, DMSO-d_6) δ 15.77; HRMS (ASAP) $[M + H]^+$ calcd for $C_{32}H_{39}N_3O_3P$ 544.2729, found 544.2737.

Supporting Information

Crystallographic Data for 8

Waiting for Lev to give crystal data.

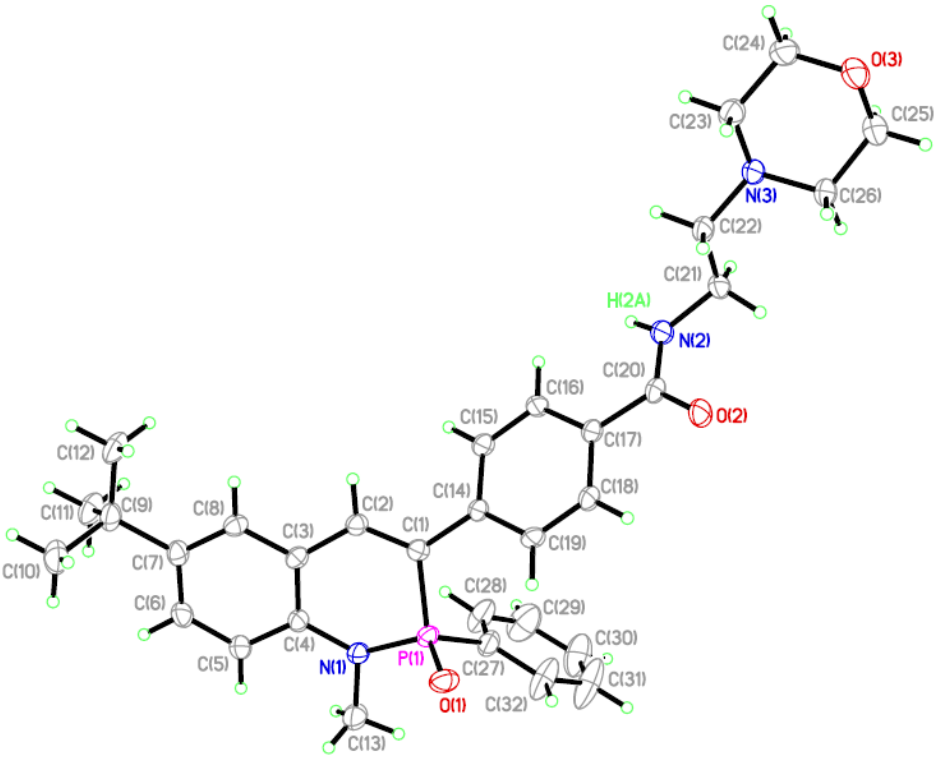

Figure E.1.1. ORTEP drawing of heterocycle **8**; thermal ellipsoids drawn at 30% probability.

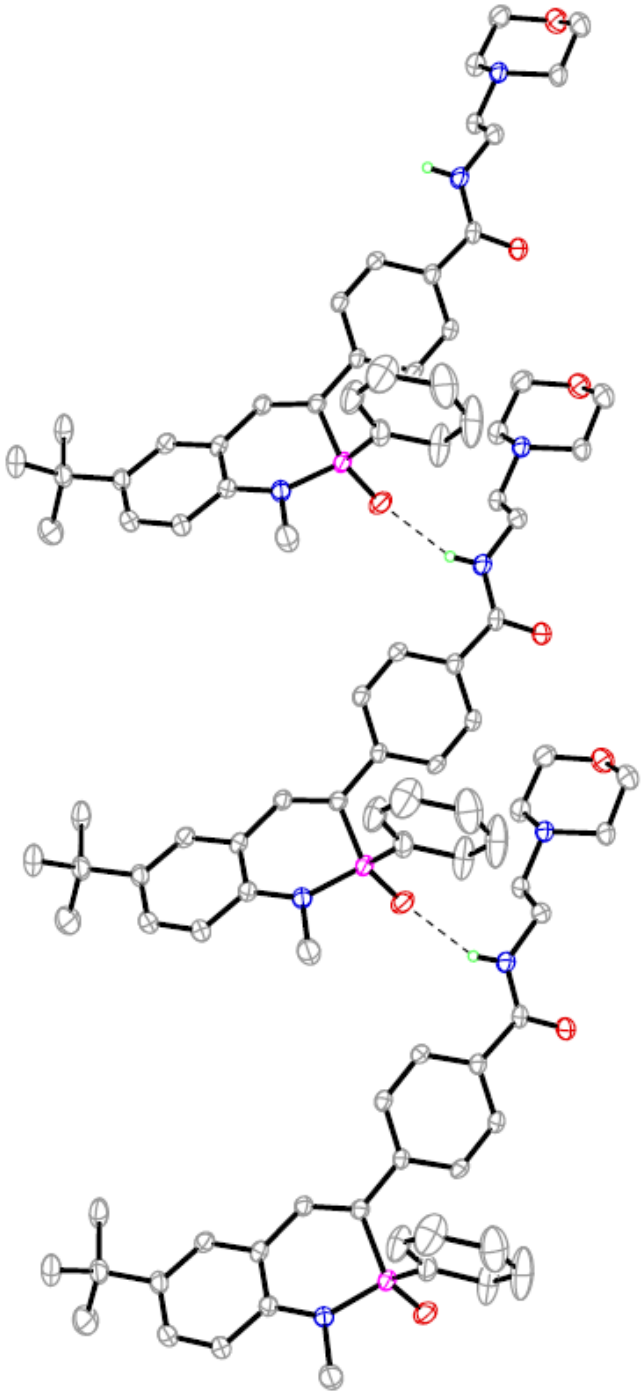

Figure E.1.2. ORTEP drawing of amide-directed hydrogen bonding seen in the solid state for heterocycle **8**; thermal ellipsoids drawn at 30% probability.

Photophysical Properties

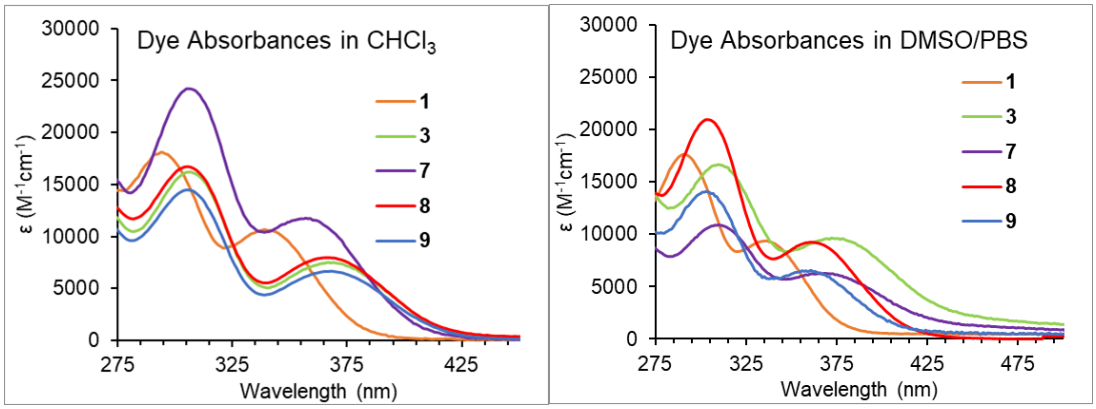

Figure E.1.3. UV-vis absorption spectra of new heterocycles in (left) $CHCl_3$ and (right) ~5% DMSO in pH 7.4 PBS buffer.

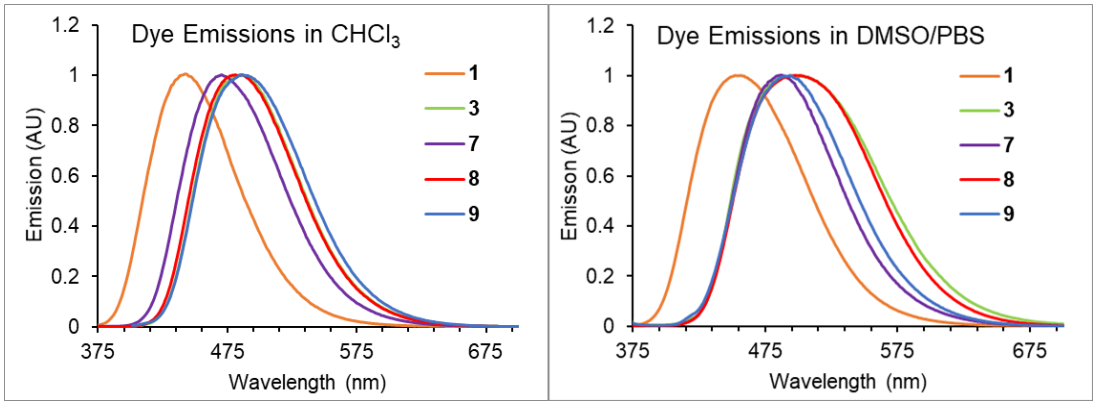

Figure E.1.4. Emission spectra of new heterocycles in (left) $CHCl_3$ and (right) ~5% DMSO in pH 7.4 PBS buffer.

Cell Images of 8 Colocalization Studies

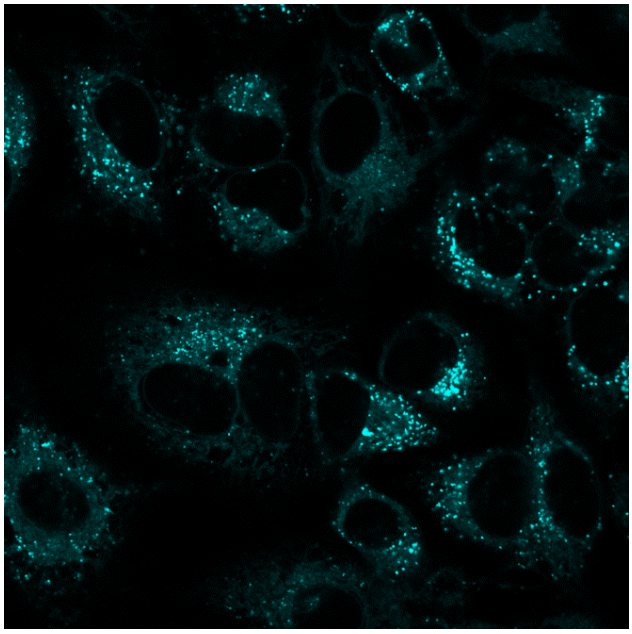

Figure E.1.5. Fluorescence image of live HeLa cells after incubation with 5 μM **8.**

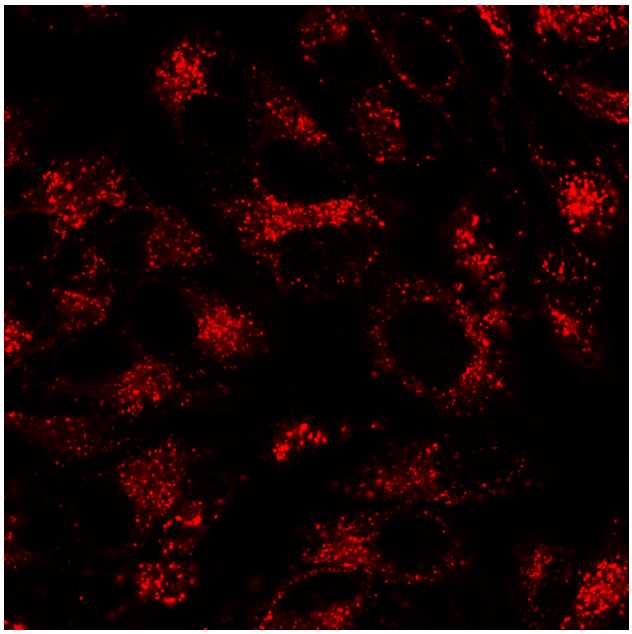

Figure E.1.6. Fluorescence image of live HeLa cells after incubation with 50 nM LysoTracker Deep Red.

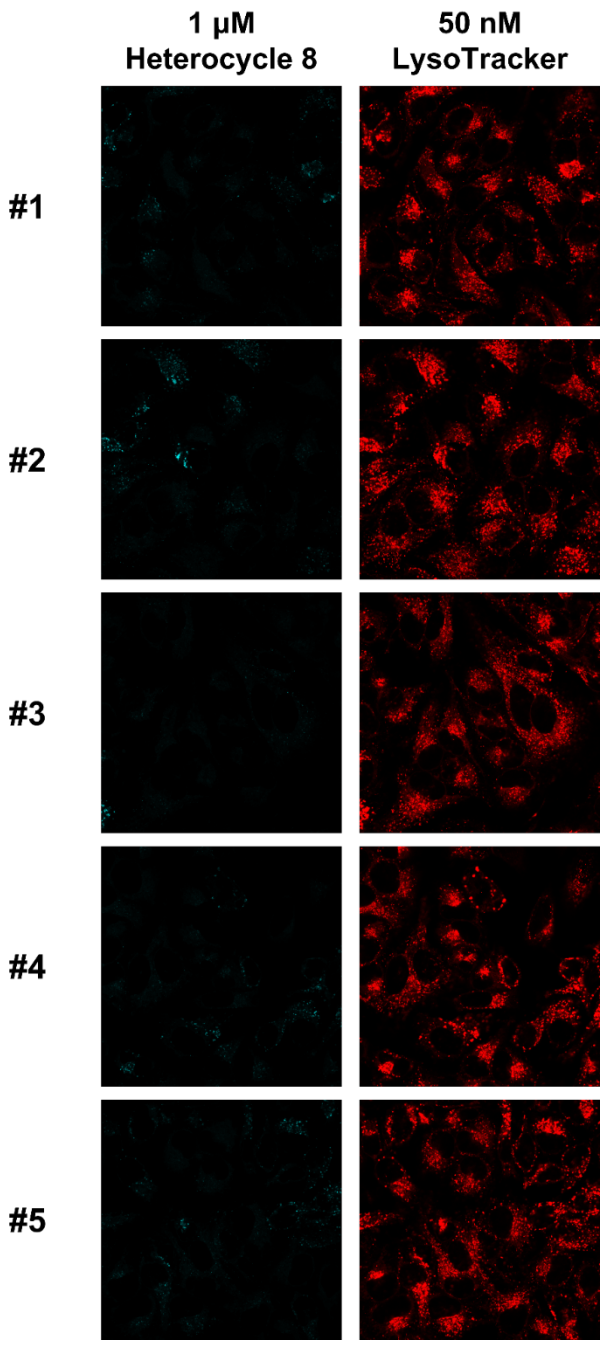

Figure E.1.7. Fluorescence images of live HeLa cells after incubation with both 1 μM solution of **8** and 50 nM LysoTracker Deep Red. Left column shows emission of **8**, right column shows emission of LysoTracker Deep Red. Average Pearson correlation value for colocalization: 0.49.

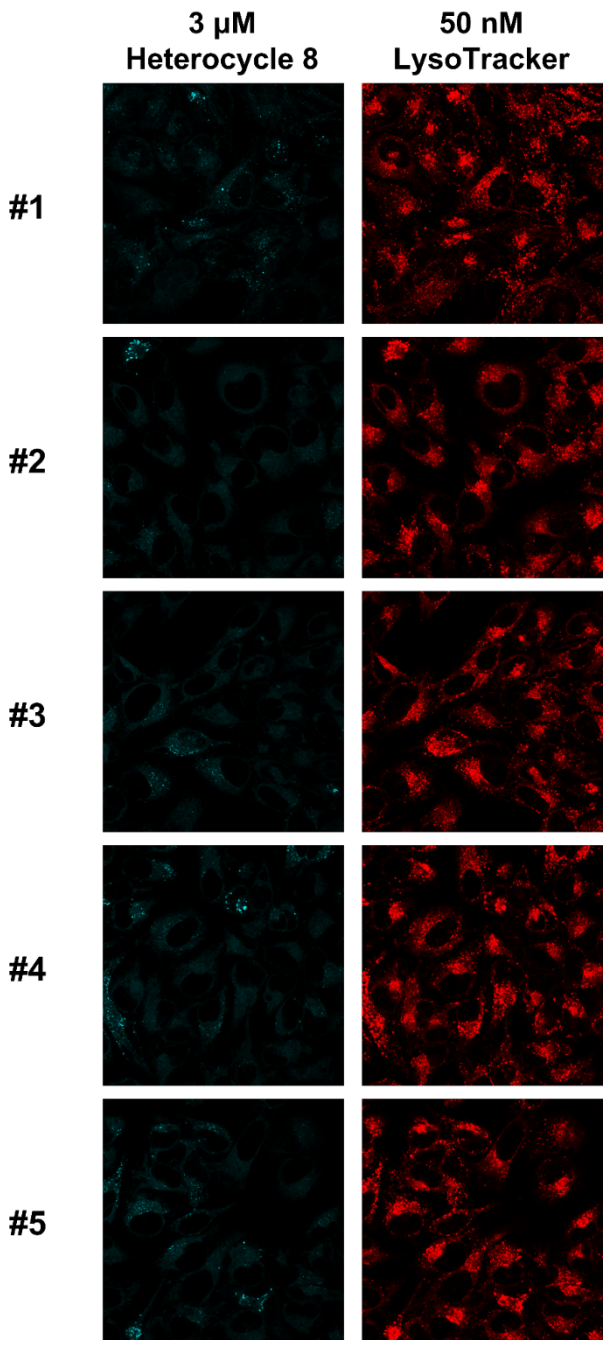

Figure E.1.8. Fluorescence images of live HeLa cells after incubation with both 3 μM solution of **8** and 50 nM LysoTracker Deep Red. Left column shows emission of **8**, right column shows emission of LysoTracker Deep Red. Average Pearson correlation value for colocalization: 0.61.

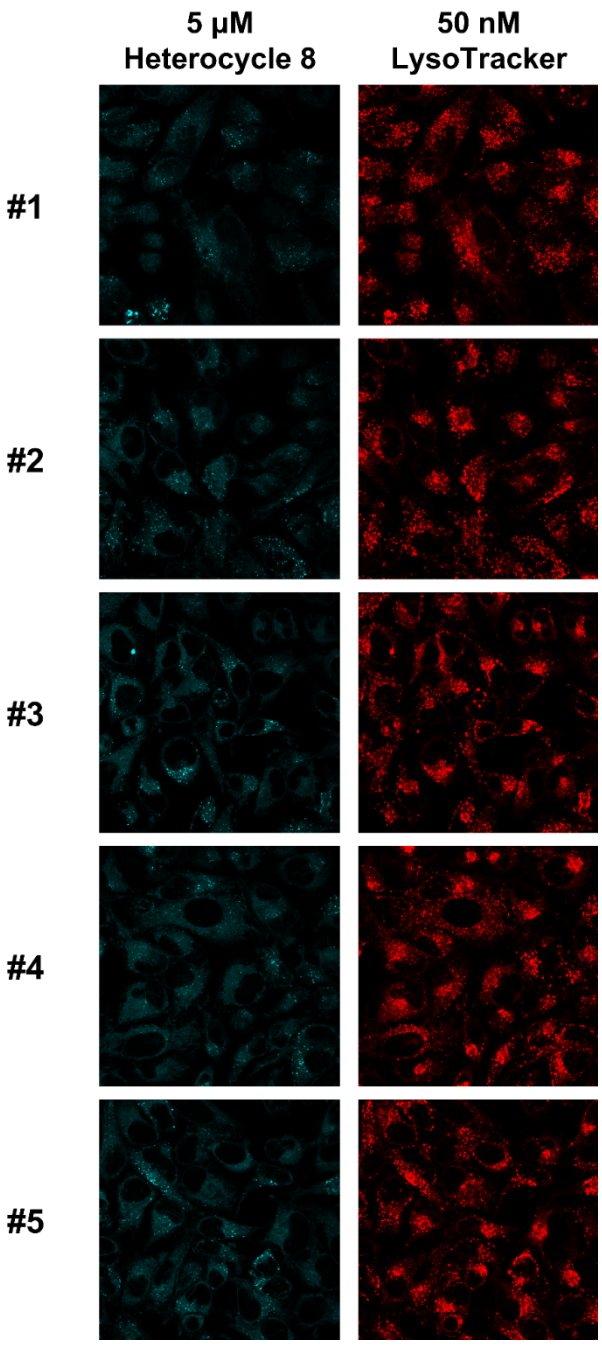

Figure E.1.9. Fluorescence images of live HeLa cells after incubation with both 5 µM solution of **8** and 50 nM LysoTracker Deep Red. Left column shows emission of **8**, right column shows emission of LysoTracker Deep Red. Average Pearson correlation value for colocalization: 0.65.

NMR Spectra

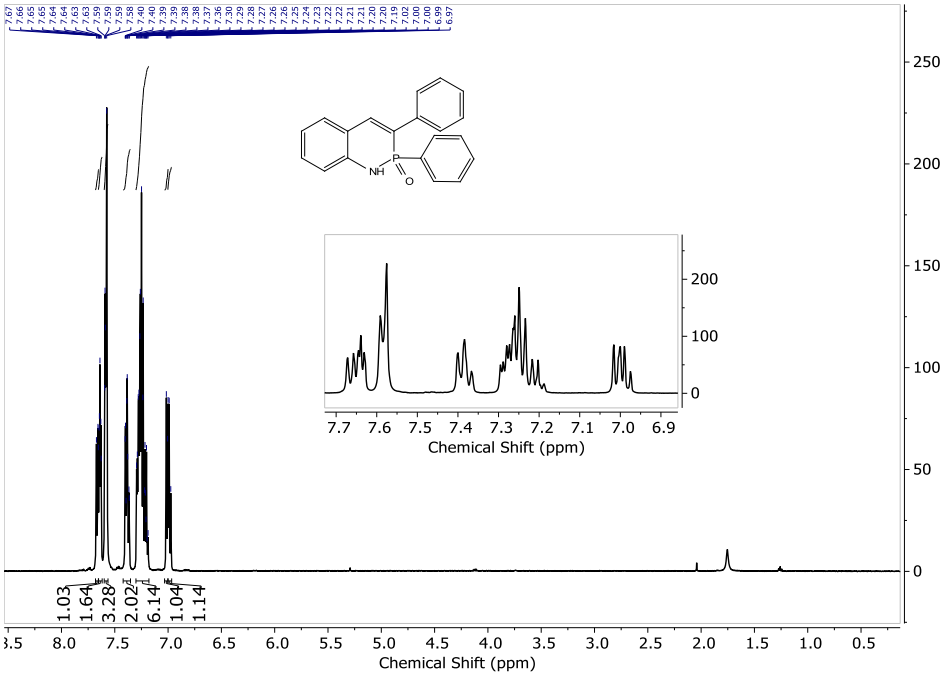

Figure E.1.10. ^{1}H NMR of **1**.

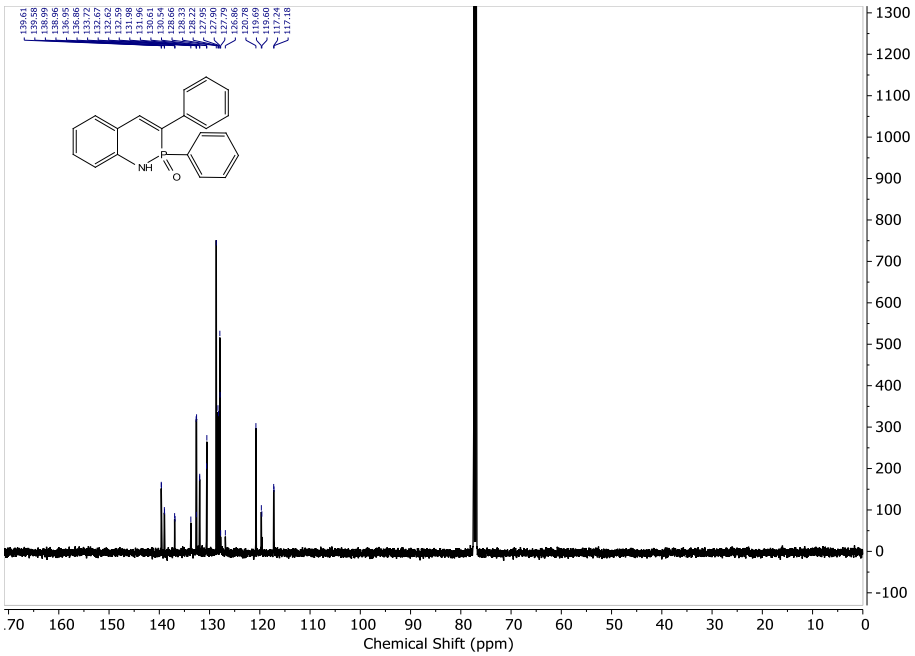

Figure E.1.11. ^{13}C NMR of **1**.

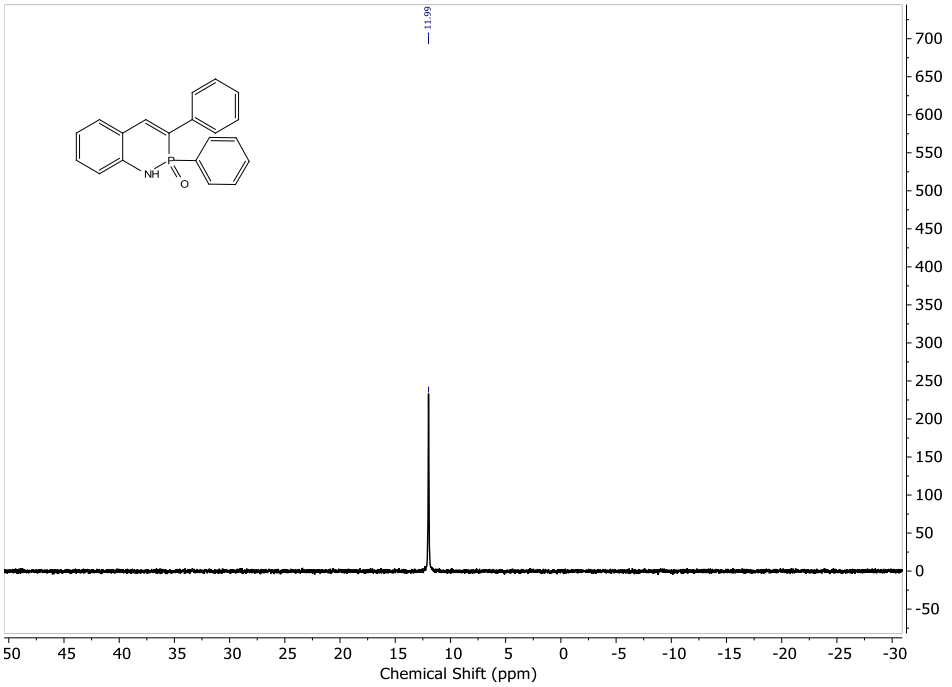

Figure E.1.12. ^{31}P NMR of **1**.

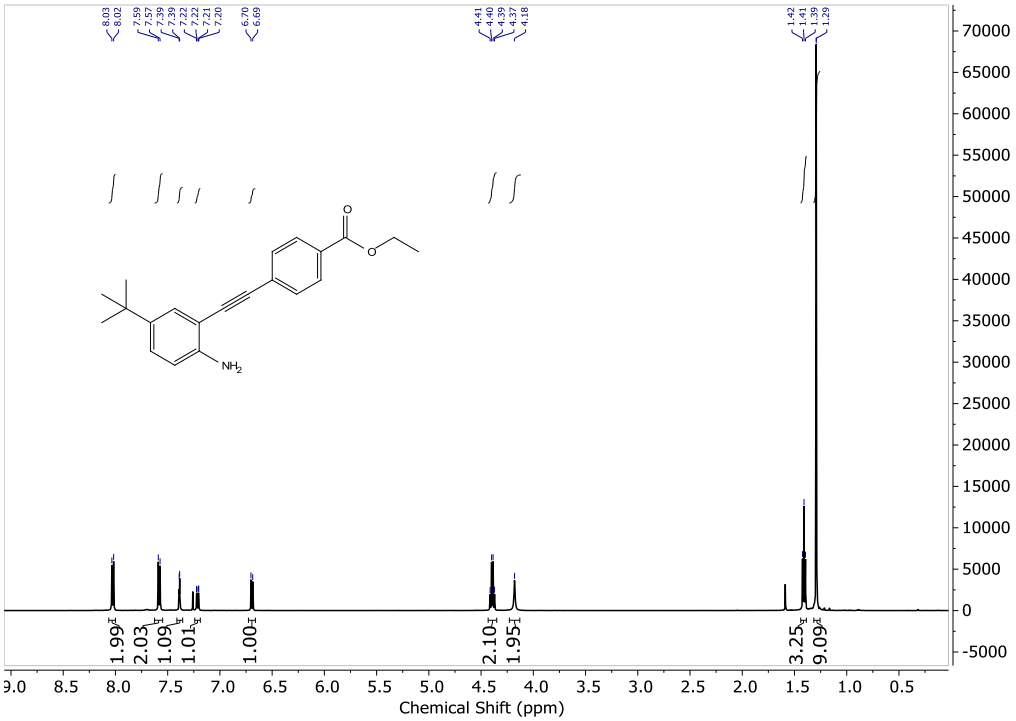

Figure E.1.13. ^{1}H NMR of **6**.

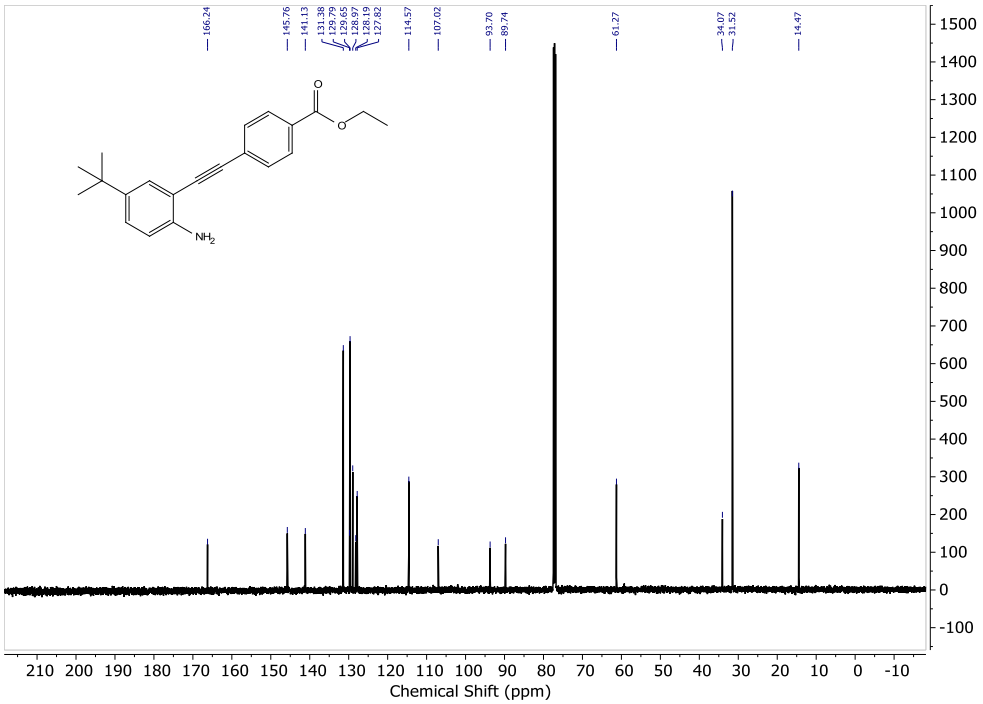

Figure E.1.14. ^{13}C NMR of **6**.

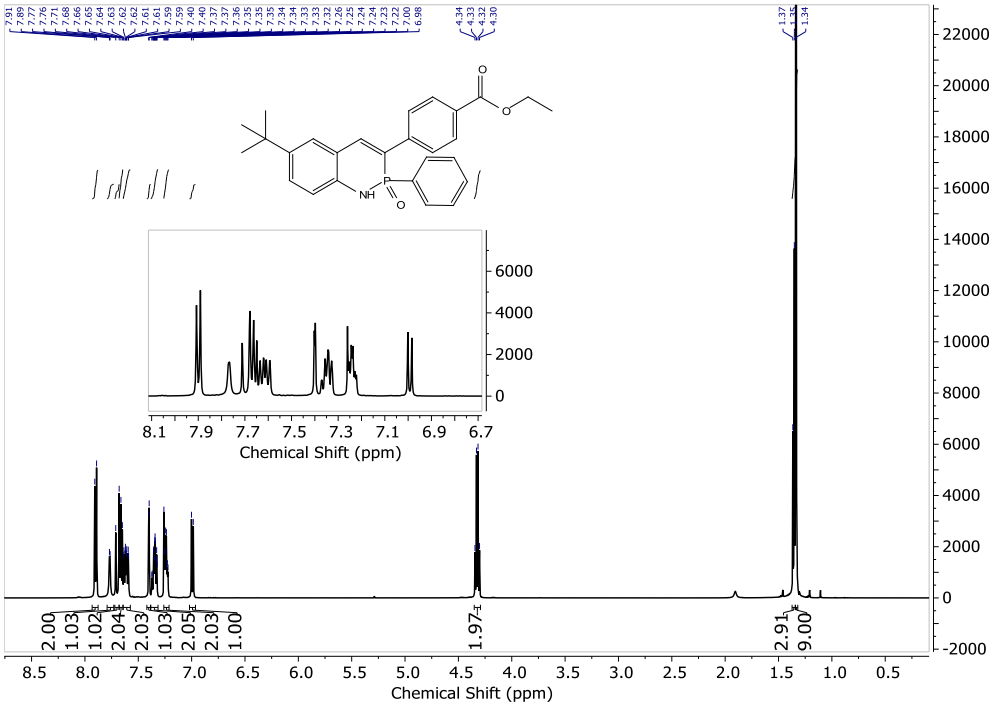

Figure E.1.15. ^{1}H NMR of **7**.

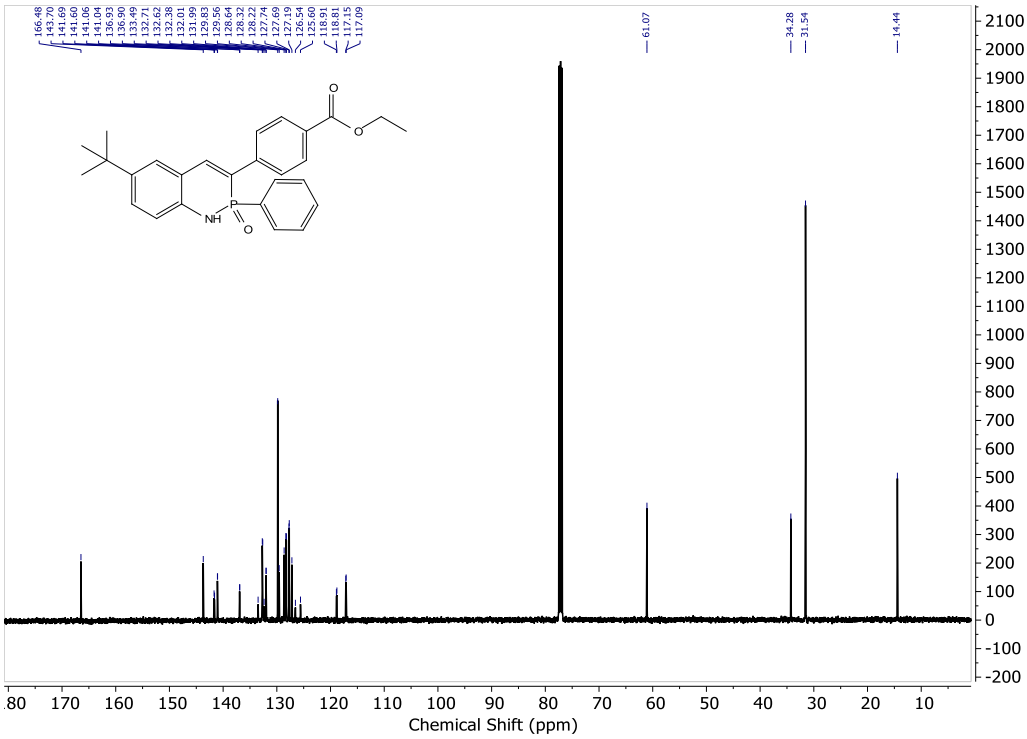

Figure E.1.16. ^{13}C NMR of **7**.

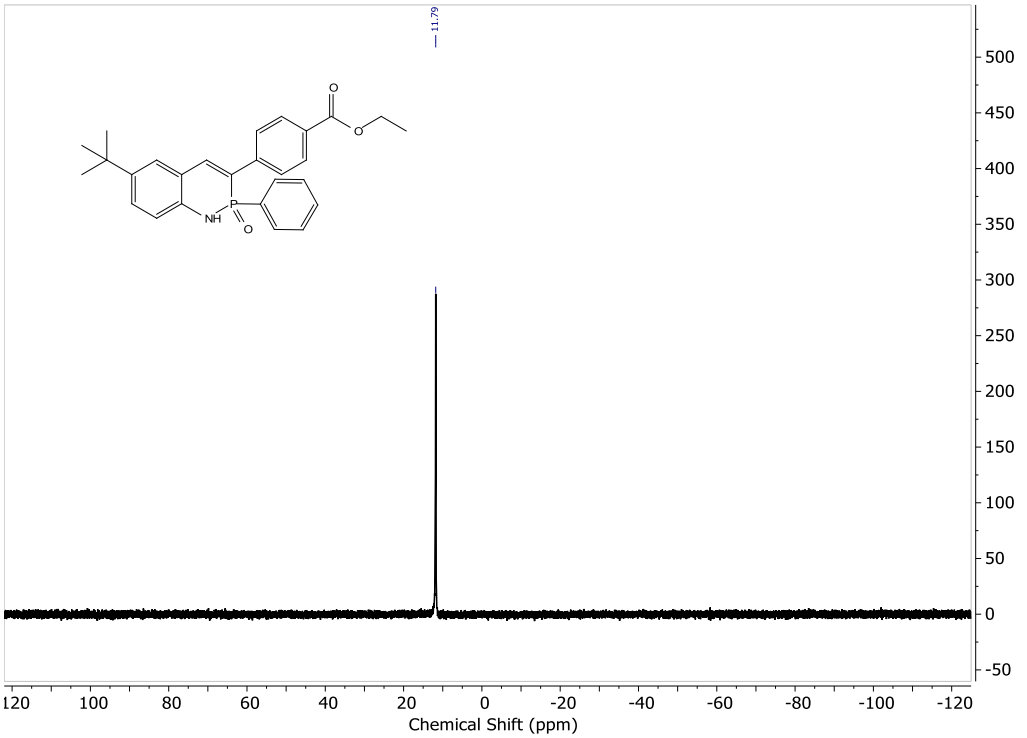

Figure E.1.17. ^{31}P NMR of **7**.

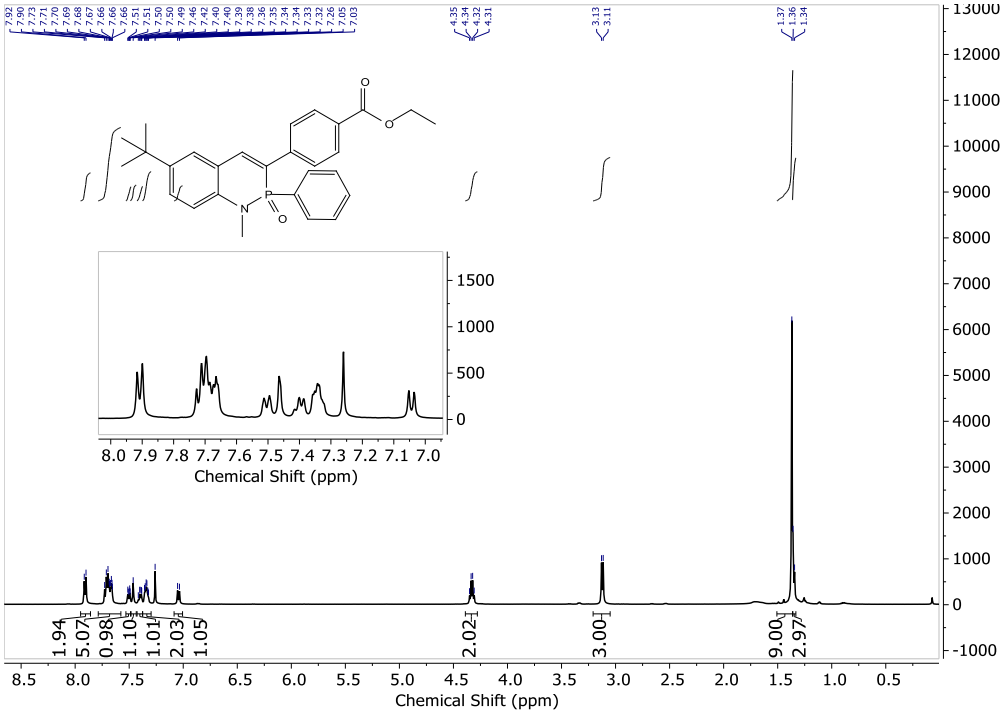

Figure E.1.18. ^{1}H NMR of **3**.

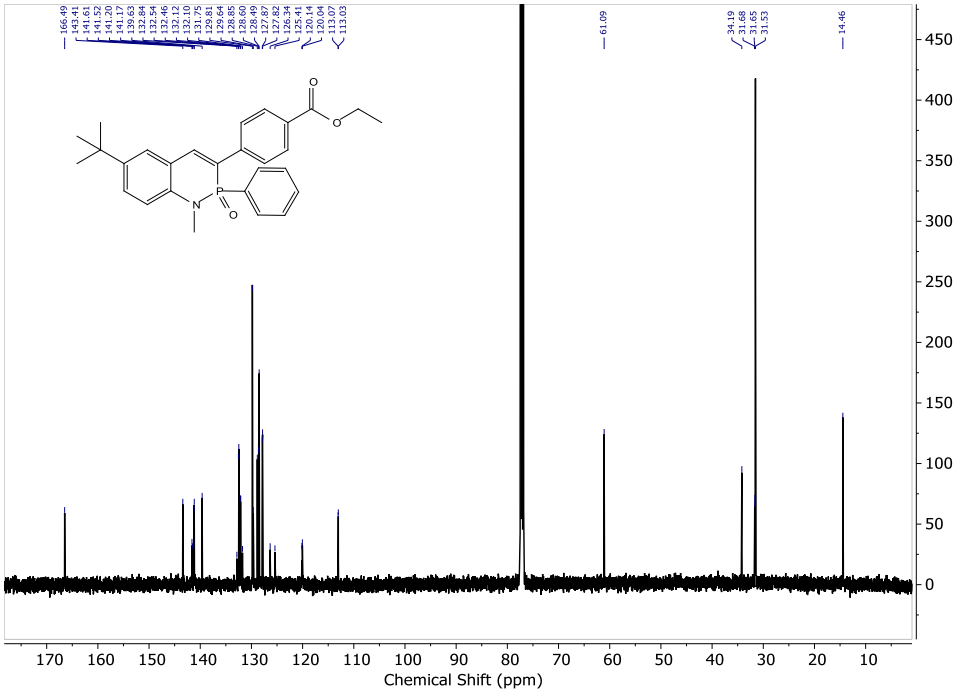

Figure E.1.19. ^{13}C NMR of **3**.

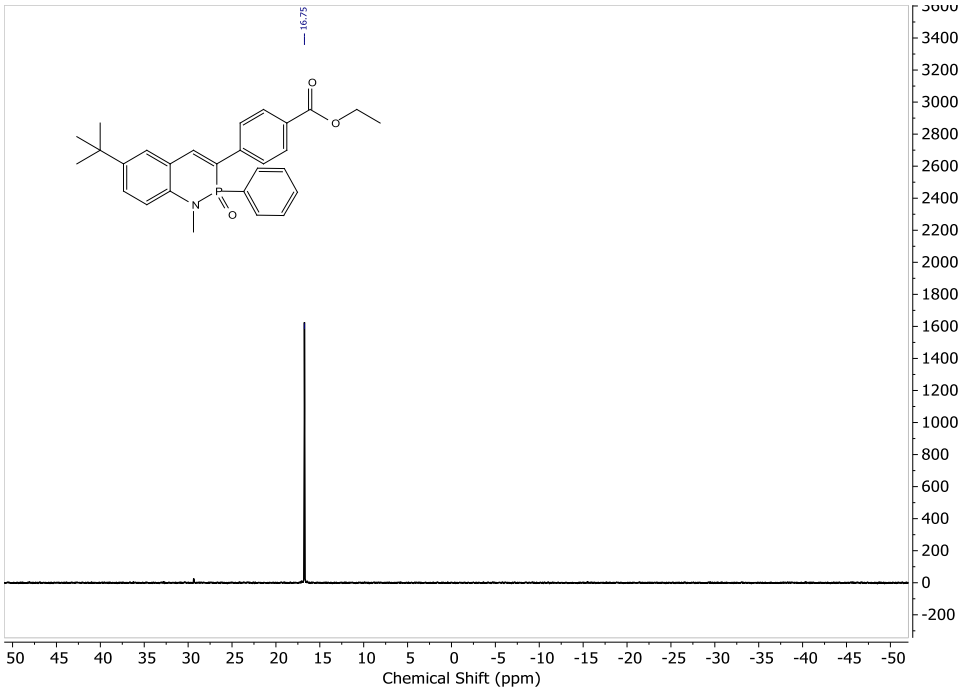

Figure E.1.20. ^{31}P NMR of **3**.

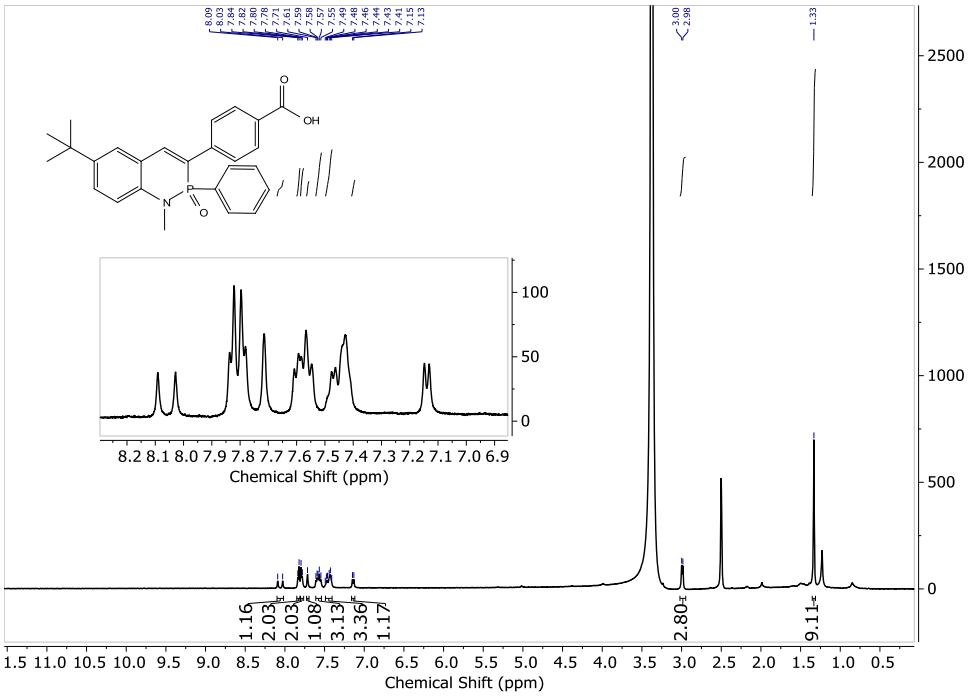

Figure E.1.21. ^{1}H NMR of **9**.

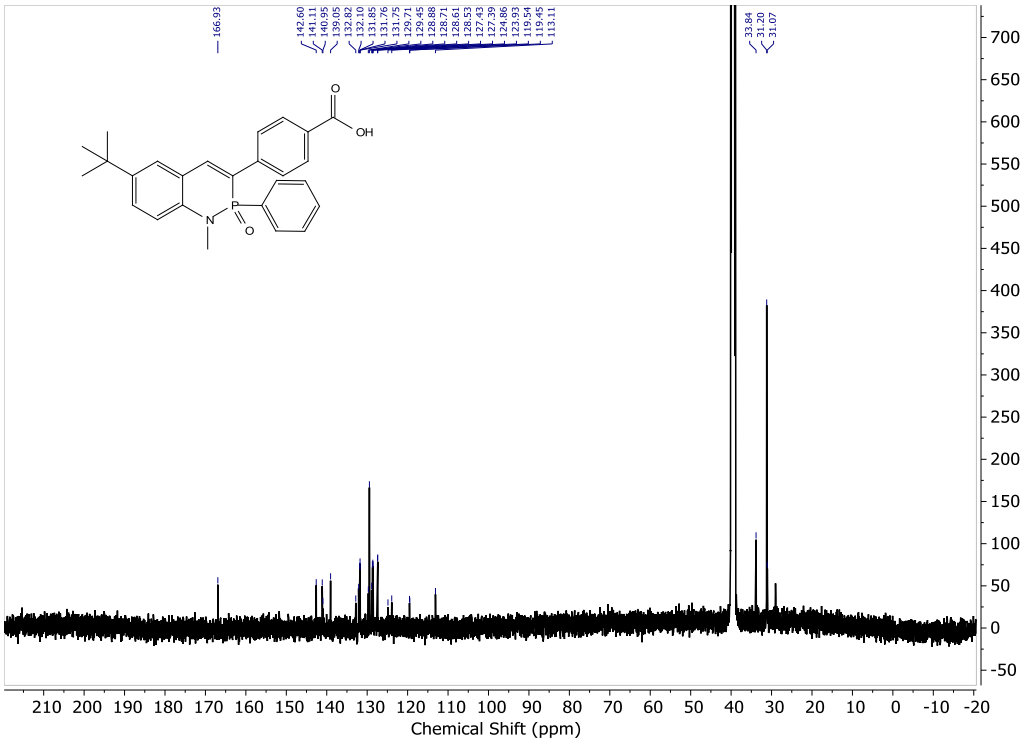

Figure E.1.22. ^{13}C NMR of **9**.

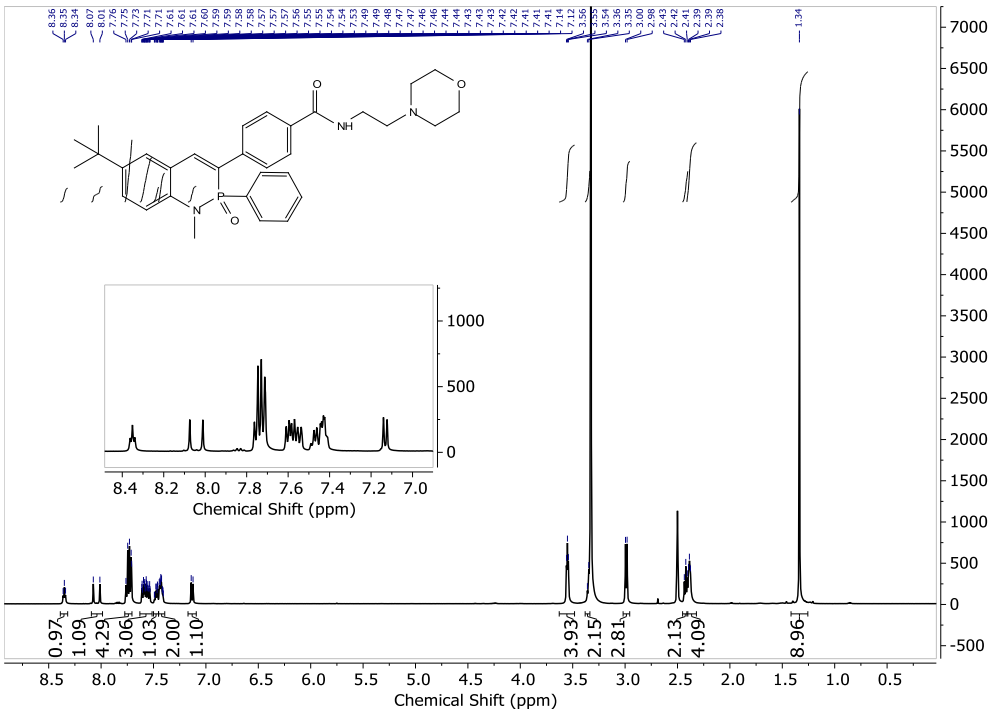

Figure E.1.23. ^{1}H NMR of **8**.

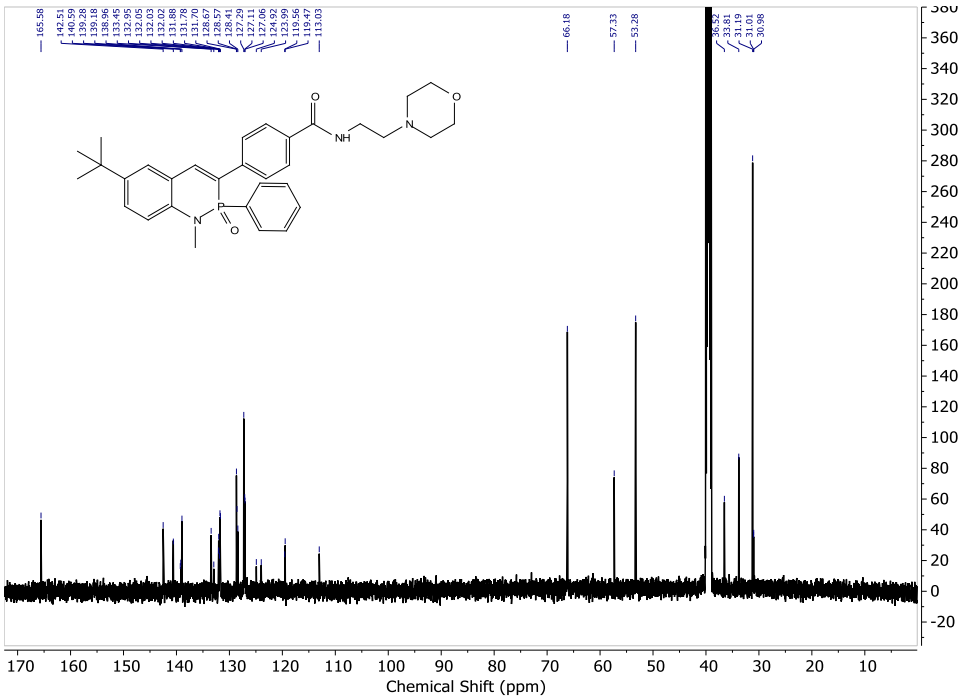

Figure E.1.24. ^{13}C NMR of **9**.

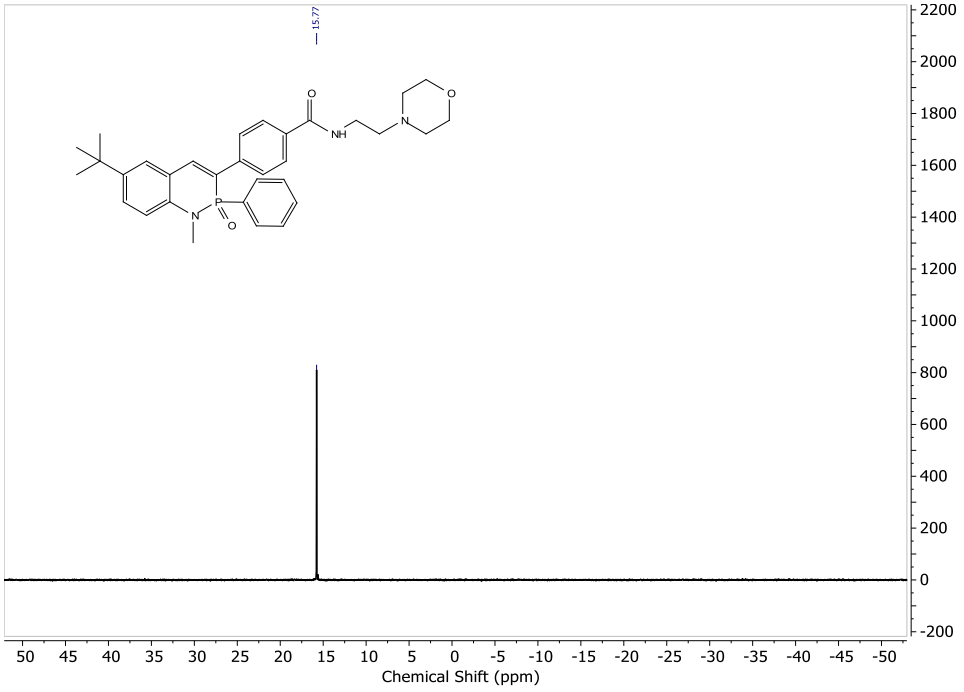

Figure E.1.25. ^{31}P NMR of **9**.

References

(1) Lakowicz, J. R. (**2006**) Principles of Fluorescence Spectroscopy, 3rd ed., Springer, New York.

(2) Waggoner, A., and Kenneth, S. Enzymol. **1995**, *246*, 362–373.

(3) Johnson, I. *Histochem. J.* **1998**, *30*, 123–140.

(4) Petit, J.-M., Denis-Gay, M., and Ratinaud, M.-H. *Biol. Cell* **1993** *78*, 1–13.

(5) Johnsson, N., and Johnsson, K. *ACS Chem. Biol.* **2007**, 31–38.

(6) Goddard, J.-P., and Reymond, J.-L. *Curr. Opin. Biotechnol.* **2004**, *15*, 314.

(7) Giepmans, B. N. G., Adams, S. R., Ellisman, M. H., and Tsien, R. Y. *Science* **2006**, *312*, 217–224.

(8) Zhang, J., Campbell, R. E., Ting, A. Y., and Tsien, R. Y. *Nat. Rev. Mol. Cell Biol*. **2002**, *3* 906–918.

(9) Valeur, B. (**2002**) Molecular Fluorescence: Principles and Applications, Wiley-VCH, Weinheim.

(10) Frangioni, J. V. In vivo near-infrared fluorescence imaging *Curr. Opin. Chem. Biol.* **2003**, *7,* 626–634.

(11) Wolfbeis, O. S. (**1985**) The fluorescence of organic natural products. In Molecular Luminescence Spectroscopy: Methods and Applications—Part 1 (Schulman, S. G., Ed.), pp 167– 317, Wiley, New York.

(12) Sun, W.-C., Gee, K. R., and Haugland, R. P. (**1998**) Synthesis of novel fluorinated coumarins: Excellent UV-light excitable fluorescent dyes *Bioorg. Med. Chem. Lett.* **1998** *8*, 3107–3110.

(13) Hinkeldey, B., Schmitt, A., and Jung, G. *ChemPhysChem* **2008**, *9*, 2019–2027.

(14) Song, L.; Hennink, E. J.; Young, T.; Tanke, H. J. *Biophys. J.***1995**, *68*, 2588.

(15) Sjoback, R.; Nygern, J.; Kubista, M. *Spectrochim. Acta Part A* **1995**, *51*, L7.

(16) Song, L.; Varma, C. A. G. O.; Verhoeven, J. W.; Tanke, H. *Biophys. J.***1996**, *70*, 2959.

(17) Lavis, L.D. and Raines, R.T. *ACS Chem. Biol*. **2014**, *9*, 855–866.

(18) Lavis, L.D. and Raines, R.T. *ACS Chem. Biol.* **2008**, *3*, 142–155.

(19) Bard, J.P., Johnson, D.W., Haley, M.M. *Synlett* **2020**, *31*, 1862–1877.

(20) Vonnegut, C.L.; Shonkwiler, A.M.; Khalifa, M.M.; Zakharov, L.N.; Johnson, D.W.; Haley, M.M. *Angew. Chem. Int. Ed.* **2015**, *54*, 13318–13322.

(21) McNeill, J.N., Dr. Karas, L.J., Dr. Bard. J.P, Fabrizio, K., Dr. Zakharov, L. N., Dr. MacMillan, S.N., Prof. Brozek, C.K., Prof. Wu, J.I., Prof. Johnson, D.W., Prof. Haley, M.M. *Chem. Eur. J.* **2022**, *28*, https://doi.org/10.1002/chem.202200472

(22) Bard, J.P., McNeill, J.N., Zakharov, L.N., Johnson, D.W., Haley, M.M. *Isr. J. Chem.* **2021**, *61*, 217–221.

(23) Bard, J.P.; Deng, C.-L.; Richardson, H.C.; Odulio, J.M.; Barker, J.E.; Zakharov, L.N.; Cheong, P.H.-Y.; Johnson, D.W.; Haley, M.M. *Org. Chem. Front.* **2019**, *6*, 1257–1265.

(24) Bard, J.P., Bates, H.J., Deng, C.-L., Zakharov, L.N., Johnson, D.W., Haley, M.M. *J. Org. Chem.* **2020**, *85*, 85–91

(25) Lipinski, C. A.; Lombardo, F.; Dominy, B. W.; Feeney, P. J. *Adv. Drug Deliv. Rev.* **1997**, *23*, 3–25.

(26) Kourounakis, A. P., Xanthopoulos, D., & Tzara, A. *Med. Res. Rev.* **2019**, 1–44.

(27) Nagano, T. *P. JPN. Acad. B-Phys.* **2010**, *8*, 837–847.

(28) Zhang, J., Yang, M., Mazi, W., Adhikari, K., Fang, M., Xie, F., Valenzano, L., Tiwari, A., Luo, F.-T., Liu, H. *ACS Sens.* **2016**, *1*, 158–165.

(29) Dunn, K.W., Kamocka, M.M., McDonald, J.H. *Am. J. Physiol-Cell Ph.* **2011**, *300*, C723-C742.

(30) Brouwer, A.M. *Pure Appl. Chem.* **2011**, *83*, 2213–2228.

(31) Carroll, C.N., Berryman, O.B., Johnson, C.A., Zakharov, L.N., Haley, M.M., Johnson, D.W. *Chem. Commun.*, **2009**, 2520–2522.

REFERENCES CITED

CHAPTER I

(1) Sessler, J. L.; Gale, P. A.; Cho, W.-S. *Anion Receptor Chemistry*; Royal Society of Chemistry: Cambridge, 2006.

(2) Zyryanov, G. V; Palacios, M. A.; Anzenbacher Jr., P. Rational Design of a Fluorescence-Turn-On Sensor Array for Phosphates in Blood Serum Zuschriften. *Angew. Chemie* **2007**, *119*, 7995–7998.

(3) Hruska, K. A.; Mathew, S.; Lund, R.; Qiu, P.; Pratt, R. Hyperphosphatemia of Chronic Kidney Disease. *Kidney Int.* **2008**, *74* (2), 148–157.

(4) Schmidt, R. F.; Thews, G. *Human Physiology*, 2nd ed.; Springer: Berlin, 1989.

(5) Kanbay, M.; Goldsmith, D.; Akcay, A.; Covic, A. Phosphate - The Silent Stealthy Cardiorenal Culprit in All Stages of Chronic Kidney Disease: A Systematic Review. *Blood Purif.* **2009**, *27* (2), 220–230.

(6) Feng, H.; Wang, Y.; Jia, H.; Zhang, R.; Han, Q.; Meng, Q.; Zhiqiang, Z. Selective Detection of Inorganic Phosphates in Live Cells Based on a Responsive Fluorescence Probe. *New J. Chem.* **2017**, *41*, 9623–9630.

(7) Scott, C. C.; Gruenberg, J. Ion Flux and the Function of Endosomes and Lysosomes: PH Is Just the Start: The Flux of Ions across Endosomal Membranes Influences Endosome Function Not Only through Regulation of the Luminal PH. *BioEssays* **2011**, *33* (2), 103–110.

(8) Jentsch, T. J.; Stein, V.; Weinreich, F.; Zdebik, A. A. Molecular Structure and Physiological Function of Chloride Channels. *Physiol. Rev.* **2002**, *82* (2), 503–568.

(9) Berend, K.; Van Hulsteijn, L. H.; Gans, R. O. B. Chloride: The Queen of Electrolytes? *Eur. J. Intern. Med.* **2012**, *23* (3), 203–211.

(10) Beck, A.; Ernst, M. Kinetic Modeling and Selectivity of Anion Exchange in Donnan Dialysis. *J. Memb. Sci.* **2015**, *479*, 132–140.

(11) Matsuyama, K.; Sen, A. C.; Perrin, J. H. The Effects of PH, Calcium and Chloride Ions on the Binding of Tolmetin to Human Serum Albumin: Circular Dichroic, Dialysis and Fluorometric Measurements. *J. Pharm. Pharmacol.* **1987**, *39* (3), 190–195.

(12) Scanziani, M.; Häusser, M. Electrophysiology in the Age of Light. *Nature* **2009**, *461* (7266), 930–939.

(13) Saunders, J. H. Liquid and Solid-State Cl- -Sensitive Microelectrodes. Characteristics and Application to Intracellular Cl- Activity in Balanus Photoreceptor. *J. Gen. Physiol.* **1977**, *70* (4), 507–530.

(14) Nagai, T.; Ibata, K.; Park, E. S.; Kubota, M.; Mikoshiba, K.; Miyawaki, A. A Variant of Yellow Fluorescent Protein with Fast and Efficient Maturation for Cell-Biological Applications. *Nat. Biotechnol.* **2002**, *20*, 87–90.

(15) Tutol, J. N.; Peng, W.; Dodani, S. C. Discovery and Characterization of a Naturally Occurring, Turn-On Yellow Fluorescent Protein Sensor for Chloride. *Biochemistry* **2019**, *58* (1), 31–35.

(16) Yoon, D. W.; Gross, D. E.; Lynch, V. M.; Lee, C. H.; Bennett, P. C.; Sessler, J. L. Real-Time Determination of Chloride Anion Concentration in Aqueous-DMSO Using a Pyrrole-Strapped Calixpyrrole Anion Receptor. *Chem. Commun.* **2009**, No. 9, 1109–1111.

(17) Langton, M. J.; Serpell, C. J.; Beer, P. D. Anion Recognition in Water: Recent Advances from a Supramolecular and Macromolecular Perspective. *Angew. Chem. Int. Ed.* **2016**, *55* (6), 1974–1987.

(18) Yu, X. H.; Hong, X. Q.; Mao, Q. C.; Chen, W. H. Biological Effects and Activity Optimization of Small-Molecule, Drug-like Synthetic Anion Transporters. *Eur. J. Med. Chem.* **2019**, *184*, 111782.

(19) Liu, Y.; Zhao, W.; Chen, C.-H.; Flood, A. H. Chloride Capture Using a C–H Hydrogen-Bonding Cage. *Science* **2019**, *365*, 159–161.

(20) Tutol, J. N.; Lee, J.; Chi, H.; Faizuddin, F. N.; Abeyrathna, S. S.; Zhou, Q.; Morcos, F.; Meloni, G.; Dodani, S. C. A Single Point Mutation Converts a Proton-Pumping Rhodopsin into a Red-Shifted, Turn-on Fluorescent Sensor for Chloride. *Chem. Sci.* **2021**, *12*, 5655–5663.

(21) Watt, M. M.; Engle, J. M.; Fairley, K. C.; Robitshek, T. E.; Haley, M. M.; Johnson, D. W. "Off-on" Aggregation-Based Fluorescent Sensor for the Detection of Chloride in Water. *Org. Biomol. Chem.* **2015**, *13* (14), 4266–4270.

(22) Khatua, S.; Choi, S. H.; Lee, J.; Kim, K.; Do, Y.; Churchill, D. G. Aqueous Fluorometric and Colorimetric Sensing of Phosphate Ions by a Fluorescent Dinuclear Zinc Complex. *Inorg. Chem.* **2009**, *48* (7), 2993–2999.

(23) Zhang, Y. M.; Lin, Q.; Wei, T. B.; Wang, D. D.; Yao, H.; Wang, Y. L. Simple Colorimetric Sensors with High Selectivity for Acetate and Chloride in Aqueous Solution. *Sensors Actuators, B Chem.* **2009**, *137* (2), 447–455.

(24) Bazany-Rodríguez, I. J.; Martínez-Otero, D.; Barroso-Flores, J.; Yatsimirsky, A. K.; Dorazco-González, A. Sensitive Water-Soluble Fluorescent Chemosensor for Chloride Based on a Bisquinolinium Pyridine-Dicarboxamide Compound. *Sensors Actuators, B Chem.* **2015**, *221*, 1348–1355.

(25) Huang, X. H.; Lu, Y.; He, Y. B.; Chen, Z. H. A Metal-Macrocycle Complex as a Fluorescent Sensor for Biological Phosphate Ions in Aqueous Solution. *Eur. J. Org. Chem.* **2010**, No. 10, 1921–1927.

(26) Martí, I.; Bolte, M.; Burguete, M. I.; Vicent, C.; Alfonso, I.; Luis, S. V. Tight and Selective Caging of Chloride Ions by a Pseudopeptidic Host. *Chem. Eur. J.* **2014**, *20* (24), 7458–7464.

(27) Kim, D. S.; Lynch, V. M.; Nielsen, K. A.; Johnsen, C.; Jeppesen, J. O.; Sessler, J. L. A Chloride-Anion Insensitive Colorimetric Chemosensor for Trinitrobenzene and Picric Acid. *Anal. Bioanal. Chem.* **2009**, *395* (2), 393–400.

(28) Buhlmann, P.; Nishizawa, S.; Xiao, K. P.; Umezawa, Y. Strong Hydrogen Bond-Mediated Complexation of H2PO4- by Neutral Bis-Thiourea Hosts. *Tetrahedron* **1997**, *53* (5), 1647–1654.

(29) Scherer, M.; Sessler, J. L.; Gebauer, A.; Lynch, V. A Bridged Pyrrolic Ansa-Ferrocene. A New Type of Anion Receptor. *Chem. Commun.* **1998**, 85–86.

(30) Snowden, T. S.; Anslyn, E. V. Anion Recognition: Synthetic Receptors for Anions and Their Application in Sensors. *Curr. Opin. Chem. Biol.* **1999**, *3* (6), 740–746.

(31) Sessler, J. L.; Cho, D. G.; Lynch, V. Diindolylquinoxalines: Effective Indole-Based Receptors for Phosphate Anion. *J. Am. Chem. Soc.* **2006**, *128* (51), 16518–16519.

(32) Prakash, V.; Saha, S.; Chakraborty, K.; Krishnan, Y. Rational Design of a Quantitative, PH-Insensitive, Nucleic Acid Based Fluorescent Chloride Reporter. *Chem. Sci.* **2016**, *7* (3), 1946–1953.

(33) Chakraborty, K.; Veetil, A. T.; Jaffrey, S. R.; Krishnan, Y. Nucleic Acid-Based Nanodevices in Biological Imaging. *Annu. Rev. Biochem.* **2016**, *85*, 349–373.

(34) Labuda, J.; Oliveira Brett, A. M.; Evtugyn, G.; Fojta, M.; Mascini, M.; Ozsoz, M.; Palchetti, I.; Paleček, E.; Wang, J. Electrochemical Nucleic Acid-Based Biosensors: Concepts, Terms, and Methodology (IUPAC Technical Report). *Pure Appl. Chem.* **2010**, *82* (5), 1161–1187.

(35) Jin, J.; Ouyang, X.; Li, J.; Jiang, J.; Wang, H.; Wang, Y.; Yang, R. Nucleic Acid-Modulated Silver Nanoparticles: A New Electrochemical Platform for Sensing Chloride Ion. *Analyst* **2011**, *136* (18), 3629–3634.

(36) Evans, N. H.; Beer, P. D. A Ferrocene Functionalized Rotaxane Host System Capable of the Electrochemical Recognition of Chloride. *Org. Biomol. Chem.* **2011**, *9* (1), 92–100.

(37) Parks, F. C.; Sheetz, E. G.; Stutsman, S. R.; Lutolli, A.; Debnath, S.; Raghavachari, K.; Flood, A. H. Revealing the Hidden Costs of Organization in Host-Guest Chemistry Using Chloride-Binding Foldamers and Their Solvent Dependence. *J. Am. Chem. Soc.* **2022**, *144* (3), 1274–1287.

(38) Liu, Y.; Parks, F. C.; Sheetz, E. G.; Chen, C. H.; Flood, A. H. Polarity-Tolerant Chloride Binding in Foldamer Capsules by Programmed Solvent-Exclusion. *J. Am. Chem. Soc.* **2021**, *143* (8), 3191–3204.

(39) Hua, Y.; Liu, Y.; Chen, C. H.; Flood, A. H. Hydrophobic Collapse of Foldamer Capsules Drives Picomolar-Level Chloride Binding in Aqueous Acetonitrile Solutions. *J. Am. Chem. Soc.* **2013**, *135* (38), 14401–14412.

(40) John, E. A.; Massena, C. J.; Berryman, O. B. Helical Anion Foldamers in Solution. *Chem. Rev.* **2020**, *120* (5), 2759–2782.

(41) Suk, J.; Jeong, K.-S. Indolocarbazole-Based Foldamers Capable of Binding Halides in Water. *J. Am. Chem. Soc. Commun.* **2008**, *130* (36), 11868–11869.

(42) Hua, Y.; Flood, A. H. Flipping the Switch on Chloride Concentrations with a Light-Active Foldamer. *J. Am. Chem. Soc.* **2010**, *132* (37), 12838–12840.

(43) Gale, P. A.; Caltagirone, C. Anion Sensing by Small Molecules and Molecular Ensembles. *Chem. Soc. Rev.* **2015**, *44* (13), 4212–4227.

(44) Tutol, J. N.; Kam, H. C.; Dodani, S. C. Identification of MNeonGreen as a PH-Dependent, Turn-On Fluorescent Protein Sensor for Chloride. *ChemBioChem* **2019**, *20* (14), 1759–1765.

(45) Zhang, P. F.; Yang, G. P.; Li, G. P.; Yang, F.; Liu, W. N.; Li, J. Y.; Wang, Y. Y. Series of Water-Stable Lanthanide Metal-Organic Frameworks Based on Carboxylic Acid Imidazolium Chloride: Tunable Luminescent Emission and Sensing. *Inorg. Chem.* **2019**, *58* (20), 13969–13978.

(46) Miyaji, H.; Sessler, J. L. Off-the-Shelf Colorimetric Anion Sensors. *Angew. Chem. Int. Ed.* **2001**, *40* (1), 154–157.

(47) Carroll, C. N.; Berryman, O. B.; Johnson, C. A.; Zakharov, L. N.; Haley, M. M.; Johnson, D. W. Protonation Activates Anion Binding and Alters Binding Selectivity in New Inherently Fluorescent 2,6-Bis(2-Anilinoethynyl)Pyridine Bisureas. *Chem. Commun.* **2009**, No. 18, 2520–2522.

(48) Carroll, C. N.; Coombs, B. A.; McClintock, S. P.; Johnson, C. A.; Berryman, O. B.; Johnson, D. W.; Haley, M. M. Anion-Dependent Fluorescence in Bis(Anilinoethynyl)Pyridine Derivatives: Switchable ON-OFF and OFF-ON Responses. *Chem. Commun.* **2011**, *47* (19), 5539–5541.

(49) Tresca, B. W.; Zakharov, L. N.; Carroll, C. N.; Johnson, D. W.; Haley, M. M. Aryl C-H···Cl-Hydrogen Bonding in a Fluorescent Anion Sensor. *Chem. Commun.* **2013**, *49* (65), 7240–7242.

(50) Gavette, J. V.; Mills, N. S.; Zakharov, L. N.; Johnson, C. A.; Johnson, D. W.; Haley, M. M. An Anion-Modulated Three-Way Supramolecular Switch That Selectively Binds Dihydrogen Phosphate, $H_2PO_4^-$. *Angew. Chemie. Ed.* **2013**, *52* (39), 10270–10274.

(51) Hartle, M. D.; Hansen, R. J.; Tresca, B. W.; Prakel, S. S.; Zakharov, L. N.; Haley, M. M.; Pluth, M. D.; Johnson, D. W. A Synthetic Supramolecular Receptor for the Hydrosulfide Anion. *Angew. Chem. Int. Ed.* **2016**, *55* (38), 11480–11484.

(52) Eytel, L. M.; Gilbert, A. K.; Görner, P.; Zakharov, L. N.; Johnson, D. W.; Haley, M. M. Do CH–Anion and Anion–π Interactions Alter the Mechanism of 2:1 Host–Guest Complexation in Arylethynyl Monourea Anion Receptors? *Chem. Eur. J.* **2017**, *23* (17), 4051–4054.

(53) Würthner, F.; Kaiser, T. E.; Saha-Möller, C. R. J-Aggregates: From Serendipitous Discovery to Supramolecular Engineering of Functional Dye Materials. *Angew. Chem. Int. Ed.* **2011**, *50* (15), 3376–3410.

(54) Schmidtchen, F. P.; Berger, M. Artificial Organic Host Molecules for Anions. *Chem. Rev.* **1997**, *97* (5), 1609–1646.

(55) Palacios, M. A.; Nishiyabu, R.; Marquez, M.; Anzenbacher, P. Supramolecular Chemistry Approach to the Design of a High-Resolution Sensor Array for Multianion Detection in Water. *J. Am. Chem. Soc.* **2007**, *129* (24), 7538–7544.

(56) Robertson, C. C.; Perutz, R. N.; Brammer, L.; Hunter, C. A. A Solvent-Resistant Halogen Bond. *Chem. Sci.* **2014**, *5* (11), 4179–4183.

(57) Metrangolo, P.; Neukirch, H.; Pilati, T.; Resnati, G. Halogen Bonding Based Recognition Processes: A World Parallel to Hydrogen Bonding. *Acc. Chem. Res.* **2005**, *38* (5), 386–395.

(58) Desiraju, G. R.; Ho, P. S.; Kloo, L.; Legon, A. C.; Marquardt, R.; Metrangolo, P.; Politzer, P.; Resnati, G.; Rissanen, K. Definition of the Halogen Bond (IUPAC Recommendations 2013). *Pure Appl. Chem.* **2013**, *85* (8), 1711–1713.

(59) Clark, T.; Hennemann, M.; Murray, J. S.; Politzer, P. Halogen Bonding: The σ-Hole. *J. Mol. Model.* **2007**, *13* (2), 291–296.

(60) Cavallo, G.; Metrangolo, P.; Milani, R.; Pilati, T.; Priimagi, A.; Resnati, G.; Terraneo, G. The Halogen Bond. *Chem. Rev.* **2016**, *116*, 2478–2601.

(61) Beale, T. M.; Chudzinski, M. G.; Sarwar, M. G.; Taylor, M. S. Halogen Bonding in Solution: Thermodynamics and Applications. *Chem. Soc. Rev.* **2013**, *42* (4), 1667–1680.

(62) Lohrman, J. A.; Deng, C.-L.; Shear, T. A.; Zakharov, L. N.; Haley, M. M.; Johnson, D. W. Methanesulfonyl-Polarized Halogen Bonding Enables Strong Halide Recognition in an Arylethynyl Anion Receptor. *Chem. Commun.* **2019**, *55*, 1919–1922.

CHAPTER II

(1) Sessler, J. L.; Gale, P. A.; Cho, W.-S. *Anion Receptor Chemistry*; Royal Society of Chemistry: Cambridge, 2006.

(2) Zyryanov, G. V; Palacios, M. A.; Anzenbacher Jr., P. Rational Design of a Fluorescence-Turn-On Sensor Array for Phosphates in Blood Serum Zuschriften. *Angew. Chemie* **2007**, *119*, 7995–7998.

(3) Schmidt, R. F.; Thews, G. *Human Physiology*, 2nd ed.; Springer: Berlin, 1989.

(4) Hruska, K. A.; Mathew, S.; Lund, R.; Qiu, P.; Pratt, R. Hyperphosphatemia of Chronic Kidney Disease. *Kidney Int.* **2008**, *74* (2), 148–157.

(5) Kanbay, M.; Goldsmith, D.; Akcay, A.; Covic, A. Phosphate - The Silent Stealthy Cardiorenal Culprit in All Stages of Chronic Kidney Disease: A Systematic Review. *Blood Purif.* **2009**, *27* (2), 220–230.

(6) Daniel, T. C.; Sharpley, A. N.; Lemunyon, J. L. Agricultural Phosphorus and Eutrophication: A Symposium Overview. *J. Environ. Qual.* **1998**, *27* (2), 251–257.

(7) Lohrman, J. A.; Deng, C.-L.; Shear, T. A.; Zakharov, L. N.; Haley, M. M.; Johnson, D. W. Methanesulfonyl-Polarized Halogen Bonding Enables Strong Halide Recognition in an Arylethynyl Anion Receptor. *Chem. Commun.* **2019**, *55*, 1919–1922.

(8) Adamczyk, M.; Rege, S. Microwave Assisted Sulfopropylation of N-Heterocycles Using 1,3-Propane Sultone. *Tetrahedron Lett.* **1998**, *39* (52), 9587–9588.

(9) Laschewsky, A. Structures and Synthesis of Zwitterionic Polymers. *Polymers (Basel).* **2014**, *6* (5), 1544–1601.

(10) Liu, H. F.; Zeng, F. X.; Deng, L.; Liao, B.; Pang, H.; Guo, Q. X. Brønsted Acidic Ionic Liquids Catalyze the High-Yield Production of Diphenolic Acid/Esters from Renewable Levulinic Acid. *Green Chem.* **2013**, *15* (1), 81–84.

(11) Delgado, J. D.; Schlenoff, J. B. Static and Dynamic Solution Behavior of a Polyzwitterion Using a Hofmeister Salt Series. *Macromolecules* **2017**, *50*, 4455–4464.

(12) Kunz, W.; Henle, J.; Ninham, B. W. 'Zur Lehre von Der Wirkung Der Salze' (about the Science of the Effect of Salts) : Franz Hofmeister's Historical Papers. *Curr. Opin. Colloid Interface Sci.* **2004**, *9*, 19–37.

(13) Hofmeister, F.; Zur Lehre, V. D. W. D. S. Hofmeister Paper. *Naunyn-Schmiedeberg's Arch. Pharmacol.* **1888**, *24*, 247.

(14) He, Y.; Shao, Q.; Chen, S.; Jiang, S. Water Mobility : A Bridge between the Hofmeister Series of Ions and the Friction of Zwitterionic Surfaces in Aqueous Environments. *J. Phys. Chem. C* **2011**, *115*, 15525–15531.

(15) Feng, H.; Wang, Y.; Jia, H.; Zhang, R.; Han, Q.; Meng, Q.; Zhiqiang, Z. Selective Detection of Inorganic Phosphates in Live Cells Based on a Responsive Fluorescence Probe. *New J. Chem.* **2017**, *41*, 9623–9630.

(16) Hermanson, G. T. The Reactions of Bioconjugation. In *Bioconjugate Techniques*; Academic Press, 2013; pp 229–258.

(17) Yang, N. J.; Hinner, M. J. Getting Across the Cell Membrane: An Overview for Small Molecules, Peptides, and Proteins. *Methods Mol. Biol.* **2015**, *1266*, 29–53.

CHAPTER III

(1) Berend, K.; Van Hulsteijn, L. H.; Gans, R. O. B. Chloride: The Queen of Electrolytes? *Eur. J. Intern. Med.* **2012**, *23* (3), 203–211.

(2) Meletis, C. D. Iodine: Health Implications of Deficiency. *J. Evid. Based. Complementary Altern. Med.* **2011**, *16*, 190–194.

(3) Bowman-James, K. Supramolecular Cages Trap Pesky Anions. *Science* **2019**, *365* (6449), 124–125.

(4) Pancholi, J.; Beer, P. D. Halogen Bonding Motifs for Anion Recognition. *Coord. Chem. Rev.* **2020**, *416*, 213281.

(5) Hein, R.; Beer, P. D. Halogen Bonding and Chalcogen Bonding Mediated Sensing. *Chem. Sci.* **2022**, 7098–7125.

(6) Kunz, W.; Henle, J.; Ninham, B. W. 'Zur Lehre von Der Wirkung Der Salze' (about the Science of the Effect of Salts) : Franz Hofmeister's Historical Papers. *Curr. Opin. Colloid Interface Sci.* **2004**, *9*, 19–37.

(7) Gregory, K. P.; Elliott, G. R.; Robertson, H.; Kumar, A.; Wanless, E. J.; Webber, G. B.; Craig, V. S. J.; Andersson, G. G.; Page, A. J. Understanding Specific Ion Effects and the Hofmeister Series. *Phys. Chem. Chem. Phys.* **2022**, *24* (21), 12682–12718.

(8) Liu, Y.; Zhao, W.; Chen, C.-H.; Flood, A. H. Chloride Capture Using a C–H Hydrogen-Bonding Cage. *Science* **2019**, *365*, 159–161.

(9) Robertson, C. C.; Wright, J. S.; Carrington, E. J.; Perutz, R. N.; Hunter, C. A.; Brammer, L. Hydrogen Bonding: Vs. Halogen Bonding: The Solvent Decides. *Chem. Sci.* **2017**, *8* (8), 5392–5398.

(10) Tresca, B. W.; Zakharov, L. N.; Carroll, C. N.; Johnson, D. W.; Haley, M. M. Aryl C-H···Cl-Hydrogen Bonding in a Fluorescent Anion Sensor. *Chem. Commun.* **2013**, *49* (65), 7240–7242.

(11) Watt, M. M.; Engle, J. M.; Fairley, K. C.; Robitshek, T. E.; Haley, M. M.; Johnson, D. W. "Off-on" Aggregation-Based Fluorescent Sensor for the Detection of Chloride in Water. *Org. Biomol. Chem.* **2015**, *13* (14), 4266–4270.

(12) Carroll, C. N.; Coombs, B. A.; McClintock, S. P.; Johnson, C. A.; Berryman, O. B.; Johnson, D. W.; Haley, M. M. Anion-Dependent Fluorescence in Bis(Anilinoethynyl)Pyridine Derivatives: Switchable ON-OFF and OFF-ON Responses. *Chem. Commun.* **2011**, *47* (19), 5539–5541.

(13) Lipinski, C. A.; Lombardo, F.; Dominy, B. W.; Feeney, P. J. Experimental and Computational Approaches to Estimate Solubility and Permeability in Drug Discovery and Development Settings. *Adv. Drug Deliv. Rev.* **2012**, *64* (SUPPL.), 4–17.

(14) Lipinski, C. A. Lead- and Drug-like Compounds: The Rule-of-Five Revolution. *Drug Discov. Today Technol.* **2004**, *1* (4), 337–341.

(15) Corradi, E.; Meille, S. V.; Messina, M. T.; Metrangolo, P.; Resnati, G. Halogen Bonding versus Hydrogen Bonding in Driving Self-Assembly Processes. *Angew. Chem. Int. Ed.* **2000**, *39* (10), 1782–1786.

(16) Fargher, H. A.; Lau, N.; Zakharov, L. N.; Haley, M. M.; Johnson, D. W.; Pluth, M. D. Expanding Reversible Chalcogenide Binding: Supramolecular Receptors for the Hydroselenide (HSe−) Anion. *Chem. Sci.* **2019**, *10* (1), 67–72.

(17) Lee, L. M.; Tsemperouli, M.; Poblador-Bahamonde, A. I.; Benz, S.; Sakai, N.; Sugihara, K.; Matile, S. Anion Transport with Pnictogen Bonds in Direct Comparison with Chalcogen and Halogen Bonds. *J. Am. Chem. Soc.* **2019**, *141* (2), 810–814.

(18) Taylor, M. S. Anion Recognition Based on Halogen, Chalcogen, Pnictogen and Tetrel Bonding. *Coord. Chem. Rev.* **2020**, *413*, 213270.

(19) Borissov, A.; Marques, I.; Lim, J. Y. C.; Félix, V.; Smith, M. D.; Beer, P. D. Anion Recognition in Water by Charge-Neutral Halogen and Chalcogen Bonding Foldamer Receptors. *J. Am. Chem. Soc.* **2019**, *141* (9), 4119–4129.

(20) Robertson, C. C.; Perutz, R. N.; Brammer, L.; Hunter, C. A. A Solvent-Resistant Halogen Bond. *Chem. Sci.* **2014**, *5* (11), 4179–4183.

(21) Bunchuay, T.; Docker, A.; Martinez-Martinez, A. J.; Beer, P. D. A Potent Halogen-Bonding Donor Motif for Anion Recognition and Anion Template Mechanical Bond Synthesis. *Angew. Chem. Int. Ed.* **2019**, *58* (39), 13823–13827.

(22) Lohrman, J. A.; Deng, C.-L.; Shear, T. A.; Zakharov, L. N.; Haley, M. M.; Johnson, D. W. Methanesulfonyl-Polarized Halogen Bonding Enables Strong Halide Recognition in an Arylethynyl Anion Receptor. *Chem. Commun.* **2019**, *55*, 1919–1922.

(23) Decato, D. A.; Riel, A. M. S.; Berryman, O. B. Anion Influence on the Packing of 1,3-Bis(4-Ethynyl-3-Iodopyridinium)-Benzene Halogen Bond Receptors. *Crystals* **2019**, *9*, 522.

(24) Riel, A. M. S.; Decato, D. A.; Sun, J.; Massena, C. J.; Jessop, M. J.; Berryman, O. B. The Intramolecular Hydrogen Bonded-Halogen Bond: A New Strategy for Preorganization and Enhanced Binding. *Chem. Sci.* **2018**, *9* (26), 5828–5836.

(25) Giese, M.; Albrecht, M.; Krappitz, T.; Peters, M.; Gossen, V.; Raabe, G.; Valkonen, A.; Rissanen, K. Cooperativity of H-Bonding and Anion–π Interaction in the Binding of Anions with Neutral π-Acceptors. *Chem. Commun.* **2012**, *48* (80), 9983–9985.

(26) Giese, M.; Albrecht, M.; Rissanen, K. Experimental Investigation of Anion-π Interactions - Applications and Biochemical Relevance. *Chem. Commun.* **2016**, *52* (9), 1778–1795.

(27) Desiraju, G. R.; Ho, P. S.; Kloo, L.; Legon, A. C.; Marquardt, R.; Metrangolo, P.; Politzer, P.; Resnati, G.; Rissanen, K. Definition of the Halogen Bond (IUPAC Recommendations 2013). *Pure Appl. Chem.* **2013**, *85* (8), 1711–1713.

(28) Brynn Hibbert, D.; Thordarson, P. The Death of the Job Plot, Transparency, Open Science and Online Tools, Uncertainty Estimation Methods and Other Developments in Supramolecular Chemistry Data Analysis. *Chem. Commun.* **2016**, *52* (87), 12792–12805.

(29) Thordarson, P. Determining Association Constants from Titration Experiments in Supramolecular Chemistry. *Chem. Soc. Rev.* **2011**, *40* (3), 1305–1323.

(30) Robinson, S. W.; Mustoe, C. L.; White, N. G.; Brown, A.; Thompson, A. L.; Kennepohl, P.; Beer, P. D. Evidence for Halogen Bond Covalency in Acyclic and Interlocked Halogen-Bonding Receptor Anion Recognition. *J. Am. Chem. Soc.* **2015**, *137* (1), 499–507.

(31) Fargher, H. A.; Lau, N.; Richardson, H. C.; Cheong, P. H. Y.; Haley, M. M.; Pluth, M. D.; Johnson, D. W. Tuning Supramolecular Selectivity for Hydrosulfide: Linear Free Energy Relationships Reveal Preferential C-H Hydrogen Bond Interactions. *J. Am. Chem. Soc.* **2020**, *142* (18), 8243–8251.

CHAPTER IV

(1) Sessler, J. L.; Gale, P. A.; Cho, W.-S. *Anion Receptor Chemistry*; Royal Society of Chemistry: Cambridge, 2006.

(2) Scott, C. C.; Gruenberg, J. Ion Flux and the Function of Endosomes and Lysosomes: pH Is Just the Start: The Flux of Ions across Endosomal Membranes Influences Endosome Function Not Only through Regulation of the Luminal PH. *BioEssays* **2011**, *33* (2), 103–110.

(3) Jentsch, T. J.; Stein, V.; Weinreich, F.; Zdebik, A. A. Molecular Structure and Physiological Function of Chloride Channels. *Physiol. Rev.* **2002**, *82* (2), 503–568.

(4) Berend, K.; Van Hulsteijn, L. H.; Gans, R. O. B. Chloride: The Queen of Electrolytes? *Eur. J. Intern. Med.* **2012**, *23* (3), 203–211.

(5) Burrows, E. F.; Southern, K. W.; Noone, P. G. Sodium Channel Blockers for Cystic Fibrosis. *Cochrane Database Syst. Rev.* **2014**, *2014* (4).

(6) Mishra, A.; Greaves, R.; Massie, J. The Relevance of Sweat Testing for the Diagnosis of Cystic Fibrosis in the Genomic Era. *Clin. Biochem. Rev.* **2005**, *26* (4), 135–153.

(7) Gibson, L. E.; Cooke, R. E. A Test for Concentration of Electrolytes in Sweat in Cystic Fibrosis of the Pancreas Utilizing Pilocarpine by Iontophoresis. *Pediatrics* **1959**, *23* (3), 545–549.

(8) Servidoni, M. F.; Gomez, C. C. S.; Marson, F. A. L.; Toro, A. A. D. C.; Ribeiro, M. Â. G. de O.; Ribeiro, J. D.; Ribeiro, A. F. Sweat Test and Cystic Fibrosis: Overview of Test Performance at Public and Private Centers in the State of São Paulo, Brazil. *J. Bras. Pneumol.* **2017**, *43* (2), 121–128.

(9) Gokdemir, Y.; Karadag, B. T. Sweat Testing and Recent Advances. *Front. Pediatr.* **2021**, *9* (May), 1–8.

(10) Watt, M. M.; Engle, J. M.; Fairley, K. C.; Robitshek, T. E.; Haley, M. M.; Johnson, D. W. "Off-on" Aggregation-Based Fluorescent Sensor for the Detection of Chloride in Water. *Org. Biomol. Chem.* **2015**, *13* (14), 4266–4270.

(11) Parks, F. C.; Sheetz, E. G.; Stutsman, S. R.; Lutolli, A.; Debnath, S.; Raghavachari, K.; Flood, A. H. Revealing the Hidden Costs of Organization in Host-Guest Chemistry Using Chloride-Binding Foldamers and Their Solvent Dependence. *J. Am. Chem. Soc.* **2022**, *144* (3), 1274–1287.

(12) Chen, Y.; Wu, G.; Chen, L.; Tong, L.; Lei, Y.; Shen, L.; Jiao, T.; Li, H. Selective Recognition of Chloride Anion in Water. *Org. Lett.* **2020**, *22*, 4878–4882.

(13) Lohrman, J. A.; Deng, C.-L.; Shear, T. A.; Zakharov, L. N.; Haley, M. M.; Johnson, D. W. Methanesulfonyl-Polarized Halogen Bonding Enables Strong Halide Recognition in an Arylethynyl Anion Receptor. *Chem. Commun.* **2019**, *55*, 1919–1922.

(14) Foster, N. I.; Heindel, N. D.; Burns, H. D.; Muir, W. Aryl Iodides from Anilines via Triazene Intermediates. *Synth. Commun.* **1980**, 572–573.